

Exploring New Physics with Astrophysical Neutrinos at IceCube

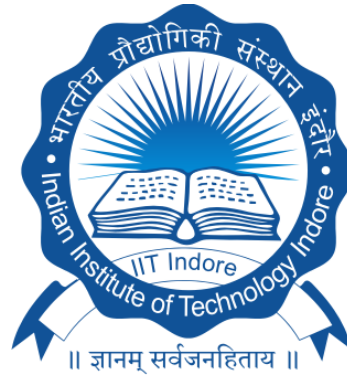
PhD THESIS

by

Sujata

Supervisor

Prof. Subhendu Rakshit



DEPARTMENT OF PHYSICS

INDIAN INSTITUTE OF TECHNOLOGY INDORE

INDORE - 453552, INDIA

Roll No.: 1501151007

December 2020

Exploring New Physics with Astrophysical Neutrinos at IceCube

Thesis submitted in partial fulfillment of the requirements for the award of the degree

DOCTOR OF PHILOSOPHY

by

Sujata

Supervisor: Prof. Subhendu Rakshit



Department of Physics,
Indian Institute of Technology Indore,
Khandwa Road, Simrol, Indore - 453552, India

Roll No.: 1501151007

December 2020



INDIAN INSTITUTE OF TECHNOLOGY INDORE

CANDIDATE'S DECLARATION

I hereby certify that the work which is being presented in the thesis entitled **Exploring New Physics with Astrophysical Neutrinos at IceCube** in the partial fulfillment of the requirements for the award of the degree of **DOCTOR OF PHILOSOPHY** and submitted in the **DEPARTMENT OF PHYSICS, Indian Institute of Technology Indore**, is an authentic record of my own work carried out during the time period from July 2015 to December 2020 under the supervision of Prof. Subhendu Rakshit, Indian Institute of Technology Indore.

The matter presented in this thesis has not been submitted by me for the award of any other degree of this or any other institute.

Sujata
12/12/2020

Signature of the student with date
(Sujata)

This is to certify that the above statement made by the candidate is correct to the best of my knowledge.

Subhendu Rakshit

15.12.2020

Signature of Thesis Supervisor with date
(Prof. Subhendu Rakshit)

Sujata has successfully given her Ph.D. Oral Examination held on **02/12/2021**.

Subhendu Rakshit

Signature of Thesis Supervisor
(Prof. Subhendu Rakshit)

Dedicated
to
My Grandparents

LIST OF PUBLICATIONS

A. Published:

1. Pandey S., Karmakar S. and Rakshit S., Interactions of Astrophysical Neutrinos with Dark Matter: A model building perspective, *JHEP* **01** (2019) 095 (DOI:10.1007/JHEP01(2019)095).
2. Pandey S., Karmakar S. and Rakshit S., Strong constraints on non-standard neutrino interactions: LHC vs. IceCube, *JHEP* **11** (2019) 046 (DOI:10.1007/JHEP11(2019)046).
3. Karmakar S., Pandey S. and Rakshit S., Astronomy with energy dependent flavour ratios of extragalactic neutrinos, *JHEP* **10** (2021) 004 (DOI:10.1007/JHEP10(2021)004).

C. Conference proceedings:

1. Pandey S., Can New Interactions with Dark Matter lead to Flux Change of Astrophysical Neutrinos at Icecube?, *Springer Proc. Phys.* **261** (2021) 977-980 (DOI:10.1007/978-981-33-4408-2_141).
2. Karmakar S., Pandey S. and Rakshit S., Extragalactic Neutrinos: A Window to New Physics, *Springer Proc. Phys.* **248** (2020) 229-236 (DOI:10.1007/978-981-15-6292-1_28).
3. Pandey S., Karmakar S. and Rakshit S., Exploring Neutrino-Dark Matter Interaction via Astrophysical Neutrinos at IceCube, *Andromeda Conference Proceedings* (DOI: 10.31526/ACP.NDM-2020.11).

Acknowledgements

I would like to thank my PhD supervisor, Prof. Subhendu Rakshit, for his continuous guidance, prompt responses and unwavering support throughout my time at IIT Indore. I am grateful to my PSPC members Prof. Manavendra Mahato and Prof. Swadesh Kumar Sahoo, for their patience and motivation. I also acknowledge Dr. Debanjan Bose for his valuable comments and fruitful discussions.

PhD can be a long journey, but thanks to my friends and lab-mates it has not been a lonely one. I appreciate the camaraderie of 507 A: Dhruv, Shiva, Swapnesh, Kajal, Ouseph and Avik. Siddhartha Da has not only been my collaborator but a fellow commiserator and a confidant. I acknowledge my friends: Sudhir, Sarvesh, Sayan, Tamalika, Shraddha, Amitesh and Debodirna for being with me through thick and thin. Thanks to all the hostel-mates Shweta, Anjali, Ankita Di, Lichchhavi, Nivedita, Surabhi and Nidhi for the good times.

It would have been impossible to complete this degree without the support of my two families. My sincere thanks to both my mummy(s) and papa(s) for their wise advice and kind understanding. Thanks for your determination when mine used to fall short. Raj, thank you for being the person I could count on, irrespective of anything or everything. Last, but very opposite of the least, my heartfelt gratitude to my better half Aditya for his partnership in the journey.

The present work is supported by the Department of Science and Technology, India via SERB grant EMR/2014/001177.

(Sujata)

Contents

Acknowledgements	vii
1 Introduction	1
1.1 Symmetries and Gauge invariance	2
1.2 The Standard Model Revisited	4
1.3 Electroweak Interaction	5
1.3.1 Neutrinos in the Standard Model	6
1.3.2 Neutrino-Nucleon interaction	9
1.4 Higgs Mechanism	13
1.5 Neutrino Mass	15
1.6 Neutrino Oscillations in Vacuum	17
1.7 Neutrino Oscillations in Matter	21
1.8 Dark Matter	28
1.8.1 Evidences of Dark Matter	29
1.8.2 Dark Matter Candidates	31
1.9 Motivation and Organisation of the Thesis	32
2 Aspects of Astrophysical Neutrinos	37
2.1 Cosmic Rays	39
2.1.1 Hillas Criterion	41
2.2 Acceleration of Cosmic Rays	41
2.2.1 Fermi Acceleration Mechanism	41

2.2.2	Diffusive Shock Acceleration	44
2.3	Production of Astrophysical Neutrinos	47
2.4	Relation with Multi-messengers	49
2.4.1	Relationship of Low Energy Gamma Rays and High En- ergy Cosmic Rays with Intermediate Energy Neutrinos	52
2.4.2	Waxman-Bahcall Bound	54
2.5	Sources of Astrophysical Neutrinos	55
2.5.1	Active Galactic Nuclei	55
2.5.2	Galaxy Clusters	57
2.5.3	Starburst Galaxy	58
2.5.4	Gamma Ray Burst	58
2.5.5	Low Luminosity and Choked Gamma Ray Bursts	59
2.5.6	Cosmogenic Neutrinos	60
2.5.7	Decaying Dark Matter	62
2.6	Observation of Astrophysical Neutrinos	62
2.7	IceCube	64
2.7.1	Detection of high energy neutrinos	66
2.7.2	Signals Observed	66
2.7.3	IceCube Observations	68
2.8	ANTARES	75
2.9	ANITA	76
2.10	Future Detectors	76
2.10.1	IceCube Upgrade and IceCube-Gen2	77
2.10.2	KM3NeT	78
2.10.3	Baikal-GVD	78
2.10.4	GRAND	79

3	Interactions of Astrophysical Neutrinos with Dark Matter: A model building perspective	83
3.1	Dark Matter Candidates	85
3.2	Effective Interactions	87
3.2.1	Topology I	89
3.2.2	Topology II	94
3.2.3	Topology III	95
3.2.4	Topology IV	96
3.3	The Renormalisable Models	98
3.3.1	Description of the models	98
3.3.2	Thermal Relic Dark Matter	101
3.3.3	Ultralight Scalar Dark Matter	104
3.4	Summary	110
4	Astronomy with Energy Dependent Flavour Ratios of Extragalactic Neutrinos	115
4.1	Neutrino Astronomy	117
4.2	Neutrino Oscillations in a dark matter halo	119
4.3	Energy dependence of flavour ratios	124
4.4	Summary and outlook	134
5	Strong constraints on non-standard neutrino interactions: LHC vs. IceCube	139
5.1	NSI and existing constraints	141
5.2	Implementation of the constraints	144
5.3	Constraints on NSI interactions from LHC and IceCube	146
5.3.1	Z' with renormalisable and effective coupling to neutrinos	147
5.3.2	Contact type interactions	154
5.4	Summary	160

6	Conclusion	165
7	Appendices	171
7.1	Cross-section of neutrino-DM interaction	171
7.1.1	Kinematics	171
7.1.2	Amplitudes of various renormalisable neutrino-DM interactions	172
7.2	Anomaly cancellation for vector-mediated scalar DM model . . .	173
7.3	Summary of neutrino-DM interactions for scalar DM	175
7.4	A UV-complete model for vector-mediated ultralight scalar DM .	176
7.5	Extracting constraints on NSI from CC neutrino-nucleon cross-section	179
7.6	Differential cross-sections and interference effects	180
	References	183

Figures

1.1	Electron spectrum vs. energy in beta decay. (Figure courtesy: Ref. [4].)	2
1.2	Feynman diagram for neutrino-nucleon interaction. (Figure courtesy: Ref. [8].)	10
1.3	Cross-section of (anti)neutrino-nucleon interaction. Here the solid and dashed lines denote DIS for neutrino and antineutrino respectively. (Figure courtesy: Ref. [21].)	13
2.1	Cosmic ray spectrum from various experiments. (Figure courtesy: Ref. [122].)	40
2.2	Hillas diagram. The solid red and blue lines represent the magnetic field B and size R required to confine a 10^{20} eV of proton and iron respectively. (Figure courtesy: Ref. [129].)	42
2.3	A charged particle deflected by the magnetic cloud.	42
2.4	(a) Velocities of upstream (v_1) and downstream medium (v_2) observed from shock rest frame. (b) Left, and right diagrams represent the velocities of shock and medium in upstream, and downstream rest frames respectively. (Figure courtesy: Ref. [131].) . .	45
2.5	The solid blue and green lines represent the gamma ray spectrum and cosmic ray spectrum respectively. A The blue dashed, solid line are the neutrino, gamma ray flux from pp process from pion decay from a source. B Neutrino flux from a source with $\Gamma = 2$ in calorimetric limit. C Green dotted line depicts the cosmogenic neutrinos. (Figure courtesy: Ref. [139].)	53

2.6	Spectral energy distribution (SED) of BL Lacs. (Figure courtesy: Ref. [156].)	57
2.7	Limit on high energy neutrino flux from IceCube data. The black solid, and dotted lines represent upper limit on neutrino flux from 9 years, and seven years of data respectively. The purple [179], cyan, and green lines [180] are cosmogenic neutrino fluxes assuming optimistic scenario. (Figure courtesy: Ref. [181].)	61
2.8	IceCube detector. (Figure courtesy: Ref. [194].)	64
2.9	Track, cascade and double-bang signals at IceCube. (Figure courtesy: Ref. [203].)	68
2.10	Left panel: Number of events vs. neutrino energy; Right panel: Number of events vs. cosine of declination angle observed in 7.5 years at IceCube. (Figure courtesy: Ref. [207].)	70
2.11	Flavour ratio allowed by 68%, 95% CL given by solid and dashed black line respectively after including a tau neutrino event. (Figure courtesy: Ref. [209].)	71
2.12	Neutrino-nucleon cross-section vs. neutrino energy for 7.5 years and 6 years of HESE IceCube data given by black and orange error bars up to 1σ CL respectively. (Figure courtesy: Ref. [214].)	72
2.13	IC-170922A 50% and 90% containment regions given by grey and red dashed lines respectively. Regions of high energy gamma ray excess seen at MAGIC and Fermi LAT shown by the yellow and blue lines respectively. (Figure courtesy: Ref. [155].)	73
2.14	IceCube observations from the direction of TXS 0506+056 from 5th April, 2008 to 31st October, 2017. (Figure courtesy: Ref. [218].)	74
2.15	Left plot represents the sensitivities of the detectors at 90 per cent CL. The right plot represents the discovery potential for the sources [239].	80
2.16	The blue solid, dashed lines represent the sensitivity and discovery potential for IceCube-Gen2 after 15 years of running. (Figure courtesy: Ref. [241].)	81

3.1	Topologies of effective neutrino-DM interactions. Fig. (a), (b), (c) and (d) represent topology I, II, III and IV respectively.	89
3.2	Cross-section vs. mass of DM. Blue line represents cross-section for $m_\nu = 0.1$ eV, $c_l^{(3)}/\Lambda = 0.5$ GeV ⁻¹ for interaction (3) under Topology I. Grey line represents the required cross-section to induce 1% suppression of incoming flux.	93
3.3	(a) Cross-section vs. incoming neutrino energy. (b) Cross-section vs. mass of DM. Grey line represents the required cross-section to induce 1% suppression of incoming flux. The dashed and solid blue lines represent cross-sections for $m_{Z'} = 5, 10$ MeV respectively, (a) with $m_{\text{DM}} = 0.5$ eV and (b) with $E_\nu = 1$ PeV. In both plots, $c_l^{(9)}/\Lambda = 3.8 \times 10^{-3}$ GeV ⁻¹ and $C_1 = 1$	96
3.4	Renormalisable cases of neutrino-DM scattering with (a) fermion, (b) scalar and (c) vector mediator.	99
3.5	Mass of the mediator vs. mass of DM for (a) fermion-mediated, (b) scalar-mediated and (c) vector-mediated neutrino-DM interactions. The blue and pink regions are allowed from relic density of DM and collisional damping respectively. The region at the left side of the vertical black line is ruled out from the constraint coming from N_{eff}	105
3.6	Fermion-mediated neutrino-DM scattering. (a) Cross-section vs. incoming neutrino energy. Green and blue lines represent cross-sections for $m_\nu = 10^{-2}, 10^{-5}$ eV respectively with $m_F = 10$ GeV. Red and orange lines represent cross-sections for $m_\nu = 10^{-2}, 10^{-5}$ eV respectively with $m_F = 100$ GeV. Here $C_L = 0.88$, $m_{\text{DM}} = 10^{-22}$ eV. (b) Cross-section vs. mass of DM. Green and red lines represent $m_F = 10, 100$ GeV respectively for $m_\nu = 10^{-2}$ eV. Here $C_L = 0.88$, $E_\nu = 1$ PeV. Grey line represents the required cross-section to induce 1% suppression of incoming neutrino flux.	106

3.7	Cross-section vs. mass of DM in scalar-mediated neutrino-DM scattering. The blue and grey lines represent the cross-section with scalar mediator and the same required to induce 1% suppression of incoming flux respectively. Here, energy of incoming neutrino $E_\nu = 1$ PeV, mediator mass $m_\Delta = 200$ GeV and $f_i g_\Delta v_\Delta = 0.1$ eV.	108
3.8	Vector-mediated neutrino-DM scattering. (a) Cross-section vs. incoming neutrino energy. (b) Cross-section vs. mass of DM. Blue and grey lines represent the calculated cross-section and required cross-section to induce 1% suppression of incoming flux respectively. Here, the mediator mass $m_{Z'} = 10$ MeV, and the couplings $g' f' = 10^{-3}$. For (a), $m_{\text{DM}} = 10^{-6}$ eV and for (b), the energy of incoming neutrino $E_\nu = 1$ PeV.	109
4.1	Energy dependence of flavour ratios for (a) neutrinos (f_α^D) and (b) antineutrinos ($f_\alpha^{\bar{D}}$), and (c) the average of neutrinos and antineutrinos (F_α^D). The blue, orange and green lines represent flavour ratio for e , μ and τ flavours. Solid and dashed lines stand for $a = 10^{-5}$ pc (non-adiabatic case) and $a = 5$ pc (adiabatic case) respectively.	126
4.2	Track to shower ratio vs. neutrino energy for varying values of (a) radius of the solitonic core a , (b) DM density at its centre ρ_0 , and (c) G'_F/m_{DM} . In (b), the solid and dotted lines correspond to $a = 1$ pc (adiabatic case) and 10^{-5} pc (non-adiabatic case) respectively.	129

5.1	Constraints on NSI described by eq. (5.4) for $m_{Z'} = 5$ GeV. The brown line represents the total SM neutrino-nucleon cross-section [10]. The red line and the light red band denote the central value and 1σ allowed range of $\sigma_{\nu N}^{tot}$ from IceCube observation of track events respectively [360]. Similarly, the green points and related error bars in the y -direction stand for the central values and 1σ allowed ranges in $\sigma_{\nu N}^{tot}$ measured from the IceCube observation of shower events at different energy bins respectively [213]. In presence of a Z' with mass $m_{Z'} = 5$ GeV and interactions as in eq. (5.4), (i) the magenta line depicts the value of $\sigma_{\nu N}^{tot}$ with the NSI parameter ϵ set at its maximum allowed value from LHC, $\epsilon = 12$, (ii) the black line represents the value of $\sigma_{\nu N}^{tot}$ with ϵ set at its maximum allowed value from IceCube, $\epsilon = 2$	151
5.2	Constraints on Z' induced NSI in presence of interactions expressed in eq. (5.4), (5.6) and (5.7) respectively as functions of Z' mass. The pink and grey regions are excluded from LHC and IceCube respectively.	152
5.3	Constraints on NSI described by eq. (5.6) in presence of a Z' of mass 5 GeV. Colour coding is the same as in fig. 5.1.	153
5.4	Constraints on NSI described by eq. (5.7) in presence of a Z' of mass 5 GeV. Colour coding is the same as in fig. 5.1.	154
5.5	The maximum allowed values of NC neutrino-nucleon cross-section in presence of NSI appearing in eq. (5.8). Colour coding is the same as in fig. 5.1.	156
5.6	Constraints on NSI described by eq. (5.9). Colour coding is the same as in fig. 5.1.	157
5.7	Constraints on NSI appearing in eq. (5.10). Colour coding is the same as in fig. 5.1.	157
5.8	Constraints on NSI appearing in eq. (5.11). Colour coding is the same as in fig. 5.1.	159

Tables

1.1	Charges of the particles under the SM. Here, $l = \{e, \mu, \tau\}$, $\nu_l = \{\nu_e, \nu_\mu, \nu_\tau\}$, $U = \{u, c, t\}$, and $D = \{d, s, b\}$ represent the three generations of leptons and quarks. ϕ is the Higgs doublet. . . .	5
3.1	Thermally averaged DM annihilation cross-section and the cross-section for neutrino-DM elastic scattering for thermal DM. . . .	103
7.1	Summary of neutrino-DM effective interactions. c_l and $c_{e,\mu,\tau}$ represent the coefficients of interactions for the gauge non-invariant and gauge-invariant forms respectively. The colour coding for the constraints is: $Z \rightarrow inv$, LEP monophoton+ \cancel{E}_T , $Z \rightarrow \mu^+\mu^-$, $Z \rightarrow \tau^+\tau^-$, BBN and $(g-2)_{e,\mu}$. We also remark whether the interactions are favoured in context of the 1% flux suppression criteria as mentioned earlier.	175
7.2	Summary of renormalisable neutrino-DM interactions. Colour coding is the same as in table 2.1.	176
7.3	Quantum numbers of the particles in the model.	178
7.4	Constraints on coupling of light vector boson Z' of mass 10 MeV.	179

Chapter 1

Introduction

In 1914, James Chadwick made a bizarre observation while conducting the beta decay experiment. It was expected that the neutrons decay to protons and electrons, and since it was a two body decay, the electron would manifest having fixed energy. But on observation, he found that electrons, produced during beta decay, had a range of energy as can be seen in fig. 1.1. In his desperation to uphold the law of conservation of energy in 1929, Pauli proposed a neutral fermion, which at that time, he called ‘neutron’ (as neutrons were not discovered yet). Later, after the discovery of neutrons by James Chadwick in 1932, this accompanying particle in beta decay got its name ‘neutrino’ or the little neutral one. This new particle was believed to be undetectable since it interacts very weakly, *i.e.*, the cross-section is much less as compared to electromagnetic interaction. However, in 1956 Reines and Cowan detected electron antineutrinos by directing them to a water detector with CdCl_2 , *via* the process $\bar{\nu}_e p \rightarrow ne^+$ [1]. The first pulse is that the positron annihilates the electron in the detector to produce two 0.5 MeV photons, which were detected. Also, there is a second pulse by the capture of the neutron in the cadmium leading to a delayed coincidence. Later on, muon neutrino was discovered from pion decay at the Brookhaven National Laboratory in 1962 [2] and tau neutrino at the DONUT experiment at CERN in 2000 [3]. These neutrinos are associated with a family of charged leptons whose mass and interactions are successfully explained by the Standard Model (SM) of particle physics. The SM is a theory based on Lorentz and gauge invariance. All the particles known to us interact *via* either one or in the combination of the three forces,

i.e., the electromagnetic, the electroweak and the strong force and all the particles interact gravitationally. The former three are well described by the SM, whereas the gravitational interaction, which is based on coordinate invariance, does not find its explanation within the SM framework. In this chapter, the SM is revisited, and its successes and failures in the context of neutrinos are discussed.

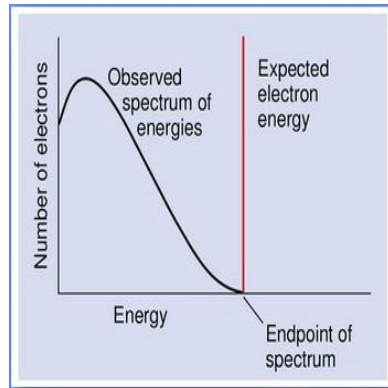


Figure 1.1. Electron spectrum vs. energy in beta decay. (Figure courtesy: Ref. [4].)

1.1 Symmetries and Gauge invariance

Noether's theorem states that for every continuous symmetry of the Lagrangian, there exists a conserved quantity [5]. In this context let us consider the free Dirac Lagrangian

$$\mathcal{L} = \bar{\Psi}(i\cancel{\partial} - m)\Psi,$$

where, Ψ is a Dirac field with mass m . Under the transformation, $\Psi \rightarrow \Psi' = e^{i\beta}\Psi$, it is evident that in the case of global transformation, *i.e.*, when β is not a function of space-time, \mathcal{L} remains invariant. But the invariance does not hold for local transformation. If β is a function of space-time

$$\mathcal{L} \rightarrow \mathcal{L}' = \bar{\Psi}(i\cancel{\partial} - m)\Psi - \bar{\Psi}\gamma^\mu\partial_\mu\beta\Psi.$$

Thus \mathcal{L} is not invariant under a local transformation. The invariance can be restored by the addition of a gauge field A_μ that transforms as, $A_\mu \rightarrow A'_\mu = A_\mu + (1/Q)\partial_\mu\beta$ and defining the kinetic term with a covariant derivative $\partial_\mu \rightarrow D_\mu = \partial_\mu - iQA_\mu$. Hence, one obtains a U(1) gauge invariant Lagrangian

$$\begin{aligned}\mathcal{L} &= \bar{\Psi}(i\not{D} - m)\Psi, \\ &= \bar{\Psi}(i\not{\partial} - m)\Psi + Q\bar{\Psi}\gamma^\mu\Psi A_\mu.\end{aligned}$$

As can be seen from the transformation of A_μ , the mass term of A_μ will break the symmetry, hence its mass term is forbidden. Therefore in $U(1)_{em}$, photons do not have mass. On adding the kinetic term for A_μ , the Quantum electrodynamics (QED) Lagrangian can be written as,

$$\mathcal{L}_{U(1)_{em}} = \bar{\Psi}(i\not{\partial} - m)\Psi + Q\bar{\Psi}\gamma^\mu\Psi A_\mu - \frac{1}{4}F_{\mu\nu}F^{\mu\nu},$$

where, $F_{\mu\nu} = \partial_\mu A_\nu - \partial_\nu A_\mu$ and Q is the conserved electric charge of field Ψ under the $U(1)_{em}$ symmetry.

Similarly, for SU(N) multiplet field ψ , which transforms as

$$\psi \rightarrow \psi' = e^{i\alpha^i T^i} \psi,$$

where, T^i represents the generators of the group that satisfies Lie Algebra: $[T^i, T^j] = if^{ijk}T^k$, and f^{ijk} are the structure constants. Also, in the case of non-abelian gauge theory, the gauge fields transform as: $A_\mu^i \rightarrow A_\mu^{\prime i} = A_\mu^i - \frac{1}{g}\partial_\mu\alpha^i - f^{ijk}\alpha^j A_\mu^k$. Finally, one obtains the gauge invariant Lagrangian for the SU(N) group analogous to the abelian group, given as

$$\mathcal{L}_{SU(N)} = \bar{\psi}(i\not{D} - m)\psi + g(\bar{\psi}\gamma^\mu T^i\psi)A_\mu^i - \frac{1}{4}(A_{\mu\nu}^i)^2, \quad (1.1)$$

where $A_{\mu\nu}^i = \partial_\mu A_\nu^i - \partial_\nu A_\mu^i - gf^{ijk}A_\mu^j A_\nu^k$ and g is the coupling strength associated with SU(N) group. Strong interactions, described by invoking a SU(3) group symmetry, have the same form as given in eq. (1.1). The

quarks, ψ_q are triplets under this group and there are eight vector bosons, G_μ^i , where $i = 1, 2, \dots, 8$, that mediate the interaction. The Quantum chromodynamics (QCD) Lagrangian is given as

$$\mathcal{L}_{\text{SU}(3)_C} = \bar{\psi}_q(i\not{\partial} - m)\psi_q + g_s(\bar{\psi}_q\gamma^\mu T^i\psi_q)G_\mu^i - \frac{1}{4}(G_{\mu\nu}^i)^2,$$

where g_s is the coupling strength of the strong interaction.

1.2 The Standard Model Revisited

The Standard Model is a gauge theory, based on three local symmetry groups, namely $\text{SU}(3)_C \times \text{SU}(2)_L \times \text{U}(1)_Y$, where C , L , and Y stands for colour, left chirality and electroweak hypercharge respectively. The $\text{SU}(3)_C$ describes the strong interaction, and $\text{SU}(2)_L \times \text{U}(1)_Y$ governs the electroweak interaction. The electromagnetic interaction is described by the remnant group $\text{U}(1)_{em}$, after the breaking of $\text{SU}(2)_L \times \text{U}(1)_Y$. Hence, out of four interactions known to humanity, *i.e.*, electroweak, electromagnetic, strong and gravitational interaction, the SM successfully describes the former three. The number of gauge bosons present in the SM corresponds to the number of generators of the group. Thus the strong interaction is mediated by eight gauge bosons called gluons, and the messengers of electroweak interactions are four vector bosons W^\pm, Z and photon (γ). Other than gauge bosons, the SM consists of 12 fermions, 6 quarks and 6 leptons, and 1 scalar doublet, the Higgs field (ϕ). The quarks interact *via* electroweak, strong and electromagnetic (EM) interactions, whereas the charged leptons participate in electroweak and EM interaction, while neutrinos take part only in weak interactions. There are three generations of quarks and leptons, of which, the left-handed fields belong to $\text{SU}(2)_L$ doublet, whereas the right-handed are singlets under $\text{SU}(2)_L$. Both the left-handed and right-handed fermion fields are charged under $\text{U}(1)_Y$. The Higgs field generates the mass of the fermions and massive gauge bosons *via* spontaneous electroweak symmetry breaking, called the Higgs mecha-

nism. The particle content and the corresponding charge under the SM gauge group can be seen in table 1.1.

	Fields	$SU(3)_C$	T^3	Y	$Q = T_3 + Y/2$
Lepton doublet	$\psi_L^\ell = \begin{pmatrix} \nu_{lL} \\ l_L \end{pmatrix}$	1	$1/2$ $-1/2$	-1	0 -1
Lepton singlet	l_R	1	0	-2	-1
Quark doublet	$\psi_L^q = \begin{pmatrix} U_L \\ D_L \end{pmatrix}$	3	$1/2$ $-1/2$	$1/3$	$2/3$ $-1/3$
Quark singlets	U_R	3	0	$4/3$	$2/3$
	D_R	3	0	$-2/3$	$-1/3$
Higgs doublet	$\phi = \begin{pmatrix} \phi^+ \\ \phi^0 \end{pmatrix}$	1	$1/2$ $-1/2$	1	1 0

Table 1.1. Charges of the particles under the SM. Here, $l = \{e, \mu, \tau\}$, $\nu_l = \{\nu_e, \nu_\mu, \nu_\tau\}$, $U = \{u, c, t\}$, and $D = \{d, s, b\}$ represent the three generations of leptons and quarks. ϕ is the Higgs doublet.

1.3 Electroweak Interaction

In the case of $SU(2)_L \times U(1)_Y$, the left-handed fields and right-handed fields transform differently

$$\begin{aligned}\psi_L &\rightarrow \psi'_L = e^{i[\alpha^i T^i + \beta Y/2]} \psi_L, \\ \psi_R &\rightarrow \psi'_R = e^{i\beta Y/2} \psi_R,\end{aligned}\tag{1.2}$$

where, T^i denotes the three generators of $SU(2)_L$ group and $\psi_{R(L)} = (1 \pm \gamma_5)/2 \psi$. The generators are expressed as $T^i = \sigma^i/2$, where σ^i represent the Pauli matrices, given as

$$\sigma^1 = \begin{pmatrix} 0 & 1 \\ 1 & 0 \end{pmatrix}, \quad \sigma^2 = \begin{pmatrix} 0 & -i \\ i & 0 \end{pmatrix}, \quad \sigma^3 = \begin{pmatrix} 1 & 0 \\ 0 & -1 \end{pmatrix}.$$

The $SU(2)_L \times U(1)_Y$ Lagrangian obtained in analogy to Sec. 1.1 reads

$$\begin{aligned}\mathcal{L}_{EW} = & \bar{\psi}_L (i\cancel{\partial} - \frac{g}{2} \sigma^i W^i - \frac{g'}{2} Y \cancel{B}) \psi_L + \bar{\psi}_R (i\cancel{\partial} - \frac{g'}{2} Y \cancel{B}) \psi_R \\ & - \frac{1}{4} W_{\mu\nu}^i W_i^{\mu\nu} - \frac{1}{4} B_{\mu\nu} B^{\mu\nu},\end{aligned}\tag{1.3}$$

where, B_μ , W_μ^i are the vector bosons associated with $U(1)_Y$, $SU(2)_L$, and their kinetic terms are given as $B_{\mu\nu} = \partial_\mu B_\nu - \partial_\nu B_\mu$, $W_{\mu\nu}^i = \partial_\mu W_\nu^i - \partial_\nu W_\mu^i - gf^{ijk}W_\mu^jW_\nu^k$, g and g' are the coupling strengths under $SU(2)_L$ and $U(1)_Y$ respectively. As mentioned earlier, the left-handed fermion fields are doublets under $SU(2)_L$, while the right handed ones are singlets. On the other hand, all the SM fermions are charged under $U(1)_Y$. This charge is called the electroweak (EW) hypercharge, represented as Y . The $U(1)_{em}$ is the remnant symmetry after the breaking of electroweak symmetry $SU(2)_L \times U(1)_Y$ and the hypercharge (Y) is related to the EM charge (Q) and the third component of the electroweak isospin (T_3) as, $Y/2 = Q - T_3$.

1.3.1 Neutrinos in the Standard Model

In this section, we will discuss the interaction of neutrinos with other SM particles within the SM framework. As mentioned earlier, in the Standard Model neutrinos interact only *via* weak interaction. Leptons and quarks are $SU(2)_L$ doublets which can be represented as

$$\psi_L^{\ell T} = (\nu_{lL}, l_L), \quad \psi_L^{qT} = (U_L, D_L),$$

where, l , U , D represents leptons, up and down quarks respectively and $l = \{e, \mu, \tau\}$, $U = \{u, c, t\}$, $D = \{d, s, b\}$, as given in table 1.1. Thus the Lagrangian obtained after assigning appropriate hypercharges to the doublet fields from eq. (1.3) is given as

$$\begin{aligned} \mathcal{L}_f = & -\frac{1}{2}\bar{\psi}_L^\ell(g\sigma^iW^i - g'\not{B})\psi_L^\ell - \frac{1}{2}\bar{\psi}_L^q(g\sigma^iW^i + \frac{1}{3}g'\not{B})\psi_L^q \\ & + g'\bar{l}_R\not{B}l_R - \frac{2}{3}g'\bar{U}_R\not{B}U_R + \frac{1}{3}g'\bar{D}_R\not{B}D_R. \end{aligned}$$

Considering only the leptonic part of the Lagrangian one obtains

$$\mathcal{L}_\ell = -\frac{1}{2} \begin{pmatrix} \bar{\nu}_{lL} & \bar{l}_L \end{pmatrix} \begin{pmatrix} gW^3 - g'\not{B} & g(W^1 - iW^2) \\ g(W^1 + iW^2) & -gW^3 - g'\not{B} \end{pmatrix} \begin{pmatrix} \nu_{lL} \\ l_L \end{pmatrix} + g'\bar{l}_R\not{B}l_R.$$

The diagonal part of the Lagrangian defines the neutral current (NC) interaction, whereas off-diagonal parts lead to charged current (CC) interaction. Taking the CC interaction and defining $W_\mu^+ = (W_\mu^1 - iW_\mu^2)/\sqrt{2}$ and $W_\mu^- = (W_\mu^1 + iW_\mu^2)/\sqrt{2}$, the CC Lagrangian is given as

$$\mathcal{L}_{CC} = -\frac{g}{\sqrt{2}}\bar{\nu}_{lL}W^+l_L + \text{h.c.} \quad (1.4)$$

On the other hand, NC interaction can be explicitly expressed as

$$\mathcal{L}_{NC} = -\frac{1}{2}\bar{\nu}_{lL}(gW^3 - g'\not{B})\nu_{lL} + \frac{1}{2}\bar{l}_L(gW^3 + g'\not{B})l_L + g'\bar{l}_R\not{B}l_R. \quad (1.5)$$

The QED Lagrangian is a part of the EW Lagrangian, therefore the photon field A_μ and Z_μ are obtained by appropriately rotating the fields W_μ^3 and B_μ by the Weinberg angle θ_W [6]

$$\begin{aligned} A_\mu &= \sin\theta_W W_\mu^3 + \cos\theta_W B_\mu, \\ Z_\mu &= \cos\theta_W W_\mu^3 - \sin\theta_W B_\mu. \end{aligned} \quad (1.6)$$

Putting eq. (1.6) into the Lagrangian in eq. (1.5), one obtains

$$\begin{aligned} \mathcal{L}_{NC} = -\frac{1}{2} & \left[\bar{\nu}_{lL} \left\{ (g \cos\theta_W + g' \sin\theta_W)\not{Z} - (g' \cos\theta_W - g \sin\theta_W)\not{A} \right\} \nu_{lL} \right. \\ & - \bar{l}_L \left\{ (g \cos\theta_W - g' \sin\theta_W)\not{Z} + (g' \cos\theta_W + g \sin\theta_W)\not{A} \right\} l_L \\ & \left. - 2g'\bar{l}_R(-\sin\theta_W\not{Z} + \cos\theta_W\not{A})l_R \right]. \end{aligned} \quad (1.7)$$

As neutrinos do not interact with photons, from the above equation $g' \cos\theta_W = g \sin\theta_W$, which implies $\tan\theta_W = g'/g$. Also, as electron has the electric charge e , $g' \cos\theta_W = g \sin\theta_W = e$. Hence, the NC Lagrangian can be written as

$$\begin{aligned} \mathcal{L}_{NC} = -\frac{g}{2 \cos\theta_W} & \left\{ \bar{\nu}_{lL}\not{Z}\nu_{lL} - (1 - 2 \sin^2\theta_W)\bar{l}_L\not{Z}l_L + 2 \sin^2\theta_W\bar{l}_R\not{Z}l_R \right\} \\ & + g \sin\theta_W\bar{l}l. \end{aligned} \quad (1.8)$$

Coming to the quark coupling with the electroweak vector boson, the Lagrangian can be written as

$$\mathcal{L}_q = -\frac{1}{2} \begin{pmatrix} \bar{U}_L & \bar{D}_L \end{pmatrix} \begin{pmatrix} gW^3 + g'\not{B}/3 & g(W^1 - iW^2) \\ g(W^1 + iW^2) & -gW^3 + g'\not{B}/3 \end{pmatrix} \begin{pmatrix} U_L \\ D_L \end{pmatrix} \\ - \frac{2g'}{3} \bar{U}_R \not{B} U_R + \frac{g'}{3} \bar{D}_R \not{B} D_R.$$

And the charged current and neutral current parts are given as

$$\mathcal{L}_{CC}^q = -\frac{g}{\sqrt{2}} \bar{U}_L W^+ D_L + \text{h.c.}, \\ \mathcal{L}_{NC}^q = -g \sin \theta_W \left(\frac{2}{3} \bar{U} \gamma^\mu U - \frac{1}{3} \bar{D} \gamma^\mu D \right) A_\mu - \frac{g}{2 \cos \theta_W} \left[\bar{U} \gamma^\mu (g_V^u - g_A^u \gamma^5) U \right. \\ \left. + \bar{D} \gamma^\mu (g_V^d - g_A^d \gamma^5) D \right] Z_\mu, \quad (1.9)$$

where, $U = U_L + U_R$, $D = D_L + D_R$, $g_V^u = \frac{1}{2} - \frac{4}{3} \sin^2 \theta_W$, $g_V^d = -\frac{1}{2} + \frac{2}{3} \sin^2 \theta_W$, $g_A^u = \frac{1}{2}$ and $g_A^d = -\frac{1}{2}$. The total number of light neutrino flavours was first determined at LEP by the NC interaction of the neutrinos. In the LEP experiment, the invisible decay of Z boson is very precisely measured. The total invisible decay width of Z boson (Γ_{inv}), when compared with the expected decay width to a single ν flavour ($\Gamma_{Z \rightarrow \nu\nu}$), the number of neutrino flavours were obtained [7]

$$N_\nu = \frac{\Gamma_{inv}}{\Gamma_{Z \rightarrow \nu\nu}} = 2.984 \pm 0.008.$$

Also, for the SM, the CC and NC interactions lead to the conservation of lepton numbers. There are three lepton numbers L_e, L_μ and L_τ . The first, second, and third generation of the lepton doublets are charged under L_e, L_μ and L_τ , respectively. The particles and antiparticles have a lepton number of +1 and -1, respectively. The conservation of lepton numbers is an accidental symmetry of the SM.

1.3.2 Neutrino-Nucleon interaction

As can be seen from eq. (1.5), (1.7) and (1.9), in the SM, neutrinos interact with charged leptons and quarks *via* W and Z exchange. At lower energy, neutrino undergoes quasielastic charged current interaction or elastic neutral current interaction, and under both the neutrino interacts with the nucleon as a whole. Whereas, at energy higher than a few GeV, neutrinos undergo a deep inelastic scattering (DIS), where it interacts with the constituent of the nucleon, *i.e.*, (anti)quarks, called partons. At energies less than a few GeV neutrino interacts with the nucleon as:

$$\begin{aligned}\nu_l + n &\rightarrow p + l^-, \\ \bar{\nu}_l + p &\rightarrow n + l^+.\end{aligned}$$

For $l = e$, the former of above interactions is referred to as inverse beta decay and ν_e were first detected *via* this process by Cowan and Reines [1]. Out of the three flavours, ν_e and ν_μ are produced in the laboratory experiments *via* beta decays and pion decay respectively. However, ν_τ are produced by leptonic decay of the charmed meson D_s .

Charged Current DIS: Neutrino-nucleon interaction above a few GeV undergoes a Deep Inelastic Scattering (DIS) given as

$$\begin{aligned}\nu_l + N &\rightarrow l^- + X, \\ \bar{\nu}_l + N &\rightarrow l^+ + X,\end{aligned}$$

where, X denotes hadrons and $N = n, p$. In the case of DIS as the energy of neutrino, E , is much higher than mass of the nucleon, m_N , the leptons, hadrons and partons are essentially massless. Let p_ν , p_N , p_q , p_l , and p_X be the four momenta of incoming ν_l , N , parton, outgoing lepton and hadron respectively, and $q = p_\nu - p_l$, *i.e.*, momentum transferred to parton.

The momentum of hadron can be written as $p_X = p_q + q$ and since

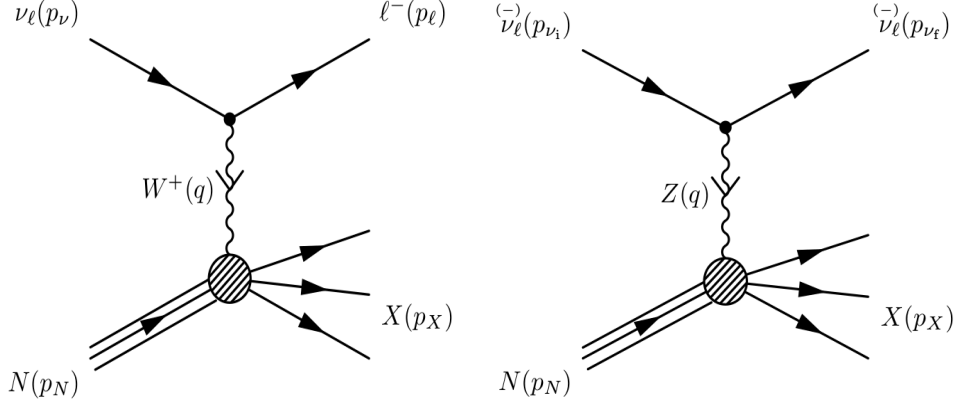


Figure 1.2. Feynman diagram for neutrino-nucleon interaction. (Figure courtesy: Ref. [8].)

the mass of hadrons is negligible

$$\begin{aligned}
 (p_q + q)^2 &= 0, \\
 \implies p_q^2 + 2p_q \cdot q + q^2 &= 0, \\
 \implies 2p_q \cdot q - Q^2 &= 0, \\
 \implies 2xp_N \cdot q &= Q^2, \\
 \implies x &= \frac{Q^2}{2p_N \cdot q}, \tag{1.10}
 \end{aligned}$$

where $Q^2 = -q^2$. Clearly, from eq. (1.10) it can be seen that x is the fraction of momentum transferred to the parton out of that of the nucleon.

Also, defining another variable

$$y = \frac{p_N \cdot q}{p_N \cdot p_\nu},$$

which in the lab frame simplifies to $y = \frac{q^0}{p_\nu^0} = \frac{q^0}{E}$. Here, $1 - y$ denotes the fraction of energy transferred to the lepton. For DIS the Mandelstam variables are

$$\begin{aligned}
 \hat{s} &= (p_\nu + p_q)^2 = 2p_\nu \cdot p_q = 2xp_\nu \cdot p_N = xs, \\
 \hat{t} &= q^2 = -Q^2 = -2xp_N \cdot q = -2xyp_N \cdot p_\nu = -2xym_N E, \\
 \hat{u} &= -\hat{s} - \hat{t} = -(1 - y)xs,
 \end{aligned}$$

where \hat{s} , \hat{t} , \hat{u} are the Mandelstam variables for partons and $s = 2m_N E$.

As can be seen from the above equations, all the Mandelstam variables for DIS depend on two variables namely the fraction of energy transferred to the produced lepton, $y = 1 - E_l/E$, and the fraction of energy transferred to the parton, $x = Q^2/(2m_N E y)$. y , x and E_l are the inelasticity, Bjorken scaling parameter [9] and outgoing lepton energy respectively. As mentioned earlier, the nucleons are composed of partons and hence the cross-section of this interaction depends on the probability of finding a certain quark in the nucleon given by the parton distribution function (PDF), $f_i(x, Q^2)$. The double-differential neutrino-nucleon DIS cross-section of CC interaction is given as [10, 11]

$$\frac{d^2 \sigma_{\nu N}}{dx dy} = \frac{2G_F^2 m_N E x}{\pi} \frac{M_W^4}{(M_W^2 + Q^2)^2} \left(f_q(x, Q^2) + (1-y)^2 f_{\bar{q}}(x, Q^2) \right). \quad (1.11)$$

For isoscalar targets such as ice, the number of protons is equal to neutrons, and their average is taken into account, *i.e.*, $N = (n + p)/2$. Here, $f_{q,\bar{q}}(x, Q^2)$ are certain combinations of parton distribution function (PDF) of the quarks and antiquarks

$$f_q = \frac{(f_u + f_d)}{2} + f_s + f_b, \quad f_{\bar{q}} = \frac{(f_{\bar{u}} + f_{\bar{d}})}{2} + f_c + f_t,$$

where, $f_{i(\bar{i})}$ are the individual PDFs for the quarks and antiquarks, with $i = u, d, c, s, t, b$.

In order to evaluate $\sigma_{\nu N}$ for neutrino energy E , the PDFs are required to be known in the x -range $\{x_{min}, 1\}$ with, $x_{min} \sim Q^2/(2m_N E) \sim M_W^2/(2m_N E)$. Thus for the calculation of neutrino-nucleon cross-section for astrophysical neutrinos of energy up to PeV, PDFs for $x \gtrsim 10^{-4}$ are required. These are known from ep collisions at HERA [12, 13] for $x \gtrsim 2 \times 10^{-5}$. Also, LHCb significantly reduces the uncertainties in PDF for such small values of x [14–16]. The differential cross-sections for antineutrinos are obtained by replacing f_q by $f_{\bar{q}}$ and vice-versa. The cross-section obtained after folding the eq. (1.11) with the CT10 PDF, increases

with energy [10] as depicted in fig. 1.3.

Neutral Current DIS: Neutrino-nucleon interaction by the exchange of a Z boson is Neutral Current (NC) interaction

$$\nu_l N \rightarrow \nu_l X.$$

The cross-section for NC DIS is given as

$$\frac{d^2\sigma_{\nu N}}{dxdy} = \frac{2G_F^2 m_N E x}{\pi} \frac{M_Z^4}{(M_Z^2 + Q^2)^2} \left(f_q(x, Q^2) + (1-y)^2 f_{\bar{q}}(x, Q^2) \right),$$

Here, as well, $f_{q,\bar{q}}(x, Q^2)$ are combinations of parton distribution function (PDF) of the quarks and antiquarks:

$$\begin{aligned} f_q &= \frac{(f_u + f_d)}{2} (L_u^2 + L_d^2) + \frac{(f_{\bar{u}} + f_{\bar{d}})}{2} (R_u^2 + R_d^2) \\ &\quad + (f_s + f_b)(R_d^2 + L_d^2) + (f_c + f_t)(R_u^2 + L_u^2), \\ f_{\bar{q}} &= \frac{(f_u + f_d)}{2} (R_u^2 + R_d^2) + \frac{(f_{\bar{u}} + f_{\bar{d}})}{2} (L_u^2 + L_d^2) \\ &\quad + (f_s + f_b)(R_d^2 + L_d^2) + (f_c + f_t)(L_u^2 + R_u^2), \end{aligned}$$

with,

$$\begin{aligned} L_u &= 1 - 4/3 \sin^2 \theta_W, & L_d &= -1 + 2/3 \sin^2 \theta_W, \\ R_u &= -4/3 \sin^2 \theta_W, & R_d &= 2/3 \sin^2 \theta_W. \end{aligned}$$

Glashow Resonance: The neutrino-electron interaction which is a t -channel process, leads to a very small cross-section as compared to the neutrino-nucleon interaction. However, electron antineutrino-electron interaction can happen *via* s -channel, $\bar{\nu}_e e^- \rightarrow W^{-(*)} \rightarrow hadron$, at resonance, *i.e.*, $\sqrt{2Em_e} = M_W$. The differential cross-section of the above process at resonance is given as

$$\begin{aligned} \frac{d}{dy} \sigma(\bar{\nu}_e e \rightarrow hadrons) &= \frac{d}{dy} \sigma(\bar{\nu}_e e \rightarrow \bar{\nu}_\mu \mu) \times \frac{\Gamma(W \rightarrow hadrons)}{\Gamma(W \rightarrow \bar{\nu}_\mu \mu)}, \\ &= 6.7 \times \frac{2G_F^2 m_e E}{\pi} \frac{M_W^2}{\Gamma_W^2} (1-y)^2. \end{aligned}$$

Here, m_e , M_W , Γ_W , and $\Gamma(W \rightarrow X)$ are electron mass, W boson mass, total decay width and partial decay width of W boson respectively. The resonance happens at neutrino energy around 6.3 PeV and is popularly called Glashow resonance after the name of the physicist who proposed it [17]. At $E = 6.3$ PeV, the cross-section comes out to be around 3.41×10^{-31} cm², which is around 240 times greater than neutrino-nucleon CC interaction [17–20], as shown in fig. 1.3. The effect of the Glashow resonance is decided by the full width at half maximum (FWHM) of the cross-section, *i.e.*, for energy range from $(M_W - 2\Gamma_W)^2/(2m_e) = 5.7$ PeV to $(M_W + 2\Gamma_W)^2/(2m_e) = 7$ PeV. The observed signals from such events are hadronic showers, which are expected to show up as excess in the number of events at IceCube around the above energy range.

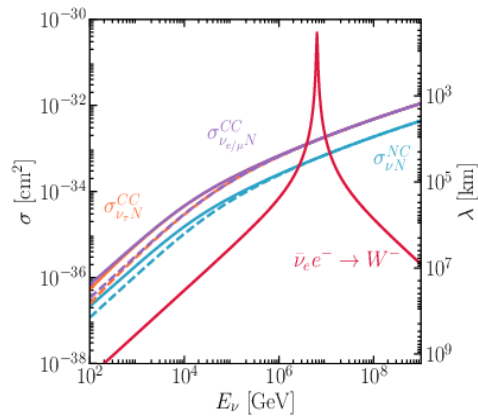


Figure 1.3. Cross-section of (anti)neutrino-nucleon interaction. Here the solid and dashed lines denote DIS for neutrino and antineutrino respectively. (Figure courtesy: Ref. [21].)

1.4 Higgs Mechanism

All the particles in the SM get their mass *via* the Higgs mechanism [22–25].

Higgs is a doublet under SM and is given as

$$\phi(x) = \begin{pmatrix} \phi^+(x) \\ \phi^0(x) \end{pmatrix},$$

where, $\phi^+(x)$, and $\phi^0(x)$ are charged and neutral complex scalars respectively. Under $SU(2)_L \times U(1)_Y$ transformation, the invariant Lagrangian governing the Higgs interaction is

$$\begin{aligned}\mathcal{L}_H &= (D^\mu \phi)^\dagger (D_\mu \phi) - \mu^2 \phi^\dagger \phi - \lambda (\phi^\dagger \phi)^2 + \mathcal{L}_{\ell\ell H} + \mathcal{L}_{qqH}, \\ \mathcal{L}_{\ell\ell H} &= Y_\ell \bar{\psi}_L^\ell \phi l_R + \text{h.c.}, \quad \mathcal{L}_{qqH} = Y_d \bar{\psi}_L^q \phi D_R + Y_u \bar{\psi}_L^q \tilde{\phi} U_R + \text{h.c.},\end{aligned}$$

where, $D_\mu = (\partial_\mu + i\frac{g}{2}\sigma^i W_\mu^i + i\frac{g'}{2}Y B_\mu)$, $\tilde{\phi} = i\sigma^2 \phi^*$ and Y_ℓ, Y_u, Y_d are the Yukawa couplings for leptons, U and D quarks respectively. As can be seen from the above equation the Higgs potential is $V(\phi) = \mu^2 \phi^\dagger \phi + \lambda (\phi^\dagger \phi)^2$ and if $\mu^2 < 0$, for a positive value of λ there exist a minima in the potential at $\phi^\dagger \phi = \mu^2/(2\lambda)$. This makes it possible to realise spontaneous symmetry breaking: $SU(2)_L \times U(1)_Y \rightarrow U(1)_{em}$. The minimum of the field corresponds to its vacuum and as Higgs attains its vacuum expectation value (vev), $v = \sqrt{\mu^2/(2\lambda)}$, the doublet can be written as

$$\phi(x) = \frac{1}{\sqrt{2}} e^{i\frac{\chi^i(x)\sigma^i}{2v}} \begin{pmatrix} 0 \\ v + H(x) \end{pmatrix},$$

where, $H(x)$ is the physical scalar and scalars $\chi^{1,2,3}$ can be set to zero by gauge fixing. This particular choice of gauge is called unitary gauge and under it the doublet can be written as,

$$\phi(x) = \frac{1}{\sqrt{2}} \begin{pmatrix} 0 \\ v + H(x) \end{pmatrix}.$$

The Yukawa term for leptons, after Higgs attains the vev, reads

$$\mathcal{L}_{\ell\ell H} = -Y_\ell \frac{v + H}{\sqrt{2}} \bar{l}_L l_R + \text{h.c.}$$

From the above equation, it can be inferred that the Lagrangian is not invariant under $SU(2)_L \times U(1)_Y$, but conserves only the EM charge. The mass of the fermions, $m_l = Y_\ell v/\sqrt{2}$, is a parameter of the SM and is measured experimentally. Therefore, though the SM gives a mechanism

by which fermions attain their mass, it fails to explain the hierarchy in the fermion mass spectrum. Hence, it is believed that the SM is a low energy effective theory of a more elaborate theory which operates at higher energy scales. The incompleteness of the SM can be realised by the fact that neutrinos, as they come with only as left-handed fields, do not find any explanation of their masses in the SM framework. These observations along with others, *e.g.*, the existence of dark matter (DM), dark energy (DE), baryon asymmetry, *etc.*, exemplify the pressing need for new physics in order to address the shortcomings of the SM.

1.5 Neutrino Mass

The evidence of neutrino mass came from the observations of atmospheric and solar neutrinos. Atmospheric neutrinos are of energy \sim GeV produced in the Earth atmosphere, whereas solar neutrinos have energy around MeV and are produced in the interiors of the Sun. The observations of atmospheric and solar neutrinos are as follows:

Atmospheric Neutrinos: The cosmic rays interact with nucleon in the atmosphere, and this leads to the production of π and K , which in turn decay to produce neutrinos, in the ratio $\nu_e : \nu_\mu = 1 : 2$. But on observation of atmospheric neutrinos at SuperKamiokande (SK) [26], it was found that:

- Low energy, *i.e.*, sub-GeV upgoing ν_μ events were always less than expected. Here, the upgoing events were the neutrinos that cross the Earth to reach the detector, *i.e.*, zenith angle $> \pi/2$, whereas, the downgoing events are the neutrinos that reach the detector from directly above without crossing the Earth matter, *i.e.*, zenith angle $< \pi/2$. It was seen that the depletion of downgoing ν_μ was less than that of upgoing ones. This is because the upgoing events travel a longer distance than the downgoing neutrinos which reach the detector from above.
- The number of multi-GeV upgoing ν_μ events were less than what was expected. On the other hand, the number of downgoing multi-GeV ν_μ events almost agree with the expected flux.

- The observed flux of ν_e matched the expected flux.

From the above observations, it was inferred that ν_μ were getting converted to ν_τ with the probability $\propto L/E$, where L is the length traversed by neutrinos and E is neutrino energy. It was seen at SK that the conversion of one flavour of neutrinos to another has an oscillatory nature and was explained *via* neutrino oscillation and, as discussed in the next section, the probability of conversion neutrino flavour, from ν_μ to ν_τ is given by,

$$P_{\mu\tau} = \sin^2 2\theta_{23} \sin^2 \left(\frac{\Delta m_{32}^2 L}{4E} \right), \quad (1.12)$$

where $\Delta m_{32}^2 = m_3^2 - m_2^2$, the mass square difference of two neutrino mass states, and θ_{23} is the mixing angle which corresponds to the mixing between the two flavours under consideration. K2K, an accelerator based experiment in Japan, produced \sim GeV neutrinos, was among the first experiments to confirm neutrino oscillation as the solution of atmospheric neutrino problem with $\Delta m_{32}^2 = (1.5 - 3.5) \times 10^{-3} \text{ eV}^2$, $\sin^2 2\theta_{23} > 0.92$ [27].

Solar Neutrinos: Sun produces ν_e *via* nuclear fission and these neutrinos are detected by CC interaction, through the process ${}^{71}\text{Ga} + \nu_e \rightarrow {}^{71}\text{Ge} + e^-$ on earth. Similar to the atmospheric neutrino problem the solar neutrino problem is nothing but the disappearance of ν_e as detected at earth. KamioKande detected ν_e *via* elastic scattering of $\nu_e e^- \rightarrow \nu_e e^-$ and the observations revealed that the flux of ν_e is deficient by a factor of ~ 2 , which was later confirmed by SuperKamiokande [28]. SNO [29] which relied on heavy water for detection, observed all the three flavours of neutrinos *via*: a) $\nu_e e^- \rightarrow \nu_e e^-$, b) $\nu_e \text{D} \rightarrow \nu_e \text{pp}$, c) $\nu_\ell \text{D} \rightarrow \nu_\ell \text{D}$. The detection of ν_τ and ν_μ illustrated that ν_e is oscillating to ν_μ and ν_τ . The KamLand experiment in Japan, which produced \sim MeV neutrinos, confirmed neutrino oscillations with values of $\Delta m_{21}^2 = (7.2 - 9.5) \times 10^{-5} \text{ eV}^2$, $\sin^2 2\theta_{12} = 0.21 - 0.37$ at 3σ CL [30], as the solution of solar neutrino problem. Thus, there are two mass square differences for three neutrinos. This allows for the arranging of masses of neutrinos in two ways: a) Normal Hierarchy ($m_1 < m_2 < m_3$) b) Inverted Hierarchy ($m_3 < m_1 < m_2$), where

m_i stands for neutrino mass.

Dirac and Majorana Neutrino Mass: As neutrinos do not carry EM charge they can have Dirac and/or Majorana mass. Majorana mass can be described by only one Weyl spinor and their conjugate can be related as $\psi^c = -\eta_c^* C \bar{\psi}^T$, where η_c is phase and in Dirac basis, $C = i\gamma^2\gamma^0$ [31]. Majorana neutrino is its own antiparticle and is given as, $\nu^M = \nu_L + \nu_L^c$ and the mass term is written as $\mathcal{L}_M = -m_M \bar{\nu}_L \nu_L^c + \text{h.c.}$ The Majorana mass term can be generated by the dim-5 Weinberg operator [32] using the SM fields given as

$$\mathcal{L}_M = \frac{c}{\Lambda} (\psi_L^{\ell T} C \tilde{\phi}) (\tilde{\phi}^T \psi_L^\ell).$$

As Higgs gets vev this term reduces to $\mathcal{L}_M = cv^2 \bar{\nu}_L \nu_L^c / (2\Lambda)$. As $\Sigma m_i \leq 0.2$ eV [33], which implies $cv^2/\Lambda \lesssim 0.2$ eV, leading to $\Lambda/c \gtrsim 1.6 \times 10^{14}$ GeV, which demarcates the energy scale of new physics required to explain neutrino mass. In the SM, lepton number is an accidental symmetry but in BSM theories, such as this, it is not conserved.

Dirac mass can be generated similar to other SM fermions, though it requires the addition of extra particle ν_R to the SM. ν_R are singlet under the SM and the mass term of the Lagrangian reads,

$$\mathcal{L}_D = Y_\nu \bar{\psi}_L^\ell \tilde{\phi} \nu_R + \text{h.c.}$$

After symmetry breaking the above Lagrangian reduces to $\mathcal{L}_D = Y_\nu v \bar{\nu}_L \nu_R / \sqrt{2} + \text{h.c.}$ Since $\Sigma m_i \leq 0.2$ eV, $Y_\nu v \lesssim 0.2$ eV and $Y_\nu \lesssim 7.8 \times 10^{-13}$. This Yukawa coupling is several orders of magnitude lower than that of SM fermions; hence they are considered unnatural [34]. The lepton number conservation holds good in the case of Dirac mass.

1.6 Neutrino Oscillations in Vacuum

Neutrinos are produced and detected in the flavour basis, *i.e.*, ν_α , where $\alpha = e, \mu, \tau$, but they propagate in another basis which is called the mass basis. The mass basis is generally denoted by ν_i , where $i = 1, 2, 3$ and each

ν_α can be expressed as the superposition of ν_i . The neutrino states in the two basis are related by a unitary transformation, given as:

$$\nu_\alpha = U \nu_i, \quad (1.13)$$

where, U is the mixing matrix, referred to as PMNS matrix [35, 36]. Neutrino oscillations in vacuum are quite different from that of matter. In this section we discuss the neutrino oscillations in vacuum. The neutrino propagation in mass basis can be expressed by the Schrödinger equation:

$$\frac{i\partial\nu_i(t)}{\partial t} = H\nu_i(t). \quad (1.14)$$

In mass basis, the Hamiltonian H is diagonal. For two neutrino flavours, H and U are expressed as:

$$H = \begin{pmatrix} E_1 & 0 \\ 0 & E_2 \end{pmatrix}, \quad U = \begin{pmatrix} \cos\theta & \sin\theta \\ -\sin\theta & \cos\theta \end{pmatrix}, \quad (1.15)$$

where, θ is the mixing angle and E_i are the eigenvalues of H . From eq. (1.14) and (1.15), the neutrino state at time t can be given as,

$$\frac{i\partial\nu_i(t)}{\partial t} = E_i\nu_i(t) \implies \nu_i(t) = \exp(-iE_it) \nu_i(0).$$

As H is diagonal in mass basis, the amplitude of transition from one mass state to another is 0. Hence, the amplitude for two states can be expressed as a 2×2 matrix, given as $\tilde{S}(0, t) = \text{diag}(\exp(-iE_1t), \exp(-iE_2t))$. The square of (i, j) elements of $\tilde{S}(0, t)$ gives the probability of transition from i mass state to j . Thus, the neutrino states at time t , in flavour basis is given as,

$$\begin{aligned} \nu_\alpha(t) &= U_{\alpha i} \exp(-iE_it) \nu_i(0), \\ &= U_{\alpha i} \exp(-iE_it) U_{i\beta}^\dagger \nu_\beta(0), \\ &= U_{\alpha i} \exp(-iE_it) U_{\beta i}^* \nu_\beta(0). \end{aligned} \quad (1.16)$$

Here, the amplitudes of transition are denoted by the elements of $(S_f)_{\alpha\beta} = U_{\alpha i}^* \exp(-iE_i t) U_{\beta i}$. Also, for three flavours, the mixing matrix is given as:

$$U = \begin{pmatrix} 1 & 0 & 0 \\ 0 & \cos \theta_{23} & \sin \theta_{23} \\ 0 & -\sin \theta_{23} & \cos \theta_{23} \end{pmatrix} \begin{pmatrix} \cos \theta_{13} & 0 & \sin \theta_{13} e^{-i\delta_{CP}} \\ 0 & 1 & 0 \\ -\sin \theta_{13} e^{i\delta_{CP}} & 0 & \cos \theta_{13} \end{pmatrix} \\ \times \begin{pmatrix} \cos \theta_{12} & \sin \theta_{12} & 0 \\ -\sin \theta_{12} & \cos \theta_{12} & 0 \\ 0 & 0 & 1 \end{pmatrix},$$

where, θ_{ij} and δ_{CP} are the mixing angles and CP violating Dirac phase respectively. In vacuum: $31.61^\circ \leq \theta_{12} \leq 36.27^\circ$, $41.1^\circ \leq \theta_{23} \leq 51.3^\circ$, $8.22^\circ \leq \theta_{13} \leq 8.98^\circ$ and $0.8\pi \leq \delta_{CP} \leq 1.98\pi$, with their best fit values given as: $\theta_{12} = 33.82^\circ$, $\theta_{23} = 48.60^\circ$, $\theta_{13} = 8.60^\circ$ and $\delta_{CP} = 1.22\pi$ [37]. The probability of conversion from flavour β to α is obtained *via* square of the amplitude, *i.e.*,

$$P_{\beta\alpha} = |(S_f)_{\alpha\beta}|^2 = |U_{\alpha i}^* \exp(-iE_i t) U_{\beta i}|^2 = U_{\alpha i}^* U_{\beta i} U_{\beta k}^* U_{\alpha k} \exp(-i(E_i - E_k)t). \quad (1.17)$$

Since neutrino mass is rather small, $\Sigma m_i \leq 0.2$ eV [33], $E_k = \sqrt{p^2 + m_k^2} \sim E + m_k^2/(2E)$, where E is the energy of each mass state, and is much greater than the mass of the neutrinos. Therefore, the difference of energy of the two neutrinos, in the eq. (1.17), can be written as $E_k - E_i = \Delta m_{ki}^2/(2E)$, where $\Delta m_{ki}^2 = m_k^2 - m_i^2$. Hence, the probability of flavour conversion reads

$$P_{\beta\alpha} = U_{\alpha i}^* U_{\beta i} U_{\beta k}^* U_{\alpha k} \exp(-i\Delta m_{ki}^2 t/(2E)), \\ = \sum_{i=k} |U_{\alpha i}^*|^2 |U_{\beta k}|^2 + \sum_{i \neq k} U_{\alpha i}^* U_{\alpha k} U_{\beta i} U_{\beta k}^* \exp(-i\Delta m_{ki}^2 t/(2E)), \\ = |U_{\alpha i}|^2 |U_{\beta i}|^2 + \sum_{i>k} 2\text{Re} \left[U_{\alpha i}^* U_{\alpha k} U_{\beta i} U_{\beta k}^* \cos(\Delta m_{ki}^2 t/(2E)) \right].$$

As one can infer from the above equation, the mass square difference leads to the probability of flavour conversion with time t . Hence, $P_{\beta\alpha}$ is referred to as oscillation probability, and the phenomenon of this oscillatory flavour

conversion is called neutrino oscillation. As mentioned earlier, there are compelling evidences that neutrinos are massive particles. If the time of propagation T is much greater than the oscillation time period $T_{osc} = 2E/\Delta m_{ki}^2$, then the time dependence of the probability gets averaged out, *i.e.*,

$$\langle \cos(t/T_{osc}) \rangle = \lim_{T \rightarrow \infty} \frac{\int_0^T dt \cos(t/T_{osc})}{\int_0^T dt} = \lim_{T \rightarrow \infty} \frac{\sin(T/T_{osc})}{T/T_{osc}} = 0.$$

Thus, the information of the length and mass square difference is lost. This is the case with the high energy astrophysical neutrinos that travel cosmological distances from their source to the Earth. Thus the probability of the oscillation reads,

$$P_{\beta\alpha} = |U_{\beta i}|^2 |U_{\alpha i}|^2. \quad (1.18)$$

As it will be discussed in the next chapter, astrophysical high energy neutrinos are produced *via* pp and $p\gamma$ interactions at source, leading to the production of charged pions (π^+ , π^-). Each charged pion decays to give 2 muon (anti)neutrinos and 1 electron neutrino and no tau neutrinos; hence the flavour ratio at the source $f_\alpha^S = (1 : 2 : 0)$. These neutrinos escape from the source, but as the length of propagation, $\mathcal{O}(1)$ Gpc, is much larger than oscillation length, $2E/\Delta m_{21}^2 \lesssim 10^{-3}$ pc for $E \lesssim 1$ PeV, they get averaged out. In standard scenario, where there is no interaction during production and detection, the flavour ratio of neutrinos at the detector is given as

$$f_\alpha^D = P_{\alpha\beta} f_\beta^S = |U_{ei}|^2 (|U_{ei}|^2 + 2|U_{\mu i}|^2).$$

As $|U_{\mu i}|^2 \sim |U_{\tau i}|^2$ for vacuum oscillations and $|U_{ei}|^2 + |U_{\mu i}|^2 + |U_{\tau i}|^2 = 1$, $|U_{e1}|^2 + |U_{e2}|^2 + |U_{e3}|^2 = 1$ for unitary matrix, the flavour ratio at the detector $\simeq (1 : 1 : 1)$. This equality is exact in the case when $\theta_{13} = 0$. However, in the presence of interacting matter/ dark matter of significant density, there can be deviation from the standard scenario in the detected flavour ratio.

1.7 Neutrino Oscillations in Matter

In constant matter density, the mixing matrix in matter (U_M) is constant and eq. (1.17) faithfully expresses the probability of flavour conversion with a simple substitution of $U \rightarrow U_M$. On the other hand, in the presence of varying matter density, the mixing matrix varies during neutrino propagation [38]. The evolution of state for constant or slowly changing matter density, from eq. (1.14), reads

$$\frac{i\partial}{\partial t} \begin{pmatrix} \nu_e \\ \nu_\mu \end{pmatrix} = \frac{1}{2E} U_M \begin{pmatrix} M_1^2 & 0 \\ 0 & M_2^2 \end{pmatrix} U_M^\dagger \begin{pmatrix} \nu_e \\ \nu_\mu \end{pmatrix},$$

where $M_1^2/(2E)$ and $M_2^2/(2E)$ are the eigenvalues of an arbitrary Hamiltonian with matter effect. Hence, in the presence of matter density significantly varying with time, the equation of states in the mass basis is given as

$$\begin{aligned} \frac{i\partial}{\partial t} U_M \begin{pmatrix} \nu_1 \\ \nu_2 \end{pmatrix} &= \frac{1}{2E} U_M \begin{pmatrix} M_1^2 & 0 \\ 0 & M_2^2 \end{pmatrix} \begin{pmatrix} \nu_1 \\ \nu_2 \end{pmatrix}, \\ \Rightarrow \frac{i\partial}{\partial t} \begin{pmatrix} \nu_1 \\ \nu_2 \end{pmatrix} &= \left[\frac{1}{2E} \begin{pmatrix} M_1^2 & 0 \\ 0 & M_2^2 \end{pmatrix} - U_M^\dagger \frac{i\partial U_M}{\partial t} \right] \begin{pmatrix} \nu_1 \\ \nu_2 \end{pmatrix}, \\ \Rightarrow \frac{i\partial}{\partial t} \begin{pmatrix} \nu_1 \\ \nu_2 \end{pmatrix} &= \left[\frac{1}{2E} \begin{pmatrix} M_1^2 & 0 \\ 0 & M_2^2 \end{pmatrix} - i \begin{pmatrix} \cos \theta_m & -\sin \theta_m \\ \sin \theta_m & \cos \theta_m \end{pmatrix} \right. \\ &\quad \left. \times \begin{pmatrix} -\sin \theta_m \frac{d\theta_m}{dt} & \cos \theta_m \frac{d\theta_m}{dt} \\ -\cos \theta_m \frac{d\theta_m}{dt} & -\sin \theta_m \frac{d\theta_m}{dt} \end{pmatrix} \right] \begin{pmatrix} \nu_1 \\ \nu_2 \end{pmatrix}, \\ \Rightarrow \frac{i\partial}{\partial t} \begin{pmatrix} \nu_1 \\ \nu_2 \end{pmatrix} &= \begin{pmatrix} \frac{M_1^2}{2E} & \frac{-i\partial\theta_m}{\partial t} \\ \frac{i\partial\theta_m}{\partial t} & \frac{M_2^2}{2E} \end{pmatrix} \begin{pmatrix} \nu_1 \\ \nu_2 \end{pmatrix}, \end{aligned}$$

One can redefine the fields with a overall phase factor $\nu'_i = \exp[i(M_1^2 + M_2^2)t/(4E)] I_2 \nu_i$, where I_2 is the identity matrix. Thus on redefinition, the

evolution equation gets modified as

$$\begin{aligned} \frac{i\partial}{\partial t} \begin{pmatrix} \nu'_1 \\ \nu'_2 \end{pmatrix} + \frac{(M_1^2 + M_2^2)t}{4E} I_2 \begin{pmatrix} \nu'_1 \\ \nu'_2 \end{pmatrix} &= \begin{pmatrix} \frac{M_1^2 - i\partial\theta_m}{2E} \\ \frac{i\partial\theta_m}{\partial t} \frac{M_2^2}{2E} \end{pmatrix} \begin{pmatrix} \nu'_1 \\ \nu'_2 \end{pmatrix}, \\ \implies i\frac{\partial}{\partial t} \begin{pmatrix} \nu'_1 \\ \nu'_2 \end{pmatrix} &= \begin{pmatrix} \frac{-(M_2^2 - M_1^2)}{4E} & \frac{-i\partial\theta_m}{\partial t} \\ \frac{i\partial\theta_m}{\partial t} & \frac{(M_2^2 - M_1^2)}{4E} \end{pmatrix} \begin{pmatrix} \nu'_1 \\ \nu'_2 \end{pmatrix}. \end{aligned} \quad (1.19)$$

As can be followed from the above equation, if the magnitude of difference between the off-diagonal elements is much less than the diagonal elements of the mass matrix, then the neutrino remains in the original mass state during propagation. This is called adiabatic propagation of neutrinos. Whereas, if the off-diagonal elements are comparable to the diagonal elements, then the particle can jump from one mass state to another. This is called non-adiabatic propagation [39]. The measure of adiabaticity in propagation is evaluated by the ratio of the diagonal elements to that of the off-diagonal elements, also called the adiabaticity parameter. This can be expressed as:

$$\gamma = \frac{(M_1^2 - M_2^2)/4E}{\partial\theta_m/\partial t}. \quad (1.20)$$

The value of $\partial\theta_m/\partial t$ is related to the change in matter density.

Effective Potential in Matter: When neutrons propagate in matter, their evolution equation is influenced by the effective potentials due to coherent interactions with the medium *via* elastic CC and NC interactions. Using eq. (1.4), for low energy, the effective CC scattering the Hamiltonian corresponds to

$$H_{eff}(x) = \frac{G_F}{\sqrt{2}} [\bar{\nu}_e(x)\gamma^\rho(1 - \gamma^5)e(x)][\bar{e}(x)\gamma_\rho(1 - \gamma^5)\nu_e(x)].$$

Using Fierz transformation the above equation becomes

$$H_{eff}(x) = \frac{G_F}{\sqrt{2}} [\bar{\nu}_e(x)\gamma^\rho(1 - \gamma^5)\nu_e(x)][\bar{e}(x)\gamma_\rho(1 - \gamma^5)e(x)].$$

In order for the scattering to be coherent, the initial and final four-momentum and helicity of the electrons in the medium must be the same.

For a finite normalization volume V , the average of $H_{eff}(x)$ over the electron background is given as

$$\begin{aligned} \bar{H}_{eff} &= \frac{G_F}{\sqrt{2}} [\bar{\nu}_e(x) \gamma^\rho (1 - \gamma^5) \nu_e(x)] \int d^3 p_e f(E_e, T) \\ &\quad \times \frac{1}{2} \sum_{h_e = \pm 1} \langle e_{p_e, h_e} | [\bar{e}(x) \gamma_\rho (1 - \gamma^5) e(x)] | e_{p_e, h_e} \rangle. \end{aligned} \quad (1.21)$$

Using $|e_{p_e, h_e}\rangle = (a_e^{(h_e)}(p_e) / \sqrt{2E_e V}) |0\rangle$, the average over electron helicity simplifies

$$\begin{aligned} &\frac{1}{2} \sum_{h_e = \pm 1} \langle e_{p_e, h_e} | [\bar{e}(x) \gamma_\rho (1 - \gamma^5) e(x)] | e_{p_e, h_e} \rangle \\ &= \frac{1}{4E_e V} \text{Tr} \left[\sum_{h_e = \pm 1} u_e^{h_e}(p_e) \bar{u}_e^{h_e}(p_e) \gamma_\rho (1 - \gamma^5) \right] \\ &= \frac{1}{4E_e V} \text{Tr} [(\gamma_a p_{ea} + m_e) \gamma_\rho (1 - \gamma^5)] = \frac{p_{e\rho}}{E_e V}. \end{aligned} \quad (1.22)$$

Substituting eq. (1.22) in (1.21) one obtains

$$\bar{H}_{eff} = \frac{G_F}{\sqrt{2}} \int d^3 p_e f(E_e, T) [\bar{\nu}_e(x) \gamma^\rho \frac{p_{e\rho}}{E_e V} (1 - \gamma^5) \nu_e(x)].$$

The integral over $d^3 p_e$ in the above equation is given as

$$\begin{aligned} \int d^3 p_e f(E_e, T) \gamma^\rho \frac{p_{e\rho}}{E_e} &= \int d^3 p_e f(E_e, T) (\gamma^0 - \frac{p_i \cdot \gamma^i}{E_e}) \\ &= N_e V \gamma^0, \end{aligned}$$

where we use $\int d^3 p_e f(E_e, T) = N_e V$, which is the total number of electrons in volume V . Hence, finally the average effective Hamiltonian has the form

$$\bar{H}_{eff} = V_{CC} [\bar{\nu}_e(x) \gamma^0 P_L \nu_e(x)],$$

where $V_{CC} = \sqrt{2} G_F N_e$. The NC interaction is equally felt by all the flavours of neutrinos, hence this term can be gotten rid of field redefinition, and does not affect the effective matter potential.

For two neutrino case, where the matter effect is only felt by the

electron neutrino, the Hamiltonian in the flavour basis is given as,

$$\begin{aligned}
 H_f &= \frac{1}{2E} \left[U \begin{pmatrix} m_1^2 & 0 \\ 0 & m_2^2 \end{pmatrix} U^\dagger + \begin{pmatrix} A & 0 \\ 0 & 0 \end{pmatrix} \right], \\
 &= \frac{1}{4E} \left[(m_1^2 + m_2^2 + A)I_2 + \begin{pmatrix} A - \Delta m_{21}^2 \cos 2\theta & \Delta m_{21}^2 \sin 2\theta \\ \Delta m_{21}^2 \sin 2\theta & -A + \Delta m_{21}^2 \cos 2\theta \end{pmatrix} \right],
 \end{aligned} \tag{1.23}$$

where, m_i is the mass of ν_i and $A = \sqrt{2}G_F N_e E$. Antineutrinos interacting with matter follow the same equation of motion given in eq. (1.23) with the following changes due to CP symmetry: $A \rightarrow -A$ and $U \rightarrow U^*$ [40]. For two generations of neutrino $U = U^*$. The effective mass square and the mixing angles of the Hamiltonian H_f are given as,

$$\begin{aligned}
 M_{2,1}^2 &= \frac{1}{2} \left[(m_1^2 + m_2^2 + A) \pm \{(A - \Delta m_{21}^2 \cos 2\theta)^2 + (\Delta m_{21}^2 \sin 2\theta)^2\}^{1/2} \right], \\
 \tan 2\theta_m &= \frac{\Delta m_{21}^2 \sin 2\theta}{\Delta m_{21}^2 \cos 2\theta - A}.
 \end{aligned} \tag{1.24}$$

Following eq. (1.24), the rate of change of mixing angles can be written as:

$$\frac{\partial \theta_m}{\partial t} = \frac{1}{2} \frac{\Delta m_{21}^2 \sin 2\theta}{(A - \Delta m_{21}^2 \cos 2\theta)^2 + (\Delta m_{21}^2 \sin 2\theta)^2} \frac{\partial A}{\partial t}. \tag{1.25}$$

Substituting these values in eq. (1.20), the adiabaticity parameter reads

$$\gamma = \frac{(M_1^2 - M_2^2)^3}{2E \Delta m_{21}^2 \sin^2 2\theta |\partial A / \partial t|}. \tag{1.26}$$

If $\gamma \geq 1$, the neutrino propagation is adiabatic, otherwise it is non-adiabatic, and it becomes extremely non-adiabatic at $\gamma \sim 0$. γ is minimum when the difference in the square of effective mass is minimum, which happens when $A = \Delta m_{21}^2 \cos 2\theta$. This is called the resonance condition, and at this point, the mixing angle θ_m is $\pi/4$, which facilitates maximum mixing between the flavour states. The adiabaticity parameter at resonance reads,

$$\gamma_R = \frac{\Delta m_{21}^2 \sin^2 2\theta}{2E \cos 2\theta |d \ln n_e(x) / dx|_R}, \tag{1.27}$$

where, $x = ct$. Similar to eq. (1.16), the amplitude of evolution in the flavour basis for a non-adiabatic case is given as

$$\begin{aligned}
S_f &= U(t)\tilde{S}(t,0)U^\dagger, \\
&= \begin{pmatrix} U_{e1}(t) & U_{e2}(t) \\ U_{\mu1}(t) & U_{\mu2}(t) \end{pmatrix} \begin{pmatrix} S_{11} & S_{21}^* \\ S_{21} & S_{11}^* \end{pmatrix} \begin{pmatrix} U_{e1}^*(0) & U_{\mu1}^*(0) \\ U_{e2}^*(0) & U_{\mu2}^*(0) \end{pmatrix}, \\
&= \begin{pmatrix} \cos\theta_m(t) & \sin\theta_m(t) \\ -\sin\theta_m(t) & \cos\theta_m(t) \end{pmatrix} \begin{pmatrix} S_{11} & S_{21}^* \\ S_{21} & S_{11}^* \end{pmatrix} \\
&\quad \times \begin{pmatrix} \cos\theta_m(0) & -\sin\theta_m(0) \\ \sin\theta_m(0) & \cos\theta_m(0) \end{pmatrix},
\end{aligned}$$

where $\theta_m(t)$ and $\theta_m(0)$ are the initial and final effective mixing angle at time 0 and t respectively. $\tilde{S}(t,0)$ is the amplitude matrix in the mass basis. Owing to the off-diagonal elements of $\tilde{S}(t,0)$, there can be transition between $\nu_1 - \nu_2$ states in the non-adiabatic case. Also, as $\tilde{S}(t,0)$ is unitary matrix, meaning $|S_{11}|^2 + |S_{12}|^2 = 1$ and the probability of conversion from $\nu_\alpha \rightarrow \nu_\beta$ is given as $|(S_f)_{\alpha\beta}|^2$. Hence, the survival probability of ν_e is given as

$$\begin{aligned}
|(S_f)_{ee}(t,0)|^2 &= \frac{1}{2} \left[1 + \cos 2\theta_m(t) \cos 2\theta_m(0) \right] - |S_{12}|^2 \cos 2\theta_m(t) \cos 2\theta_m(0) \\
&\quad + P_{int}, \tag{1.28}
\end{aligned}$$

where the interference term is

$$\begin{aligned}
P_{int} &= \frac{1}{4} \sin 2\theta_m(t) \sin 2\theta_m(0) \left[S_{11}^2 + S_{11}^{*2} + S_{12}^2 + S_{12}^{*2} \right] \\
&\quad - \frac{1}{2} \sin \left[2\theta_m(t) - 2\theta_m(0) \right] \left[S_{11} S_{12}^* + S_{12} S_{11}^* \right].
\end{aligned}$$

If the propagation length is much greater than the oscillation length, as $S_{ij} \propto \exp(-it/T_{osc})$ [39], each term of P_{int}^c has a factor of $\exp(-it/T_{osc})$, which when averaged out yields

$$\langle \exp(-it/T_{osc}) \rangle = \lim_{T \rightarrow \infty} \frac{\int_0^T dt \exp(-it/T_{osc})}{\int_0^T dt} = \lim_{T \rightarrow \infty} \frac{i \exp(-iT/T_{osc})}{T/T_{osc}} = 0.$$

Thus, on averaging out $P_{int} = 0$. Similarly, the probability of flavour transition, $\nu_\alpha \rightarrow \nu_\beta$, is given as

$$\begin{aligned} |(S_f)_{\alpha\beta}(t, 0)|^2 &= \left| U_{\beta 1}(t)(S_{11}U_{\alpha 1}^*(0) + S_{21}^*U_{\alpha 2}^*(0)) + U_{\beta 2}(t)(S_{21}U_{\alpha 1}^*(0) \right. \\ &\quad \left. + S_{11}^*U_{\alpha 2}^*(0)) \right|^2, \\ &= |U_{\beta 1}(t)|^2(1 - |S_{21}|^2)|U_{\alpha 1}(0)|^2 + |S_{21}|^2(|U_{\alpha 2}(0)|^2|U_{\beta 1}(t)|^2 \\ &\quad + |U_{\alpha 1}(0)|^2|U_{\beta 2}(t)|^2) + |U_{\beta 2}(t)|^2(1 - |S_{21}|^2)|U_{\alpha 2}(0)|^2 + P_{int}. \end{aligned}$$

With no interference terms, the above probability of flavour transition has the form

$$P_{\alpha\beta} = \begin{pmatrix} |U_{\beta 1}(t)|^2 & |U_{\beta 2}(t)|^2 \end{pmatrix} \begin{pmatrix} 1 - P_{12}^c & P_{12}^c \\ P_{12}^c & 1 - P_{12}^c \end{pmatrix} \begin{pmatrix} |U_{\alpha 1}(0)|^2 \\ |U_{\alpha 2}(0)|^2 \end{pmatrix}, \quad (1.29)$$

where $P_{ij}^c = |S_{ij}|^2$. Thus, in the case of one resonance during non-adiabatic propagation, the probability of flavour transition can be generalised as,

$$P_{\alpha\beta} = |U_{\beta i}^D|^2|U_{\alpha i}^S|^2 - P_{ij}^c(|U_{\beta i}^D|^2 - |U_{\beta j}^D|^2)(|U_{\alpha i}^S|^2 - |U_{\alpha j}^S|^2), \quad (1.30)$$

where U^D , and U^S are the mixing matrices at detector, and source respectively. In the same way, for three neutrino flavours and two resonances, $\nu_1 - \nu_3$ followed by $\nu_1 - \nu_2$, the probability of flavour transition is given as

$$\begin{aligned} P_{\alpha\beta} &= \begin{pmatrix} |U_{\beta 1}(t)|^2 & |U_{\beta 2}(t)|^2 & |U_{\beta 3}(t)|^2 \end{pmatrix} \begin{pmatrix} 1 - P_{12}^c & P_{12}^c & 0 \\ P_{12}^c & 1 - P_{12}^c & 0 \\ 0 & 0 & 1 \end{pmatrix} \\ &\quad \times \begin{pmatrix} 1 - P_{13}^c & 0 & P_{13}^c \\ 0 & 1 & 0 \\ P_{13}^c & 0 & 1 - P_{13}^c \end{pmatrix} \begin{pmatrix} |U_{\alpha 1}(0)|^2 \\ |U_{\alpha 2}(0)|^2 \\ |U_{\alpha 3}(0)|^2 \end{pmatrix}. \quad (1.31) \end{aligned}$$

Hence, for the case of two resonances, the probability of flavour conversion

can be generalised as

$$P_{\alpha\beta} = |U_{\alpha i}^S|^2 |U_{\beta i}^D|^2 - P_{ij}^c (|U_{\alpha i}^S|^2 - |U_{\alpha j}^S|^2) (|U_{\beta i}^D|^2 - |U_{\beta j}^D|^2) \\ - P_{ik}^c P_{kj}^c (|U_{\alpha i}^S|^2 - |U_{\alpha k}^S|^2) (|U_{\beta k}^D|^2 - |U_{\beta j}^D|^2). \quad (1.32)$$

As can be seen from eq. (1.31), for the non-adiabatic contributions only those terms relevant for the scenario are taken into account. For example, if the 13 resonance is followed by a 12 resonance, only the term with $P_{12}^c P_{13}^c$ is included for two resonances. Here, P_{ij}^c , jumping probability from i th state to j th state, is expressed as [41–43]

$$P_{ij}^c = \frac{\exp(-\frac{\pi}{2}\gamma_R^{ij} F_{ij}) - \exp(-\frac{\pi}{2}\gamma_R^{ij} \frac{F_{ij}}{\sin^2 \theta_{ij}})}{1 - \exp(-\frac{\pi}{2}\gamma_R^{ij} \frac{F_{ij}}{\sin^2 \theta_{ij}})}, \quad (1.33)$$

where, F_{ij} is dependent on the density profile of medium and is defined as:

$$F_{ij} = \frac{2}{\pi E \gamma_R^{ij}} \text{Im} \int_{t_R}^{t^*} dt (M_i^2 - M_j^2), \\ = \frac{2}{\pi E \gamma_R^{ij}} \text{Im} \int_{A_R}^{A^*} \frac{dA}{dA/dx} \sqrt{(A - \Delta m_{ij}^2 \cos 2\theta_{ij})^2 + (\Delta m_{ij}^2 \sin 2\theta_{ij})^2},$$

where $x = ct$, t_R , and t^* are the time at which resonance happens, and when the term $M_i^2 - M_j^2$ is zero respectively. A_R , and A^* are the values of A at time t_R , and t^* respectively. For exponential density profile, *i.e.*, $\rho \propto \exp(-x/x_0)$, using transformation $b = (A - \Delta m_{ij}^2 \cos 2\theta_{ij}) / (\Delta m_{ij}^2 \sin 2\theta_{ij})$, the above expression reads

$$F_{ij} = \frac{2x_0}{\pi E \gamma_R^{ij}} \text{Im} \int_0^i db \frac{\Delta m_{ij}^2 \sin^2 2\theta_{ij} \sqrt{1+b^2}}{\cos 2\theta_{ij} (b \tan 2\theta_{ij} + 1)}, \\ = \frac{4}{\pi \gamma_R^{ij}} \left(\frac{x_0 \Delta m_{ij}^2 \sin^2 2\theta_{ij}}{2E \cos 2\theta_{ij}} \right) \text{Im} \int_0^i db \frac{\sqrt{1+b^2}}{b \tan 2\theta_{ij} + 1}.$$

Also, for the exponentially falling matter density profile $\gamma_R^{ij} = x_0 \Delta m_{ij}^2 \sin^2 2\theta_{ij} / (2E \cos 2\theta_{ij})$. Hence, F_{ij} is given as

$$F_{ij} = \frac{4}{\pi} \text{Im} \int_0^i db \frac{\sqrt{b^2 + 1}}{(b \tan 2\theta_{ij} + 1)} = \begin{cases} 1 - \tan^2 \theta_{ij}, & \text{if } \theta_{ij} \leq \pi/4 \\ 1 - \cot^2 \theta_{ij}, & \text{if } \theta_{ij} > \pi/4. \end{cases} \quad (1.34)$$

Here, as matter effect changes only the (1,1) component of the H_f , thus ν_2 - ν_3 states never undergo resonance, *i.e.*, $P_{23}^c = 0$ [8]. Similarly, if new physics changes the $V_{\tau\tau}$ only, as discussed in Chapter 4, then the resonance never occurs for the ν_1 - ν_2 states, as such $P_{12}^c = 0$.

In addition to having mass, neutrinos stand out from the rest of the SM fermions as they do not interact with photons or gluons. Further, because of their tiny masses, they are assumed to be stable; therefore, they may be wrongly confused as dark matter particles. However, the same tiny masses make them relativistic at the time of structure formation, thereby erasing out the small scale density perturbations and disrupting the large scale structure formation. Therefore, neutrinos or any other relativistic species can account for a tiny component of dark matter (DM) in the universe. The dominant component of DM is unknown, and no SM particle can be a candidate. In the following section, we discuss the evidences of the existence of DM and some of the BSM particles that are widely perceived as DM candidates.

1.8 Dark Matter

Dark Matter is another open question in particle physics, unexplained in the SM framework. There have been several cosmological and astrophysical evidences for the existence of dark matter.

1.8.1 Evidences of Dark Matter

Galaxy Cluster

In 1933, Zwicky et al. used virial theorem to estimate the velocity dispersion of Comma galaxy cluster [44]. Velocity dispersion (σ_0) is the variance of velocity for a galaxy cluster about its mean velocity. Using virial theorem, it can be estimated as

$$\sigma_0 = \sqrt{\frac{GM}{3R}},$$

where G is the gravitational constant, and M is the mass contained within the radius R . The author estimated the dispersion velocity to be around 80 km/s for 800 observed galaxies, with an average mass of $10^9 M_\odot$, and within the radial distance of 10^6 light years. However, the observed dispersion velocity came out to be around 1000 km/s. As the dispersion velocity is proportional to the square root of mass contained inside a radial distance, the resulting missing mass was explained by the presence of invisible matter with a net contribution to the galactic mass much greater than from visible matter.

Galactic rotational curves

Further, in 1970 these speculations about the non-luminous matter were confirmed by radio observations of galactic rotational curves [45]. The observations of the circular velocity profile of the gas and stars within the galaxy beyond the luminous disc revealed a flat velocity profile. However, from the Newtonian gravity, it is known that the circular velocity is

$$v(r) = \sqrt{\frac{GM}{R}},$$

where M is the mass enclosed within the radius R . As the mass of the luminous matter contained inside the galactic disc is constant, in the absence of DM, $v(r)$ must fall as one moves away from the disc. But instead $v(r)$

stays flat, which not only confirms the presence of DM but also suggests that it has a density proportional to $1/r^2$.

Bullet Cluster

The X-ray and gravitational weak lensing observations of the two merging clusters, called the Bullet Cluster, is another evidence of the DM. The X-ray observations depict the distorted distribution of the baryons within the cluster, resembling a bullet. Whereas, the weak lensing observations showed two well separated clusters, confirming that dark matter must dominate the mass of this astrophysical system [46]. These observations of Bullet Cluster suggest that DM particles must have feeble self-interaction which reads, $\sigma/m_{\text{DM}} \leq 1.25 \text{ cm}^2 \text{ g}^{-1}$.

Cosmic Microwave Background

Cosmic Microwave Background (CMB) radiation represents the photons that were last scattered off the baryons in the primordial soup. After this, they got decoupled from the soup, and the Universe turned transparent at the epoch of recombination, *i.e.*, redshift around 1100. These photons have a remarkably uniform temperature of about 2.7 K with fluctuations of around $30 \mu\text{K}$. These tiny fluctuations are observed with great precision, that leads to the probe of various cosmological parameters, *e.g.*, relic density of dark matter, dark energy, baryonic matter, the expansion rate of the Universe, *etc.* The Λ -CDM model with cold and weakly interacting DM with a relic density of $\Omega_{\text{DM}}h^2 = 0.1186 \pm 0.0020$ [47] can fit the Planck observations very well. This is around 5 times the abundance of visible matter in the Universe. Computer simulations have shown that cold dark matter (CDM) can lead to large scale structures, which are in agreement with the observed universe [48].

1.8.2 Dark Matter Candidates

For a particle to qualify as a DM candidate, it should be cold (non-relativistic), weakly interacting and stable. There are various BSM particles ranging from ultralight, $m_{\text{DM}} \sim 10^{-22}$ eV [49] to massive compact halo objects (MACHO) of a few M_{\odot} [50], which are proposed as DM candidates.

Weakly Interacting Massive Particles (WIMPs), $m_{\text{DM}} \sim 10$ GeV are the most popular thermal DM particles in the literature, and they can be both fermions or bosons. However, from the observations of dwarf galaxies, fermionic DM of mass ≤ 70 eV is disfavoured [51]. WIMP of mass ~ 10 GeV and interaction strength similar to weak interactions can lead to correct DM relic density [52]. This is called the ‘WIMP miracle’.

However, numerical simulations with the Λ CDM model show a few tensions with cosmological observations at small, *i.e.*, galactic scales [53–55]. At galactic and sub-galactic scales, the WIMPs predict steep ‘cusp’ like features [56] at galactic centres in which the DM density ρ is expected to fall with the radius r as $1/r$. This is contrary to the observed flat ‘core’ like features, $\rho \sim r^0$ [57]. This discrepancy is known as the core/cusp problem. Also, WIMP predicts too many sub-halos of DM in the vicinity of a galactic DM halo, thus predicting the existence of many satellite galaxies which have not been observed. This is known as the missing satellite problem [58, 59]. Self-interaction among the DM particles is a viable solution to these problems [60–62].

Another candidate, ultralight bosons of mass less than around 1 eV, can exist as Bose Einstein condensate (BEC) from a very early epoch [63]. Fuzzy Dark Matter (FDM), $m_{\text{DM}} \sim 10^{-22}$ eV, are non-relativistic and can lead to structure formation, such that at large scales they mimic CDM. Whereas, at smaller scales, self-gravitating bosonic fields can support stable and localized field configurations with constant DM density known as soliton. These solitons are formed at the center of galaxy, the so called solitonic cores [49, 64–66]. In the presence of self-interactions, ultralight

scalar DM of masses $m_{\text{DM}} \gtrsim 10^{-22}$ eV also become viable [66–69]. The quantum pressure at small scales suppresses structure formation at those scales, thus leading to a smaller number of galaxies, and hence solving the missing satellite problem [49, 70, 71]. For m_{DM} much greater than 10^{-22} eV, the de Broglie wavelength which is relatively small, and the gravitational collapse is prevented with the help of tiny repulsive self-interaction with quartic coupling λ given as, $m_{\text{DM}}^4/\lambda \leq 50$ eV⁴ [67]. This leads to additional pressure against gravity, thereby stabilising the system. The observation of CMB and Lyman- α spectra disfavours the ultralight scalar DM of mass $\lesssim 10^{-21}$ eV [72]. If the DM was in thermal equilibrium with photons before recombination, in order for such a scalar to remain in a BEC in the present Universe, its mass should be $\lesssim 1.87$ eV [73].

1.9 Motivation and Organisation of the Thesis

The origin of neutrino masses and neutrino interactions are not completely known to us [74]. In literature, there is a plethora of beyond standard models (BSM), explored in an attempt to explain neutrino mass [75–81]. Some of these models have DM candidates as well, as a part of their particle content [82–84]. Also, the addition of right-handed neutrinos can lead to neutrino mass. To generate the Majorana mass term, these right-handed neutrinos have a mass greater than $\sim 10^{14}$ GeV, as discussed in Sec. 1.5. Even light sterile neutrinos are explored in the context of neutrino mass [81] and as a viable explanation of reactor anomalies, *i.e.*, LSND and Mini-BooNE. In reactor anomalies, sterile neutrinos of mass ~ 1 eV with maximal active–sterile mixing, can lead to observed ν_e – ν_μ transitions [84–88]. However, such explanations are in serious disagreement with the cosmological observations [89]. The primary constraint, in this case, is that the maximum mass of neutrinos allowed from structure formation has to be less than 0.2 eV [33]. Also, the presence of light species, *e.g.*, sterile neutri-

nos, extra gauge bosons (Z'), scalar or fermionic DM [90–93], of mass less than a few MeV, are highly constrained by the precise measurement of effective degree of freedom of relativistic particles (N_{eff}) [94, 95], discussed in Chapter 3, Sec. 3.3.2. Further, DM mass and cross-section suffers stringent bounds from the observations of relic density [96]. Thus, precise cosmological observations are essential tools for the study of dark matter and neutrinos interacting within and beyond the SM.

As we move to new physics at higher energy, the measurements from LEP [97], LHC [98–100], BABAR [101, 102], CCFR [103], oscillation experiments [88, 104] provide stringent constraints on new physics. LHC excludes heavy DM and Z' [105], RH neutrinos [106, 107], extra $SU(2)_L$ doublet bosons W_R [108], neutrino non-standard interactions (NSI) with quark, and leptons [109] with $\mathcal{O}(1)$ coupling up to \sim TeV. As in the case of NSI, another way to explore new physics is to integrate out the massive fields at lower energies and generate effective operators. This allows us to put a bound on the scale of new physics without getting into the details of the model. The constraints on such effective operators from LEP, Belle, CHARM and LHC can be followed from refs. [110–116]. Future experiments like Hyper-Kamiokande, MEMPHYS, DUNE and DARWIN can improve the bounds on neutrino-DM interactions [117].

In addition to these observations, the recent detection of astrophysical neutrinos at IceCube opens up a new avenue for explorations of such interactions beyond the scope of the present experiments. Astrophysical neutrinos at IceCube have a wide range of energy, and they travel through cosmic distances to reach earth. As the astrophysical neutrinos travel through a long column of cosmic DM, if neutrinos interact with DM, such changes are bound to show up in the observed neutrino spectrum. Significant neutrino-DM interaction changes the flux and/or flavour ratio of the neutrino spectrum. Also, the upgoing neutrinos pass through the various length of earth matter to reach IceCube, whereas the downgoing neutrinos reach the detector without any hindrance. Thus the comparison of upgoing and downgoing neutrino events can be used to determine neutrino-nucleon

interactions, both in the SM and BSM frameworks. Hence, cosmic neutrinos are ideal for the study of new interactions of neutrinos with DM as well as ordinary matter. Therefore, this thesis aims to explore the implications of a wide variety of new interactions, effective as well as renormalisable, with ordinary matter and DM. We attempt to draw a comparison among various experiments in order to understand the role of cosmic neutrinos at IceCube in the search for BSM physics. Such exploration will pave the way for a better understanding of new interactions, needed to explain various observations. The opportunity to search for these interactions grows with upcoming experiments, *e.g.*, IceCube-Gen2, KM3NeT, GRAND, *etc.*

The thesis is organised into six chapters. In the **second** chapter, we discuss the modes of production and methods of detection of extragalactic neutrinos. We briefly study the relation to other messengers and various sources of high energy neutrinos. We review the main observations of the IceCube experiment and mention the upcoming experiments for the observation of astrophysical neutrinos.

In the **third** chapter, we explore the possibility that high energy astrophysical neutrinos can interact with the dark matter on their way to the Earth. Keeping in mind that new physics might leave its signature at such energies, we have considered all possible topologies for effective interactions between neutrino and dark matter. Building models that give rise to a significant flux suppression of astrophysical neutrinos at Earth is rather difficult. Encompassing a large variety of models, a wide range of dark matter masses from 10^{-21} eV up to a TeV, this study aims at highlighting the challenges one encounters in such a model building endeavour after satisfying various cosmological constraints, collider search limits and electroweak precision measurements. The observed spectrum of high energy astrophysical neutrinos at IceCube might be indicative of absorption of such neutrinos in ultralight dark matter halos.

High energy astrophysical neutrinos interacting with ultralight dark matter can undergo flavour oscillations that induce an energy dependence

in the flavour ratios. In the **fourth** chapter, we point out that such a dependence on the neutrino energy will reflect in the track to shower ratio in neutrino telescopes like IceCube or KM3NeT. This opens up a possibility to study DM density profiles of astrophysical objects like AGN, GRB, *etc.*, which are the suspected sources of such neutrinos.

In the **fifth** chapter, we find the constraints on various non-standard interactions of neutrinos from monojet+ \cancel{E}_T searches at the LHC. Also, we show that the measurement of neutrino-nucleon cross-section from the observation of high energy astrophysical neutrino events at IceCube facilitates strong constraints on NSI as well. To this end, we pursue a comparative study of the prospects of LHC and IceCube in detecting NSI, also mentioning the role of low-energy experiments. We discuss the case of NSI with a new vector boson Z' , and it is found that for some range of $m_{Z'}$ LHC puts a more stringent bound, whereas IceCube supersedes elsewhere. We also pay special attention to the case of Z' of the mass of a few GeVs, pointing out that the IceCube constraints can surpass those from LHC and low-energy experiments. Although, for contact-type effective interactions with two neutrinos and two partons, constraints from LHC are superior. Finally, in the **sixth** chapter, we summarise our findings and draw our conclusions.

Chapter 2

Aspects of Astrophysical Neutrinos

For centuries, humanity has strived to understand astrophysical objects. Exploration of cosmic objects began with the study of photons. In the interiors of the astrophysical sources, photons are frequently absorbed and re-emitted by the atoms, which makes their escape impossible from within. Also, high energy photons with energy greater than a TeV are highly attenuated by their interactions with the background photons during their propagation towards the Earth. In addition to photons, the astrophysical objects also emit cosmic rays which are charged particles, mainly consisting of protons or heavier nuclei. The trajectory of the cosmic rays gets distorted on their way due to the deflection suffered in the presence of the cosmic magnetic field. Only cosmic rays of energy greater than around EeV can point back to their sources. Along with these messengers, there are neutrinos produced by pp and $p\gamma$ interactions at the source [118, 119]. As discussed in the previous chapter, neutrinos are neutral elementary particles that are very light and interact only weakly. For example, 10 MeV photons have a mean free path of ~ 20 cm in carbon, whereas neutrinos with the same energy can travel a distance of 1 light year in lead unabsorbed. This enables neutrinos to carry information from astrophysical objects to the detector unattenuated and undeflected. But the same weak interaction makes the Earth transparent to most of these neutrinos. Hence, observing astrophysical neutrinos is difficult, and it is compelling to build huge detectors. Various aspects of astrophysical neutrinos, their produc-

tion mechanism and detection methods, are discussed in this chapter. The motivations of studying astrophysical neutrinos are:

- Neutrinos are the most abundant particles after photons. Neutrinos interact only weakly; they travel unhindered through the intervening matter. Hence, they can give us information about regions of the Universe which are inaccessible to the traditional photon astronomy.
- Neutrinos are the only way to understand the interior of the astrophysical sources. This has been observed from the sun where the only experimental accessibility to the interior of the sun is through the observation of solar neutrinos [120]. So is the case of other astrophysical objects and observing such neutrinos is the only way for probing such sources.
- In the astrophysical objects neutrinos are produced by hadronic channels only, *i.e.*, pp and $p\gamma$. So the study of neutrino flux from such objects, *e.g.*, AGN, GRB, supernovas, is essential for the understanding of the mechanism at work, by which such high energy particles (cosmic ray, photons) are generated from the astrophysical sources [121].
- As far as energy is considered, these astrophysical objects are more powerful than any human-made accelerator ever built on earth. Neutrinos coming from these objects have energies much higher than the energy available at Large Hadron Collider (LHC). Therefore new physics at higher energies can be probed by the study of such high energy neutrinos.
- Studying flavour ratios of these incoming high energy neutrinos can help us understand neutrino oscillations at high energies. Many new physics scenarios lead to change in the neutrino oscillation at high energies; thus, this study can help us probe such new physics models.
- As these neutrinos travel through cosmological distances, they pass through the cosmic dark matter on their way. Studying the flux and flavour of such neutrinos may give us hints about the dark matter interactions they pass through. The condition for producing high energy neutrinos from a source is either the generation of high energy cosmic rays (CR) from the source or the exposure to CRs from other sources. Thus, high energy neu-

trinos at IceCube can be naturally related to the high energy cosmic rays.

2.1 Cosmic Rays

Cosmic Rays are protons and atomic nuclei of very high energy that can be detected at earth. The typical energy of cosmic ray lie between 100 TeV and about 100 EeV, following a broken power-law spectrum, $dN/dE_N \propto E_N^{-\alpha}$. The flux varies from event/(m² s) at 1 GeV to event/(km² 100 years) at 100 EeV, as shown in fig. 2.1. The cosmic ray spectrum is divided into three main regions [122]:

$$\frac{dN}{dE_N} \propto \begin{cases} E_N^{-2.7}, & \text{if } E_N < 10^{16} \text{ eV}, \\ E_N^{-3}, & \text{if } 10^{16} < E_N < 10^{18.5} \text{ eV}, \\ E_N^{-2.7}, & \text{if } 10^{18.5} < E_N < 10^{20.5} \text{ eV}, \end{cases}$$

where E_N is the energy of the nucleon detected. The cosmic ray spectrum has two breaks; the first break at around 10^{16} eV after which the spectrum becomes softer, called the knee. For the energy above the knee, the spectrum suffers another break at energy $\sim 10^{18.5}$ eV and gets harder, leading to the ankle region. A close look at the knee region from more recent observations suggests a second knee at around 4×10^{17} eV, after which the power spectrum gets steeper to $\alpha = 3.2$ before it flattens around the ankle region [7].

The spectrum up to the knee is expected to be of the galactic origin. In contrast, cosmic rays of higher energies can neither be produced nor be contained inside the galaxy; hence they are considered to have originated from the extragalactic sources. Cosmic rays up to the knee need relatively smaller detectors and can be detected by balloons and satellites upon interaction with the atmosphere [123]. At higher energies, cosmic rays interact with the atmosphere, giving rise to secondary particles, which in turn interact with the atmosphere leading to showers. Cosmic rays of energies greater than 10^{14} eV lead to extensive air showers (EAS). These

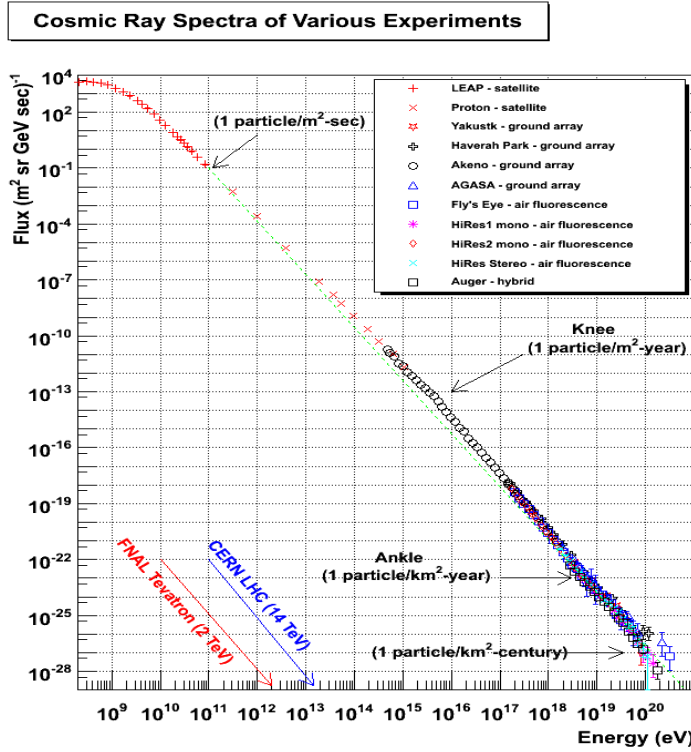


Figure 2.1. Cosmic ray spectrum from various experiments. (Figure courtesy: Ref. [122].)

showers are detected with a large surface area of sparsely placed particle detectors, *e.g.*, Pierre Auger Observatory. Pierre Auger Observatory (PAO) and Telescope Array (TA) experiments have observed high energy cosmic rays up to 4×10^{19} eV and 5.4×10^{19} eV respectively. PAO observes a mixed composition of cosmic rays with protons as the dominant component of the spectrum up to 10^{18} eV and the higher energies have heavier nuclei [124], whereas TA observes protons throughout [125]. We do not expect to observe cosmic rays of energy higher than 10^{20} eV, as protons of energy greater than ~ 70 EeV gets suppressed on their way to the Earth *via* Greisen Zatsepin Kuzmin (GZK) suppression. The GZK suppression occurs when the Ultra-high energy cosmic rays (UHECR) interact with cosmic background radiation (CMB) and lead to photo-production of pions, attenuating the cosmic rays at ultra-high energies. These pions decay to high energy gamma rays and neutrinos. The high energy gamma rays above a TeV interact with background photons, leading to the suppression

of their flux. But high energy neutrinos reach earth and can be observed *via* neutrino telescope, with energies greater than ~ 10 PeV. Such neutrinos are called cosmogenic neutrinos. Not all astrophysical sources would lead to such high energy protons and, in turn, high energy neutrinos. The astrophysical sources must have a magnetic field as well as a size appropriate to accelerate the protons to such high energies, the so called Hillas Criterion.

2.1.1 Hillas Criterion

According to the Hillas criterion [126], the maximum energy imparted to an accelerated particle is given as

$$E_{max} = BqR,$$

where B , q and R are the magnetic field of the source, the charge of the accelerated particle and gyroradius respectively. For a particle to be accelerated, R should be less than the size of the astrophysical source, *i.e.*, the accelerated particle should be confined within the source. The sources which could lead to UHECR are plotted in the Hillas plots, with their magnetic field and size, in fig. 2.2.

2.2 Acceleration of Cosmic Rays

In this section, we discuss the mechanisms for the acceleration of cosmic rays particles [127].

2.2.1 Fermi Acceleration Mechanism

In 1949, Fermi came up with a mechanism of acceleration of cosmic particles inside astrophysical objects [128]. These objects are full of magnetic turbulences, *i.e.*, the ionised ‘clouds’, which are in motion with respect to the galactic frame. As the charged particles enter these clouds, they get

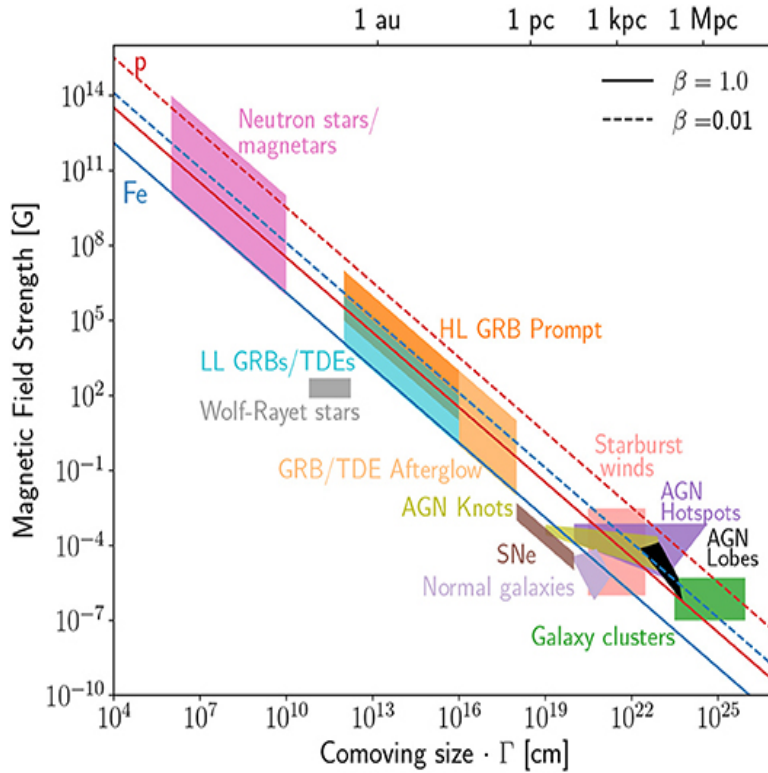


Figure 2.2. Hillas diagram. The solid red and blue lines represent the magnetic field B and size R required to confine a 10^{20} eV of proton and iron respectively. (Figure courtesy: Ref. [129].)

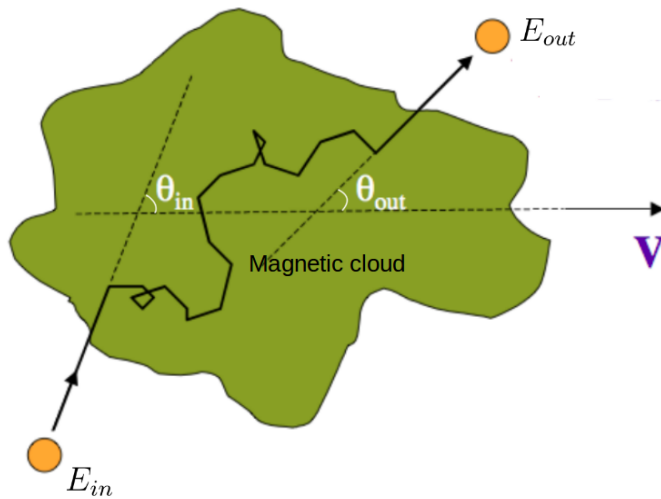


Figure 2.3. A charged particle deflected by the magnetic cloud.

reflected back, which leads to change in velocity. Let us assume a particle with a velocity $v \sim c$ encounters a cloud moving with a velocity V , then

the energy of the particle entering and leaving the cloud can be given as

$$\begin{aligned} E'_{in} &= \gamma_{cl} E_{in} (1 - \beta_{cl} \cos \theta_{in}), \\ E_{out} &= \gamma_{cl} E'_{out} (1 + \beta_{cl} \cos \theta'_{out}), \end{aligned}$$

where $E_{in(out)}$ and $\theta_{in(out)}$ is the incoming (outgoing) particle energy and angle between incoming (outgoing) particle and the cloud respectively. The primed (unprimed) index represents the quantities in cloud (galactic) frame, $\beta_{cl} = V/c$ and $\gamma_{cl} = 1/\sqrt{1 - \beta_{cl}^2}$. Assuming elastic collision, $E'_{in} = E'_{out}$, the final energy of the particle in the galactic frame is

$$E_{out} = \gamma_{cl}^2 E_{in} (1 - \beta_{cl} \cos \theta_{in}) (1 + \beta_{cl} \cos \theta'_{out}).$$

The increase in energy per unit original energy is given as

$$\frac{\Delta E}{E_{in}} = \frac{E_{out} - E_{in}}{E_{in}} = \frac{\beta_{cl}^2 - \beta_{cl} \cos \theta_{in} + \beta_{cl} \cos \theta'_{out} - \beta_{cl}^2 \cos \theta_{in} \cos \theta'_{out}}{1 - \beta_{cl}^2}.$$

As the velocity distribution of the particles inside the cloud is isotropized $\langle \cos \theta'_{out} \rangle = 0$. Whereas, the probability of particle to encounter the cloud with angle θ_{in} is proportional to the relative velocity $v - V \cos \theta_{in}$. Hence,

$$\langle \cos \theta_{in} \rangle = \frac{\int_{-1}^1 d \cos \theta_{in} \cos \theta_{in} (v - V \cos \theta_{in})}{\int_{-1}^1 d \cos \theta_{in} (v - V \cos \theta_{in})} = \frac{-2V/3}{2v} \simeq \frac{-\beta_{cl}}{3}. \quad (2.1)$$

Therefore, as the cloud moves much slower than the particle $\beta_{cl} \ll 1$, the change in energy after one encounter with the cloud is proportional to $\Delta E/E = 4\beta_{cl}^2/3$. This second order increase in energy, $\Delta E \propto \beta_{cl}^2$, makes the Fermi mechanism highly inefficient for accelerating the particles. Suppose a particle with initial energy E_0 undergoes multiple collisions with clouds separated with a length L . The time between two collisions is $t_{col} = L/c$, and the time rate of change in energy of the particles is

$$\begin{aligned} \frac{dE}{dt} &= \frac{\Delta E}{t_{col}} = \frac{4\beta_{cl}^2 c E}{3L}, \\ \implies E(t) &= E_0 \exp(t/t_{acc}), \end{aligned} \quad (2.2)$$

where, $t_{acc} = 3L/(4c\beta_{cl}^2)$. Suppose the particle leaves the system after an average time t_{esc} , then the probability of escape is $P_{esc} = dt/t_{esc}$ and the fraction of particles still within the system after time t is $\propto \exp(-t/t_{esc})$. Hence, if N_0 be the injection rate of the particles, then from eq. (2.2) their number between energy E and $E + dE$ per unit area is given as

$$\begin{aligned} ndE &= N_0 dt \exp(-t/t_{esc}), \\ \implies ndE &= N_0 \frac{t_{acc}}{E} dE \left(\frac{E}{E_0}\right)^{-\frac{t_{acc}}{t_{esc}}}, \\ \implies n &= \frac{N_0}{E_0} t_{acc} \left(\frac{E}{E_0}\right)^{-(1+\frac{t_{acc}}{t_{esc}})}. \end{aligned}$$

Here n is the differential flux from astrophysical sources, and it displays a power law behaviour, with $(1 + t_{acc}/t_{esc})$ as the spectral index. To obtain an estimate of the efficiency of this mechanism, from eq. (2.2), keeping $\beta_{cl} = 10^{-4}$ and $L = 1$ pc, one can estimate that it will take $\sim 10^9$ years to double the energy of the charged particle [130]. Hence, in realistic scenarios, the Fermi mechanism is highly inefficient as the acceleration is rather slow.

2.2.2 Diffusive Shock Acceleration

Another method to accelerate the charged particles is the propagation of shock in the interstellar medium [130]. The region of the medium which is already in the influence of shock is called the downstream and the region to which the shock moves is called upstream. These two regions have different velocities, temperature, pressure and density. Let $T_{1(2)}$, $P_{1(2)}$, $v_{1(2)}$ and $\rho_{1(2)}$ be the temperature, pressure, velocity and density of upstream (downstream) fluid. These quantities are related by the shock conditions:

- Mass conservation: $\rho_1 v_1 = \rho_2 v_2$.
- Momentum flux conservation: $P_1 + \rho_1 v_1^2 = P_2 + \rho_2 v_2^2$.
- Energy conservation: $\rho_1 v_1 \left(\frac{v_1^2}{2} + \frac{P_1}{\rho_1} + \omega_1 \right) = \rho_2 v_2 \left(\frac{v_2^2}{2} + \frac{P_2}{\rho_2} + \omega_2 \right)$, where ω_i is the energy density of the gas given as $\omega_i = \frac{1}{\gamma_a - 1} \frac{P_i}{\rho_i}$ and γ_a is the adiabatic index, which is 5/3 for a monoatomic gas.

From the shock conditions the velocity relation can be given as

$$\frac{v_2}{v_1} = \frac{\gamma_a + M_1^{-2} \pm (1 - M_1^{-2})}{\gamma_a + 1}, \quad (2.3)$$

where $M_1 = v_1/v_s$ is the Mach number and v_s is the velocity of sound in the upstream medium given as $v_s = \sqrt{\gamma_a P_1/\rho_1}$. In the limit of strong shocks, *i.e.*, $M_1 \gg 1$, considering the negative sign in the eq. (2.3), leads to the relation $v_1 = rv_2$ where $r = (\gamma_a + 1)/(\gamma_a - 1)$ and the density of the downstream region is r times greater than the upstream. In the upstream

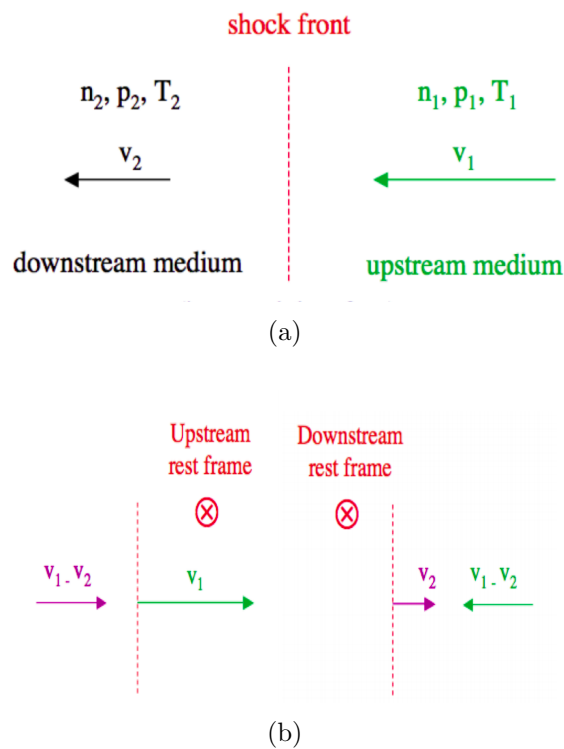


Figure 2.4. (a) Velocities of upstream (v_1) and downstream medium (v_2) observed from shock rest frame. (b) Left, and right diagrams represent the velocities of shock and medium in upstream, and downstream rest frames respectively. (Figure courtesy: Ref. [131].)

frame, the shock moves towards the upstream with a velocity v_1 and the downstream moves towards it with a velocity $v_1 - v_2 = (r - 1)v_1/r$, as shown in fig. 2.4. As the particle crosses to reach downstream, in the downstream frame, the shock seems to move away with a velocity of v_2 . However, the upstream seems to move towards it with a velocity $v_1 - v_2$, and again the particle moves into the upstream region. This cycle repeats itself and with

each cycle the particle gains in energy. Similar to the Fermi mechanism discussed above, the net increase in energy per unit initial energy in one complete cycle is given as

$$\frac{\Delta E}{E} = \frac{\beta^2 + \beta \cos \theta_{in} - \beta \cos \theta'_{out} - \beta^2 \cos \theta_{in} \cos \theta'_{out}}{1 - \beta^2},$$

where, $\beta = (v_1 - v_2)/c = (r - 1)\beta_{sh}/r$, $\theta_{in(out)}$ is the angle with which the particle enters (exits) the downstream. Here, primed (unprimed) index denote the downstream (upstream) reference frame. Only the particles moving in the direction of the shock front will cross it and get accelerated. Suppose a particle with velocity v_p making an angle θ with the shock front, then the number of particles crossing the shock between angle θ and $\theta + d\theta \propto \cos \theta d\cos \theta$. Hence,

$$\langle \cos \theta \rangle = \frac{\int_{\cos \theta_{min}}^{\cos \theta_{max}} d\cos \theta \cos^2 \theta}{\int_{\cos \theta_{min}}^{\cos \theta_{max}} d\cos \theta \cos \theta} = \frac{2}{3} \left(\frac{\cos^3 \theta_{max} - \cos^3 \theta_{min}}{\cos^2 \theta_{max} - \cos^2 \theta_{min}} \right). \quad (2.4)$$

For a particle in the upstream, as the shock moves toward it, $\theta_{min(max)} = 0(\pi/2)$. Whereas for downstream, the shock moves away from it, leading to $\theta_{min(max)} = \pi/2(\pi)$. Therefore $\langle \cos \theta_{in} \rangle = 2/3$ and $\langle \cos \theta'_{out} \rangle = -2/3$, which in turn means that $\Delta E/E \simeq 4\beta/3$. Hence, in Diffusive Shock Acceleration (DSA) the increase in energy is more efficient than Fermi mechanism.

The number of particles in the solid angle $d\Omega$, area dS and time dt , is given as

$$dN = \frac{n_0}{4\pi} \cos \theta v_p d\Omega dS dt = \frac{n_0}{2} \cos \theta v_p dS d\cos \theta dt,$$

where n_0 is the number density of the particles at the source. As the shock moves towards upstream, particles in the upstream always gets accelerated and move to downstream. But in downstream as the shock keeps on shifting away with speed v_2 , the particle can land up at a position much far away from the shock front and can eventually escape. Thus the flux that can escape from the system can be given as $\Phi_{esc} = n_0 v_2$. Whereas the flux in

the upstream is

$$\Phi_{us} = \frac{n_0}{4\pi} v_1 \int_0^{2\pi} d\phi \int_0^{-1} d \cos \theta \cos \theta \sim \frac{n_0 c}{4}. \quad (2.5)$$

Hence, the probability of escape from the system is given as $P_{es} = \Phi_{esc}/\Phi_{us} = 4\beta_{sh}/r$. If one initially injects N_0 particles with energy E_0 , after n cycles the energy of the particles is $E = (1 + 4\beta/3)^n E_0$, and the number of particles per unit area per unit time still in the system is

$$N = N_0(1 - P_{es})^n = N_0(1 - P_{es})^{\frac{\ln(E/E_0)}{\ln(1+4\beta/3)}}.$$

Using the relations $a^{\ln b} = b^{\ln a}$, $\ln(1+x) = \sum_i (-1)^{i+1} x^i / i$, $\beta \ll 1$ and $P_{es} \ll 1$, the above relation is simplified as

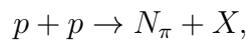
$$N = N_0 \left(\frac{E}{E_0} \right)^{\frac{\ln(1-P_{es})}{\ln(1+4\beta/3)}} = N_0 \left(\frac{E}{E_0} \right)^{-\frac{3P_{es}}{4\beta}}.$$

Thus, the differential flux can be obtained as $dN/dE \propto E^{-1-3P_{es}/(4\beta)}$. Hence, similar to Fermi mechanism we end up with a power law flux, having the spectral index $\Gamma = 1 + 3P_{es}/(4\beta) = (r+2)/(r-1)$, and for monoatomic gas $\Gamma = 2$.

2.3 Production of Astrophysical Neutrinos

The accelerated protons in the astrophysical sources lead to the production of high energy neutrinos *via* pp or $p\gamma$ interactions. These interactions are described below:

- Hadronic collision or pp interaction: pp interaction leads to the production of pions



where, N_π is pion multiplicity. Here charged and neutral pions have the equal probability of production. These pions further decay into neutrinos

and gamma rays:

$$\begin{aligned}\pi^+ &\rightarrow \mu^+ + \nu_\mu, & \pi^- &\rightarrow \mu^- + \bar{\nu}_\mu, \\ \mu^+ &\rightarrow e^+ + \nu_e + \bar{\nu}_\mu, & \mu^- &\rightarrow e^- + \bar{\nu}_e + \nu_\mu, \\ \pi^0 &\rightarrow \gamma\gamma.\end{aligned}$$

In this process, the inelasticity, *i.e.*, the fraction of energy transferred from the parent particles, to each pion, neutrino and photon are $k_\pi \sim 0.2$, $k_\nu \sim 0.25$, and $k_\gamma \sim 0.5$ respectively. Therefore 5% of the total energy of the nucleon is transferred to the neutrino, whereas 10% is transferred to photon [132].

- Pion photo-production or $p\gamma$ interaction. The production process of neutral and charged pions:

$$\begin{aligned}p + \gamma &\rightarrow p + \pi^0, \\ p + \gamma &\rightarrow n + \pi^+.\end{aligned}$$

Similar to the pp process, the inelasticity of pion and neutrinos is $k_\pi \sim 0.2$ and $k_\nu \sim 0.25$ respectively [133], and the probability of production of π^+ is same as π^0 . Hence, 5% of the nucleon energy is transferred to the neutrinos, *i.e.*, for a source at redshift z , the neutrino energy

$$E_\nu = 0.05E_p = \frac{5}{1+z} \text{ PeV} \left(\frac{\epsilon_p}{10^{17} \text{ eV}} \right), \quad (2.6)$$

where E_p , ϵ_p are the proton energy at the Earth and the source respectively. Hence, PeV neutrinos can be produced by cosmic rays with energies around the knee region of the CR spectrum.

K_π is the ratio of number of charged pions (N_{π^\pm}) over neutral pion (N_{π^0}) and it is 1, 2 for $p\gamma$ and pp interaction respectively. The probability of production of charged pion is given as,

$$P_{\pi^\pm} = \frac{N_{\pi^\pm}}{N_{\pi^\pm} + N_{\pi^0}} = \frac{K_\pi}{K_\pi + 1}. \quad (2.7)$$

2.4 Relation with Multi-messengers

As discussed in the previous section, gamma rays and neutrinos are produced from the same $p\gamma$ or pp interaction processes. Hence, the rates of production of neutrinos and gamma rays are related to the production rate of cosmic rays [133]. Apart from cosmic rays and photons, gravitational waves may be produced when a neutron star merges with a black hole or with another neutron star. These mergers are ideal for the production of high energy particles, including neutrinos as discussed in Sec. 2.5. In this section, we find out the relation between the production rates of different messengers.

Following eq. (2.7), charged pion production rate $Q_{\pi^\pm}(E_\pi)$, *i.e.*, the number of charged pions produced per unit time per unit energy is given as,

$$Q_{\pi^\pm}(E_\pi) = \frac{dN_{\pi^\pm}(E_\pi)}{dt dE_\pi} = \frac{K_\pi}{K_\pi + 1} [Q_N(E_N)]_{E_N=E_\pi/k_\pi}. \quad (2.8)$$

In optically thick sources, *i.e.*, the sources in which matter density is greater, produce more neutrinos as compared to the ones which are rare. The optical thickness of the source is taken care by the factor f_π which is given as $f_\pi = 1 - \exp(-n\sigma k_\pi \ell)$, where n , ℓ and σ are source nucleon number density, diameter of the source (assuming spherical symmetry), and cross-section of pp or $p\gamma$ interaction respectively. $f_\pi \sim 1$ for a dense source whereas $f_\pi \ll 1$ for rare sources. Hence, the energy squared rate of

production of charged pions is given as

$$E_\pi^2 Q_{\pi^\pm} = f_\pi \frac{K_\pi}{K_\pi + 1} [E_N^2 Q_N(E_N)]_{E_N = E_\pi/k_\pi}.$$

As each charged pion decays to produce 2 $\nu_\mu + \bar{\nu}_\mu$ and 1 ν_e (or $\bar{\nu}_e$), and each neutral pion produces 2 γ , the rate of production of pions, with the energy between E_l and E_h , can be related to that of neutrinos and photons as

$$N_{\pi^\pm} = \frac{1}{2} \int_{k_\nu E_l}^{k_\nu E_h} dE_\nu \frac{dN_{\nu_\mu}}{dE_\nu},$$

$$N_{\pi^0} = \frac{1}{2} \int_{k_\gamma E_l}^{k_\gamma E_h} dE_\gamma \frac{dN_\gamma}{dE_\gamma}.$$

For very small difference between E_l and E_h , dN_{ν_μ}/dE_ν is a constant and the above equations can be written as,

$$\left. \frac{dN_{\pi^\pm}}{dE_\pi} \right|_{E_\pi} = \left. \frac{k_\nu}{2} \frac{dN_{\nu_\mu}}{dE_\nu} \right|_{E_\nu = E_\pi k_\nu},$$

$$\left. \frac{dN_{\pi^0}}{dE_\pi} \right|_{E_\pi} = \left. \frac{k_\gamma}{2} \frac{dN_\gamma}{dE_\gamma} \right|_{E_\gamma = E_\pi k_\gamma}.$$

The production rates for neutrino and photon related to pion are given as,

$$Q_{\nu_\mu}(E_\nu) = \frac{2}{k_\nu} Q_{\pi^\pm}(E_\nu/k_\nu),$$

$$Q_{\nu_e}(E_\nu) = \frac{1}{k_\nu} Q_{\pi^\pm}(E_\nu/k_\nu),$$

$$Q_\gamma(E_\gamma) = \frac{2}{k_\gamma} Q_{\pi^0}(E_\gamma/k_\gamma). \quad (2.9)$$

The produced neutrinos undergo vacuum oscillation and as the path traversed by such neutrinos is much larger than the typical oscillation length of neutrinos, they get averaged out. As shown in the previous chapter, the final flavour ratio at earth is 1 : 1 : 1 and the rate of production followed

from eq. (2.9) for each flavour is given as,

$$\frac{1}{3} \sum_{\alpha} Q_{\nu_{\alpha}}(E_{\nu}) = \frac{1}{3} (Q_{\nu_{\mu}} + Q_{\nu_{e}}) = \frac{1}{k_{\nu}} Q_{\pi^{\pm}} \left(\frac{E_{\nu}}{k_{\nu}} \right). \quad (2.10)$$

Multiplying E_{ν} on both sides we obtain

$$\frac{1}{3} \sum_{\alpha} E_{\nu} Q_{\nu_{\alpha}}(E_{\nu}) = \frac{E_{\nu}}{k_{\nu}} Q_{\pi^{\pm}} \left(\frac{E_{\nu}}{k_{\nu}} \right) = E_{\pi} Q_{\pi^{\pm}}(E_{\pi}) \Big|_{E_{\pi}=E_{\nu}/k_{\nu}}. \quad (2.11)$$

Following eqs. (2.8), (2.10) and (2.11), neutrino production rate is connected to the cosmic rays as,

$$\frac{1}{3} \sum_{\alpha} E_{\nu}^2 Q_{\nu_{\alpha}}(E_{\nu}) = k_{\nu} f_{\pi} \frac{K_{\pi}}{1 + K_{\pi}} E_N^2 Q_N(E_N) \Big|_{E_N=E_{\nu}/(k_{\nu} k_{\pi})}. \quad (2.12)$$

Also, the production rate of neutrinos is related to gamma rays as,

$$\begin{aligned} \frac{1}{3} \sum_{\alpha} Q_{\nu_{\alpha}}(E_{\nu}) &= \frac{K_{\pi}}{k_{\nu}} Q_{\pi^0} \left(\frac{E_{\nu}}{k_{\nu}} \right) = \frac{k_{\gamma} K_{\pi}}{2k_{\nu}} Q_{\gamma} \left(\frac{E_{\nu} k_{\gamma}}{k_{\nu}} \right) = K_{\pi} Q_{\gamma}(2E_{\nu}), \\ \frac{1}{3} \sum_{\alpha} E_{\nu}^2 Q_{\nu_{\alpha}}(E_{\nu}) &= \frac{K_{\pi} k_{\nu}^2}{k_{\gamma}^2} [E_{\gamma}^2 Q_{\gamma}(E_{\gamma})]_{E_{\gamma}=E_{\nu} k_{\gamma}/k_{\nu}} = \frac{K_{\pi}}{4} E_{\gamma}^2 Q_{\gamma}(E_{\gamma}) \Big|_{E_{\gamma}=2E_{\nu}}. \end{aligned}$$

Initially, the produced gamma rays have the same spectral index and twice the energy of that of neutrinos. Both are produced with energies between TeV and PeV, depending on the source. But gamma rays with energies greater than a TeV tend to pair produce on interaction with infra-red photons, a part of extragalactic background light (EBL). On inverse Compton scattering with the background photon, these pairs lead to photons of lower energy, between 10 and 800 GeV, as detected by Fermi LAT [134]. These observations from Fermi LAT lead to stringent constraints on almost all models of neutrino production *via* pp process. For $p\gamma$ production of neutrinos, as the efficiency of $p\gamma$ increases, the efficiency of $\gamma\gamma$ interaction increase as well, leading to suppression of γ emission from the source. As such, the high energy gamma rays are attenuated, and such sources do not have stringent constraints on their ν counterparts. Many sources that predict high energy neutrinos and gamma rays are optically thin. As such,

these lead to the escape of gamma rays and the expected neutrino flux are severely constrained by Fermi LAT. If these gamma rays are absorbed or attenuated on their way out of the source, then these will be hidden from Fermi LAT, and hence the name hidden sources [135]. Various sources of astrophysical neutrinos are discussed in detail in Sec. 2.5.

2.4.1 Relationship of Low Energy Gamma Rays and High Energy Cosmic Rays with Intermediate Energy Neutrinos

Cosmic rays below the ankle can lead to TeV-PeV energy neutrinos and gamma rays at the source. Both γ and ν have the same spectral index as that of cosmic rays. Still, on their way, the high energy gamma rays with energy greater than ~ 1 TeV are attenuated due to interactions with the background photons [136], whereas the neutrinos reach the detector unaltered. Thus the gamma rays of energy greater than TeV shifts to around 100 GeV and can be observed at Fermi LAT. These observations put bounds on the spectral index for production of gamma rays, $\Gamma \leq 2.1$ [137]. The neutrino spectrum observed at IceCube is consistent with $\Gamma \sim 2$ for $E_\nu \gtrsim 100$ TeV, whereas the High Energy Starting Events which subtends to even lower energy predict a softer flux and hence is in marginal agreement with the bound [138]. These bounds do not apply to the sources with $p\gamma$ as their dominant process of neutrino production. For such sources the $\gamma\gamma$ interactions do not allow the emission of high energy gamma rays, and hence the connection between the neutrinos and gamma rays are difficult to observe. The blue solid (dashed) lines in fig. 2.5 shows the expected gamma rays (neutrinos) observed from $\Gamma = 2$.

In order to estimate the flux of neutrinos from a cosmic ray point source, we consider a source P located at redshift z , luminosity distance

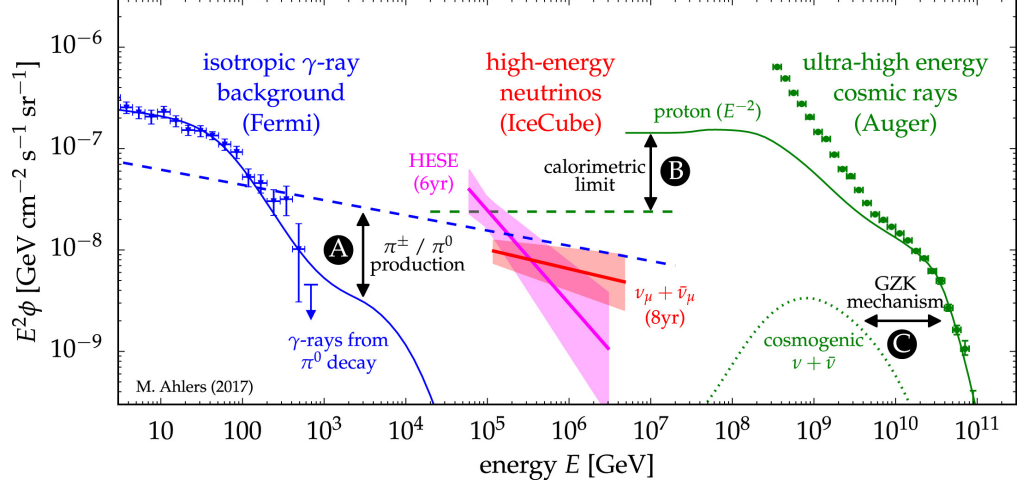


Figure 2.5. The solid blue and green lines represent the gamma ray spectrum and cosmic ray spectrum respectively. **A** The blue dashed, solid line are the neutrino, gamma ray flux from pp process from pion decay from a source. **B** Neutrino flux from a source with $\Gamma = 2$ in calorimetric limit. **C** Green dotted line depicts the cosmogenic neutrinos. (Figure courtesy: Ref. [139].)

x_L . The neutrino flux from P for each flavour is given as

$$\phi_\nu^P = \frac{(1+z)^2}{4\pi x_L^2} \frac{1}{3} \sum_\alpha Q_{\nu_\alpha}(E_\nu(1+z)),$$

where,

$$x_L(z) = (1+z)^2 \int_0^z \frac{dz'}{H(z')}. \quad (2.13)$$

$H(z) = H_0 \sqrt{\Omega_\Lambda + (1+z)^3 \Omega_m}$ is the Hubble parameter, where $H_0 \sim 70$ km/(s Mpc), $\Omega_\Lambda = 0.7$ and $\Omega_m = 0.3$. Considering all such sources distributed with density $\rho(z)$ within a comoving volume

$$dV = dz \frac{4\pi}{H(z)} \left(\frac{x_L(z)}{(1+z)} \right)^2,$$

the neutrino flux is given as

$$\phi_\nu(E_\nu) = \int_0^\infty dz \frac{\rho(z)}{4\pi H(z)} \frac{1}{3} \sum_\alpha Q_{\nu_\alpha}(E_\nu(1+z)).$$

For $Q_{\nu_\alpha}(E_\nu) \propto E_\nu^{-\Gamma}$ and $Q_{\nu_\alpha}(E_\nu) = \rho_0 Q_{\nu_\alpha}(E_\nu)$, where ρ_0 is the density at

redshift 0, the above equation reads

$$\begin{aligned} \frac{1}{3} \sum_{\alpha} E_{\nu}^2 \phi_{\nu}(E_{\nu}) &= \frac{1}{3} \int_0^{\infty} \frac{dz}{4\pi} \frac{(1+z)^{-\Gamma} \rho(z)}{H(z) \rho_0} \sum_{\alpha} E_{\nu}^2 \mathcal{Q}_{\nu\alpha}(E_{\nu}), \\ &= k_{\nu} f_{\pi} \frac{K_{\pi}}{1 + K_{\pi}} \rho_0 E_N^2 \mathcal{Q}_N(E_N) \Big|_{E_N=20E_{\nu}} \\ &\quad \times \int_0^{\infty} \frac{dz}{4\pi} \frac{(1+z)^{-\Gamma} \rho(z)}{H(z) \rho_0}. \end{aligned}$$

From the above equation, it can be inferred that the flux of astrophysical neutrinos depends on the source density distribution, $\rho(z)$. Thus, different source densities lead to different neutrino flux at the detector. For example, if one considers Star Burst Galaxies, then the source distribution follows the star formation rate (SFR), *i.e.*, $\rho(z) = \rho_0(1+z)^3$ and $\rho_0(1+1.5)^3$ for $z < 1.5$, and $1.5 < z < 4$ respectively. In the calorimetric limit $f_{\pi} = 1$, $K_{\pi} = 2$, $\Gamma = 2$ and $E_N^2 \mathcal{Q}_N(E_N)|_{E_N=10^{19.5} \text{ eV}} = 10^{44} \text{ erg}/(\text{Mpc}^3 \text{ yr})$, the neutrino flux comes out to be $E_{\nu}^2 \phi_{\nu} \sim 2 \times 10^{-8} \text{ GeV}/(\text{cm}^2 \text{ s str})$ above 100 TeV [140].

2.4.2 Waxman-Bahcall Bound

From the measurements of cosmic rays above $\sim 10^{17} \text{ eV}$, Waxman et al. [141, 142] derived an upper bound for the neutrino flux. In their work, it was assumed that the cosmic rays above this energy are proton dominated. If such cosmic rays are produced *via* an optically thin source with $f_{\pi} \lesssim 1$, and are accelerated *via* Fermi shock acceleration, the production rate of cosmic rays for the energy between 10^{19} and 10^{21} eV is given as,

$$E_N^2 \mathcal{Q}_N(E_N) \sim 10^{44} \text{ erg}/(\text{Mpc}^3 \text{ yr}).$$

If all the energy of the proton is transferred to the pion, with no loss of energy due to magnetic field in the source, then the upper bound of the neutrino flux is found to be $E_{\nu}^2 \phi_{\nu} < 2 \times 10^{-8} \text{ GeV}/(\text{cm}^2 \text{ s str})$, which is in agreement with IceCube observations for $E_{\nu} > 100 \text{ TeV}$ [140]. This bound can be avoided by

- Considering an optically thick source, *e.g.*, AGN core models.
- Sources in which neutrinos are not produced *via pp* interaction, *e.g.*, production through decaying dark matter.

Also, the derivation of Waxman-Bahcall bound assumes that high energy cosmic rays are proton dominated, which might not be the case. In ref. [143] the possibility of neutrino production *via* heavy nuclei was explored, and it was found that if such heavy nuclei are the source of high energy neutrinos, the flux of the neutrinos was around one order of magnitude lower than the Waxman-Bahcall bound.

2.5 Sources of Astrophysical Neutrinos

Different astrophysical sources lead to a different neutrino flux dominant at different energies. In this section, we study various sources of astrophysical neutrinos and their implications for multi-messenger observations.

2.5.1 Active Galactic Nuclei

Active Galactic Nuclei (AGN) are astrophysical objects characterised by a supermassive black hole (SMBH) surrounded by an accretion disc. Particle accretion leads to the production of radio, optical, X-rays and gamma rays detectable at earth. AGNs which emit radio and X-rays up to luminosity of 10^{43} erg s⁻¹ are called low luminosity AGNs (LLAGN) [144, 145]. AGNs, whose luminosity is around four or more orders of magnitude higher than LLAGN, are further classified into two types: Radio Quiet (RQ) AGN and Radio Loud (RL) AGN. RQ AGNs [146–148] have radio and X-rays as their dominant emissions, whereas RL AGNs emit radio, optical, X-rays as well as high energy gamma rays. RL jet AGNs are further divided into two classes: FR-I and FR-II. The FR-I galaxies have jets of irregular shape, low luminosity and these do not extend beyond the galaxy. On the other hand, FR-II AGN jets are more luminous, and their jets extend hundreds of kpc and overshoot their host galaxies. Blazars are the class of AGNs

whose jets are aligned towards our line of sight. The blazars emitted from aligned FR-I galaxies are called BL Lac whose luminosity lies within the range $10^{44} - 10^{45} \text{ erg s}^{-1}$. Whereas, blazars from FR-II are called flat-spectrum radio quasars (FRSQs) with the luminosity of $10^{46} - 10^{47} \text{ erg s}^{-1}$. Refs. [149, 150] provide excellent reviews on this aspect.

The BL Lac objects are generally characterised by the presence of two distinct ‘humps’ in the spectral energy distribution (SED), shown in fig. 2.6. The lower energy peak is attributed to the synchrotron emission of relativistic electrons. Whereas, the origin of the high energy peak is not clearly known. Two classes of models are proposed to explain the emission of these high energy photons at BL Lacs; the leptonic and hadronic model. In leptonic model, high energy photons are produced by inverse Compton scattering *via* relativistic electron [151]. Hence, in this framework, the gamma rays are always accompanied by a low energy photon peak, in the form of enhanced X-ray emission due to electron synchrotron radiation. This model does not lead to the production of neutrinos. However, there have been observations of high energy TeV photons without the accompanying X-rays, popularly called the orphan TeV flares from BL Lac [152, 153]. Such observations find their explanation in the framework of hadronic models [154]. In these models, the high energy gamma rays are produced along with neutrinos, *via* $p\gamma$ interaction. The detection of neutrinos from the direction of blazar will lead to the confirmation of the hadronic model. So far, as reported, only one such neutrino source has been detected [155].

Apart from blazars, neutrinos are also produced in AGN core like in FRSQ [157] and LLAGN core [145]. The dominant mode of production of neutrinos is when an accelerated proton hits a photon either within the accretion disc or in the dust cloud surrounding the accretion disc. Near the core where the density of proton is high, pp can be the dominant mode of neutrino production. However, the efficiency of $p\gamma$ mode increases with the increase in energy and surpasses the pp mode above $\sim \text{PeV}$ energy. A general characteristic of these AGNs is that they predict a peak in the

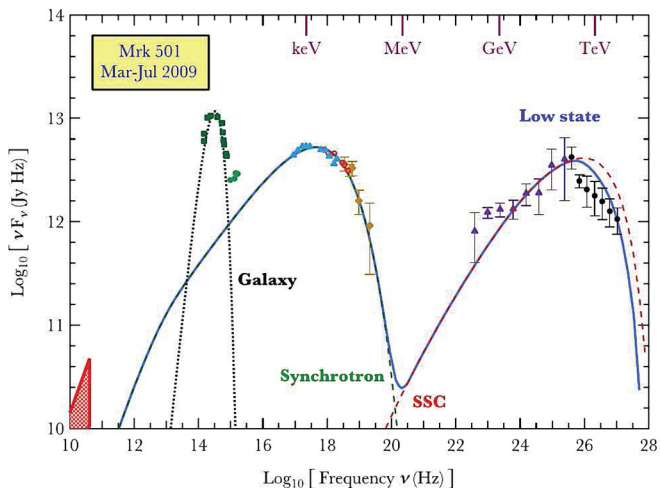


Figure 2.6. Spectral energy distribution (SED) of BL Lacs. (Figure courtesy: Ref. [156].)

neutrino flux greater than or around a few PeV and under-predict neutrinos up to energy ~ 100 TeV. Such models are in tension with IceCube observations [149, 150]. Further, in a stacking analysis conducted by IceCube collaboration, the neutrinos from EM bright AGNs were correlated with their gamma ray counterparts observed at Fermi LAT. The analysis concluded that AGNs with a spectral index of 2.5 cannot lead to neutrino flux more than 25% of the observed neutrino spectrum at IceCube [158].

2.5.2 Galaxy Clusters

Galaxy clusters are objects consisting of around 10^2 to 10^3 galaxies, bound by gravity. These massive objects are the reservoir of cosmic rays which are confined within, due to their magnetic field [159, 160]. Such galaxy clusters can lead to neutrino production mainly *via pp* interaction. There are two methods of acceleration of cosmic rays in such objects:

- *Accretion shock* : The cosmic rays can be accelerated by accretion shocks within the cluster. These sources can contribute to high energy neutrino spectrum no more than $\sim 10\%$ of the total flux seen at IceCube [161].
- *Acceleration through another source*: Cosmic rays are accelerated by a source like AGN or supernova residing inside the cluster and those high

energy cosmic rays interacting with the proton in the galaxy cluster lead to the production of high energy neutrinos [162]. These sources can be responsible for the whole neutrino spectrum seen at IceCube for spectral index from 2 to 2.2. However, the flux with spectral index steeper than the spectral index of 2.1 is in tension with the Fermi LAT observations for gamma rays [163].

2.5.3 Starburst Galaxy

Starburst galaxies (SBG) are objects in which star formation happens at a very high rate. For instance, in the Milky Way star formation happens at a rate of 3 solar mass per year, but in SBGs, the rate is at least a hundred times higher [164]. SBGs lead to the formation of many supernovas (SN) in their starburst phase. These SNs are the ultimate sites for the acceleration of CRs. Also, around 5% of SNs are much brighter with around energy two orders of magnitude greater than average SNs, the so called hypernovas (HN). SNs lead to CR with a maximum energy of around PeV, whereas, HNs lead to ~ 100 PeV CRs, *via* DSA [165]. If such SBGs hosts an AGN, the cosmic rays get accelerated to 10-100 PeV. Hence, SBGs can lead to TeV to PeV neutrinos at IceCube mainly *via* pp interaction.

The X-ray observations dictate that star formation rate (SFR) peaks at around $z \sim 2$ [166]. From the observations of Fermi LAT gamma rays and considering a spectral index of 2.3, IceCube found that SFR can lead to around 30% of the neutrino flux observed at IceCube [138].

2.5.4 Gamma Ray Burst

Gamma Ray Burst (GRB) is a catastrophic event in which there is either collapse of the core of a massive star under gravity or merger of binary objects, *i.e.*, two neutron stars or a neutron star and black hole. These events are seen by the Fermi LAT and Swift as an initial emission of gamma rays from energy $\mathcal{O}(100)$ keV to 100 GeV, which lasts for a few milliseconds

to a few minutes. This prompt emission is followed by an afterglow which has radiation from X-rays to radio waves and lasts from a few days to a few months [167]. Both the prompt emission and afterglow are expected to lead to the acceleration of cosmic rays, which in turn leads to the production of neutrinos *via* $p\gamma$ interaction. As they are optically thin, these GRBs are bright, and their EM radiations are well detected. In the observation of 4 years of IceCube data, where they have used a sample of 592 GRBs, it was found that these GRBs cannot be contributing to more than 1% of IceCube flux [168]. Apart from high energy photons, cosmic rays and neutrinos, these mergers are the sources of gravitational waves. However, till date, no neutrino event has been observed coinciding with the sources of gravitational waves [169].

2.5.5 Low Luminosity and Choked Gamma Ray Bursts

Low Luminosity GRB (LLGRB) are the class of GRB, which are EM dim [170, 171]. These are more in number as compared to the EM GRBs, but their photons can be detected for redshift $z \ll 1$. Choked GRBs [172, 173] are the ones where the stars undergo a core collapse, and the jets do not have enough momentum to leave the source or are absorbed by the stellar envelope. Fermi LAT is blind to such sources, and hence the stacking analysis of IceCube which correlates the photons to neutrinos are not applicable in such scenarios. Thus LLGRBs and Choked GRBs are “hidden” sources and these can account for neutrino flux at IceCube [174]. The jets which are absorbed by the stellar envelope can lead to neutrino production *via* $p\gamma$ interaction. The neutrinos which interact weakly escape the envelope, whereas the gamma rays are trapped within. Therefore, the LLGRBs or choked GRBs can account for the neutrinos observed at IceCube as

- They are more in number than their cousin luminous GRB.
- These cannot be constrained by neutrino-electromagnetic analysis, which

correlates the photons to neutrinos from astrophysical sources.

2.5.6 Cosmogenic Neutrinos

For cosmic rays at energies higher than a few EeV, *i.e.*, above the ankle region, the most dominant interactions that happen are:

- *Photo-disintegration*: The cosmic radiation on interaction with the heavy nucleus, breaks it into lighter nucleons. It is given as, $A + \gamma \rightarrow (A - 1) + N$, where A and N stand for nuclei mass number and nucleon respectively, *e.g.*, ${}^2_1\text{D} + \gamma \rightarrow {}^1_1\text{H} + \text{n}$.
- *Pion production*: The high energy cosmic rays interacts with CMB photons to produce pions which, in turn, decay to produce high energy neutrinos and gamma rays.

Both these interactions peak at around 50 EeV [175]. Hence, independent of the composition of cosmic rays, the cosmic rays flux must have a cut-off at this energy. Hence, on the one hand, due to high UHECR-CMB interaction cross-section, no UHECR can reach earth beyond ~ 100 Mpc, and on the other hand, the production of cosmogenic neutrinos are guaranteed. One of the main objectives of the neutrino telescope is the detection of cosmogenic neutrinos.

The flux of the cosmogenic neutrinos are dictated by three dependencies [176]:

- *Source of cosmic rays*: The sources which accelerate the cosmic rays to higher energies, *i.e.*, from Hillas Criterion has greater E_{max} , and have a flatter spectrum are more feasible for the production of cosmogenic neutrinos. Cosmogenic neutrinos estimated from various sources, like galaxies and AGNs, are constrained from the IceCube [177].
- *Redshift evolution of the cosmos*: Since the UHECR are depleted for distances farther than ~ 100 Mpc, the sources which have strong redshift (z) evolution are favoured. This means for source luminosity, L , where $L \propto (1 + z)^n$, cosmogenic neutrinos flux increases with an increase in n .
- *Chemical composition of the cosmic rays*: The cosmic rays made up of

heavier nuclei produce less flux of cosmogenic neutrinos. If the cosmic rays are made up of protons, then they predict higher flux, called the optimistic scenario.

The neutrinos observed at IceCube, *i.e.*, the TeV to PeV cannot be due

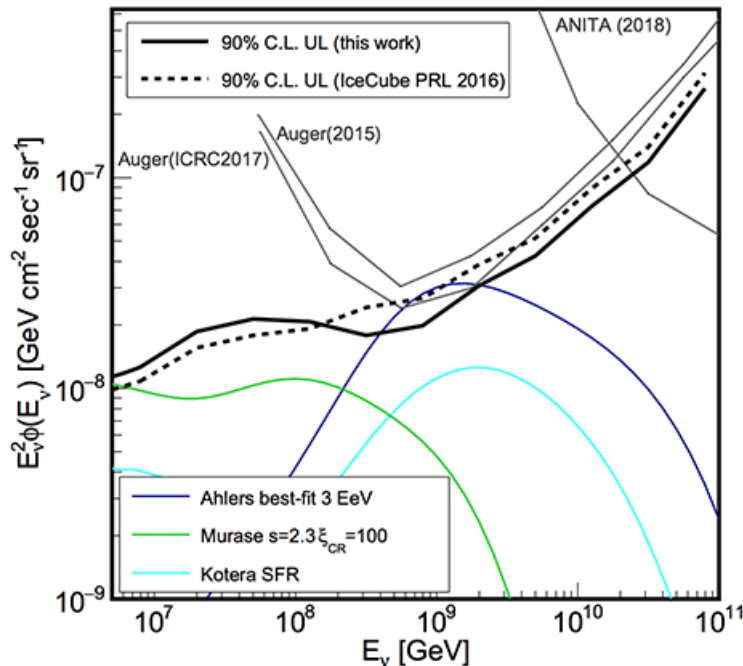


Figure 2.7. Limit on high energy neutrino flux from IceCube data. The black solid, and dotted lines represent upper limit on neutrino flux from 9 years, and seven years of data respectively. The purple [179], cyan, and green lines [180] are cosmogenic neutrino fluxes assuming optimistic scenario. (Figure courtesy: Ref. [181].)

to cosmic rays-CMB interaction as they will lead to overproduction of high energy gamma rays at Fermi LAT [178]. For the chemical composition of cosmic rays as observed at HiRes and the source distribution of SFR, it was shown that IceCube has started to constrain the optimistic scenario, as shown in fig. 2.7. If the chemical composition of the cosmic rays is purely iron, then the neutrino flux is at least two orders of magnitude below the optimistic scenario [182]. As IceCube has not observed any cosmogenic neutrinos so far, they provide the upper limit of allowed flux. This itself constraints many models of sources that predict optimistic neutrino flux.

2.5.7 Decaying Dark Matter

Although one of the properties of DM is that it should be stable, rare decays of DM, with a lifetime greater than the age of the Universe, can lead to high energy neutrinos flux at IceCube [183]. DM particles of mass $m_{\text{DM}} \sim 400 \text{ TeV}$ [184, 185] and a few PeV [186–188] have been studied in the literature as the source of astrophysical neutrinos. The lifetime of such DM is typically around 10^{28} s in order to be concordant with the observed neutrino flux at IceCube [183]. Both galactic and extragalactic DM can lead to such neutrino flux. Along with neutrinos, the decay of DM into charged particles can lead to the production of gamma rays *via* Inverse Compton scattering, in which charged particles scatter off the low energy photons in the galaxy, leading to the upscattering of the gamma rays. These high energy gamma rays lie within the energy reach of Fermi-LAT, and the non-observation of such events lead to stringent constraints on the lifetime of DM [189]. However, such constraints do not apply to the models in which the DM can only decay to neutrinos and dark fermions [190]. DM of mass $\sim 500 \text{ TeV}$ with a lifetime of $2.7 \times 10^{27} \text{ s}$ can lead to neutrino events around 100 TeV, whereas DM mass of a few PeV and lifetime $1.9 \times 10^{28} \text{ s}$ leads to PeV energy neutrinos, thereby explaining the excess in the spectrum. The neutrino flux from DM decay is generally considered along with other sources like the galaxy cluster in order to explain the entire high energy neutrino spectrum at IceCube. The scenarios in which DM decay is the only source of the high energy neutrino flux, are disfavoured [183].

2.6 Observation of Astrophysical Neutrinos

The weak interaction, which makes the neutrinos such a faithful messenger, also leads to difficulties in their detection. Also, the flux of high energy neutrinos decreases with the increase in energy. Therefore in order to detect astrophysical neutrinos, we require a large detector. Also, as the detection happens due to ultra-relativistic secondary particles emitting Cherenkov

radiation, such detectors have to be transparent. This made water or ice with huge volumes ideal for the detection of high energy neutrinos. IceCube, which is a km^3 detector made in the Antarctic ice, is functional and taking measurements for the last ten years. The predecessors of IceCube are described below:

Brief History: The need for an astrophysical neutrino detector was felt long back around 1976 with the building of Deep Underwater Muon And Neutrino Detector Project (DUMAND) experiment [191]. It was a water Cherenkov detector built in the Pacific ocean around 5 km beneath the sea. Although, due to technical difficulties, this detector could not be completed. However, the technology pioneered paved its way to smaller detectors like Lake Baikal [192]. Astronomy with a Neutrino Telescope and Abyss environmental RESearch (ANTARES) [193] experiment is built in the Mediterranean Sea and is completed on May 30, 2008, two years after the deployment of the first string. It is a 0.1 km^3 detector and will be succeeded by Cubic Kilometre Neutrino Telescope (KM3NeT) [194]. The first string of KM3NeT was successfully installed in 2019. Antarctic Muon and Neutrino Detector Array (AMANDA) [195], which is the optical Cherenkov detector built in the South Pole ice in the year 1997. It worked on ten strings, after which it was upgraded to AMANDA II with 19 strings, which was operational from 2000 to 2005. AMANDA II observed around 6595 of upgoing high energy atmospheric neutrino events in 3.8 years [196]. It served as the precursor of IceCube, which was completed in 2010. IceCube was the first to observe PeV neutrino events, which had astrophysical sources with 5.7σ confidence. Within three years of its observation, in 2013, IceCube had observed 37 neutrino events in the energy range of 30 TeV to 2 PeV [197].

2.7 IceCube

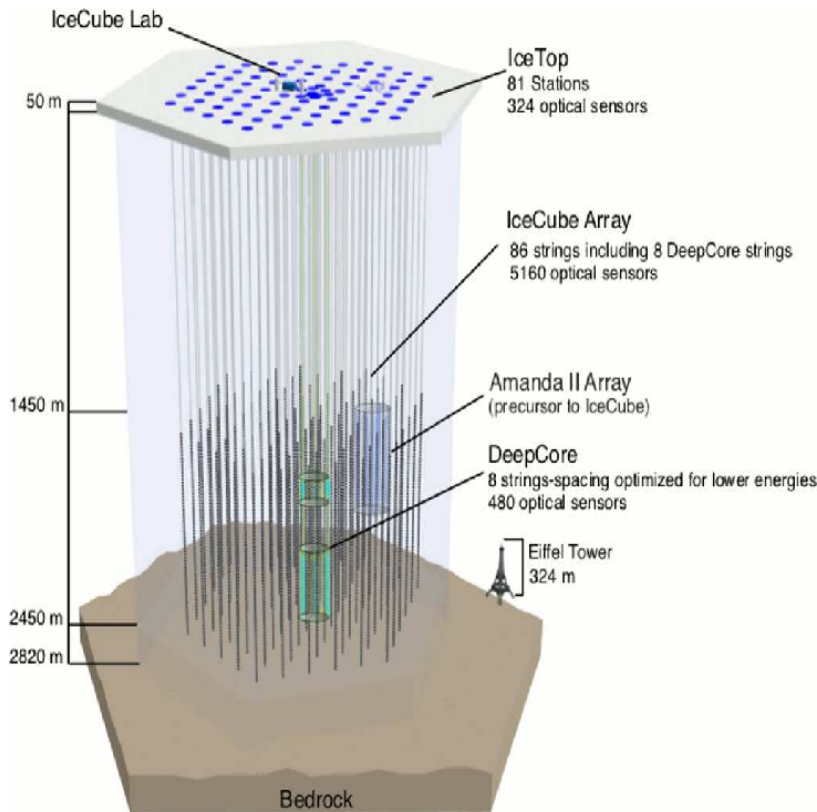


Figure 2.8. IceCube detector. (Figure courtesy: Ref. [194].)

IceCube is a 1 km³ detector deployed at Antarctica [194]. It is instrumented with 86 vertical strings and a total of 5160 digital optical modules (DOMs). The DOMs are spherical glass pressure vessels containing photomultiplier tubes and electronic digitisers that can collect light from all directions. Photomultiplier signals are registered using fast waveform digitisers in each DOM. The direction and energy of the incoming particles are known by reconstructing the light collected by these DOMs. Each vertical string contains 60 DOMs and is deployed in about 2500 m deep holes. DOMs are located inside ice at a depth between 1.5 km to 2.5 km. Deep Antarctic ice is very pure and highly transparent; thus, Cherenkov photons can be detected easily. The 86 strings in IceCube are deployed 125 m apart, covering 1 km² of the surface. The vertical distance between two DOMs on a string is 17 m. The upper layer of ice, above 1450 m filters the cosmic rays and muons and acts as a veto. Each string is supported by a cable that

contains 30 twisted pairs; each pair is connected to two DOMs in parallel. These cables run to a counting-house at the centre of the array. Each IceCube string is independent of the other, which facilitates observation since the time of deployment of string. IceCube takes observations throughout the year; hence the uptime of 99%.

DeepCore:

The remaining six strings out of 86 are placed closer to each other, around 72 m apart, making the denser triangular looking part of IceCube called the ‘DeepCore’. Each DeepCore string has 60 DOM with a vertical spacing of 10 m for the first 10 and 7 m for the last 50. The closely spaced strings of DeepCore and denser DOMs gives DeepCore a lower threshold in terms of neutrino energy, compared to the rest of IceCube, as low as 10 GeV. DeepCore is used for the observation of atmospheric neutrinos and has been used to probe neutrino oscillations up to a TeV. The most stringent constraints on muon neutrino and sterile neutrino mixing come from the observations of atmospheric through-going muon events at DeepCore [198–200].

IceTop:

In addition to the DOMs buried into the ice, the IceCube Observatory includes IceTop to detect surface air showers. IceTop consists of 160 ice-filled tanks, each instrumented with two IceCube DOMs. Two tanks are deployed about 10 m apart, near the top of each IceCube string. Each tank is 1.8 m in diameter and filled with ice to a depth of about 50 cm. The water is frozen in a controlled manner to minimise air bubbles. The tanks are lined with reflective material to increase light collection. IceTop detects cosmic-ray air showers, with a threshold of about 300 TeV. Its main function is to study cosmic-ray flux and composition and TeV muon fluxes. IceTop is also be used to veto high-energy neutrinos in IceCube as the high energy muons can be differentiated as compared to high energy neutrinos

due to IceTop [201, 202].

2.7.1 Detection of high energy neutrinos

Neutrinos being weakly interacting particles travel through the source unattenuated and reach IceCube. At IceCube, they interact with the nucleus or electrons to give secondary charged particles. These particles are seen in the detector, depending on the flavour and interaction. For neutrinos to be detected at IceCube, they must interact with the ice and produce ultra-relativistic charged particles.

2.7.2 Signals Observed

The Cherenkov radiation, in a transparent medium as ice, is transformed from radiation to electrical signals with the help of photomultipliers, which is reconstructed to infer energies, arrival directions, arrival time and flavour of the incoming neutrinos. Neutrinos can arrive from above the sky and go through the detector, called downgoing events, or can cross through the Earth and reach it, called the upgoing events. While they interact with the ice, neutrinos can either undergo a charged current (CC) interaction or a neutral current (NC) interaction. The signals seen at IceCube help to distinguish between different events. These signals are:

Tracks:

A high energy muon neutrino on hitting the ice leads to the production of highly boosted, long-lived muon events *via* a CC interaction. The Cherenkov radiation emitted by this long-lived muon is referred to as a ‘track’. High energy muons can travel several kilometres in the ice; thus, they leave a track like signature in the detector volume. As the muon moves through the ice, its energy gets depleted, and the Cherenkov light decreases in brightness with time. The energy of the incoming muon neutrino is reconstructed by measuring the brightness of these tracks. However, on the

increasing the energy, the track length and energy loss of the muons increases, *i.e.*, $dE/dx \propto E$. As such, the muons cannot be contained inside the detector leading to poor energy estimation of high energy track events. On the other hand, due to the known starting and ending direction of the Cherenkov cone in the detector, the arrival direction of the muon tracks are reconstructed with higher precision, *i.e.*, the uncertainty in the arrival direction is around 1 degree for neutrino energy greater than 100 TeV.

Cascades:

Electron neutrino may interact with the IceCube *via* CC interaction, generating a high energy electron. Electron losses energy more rapidly than a muon predominantly *via* bremsstrahlung and gives rise to electromagnetic showers. All the flavours of neutrinos can lead to hadronic showers *via* an NC interaction. Due to the large spacing between the strings, electronic showers cannot be distinguished from the hadronic ones, as both lead to almost spherical spreading of light called a cascade. As the cascade events are contained within the detector, their energy is well estimated as compared to muon track events. The Cherenkov light has more intensity in the arrival direction, which leads to a bulge in this direction and this deviation from perfect spherical distribution leads to an estimation of arrival direction. However, the resolution of the arrival direction has more uncertainty, *i.e.*, 10-15 degrees for neutrino energy greater than 200 TeV, which is much greater as compared to the track events.

Taus:

Tau neutrino *via* CC interaction yields a tau which decays to produce either a hadronic shower (66% of times), or an electromagnetic shower (17% of time) or a muon track (17% of times). The tau neutrino, after hitting the ice first produces a hadronic shower and a tauon. The produced tau leads to a track and finally decays to produce another cascade. This leads to two cascades separated by a track signature called the ‘double bang’ event.

Instead, if the first cascade happens to be outside the fiducial volume of the detector, this is called an inverted lollipop event. Instead of a cascade, if the tau decays to a muon, this leads to a track after the first shower, which is called a lollipop event. The resolution of the two separate showers, or a shower and a track happens only at higher energy. For neutrino energy \sim PeV, the two cascades are separated at about a distance of 50 m. Thus lower energy tau events have two cascades overlapping with each other and are rather indistinguishable from the electron events. Similarly, the taus decaying into muons give tracks and are confused with muon tracks.

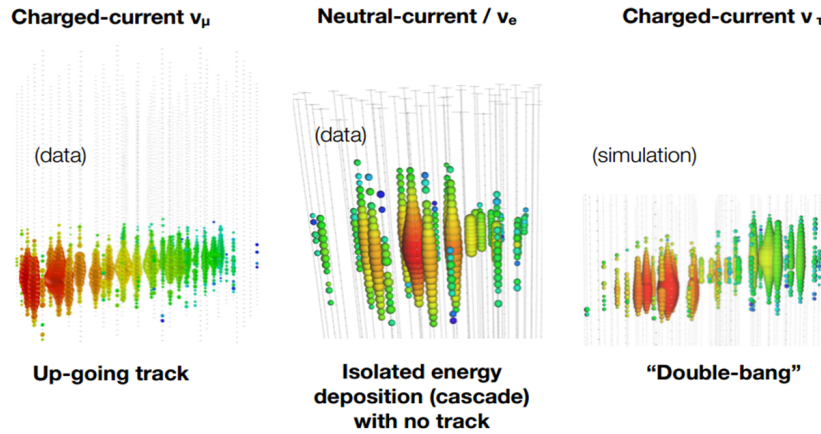


Figure 2.9. Track, cascade and double-bang signals at IceCube. (Figure courtesy: Ref. [203].)

2.7.3 IceCube Observations

The astrophysical neutrino reaching the detector is accompanied by cosmic rays, high energy muons and atmospheric neutrinos. The flux of the atmospheric neutrinos fall very steeply with respect to energy in comparison to astrophysical neutrino flux, *i.e.*, $\phi_{atm} \propto E^{-3.7}$; hence after ~ 60 TeV, the astrophysical neutrinos dominate over the atmospheric background [197]. To distinguish it from the other particles hitting the detector and giving Cherenkov radiation, IceCube typically observes HESE and throughgoing events discussed below

Throughgoing Muon Tracks:

The neutrinos coming from the northern sky have to go through the Earth before reaching the detector. Hence, the Earth acts as a filter for the cosmic rays and muons prohibiting them from reaching the detector, and only the high energy muon neutrinos can get through. These events are called throughgoing track events. The flux from the throughgoing events for the last 9.5 years, *i.e.*, May 2009 to December 2018 can be given as $d\Phi/dE = (1.44_{-0.24}^{+0.25}) (E/100 \text{ TeV})^{-2.28_{-0.09}^{+0.08}} \times 10^{-18} \text{ GeV}^{-1} \text{ cm}^{-2} \text{ s}^{-1} \text{ sr}^{-1}$ [204]. The flux has become softer than the six-year analysis, where the spectral index was 1.91 ± 0.20 [205].

High Energy Starting Events (HESE):

The particles coming from the southern sky have to pass through 1500 m of ice to reach the detector. The high energy muons get through the entire length of the ice, emitting Cherenkov radiation to reach IceCube. To differentiate them from the high energy neutrinos, only the events starting within the fiducial volume of the detector are considered. These events are generated when neutrinos interact with the ice *via* NC or CC interactions. They are called High Energy Starting Events (HESE). They include both cascades as well as tracks. The flux of the HESE for 7.5 years from 2010-2017 is given by $d\Phi/dE = (6.45_{-0.46}^{+1.46}) (E/100 \text{ TeV})^{-2.89_{-0.14}^{+0.20}} \times 10^{-18} \text{ GeV}^{-1} \text{ cm}^{-2} \text{ s}^{-1} \text{ sr}^{-1}$ [207]. The spectral index is not very different from the six-year HESE IceCube analysis, $\Gamma = 2.87_{-0.19}^{+0.20}$ [205, 206].

Most of the high energy neutrino events are observed below 250 GeV, with only a few events in the range of 500 TeV to 1 PeV. This leads to the soft spectral index of 2.89. Till date IceCube has reported observations of five events at energies above a PeV : 1) Bert with energy 1 PeV, 2) Ernie, 1.1 PeV, 3) BigBird, 2 PeV, 4) High Energy track, 2.6 PeV and 5) Hydrangea, 5.9 PeV. Bert, Ernie and BigBird are contained cascade events, and Hydrangea is an uncontained cascade event [208].

In addition to these events, the IceCube collaboration is developing

samples in which they explore uncontained cascade events for HESE and very high energy (VHE) events. VHE events have an energy range from around 10 PeV to EeV. This is done to explore Glashow events around 6.3 PeV at IceCube [20]. The highest energy event of this sample, *i.e.*, Hydrangea, is the promising candidate of the Glashow event. The number of expected Glashow events depends greatly on the spectral index and cut-off of the flux. For a spectral index of 2.2, the number of events varies from around 6 to 9 for cut-off energy of 2.2 PeV to 100 PeV respectively [20]. Hence, the behaviour of the astrophysical neutrino spectrum can be understood by the observations or paucity of Glashow events. With the increase in data, with time and detector size, the number of Glashow events can be known with better accuracy.

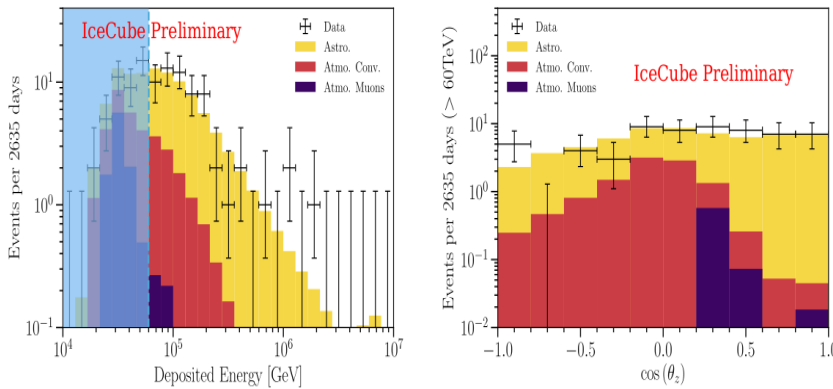


Figure 2.10. Left panel: Number of events vs. neutrino energy; Right panel: Number of events vs. cosine of declination angle observed in 7.5 years at IceCube. (Figure courtesy: Ref. [207].)

Double Cascade Events:

Tau neutrinos, as discussed earlier, give rise to two cascades separated by a track which is difficult to resolve below neutrino energy \sim PeV. According to the IceCube analysis, only one event which is most likely a double cascade event is observed [209]. It has a total energy of 89 TeV, with the first cascade energy of 9 TeV and the second cascade has the energy of 80 TeV. Both the cascades are separated by 17 m.

Flavour Ratio:

Along with the energy dependence of the flux, the observations of the high energy neutrinos lead to the estimation of the flavour ratio of neutrinos $\nu_e : \nu_\mu : \nu_\tau$ at earth. In the last 7.5 years, IceCube has observed 41 cascades, 17 tracks and 2 double cascade candidate events above 60 TeV, out of the total of 102 events above 20 TeV. Using the candidate tau neutrino events, the best fit for the flavour ratio has shifted to $(0.29 : 0.50 : 0.21)$ [209, 210], in contrast to $(0.5 : 0.5 : 0)$ as obtained from the 6 year analysis with no candidate ν_τ events [205]. The low energy degeneracy of ν_τ and ν_e , leads to large uncertainty in the flavour ratio, as shown in fig. 2.11. (Anti)Neutrinos produced *via* charged pion decay with initial flavour ratio of $(1 : 2 : 0)$ and damped muon decay with initial flavour ratio of $(0 : 1 : 0)$ are still allowed by the IceCube data. However, the neutrinos produced dominantly by neutron decay, with initial flavour ratio $(1 : 0 : 0)$, is excluded by 2σ in the case of standard neutrino oscillations. Following eq. (1.18) from the **first** chapter, the final flavour ratio at the detector for charged pion, damped muon and neutron decay are $(0.30 : 0.36 : 0.34)$, $(0.17 : 0.45 : 0.37)$ and $(0.55 : 0.17 : 0.28)$ respectively. The increase in the number of observations will lead to a decrease in the uncertainties in the flavour ratio, making any deviation from the standard scenario very evident [211]. Such a deviation may imply the presence of new physics.

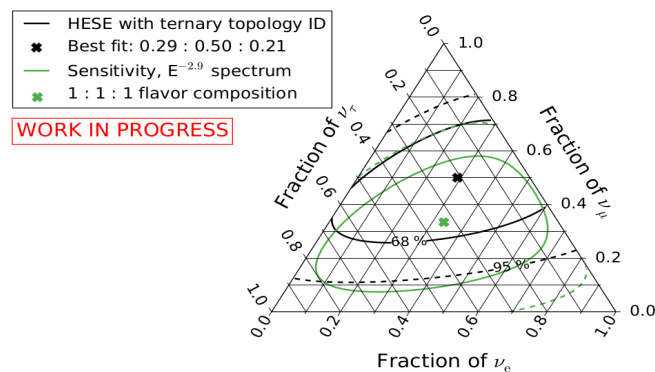


Figure 2.11. Flavour ratio allowed by 68%, 95% CL given by solid and dashed black line respectively after including a tau neutrino event. (Figure courtesy: Ref. [209].)

Neutrino Nucleon Cross-Section:

The throughgoing muon neutrinos cross the Earth to reach IceCube. Hence, they get attenuated on their way, depending on their zenith angle. IceCube collaboration used these events to constrain the neutrino-nucleon interaction at high energies from 6.3–980 TeV, using the data from 2009–2010. The best fit of the analysis preferred 1.3 times the cross-section predicted by the standard model. But the SM cross-section is allowed within 2σ confidence [212]. Bustamante et al. [213] constrained the neutrino-nucleon cross-section using six years of HESE data for energy range 18 TeV to 2 PeV at IceCube. They showed that the flux preferred the soft spectral index of around 2.4 [213]. Since the arrival direction of cascade events has larger uncertainty, the cross-section using such events had more uncertainty than track events. Further, IceCube collaboration used 7.5 years of HESE to constrain the neutrino-nucleon cross-section [214, 215]. The results from both the analysis, do not show any abrupt rise of cross-section, and the data still agree with the SM prediction within 1σ CL.

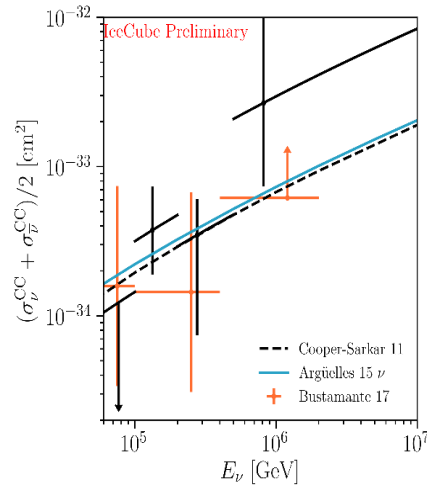


Figure 2.12. Neutrino-nucleon cross-section vs. neutrino energy for 7.5 years and 6 years of HESE IceCube data given by black and orange error bars up to 1σ CL respectively. (Figure courtesy: Ref. [214].)

Observation of blazar coincident event from TXS 0506+056:

On September 22, 2017, IceCube observed a muon neutrino event, IC-170922A, of energy 290 TeV. Within 1 min of this observation, an automatic alert was communicated worldwide to facilitate multi-messenger astronomy. The Fermi-LAT detected an excess of gamma rays from the direction of arrival pointed out by the muon neutrino event. Further, Major Atmospheric Gamma Imaging Cherenkov Telescopes (MAGIC) as well observed 400 GeV of gamma-ray events from the same direction within 24 hours of an alert [155]. These observations point out that the TXS 0506+056 is the source of the neutrino event with 3σ confidence. This observation is the first to point out the hadronic mode of the AGN emission, as neutrinos can only be produced by the hadrons in such sources. Such observations will help us to understand the mechanism at work for the production of high energy particles at AGNs. This marks the new era of multimessenger astronomy. Apart from astronomy, this event puts constraint on neutrino-DM interactions [216, 217].

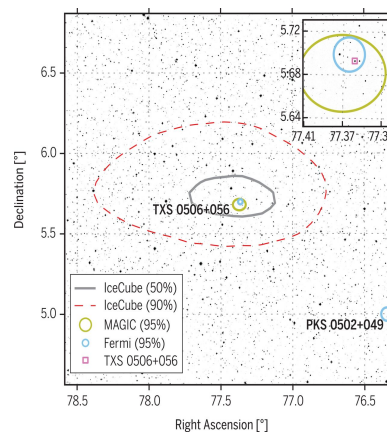


Figure 2.13. IC-170922A 50% and 90% containment regions given by grey and red dashed lines respectively. Regions of high energy gamma ray excess seen at MAGIC and Fermi LAT shown by the yellow and blue lines respectively. (Figure courtesy: Ref. [155].)

IceCube data were analysed for astrophysical neutrino events coming from this direction, and it was found that for a period of September 2014 and March 2015, there has been an excess in the number of events, with

3.5σ confidence, above the atmospheric background [218]. The number of events coming from this direction with this period is 13 ± 5 . Fig. 2.14 shows the IceCube observations from the region of IC-170922A from the duration of May 2008 to October 2017.

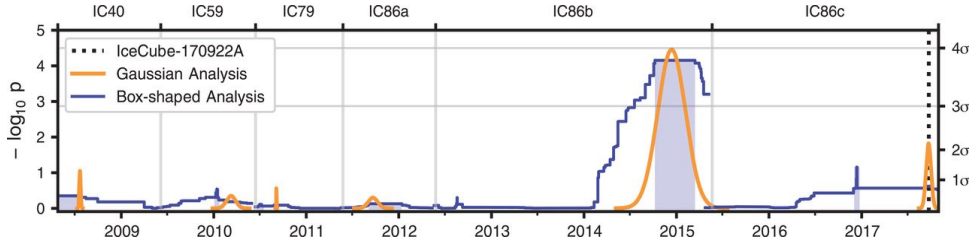


Figure 2.14. IceCube observations from the direction of TXS 0506+056 from 5th April, 2008 to 31st October, 2017. (Figure courtesy: Ref. [218].)

Critical look at IceCube Data: Expectations vs. Observations

A few important points evident from the IceCube observations from the last 7.5 years are:

(i) IceCube has observed 60 neutrino events with energy $E \gtrsim 60$ TeV, out of the total of 102 events above 20 TeV [219], with no events after a few PeV. Most of the events lie below 250 TeV, and very few events are between 400 TeV to PeV. This has been suggested in the literature as a possible gap or a dip in the observed spectrum of astrophysical neutrinos [220–222]. Moreover, the steep fall in the flux suggests a cut-off after a few PeV. With more data over time, these features may turn out to be statistically significant.

(ii) Cosmogenic neutrinos, which are guaranteed due to the interactions of ultra-high energy cosmic rays with the cosmic microwave background (CMB) photons, have not been observed yet. This rules out many models of cosmogenic neutrinos as well as other astrophysical sources which predict substantial flux above ~ 5 PeV [223]. Moreover, due to the resonant interactions of $\bar{\nu}_e$ with the electrons present in the detector *via* the W boson, an excess of events at $E \sim 6.3$ PeV is expected at IceCube within the standard model [17–19]. Such Glashow events might be observed in

astrophysical neutrino spectrum anytime soon [20].

(iii) As it was mentioned earlier, only one high energy neutrino source has been identified by IceCube: the blazar. But the overall non-observation of events with $E \gtrsim \text{PeV}$ suggests that the models of active galactic nuclei (AGN) which predict substantial neutrino flux above a few PeV might be ruled out from the present observations [149].

(iv) The puzzle is further accentuated by an excess of events at energies between 40–160 TeV [184], when one considers a power law of $E^{2-2.2}$ favoured by pp process of ν production.

(iv) The number of double bang events was expected to be 2 [224]. IceCube has observed two candidate ν_τ events, with 76% and 98% probability of them being ν_τ [210]. With more data, if any deviation in the number of ν_τ events is confirmed, it would clearly point towards new physics.

2.8 ANTARES

The ANTARES detector is built in the Mediterranean Sea, 40 km offshore of Toulon, France. It is built around 2.47 km beneath the sea and is one-tenth the volume of IceCube. It is a Cherenkov detector with an angular resolution of 4 degrees for shower events and 0.4 degrees for track event above 10 TeV. In nine years of observations, from 2007 to 2015 of the upgoing events, it has observed 19 track events with a background estimation of 13.5 ± 4 and 14 shower events with background estimation of 10.5 ± 4 in the energy range of 100 GeV to PeV. The observed diffused flux is in agreement with IceCube [225].

ANTARES, due to its location in the northern hemisphere, is suitable for the detection of neutrinos from the Galactic Centre and Southern sky. From the southern sky, the neutrinos pass through the Earth; hence there is less background from below the horizon. In collaboration with the IceCube, there have been attempts to search for neutrino point sources by taking into account the data from both experiments. Though the sensitivity to source improved by a factor of 2 in comparison to individual searches, no source

of astrophysical neutrinos was identified [226].

2.9 ANITA

Antarctic Impulsive Transient Antenna or ANITA is a balloon-borne experiment flying around 35–40 km above the Antarctic ice [227]. It is exposed to about a million of km³ of Antarctic Ice and is sensitive to neutrinos of energy greater than \sim EeV. ANITA consists of a series of radio antennas and when very high energy neutrinos interact with the nucleons in the ice or atmosphere they radiate Cherenkov radiation which is detected by the ANITA experiment.

Till date, ANITA has observed 3 events of around EeV energy [228, 229]. At these energies, due to large neutrino-nucleon cross-section, the mean free path of tau neutrinos through the Earth is around 290 km [230]; therefore, such neutrinos get absorbed before reaching the detector. Hence, detecting such high energy events is anomalous. Two of the observed EeV events at ANITA are anomalous as they travel through the ice and reach ANITA. The anomalous events cross 5740 ± 60 km and 7210 ± 55 km with energy 0.6 ± 0.4 EeV and $0.56^{+0.30}_{-0.20}$ EeV respectively. The third event came from the southern sky and had energy greater than 10 EeV.

2.10 Future Detectors

In addition to the existing high energy neutrino detectors, there are powerful upcoming neutrino detectors which will take neutrino astronomy to the next level. IceCube itself is going to be upgraded with its first upgrade to be undertaken in the Antarctic summers of 2022–2023. This upgraded version of IceCube will be called IceCube Upgrade which will be the testing ground of a much larger detector to be built, *i.e.*, IceCube-Gen2. Further ANTARES will be upgraded to KM3NeT which will be operational in the northern hemisphere. The upcoming experiments, Baikal-GVD and

GRAND, are being constructed in Russia and China, respectively. The future neutrino telescopes are briefly described as:

2.10.1 IceCube Upgrade and IceCube-Gen2

In around 2022, 7 new strings with 700 additional optical sensors, with a vertical spacing of 3 m, will be established in the DeepCore between 2150 m and 2425 m from the surface [231]. This will remarkably reduce the energy threshold above which neutrinos can be detected to $\sim \mathcal{O}$ (1–10) GeV. The detection of the photons will be improved by the inclusion of new devices like Dual optical sensors and Multi-PMT Digital Optical Module (mDOM) [232, 233]. This upgrade will improve the neutrino oscillation measurements, tau neutrino appearance observations and dark matter indirect detection bounds. IceCube Upgrade uses the optical sensors and mDOM, which are to be used in IceCube-Gen2, a much larger avatar of IceCube; hence it also serves in testing and calibrating these new devices.

IceCube-Gen2 is proposed to be a ten km³ neutrino detector with an array of optical strings placed at a separation of 250 m, twice the distance between present IceCube strings [234]. This is done to decrease the cost and increase the number of neutrino events. Present IceCube has observed only one candidate tau neutrino event and Glashow event each in the last 10 years. However, with the increase in the size of the detector, the number of events should increase to one event per year. Also, as the size of the detector increases, very high energy tracks and cascades can be contained in the detector, and this increases our sensitivity to GZK and Glashow events even more. With the increase in the number of events, the uncertainty in the flux will come mainly from systematics.

PINGU is proposed to be the part located at the centre of IceCube-Gen2, which consists of 60 DOMs with a horizontal spacing of around 5 m between two strings. PINGU shall reduce the threshold for observation of atmospheric neutrinos to 1 GeV, and will be used in the exploring neutrino mass ordering problem.

2.10.2 KM3NeT

KM3NeT will be around a cubic km array of optical sensors in the Mediterranean Sea, which will be consisting of two parts Astroparticle Research with Cosmics in Abyss (ARCA) and Oscillation Research with Cosmics in the Abyss (ORCA) [194]. The ARCA array will be 100 km offshore of Italy, and its main function will be to study diffused astrophysical neutrinos, whereas the ORCA will be 40 km offshore of France, which will focus on neutrino mass ordering. Three ARCA strings and one ORCA string have already been established in the detector. When completed, ARCA would consist of 115 strings with a height of 700 m spread in a square km area and ORCA will have six strings with a horizontal distance of 20 m and 140 m height.

KM3NeT will be able to confirm the diffuse flux seen by IceCube within a year of its operation, and due to its location in the Northern Hemisphere [235], it will be able to explore the sources of neutrino flux in partnership with IceCube. For neutrino energy greater than 100 TeV, its angular resolutions are 0.1 degree and 2 degree for track and shower events respectively, which are much better than the present IceCube detector [235].

2.10.3 Baikal-GVD

Baikal Gigaton Volume Detector (Baikal-GVD) is being built in Lake Baikal, Russia [236]. A smaller cluster with 192 optical modules was deployed in 2015 by the name of Dubna. This cluster was upgraded with the deployment of more optical modules in 2016 and 2017. After the upgrade in April 2018, Baikal GVD has a total of 846 optical modules arranged in 24 strings. By 2020-2021 Baikal GVD will have a volume of 0.4 km³. The completed detector will have a volume of 2 km³.

Baikal GVD has observed 23 atmospheric events with a background of 6 in the year 2016. The detector has searched for astrophysical cascade events for observations between April 2016 and January 2017. Within this

time it has observed around 5 events above 100 TeV. Due to its location in the Northern Hemisphere, the detector can observe the sources in the southern sky pretty well [236].

2.10.4 GRAND

Giant Radio Array for Neutrino Detection (GRAND) is proposed to be constructed as a huge array of antennae covering up an area around 20,000 km² around China [237]. These antennae will detect radio signals given out extensive air showers produced when very high energy cosmic rays, gamma rays or neutrinos interact with the rocks or atmosphere. Its energy threshold will be 100 PeV. Tau neutrinos are expected to be the most dominant detection channel for neutrinos at GRAND. As the mean interaction length of EeV tau neutrino at earth is 290 km, only the neutrinos glancing the Earth can reach the detector. The detection is based on the emission of extensive air shower emitted due to the decay of tau produced when initial tau neutrino interacts with the Earth. These air showers produce the radio signal, which will be detected by the GRAND detector.

Currently, GRANDProto35, consisting of 35 antennae, are being deployed in the Tian Shan, China. Around the year 2020, the deployment of 300 antennas will be done followed by 10000 antennas till 2025, and finally, the completion is expected in 2030 when 2,00,000 km² of the area will be instrumented making GRAND the largest detector in the world.

IceCube vs. KM3NeT: Future Prospects

The observation of the TXS 0506+056 neutrino event, starts the era of neutrino astronomy. In the future, both IceCube Upgrade and KM3NeT would have an improved potential of discovering new point sources of cosmic neutrinos. Further, the upcoming telescopes will lead to stronger constraints on many proposed neutrino fluxes compared to present IceCube constraint, discussed in Sec. 2.4.1. Owing to more sensitive detectors at IceCube-Gen2,

the angular resolution of the cascade events are improved from 10 – 15 degrees to around 5 degree, above 200 TeV. At the same time, the resolution for KM3NeT ARCA is less than 2 degrees for cascades. For tracks at energy greater than 100 TeV, IceCube-Gen2 (ARCA) has a resolution less than 1 (0.1) degree, which will lead to a better probe for sources [238]. For the discovery of a point source, the neutrino signal should be greater than the background, mainly consisting of muons and atmospheric neutrinos. The discovery potential refers to a statistically significant excess from a point source, *e.g.*, a 5σ discovery potential for the sources with E^{-2} neutrino flux, is shown in the right plot of fig. 2.15. The sensitivity, which is shown in the left plot of fig. 2.15, is the upper limit of the allowed neutrino flux with 90% CL. As can be seen from the figure, both the discovery potential and sensitivity of the KM3NeT/ARCA is an order of magnitude better than IceCube for the southern sky and rather competing for northern sky [239].

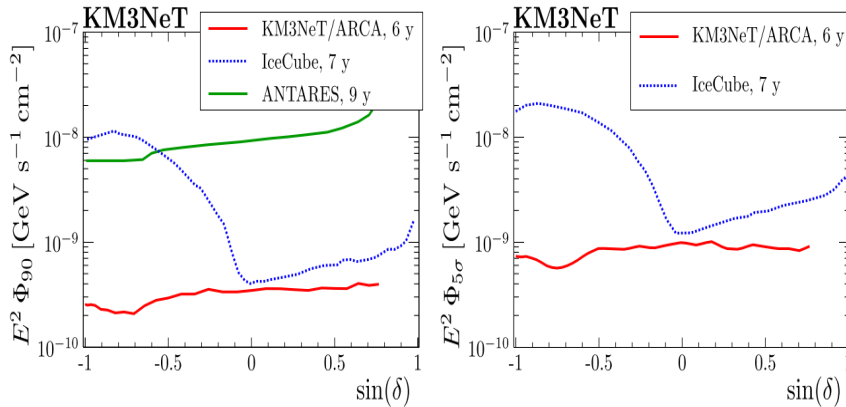


Figure 2.15. Left plot represents the sensitivities of the detectors at 90 percent CL. The right plot represents the discovery potential for the sources [239].

From the fig. 2.16 it can be seen that IceCube-Gen2 with 15 years of running time can improve the sensitivity of IceCube by a factor of around 4.5. But still, KM3NeT is more sensitive than IceCube-Gen2 when it comes to pinpointing the sources of cosmic neutrinos in the northern sky.

The IceCube Upgrade with 7 additional strings and more sensitive detectors at DeepCore, decreases the threshold of the lower energy neutrinos. By the time of its deployment 2022–2023 [240], KM3NeT/ORCA will reach

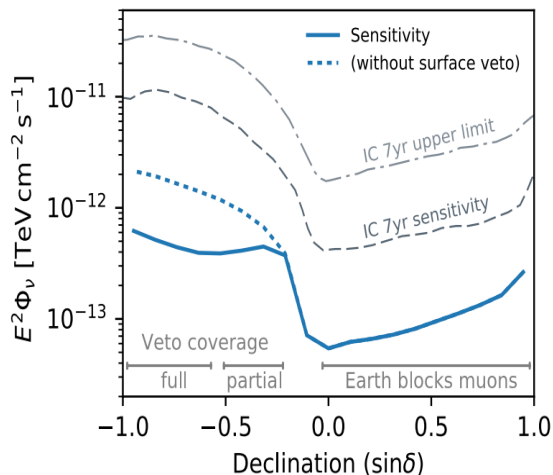


Figure 2.16. The blue solid, dashed lines represent the sensitivity and discovery potential for IceCube-Gen2 after 15 years of running. (Figure courtesy: Ref. [241].)

its completion in 2023 [242]. Both IceCube Upgrade and KM3NeT/ORCA will lead to a better measurement of oscillation parameters, tau normalisation and mass ordering. Tau normalisation is defined as the ratio of measured ν_τ events to expected ν_τ events. By observing the disappearance of ν_μ , in the throughgoing events, and attributing the resulting cascade events to ν_τ , the neutrino telescopes measure tau normalisation. The expected uncertainty in the tau normalisation for IceCube Upgrade is estimated to be 13% after three years of running at 90% CL [240]. Whereas, ORCA estimate of tau normalisation uncertainty to be around 20% at 3σ after one year [242]. Also, as the atmospheric ν_μ pass through the Earth matter, the probability of oscillation is very different from vacuum oscillations. This helps to uncover the mass ordering of the neutrinos. Using atmospheric neutrinos, IceCube is expected to reveal the mass ordering with $\sim 3\sigma$ CL in 3-8 years, and ORCA will reach $3-6\sigma$ CL in 3 years of its running [224]. Thus IceCube Upgrade and IceCube-Gen2 are competitive with both ARCA and ORCA, and the combined measurements from these experiments are expected to improve our understanding of neutrino oscillations and astrophysical sources.

Interactions of Astrophysical Neutrinos with Dark Matter: A model building perspective

IceCube has been designed to detect high energy astrophysical neutrinos of extragalactic origin. As discussed in the previous chapter, beyond neutrino energies of ~ 20 TeV the background of atmospheric neutrinos get diminished and the neutrinos of higher energies are attributed to extragalactic sources [243]. However, there is a paucity of high energy neutrino events observed at IceCube for neutrino energies greater than ~ 400 TeV [244]. There are a few events around ~ 1 PeV or higher, whose origin perhaps can be described by the decay or annihilation of very heavy new particles [186, 190, 245–250] or even without the help of any new physics [149, 251, 252]. In the framework of standard astrophysics, high energy cosmic rays of energies up to 10^{20} eV have been observed, which leads to the prediction of the existence of neutrinos of such high energies as well [141, 142, 253]. In this context, it is worth exploring whether the flux of such neutrinos can get altered due to their interactions with DM particles. However, it is challenging to build such models given the relic abundance of dark matter. Few such attempts have been made in literature but these models also suffer from cosmological and collider constraints. Hence, in this chapter, we take a model building perspective to encompass a large canvas of such interactions that can lead to appreciable flux suppression at IceCube. The results presented in this chapter are based on ref. [254].

In presence of neutrino-DM interaction, the flux of astrophysical neutrinos passing through isotropic DM background is attenuated by a factor $\sim \exp(-n\sigma L)$. Here n denotes number density of DM particles, L is the distance traversed by the neutrinos in the DM background and σ represents the cross-section of neutrino-DM interaction. The neutrino-DM interaction can produce appreciable flux suppression only when the number of interactions given by $n\sigma L$ is $\gtrsim \mathcal{O}(1)$. For lower masses of DM, the number density is significant. But the cross-section depends on both the structure of the neutrino-DM interaction vertex and the DM mass. The neutrino-DM cross-section might increase with DM mass for some particular interactions. Hence, it is essentially the interplay between DM number density and the nature of the neutrino-DM interaction, which determines whether a model leads to a significant flux suppression. As a pre-filter to identify such cases we impose the criteria that the interactions must lead to at least 1% suppression of the incoming neutrino flux. For the rest of the chapter, a flux suppression of less than 1% has been addressed as ‘not significant’. While checking an interaction against this criteria, we consider the entire energy range of the astrophysical neutrinos. If an interaction leads to 1% change in neutrino flux after considering the relevant collider and cosmological constraints in any part of this entire energy range, it passes this empirical criteria. We explore a large range of DM mass ranging from sub-eV regimes to WIMP scenarios. In the case of sub-eV DM, we investigate the ultralight scalar DM which can exist as a Bose-Einstein condensate in the present Universe.

In general, various aspects of the neutrino-DM interactions have been addressed in the literature [91, 92, 255–261]. The interaction of astrophysical neutrinos with cosmic neutrino background can lead to a change in the flux of such neutrinos as well [220, 221, 262–268]. But it is possible that the dark matter number density is quite large compared to the number density of the relic neutrinos, leading to more suppression of the astrophysical neutrino flux.

To explore large categories of models with neutrino-DM interactions,

we take into account the renormalisable as well as the non-renormalisable models. In case of non-renormalisable models, we consider neutrino-DM effective interactions up to dimension-eight. However, it is noteworthy that for a wide range of DM mass the centre-of-mass energy of the neutrino-DM scattering can be such that the effective interaction scale can be considered to be as low as ~ 10 MeV. We discuss relevant collider constraints on both the effective interactions and renormalisable models. We consider thermal DM candidates with masses ranging in MeV–TeV range as well as non-thermal ultralight DM with sub-eV masses. For the thermal DM candidates, we demonstrate the interplay between constraints from relic density, collisional damping and the effective number of light neutrinos on the respective parameter space. Only for a few types of interactions, one can obtain significant flux suppressions.

In Sec. 3.1 we discuss the nature of the DM candidates that might lead to flux suppression of neutrinos. In Sec. 3.2 we present the non-renormalisable models, *i.e.*, the effective neutrino-DM interactions categorised into four topologies. In Sec. 3.3 we present three renormalisable neutrino-DM interactions and the corresponding cross-sections in case of thermal as well as non-thermal ultralight scalar DM. Finally in Sec. 3.4 we summarise our key findings.

3.1 Dark Matter Candidates

In this section, we systematically narrow down the set of DM candidates we are interested in considering a few cosmological and phenomenological arguments.

As mentioned in Sec. 1.8.2, the Lambda cold dark matter (Λ CDM) model explains the anisotropies of cosmic microwave background quite well. The weakly interacting massive particles are interesting candidates of CDM, mostly because they appear in well-motivated BSM theories of particle physics. Nevertheless, CDM with sub-GeV masses are also allowed. The

most stringent lower bound on the mass of CDM comes from the effective number of neutrinos (N_{eff}) implied by the CMB measurements from the Planck satellite. For complex and real scalar DM as well as Dirac and Majorana fermion DM, this lower bound comes out to be ~ 10 MeV [91, 92]. Thermal DM with masses lower than ~ 10 MeV are considered hot and warm DM candidates and are allowed to make up only a negligible fraction of the total dark matter abundance [269]. The ultralight non-thermal Bose-Einstein condensate dark matter with mass $\sim 10^{-21} - 1$ eV is also a viable cold dark matter candidate [270]. In the rest of this chapter, unless mentioned otherwise, by ultralight DM we refer to the non-thermal ultralight BEC DM. As discussed in Sec. 1.8.2, ultralight DM form BEC at an early epoch and acts like a “cold” species in spite of their tiny masses [271]. Numerous searches of these kinds for DM are underway, namely ADMX [272], CARRACK [273] etc. It has been recently proposed that gravitational waves can serve as a probe of ultralight BEC DM as well [274]. But the ultralight fermionic dark matter is not a viable candidate for CDM, because it can not form such a condensate and is, therefore “hot”. The case of ultralight vector dark matter also has been studied in the literature [275].

The scalar DM can transform under $SU(2)_L$ as a part of any multiplet. In the case of a doublet or higher representations, the DM candidate along with other degrees of freedom in the dark sector couple with W^\pm, Z bosons at the tree level. This leads to stringent bounds on their masses as light DM candidates can heavily contribute to the decay width of SM gauge bosons, and hence, are ruled out from the precision experiments. Moreover, Higgs-portal WIMP DM candidates with $m_{\text{DM}} \ll m_h/2$ are strongly constrained from the Higgs invisible decay width as well. The failure of detecting DM particles in collider searches and the direct DM detection experiments rule out a vast range of parameter space for WIMPs. In light of current LUX and XENON data, amongst low WIMP DM masses, only a narrow mass range near the Higgs funnel region, *i.e.*, $m_{\text{DM}} \sim 62$ GeV, survives [276–278]. As alluded to earlier, the ultralight scalar DM can transform only as a singlet under $SU(2)_L$ because of its tiny mass.

We investigate the scenarios of scalar dark matter, both thermal and ultralight, as possible candidates to cause flux suppression of the high energy astrophysical neutrinos. Such a suppression depends on the length of the path the neutrino travels in the isotropic DM background and the mean free path of neutrinos, which depends on the cross-section of neutrino-DM interaction and the number density of DM particles. We take the length traversed by neutrinos to be ~ 200 Mpc, the distance from the nearest group of quasars [279], which yields a conservative estimate for the flux suppression. Moreover, we consider the density of the isotropic DM background to be $\sim 1.2 \times 10^{-6}$ GeV cm $^{-3}$ [280]. Comparably, in the case of WIMP DM, the number density is much smaller, making it interesting to investigate whether the cross-section of neutrino-DM interaction in these cases can be large enough to compensate for the smallness of DM number density. This issue will be addressed in a greater detail in Sec. 3.3.3.

3.2 Effective Interactions

In order to exhaust the set of higher dimensional effective interactions contributing to the process of neutrino scattering off scalar DM particles, we consider four topologies of diagrams representing all the possibilities as depicted in fig. 3.1. Topology I represents a contact type of interaction. In case of topologies II, III, and IV we consider higher dimensional interaction in one of the vertices while the neutrino-DM interaction is mediated by either a vector, a scalar or a fermion, whenever appropriate.

$\nu\bar{\nu}$ DM DM effective interactions can arise from higher dimensional gauge-invariant interactions as well. In this case, the bounds on such interactions may be more restrictive than the case where the mediators are light and hence, are parts of the low energy spectrum. In general low energy neutrino-DM effective interactions need not reflect explicit gauge invariance.

We discuss the bounds on the effective interactions based on LEP

monophoton searches and the measurement of the Z decay width. The details of our implementation of these two bounds are as follows:

- **Bounds from LEP monophoton searches**

For explicitly gauge-invariant effective interactions, $\nu\bar{\nu}$ DM DM interactions come along with l^+l^- DM DM interactions. e^+e^- DM DM interactions can be constrained from the channel $e^+e^- \rightarrow \gamma + \cancel{E}_T$ using FEMC data at DELPHI detector in LEP for $190 \text{ GeV} \leq \sqrt{s} \leq 209 \text{ GeV}$. To extract a conservative estimate on the interaction, we assume that the new contribution saturates the error in the measurement of the cross-section $1.71 \pm 0.14 \text{ pb}$ at 1σ [281]. By the same token, we consider only one effective interaction at a time. The corresponding kinematic cuts on the photon at the final state were imposed in accordance with the FEMC detector: $20.4 \leq E_\gamma$ (in GeV) ≤ 91.8 , $12^\circ \leq \theta_\gamma \leq 32^\circ$ and $148^\circ \leq \theta_\gamma \leq 168^\circ$. Here E_γ stands for the energy of the outgoing photon and θ_γ is its angle with the beam axis. We use `FeynRules-2.3.32` [282], `CalcHEP-3.6.27` [283] and `MadGraph-2.6.1` [284] for computations.

Although here we considered gauge-invariant interactions, $\nu\bar{\nu}$ DM DM interactions can be directly constrained from the monophoton searches due to the existence of the channel $e^+e^- \rightarrow \gamma\nu\bar{\nu}$ DM DM *via* a Z boson. But such bounds are generally weaker than the bounds obtained from Z decay which we are going to consider next.

$\mu^+\mu^-$ DM DM interactions can contribute to the muon decay width which is measured with an error of $10^{-4}\%$. However, the partial decay width of the muon *via* $\mu \rightarrow \nu_\mu e^- \bar{\nu}_e$ DM DM channel is negligible compared to the error. Hence, these interactions are essentially unbounded from such considerations. The percentage error in the decay width for tauon is even larger and hence, the same is true for $\tau^+\tau^-$ DM DM interactions.

- **Bounds from the leptonic decay modes of the Z -boson**

The effective $\nu\bar{\nu}$ DM DM interactions can be constrained from the invisible decay width of the Z boson which is measured to be $\Gamma(Z \rightarrow$

$inv) = 0.48 \pm 0.0015$ GeV [280]. When the gauge-invariant forms of such effective interactions are taken into account, l^+l^- DM DM interactions may be constrained from the experimental error in the partial decay width of the channel $Z \rightarrow l^+l^-$: $\Delta\Gamma(Z \rightarrow l^+l^-) \sim 0.176, 0.256, 0.276$ MeV for $\ell = e, \mu, \tau$ at 1σ [280]. To extract conservative upper limits on the strength of such interactions, one can saturate this error with the partial decay width $\Gamma(Z \rightarrow l^+l^- \text{ DM DM})$.

If such interactions are mediated by some particle, say a light Z' , then a stringent bound can be obtained by saturating $\Delta\Gamma(Z \rightarrow l^+l^-)$ with $\Gamma(Z \rightarrow l^+l^- Z')$. Similar considerations hold true for $Z \rightarrow \nu\bar{\nu}$ DM DM mediated by a Z' . We note in passing that such constraints from Z decay measurements are particularly interesting for light DM candidates.

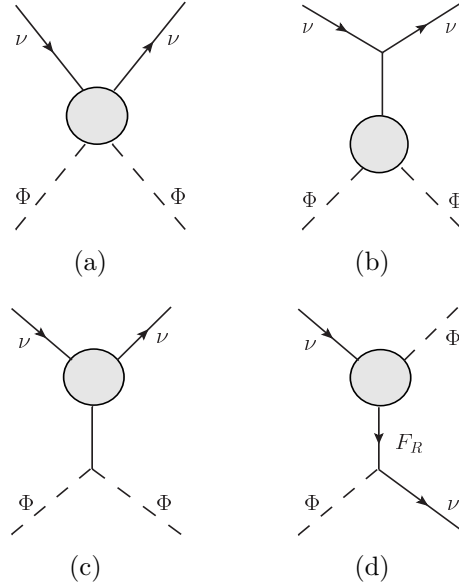


Figure 3.1. Topologies of effective neutrino-DM interactions. Fig. (a), (b), (c) and (d) represent topology I, II, III and IV respectively.

3.2.1 Topology I

In this subsection effective interactions up to dimension 8 have been considered which can give rise to neutrino-DM scattering. The phase space factor for the interaction of the high energy neutrinos with DM can be found in appendix 7.1.1.

1. A six-dimensional interaction term leading to neutrino-DM scattering can be written as,

$$\mathcal{L} \supset \frac{c_l^{(1)}}{\Lambda^2} (\bar{\nu} i \not{\partial} \nu) (\Phi^* \Phi), \quad (3.1)$$

where ν is SM neutrino, Φ is the scalar DM and Λ is the effective interaction scale.

Now, for this interaction, the constraint from Z invisible decay reads $c_l^{(1)}/\Lambda^2 \lesssim 8.8 \times 10^{-3} \text{ GeV}^{-2}$. The bounds from the measurements of the channel $Z \rightarrow l^+ l^-$ are dependent on the lepton flavours, and are found to be: $c_e^{(1)}/\Lambda^2 \lesssim 5.0 \times 10^{-3} \text{ GeV}^{-2}$, $c_\mu^{(1)}/\Lambda^2 \lesssim 6.0 \times 10^{-3} \text{ GeV}^{-2}$ and $c_\tau^{(1)}/\Lambda^2 \lesssim 6.2 \times 10^{-3} \text{ GeV}^{-2}$. The gauge-invariant form of this effective interaction leads to a five-point vertex of $\nu \bar{\nu} \Phi \Phi Z$, which in turn leads to a new four-body decay channel of the Z boson. Due to the existence of such a vertex, the bound on this interaction from the Z decay width reads $c_l^{(1)}/\Lambda^2 \lesssim 9 \times 10^{-3} \text{ GeV}^{-2}$. The electron-DM effective interactions can be further constrained from the measurements of $e^+ e^- \rightarrow \gamma + \cancel{E}_T$, leading to $c_e^{(1)}/\Lambda^2 \lesssim 10^{-4} \text{ GeV}^{-2}$. It can be seen that for the effective interaction with electrons, the bound from the measurement of the cross-section in the channel $e^+ e^- \rightarrow \gamma + \cancel{E}_T$ can be quite stringent even compared to the bounds coming from the Z decay width. Among all the constraints pertaining to such different considerations, if one assumes the least stringent bound, the interaction still leads to only $\lesssim 1\%$ flux suppression. The renormalisable model discussed in Sec. 3.3.1 is one of the scenarios that leads to the effective interaction as in eq. (3.1).

2. Another six-dimensional interaction is given as:

$$\mathcal{L} \supset \frac{c_l^{(2)}}{\Lambda^2} (\bar{\nu} \gamma^\mu \nu) (\Phi^* \partial_\mu \Phi - \Phi \partial_\mu \Phi^*). \quad (3.2)$$

The constraint from the measurement of the decay width in the $Z \rightarrow inv$ channel reads $c_l^{(2)}/\Lambda^2 \lesssim 1.8 \times 10^{-2} \text{ GeV}^{-2}$ for light DM.

The bounds on the gauge-invariant form of the interaction in eq. (3.2) from the measurement of $Z \rightarrow l^+l^-$ reads $c_e^{(2)}/\Lambda^2 \lesssim 1.7 \times 10^{-2} \text{ GeV}^{-2}$, $c_\mu^{(2)}/\Lambda^2 \lesssim 1.2 \times 10^{-2} \text{ GeV}^{-2}$ and $c_\tau^{(2)}/\Lambda^2 \lesssim 1.3 \times 10^{-2} \text{ GeV}^{-2}$. The bound from the channel $e^+e^- \rightarrow \gamma + \cancel{E}_T$ reads $c_e^{(2)}/\Lambda^2 \lesssim 2.6 \times 10^{-5} \text{ GeV}^{-2}$. Even with the value $c_l^{(2)}/\Lambda^2 \sim 10^{-2} \text{ GeV}^{-2}$, such an effective interaction does not give rise to an appreciable flux suppression due to the structure of the vertex.

3. Another five dimensional effective Lagrangian for the neutrino-DM four-point interaction is given by:

$$\mathcal{L} \supset \frac{c_l^{(3)}}{\Lambda} \bar{\nu} c_\nu \Phi^* \Phi. \quad (3.3)$$

The above interaction gives rise to neutrino mass at the loop-level which is proportional to m_{DM}^2 . This, in turn, leads to a bound on the effective interaction due to the smallness of neutrino mass,

$$\frac{c_l^{(3)}}{\Lambda} \lesssim 16\pi^2 \frac{m_\nu}{m_{\text{DM}}^2} \sim 1.6\pi^2 \left(\frac{1 \text{ eV}}{m_{\text{DM}}}\right)^2 \left(\frac{m_\nu}{0.1 \text{ eV}}\right) \text{eV}^{-1}, \quad (3.4)$$

up to a factor of $\mathcal{O}(1)$. In the ultralight regime mass of DM $\lesssim 1 \text{ eV}$. Hence eq. (3.4) does not lead to any useful constraint on $c_l^{(3)}/\Lambda$. The constraint from invisible Z decay on this interaction reads $c_l^{(3)}/\Lambda \leq 0.5 \text{ GeV}^{-1}$, independent of neutrino flavour. The gauge-invariant form of this interaction does not contain additional vertices involving the charged leptons and hence leads to no further constraints. For such a value of coupling, there can be a significant flux suppression for the entire range of ultralight DM mass, independent of the energy of the incoming neutrino as shown in fig. 3.2. On considering the BBN constraints on this interaction, the rate of $\nu\nu \rightarrow \Phi\Phi$ at temperature $\sim 2 \text{ MeV}$ must be less than Hubble expansion rate. This leads to a bound $c_l^{(3)}/\Lambda \leq 2.5 \times 10^{-5} \text{ GeV}^{-1}$ and the cross-section of $3.5 \times 10^{-34} \text{ eV}^{-2}$. Hence, $m_{\text{DM}} \lesssim 4 \times 10^{-8} \text{ eV}$ can lead to a significant flux suppression.

In passing, we note that the interaction can be written in a gauge-invariant manner at the tree-level only when Δ , a $SU(2)_L$ triplet with hypercharge $Y = 2$, is introduced. The resulting gauge-invariant term goes as $(c_l^{(3)}/\Lambda^2)(\bar{L}^c L)\Phi^*\Phi\Delta$. When Δ obtains a vacuum expectation value v_Δ , the above interaction represents an effective interaction between neutrinos and DM as in eq. (3.3). Such an interaction can arise from the mediation of another scalar triplet with mass $\sim \Lambda$. The LEP constraint on the mass of the neutral scalar other than the SM-like Higgs, arising from such a Higgs triplet reads $m_\Delta \gtrsim 72$ GeV [285]. Furthermore, theoretical bounds, constraints from T -parameter and Higgs signal strength in the diphoton channel dictate that $m_\Delta \gtrsim 150$ GeV [286] for $v_\Delta \sim 1$ GeV. For smaller values of v_Δ , such as $v_\Delta \sim 10^{-4}$ GeV, the bound can be even stronger, $m_\Delta \gtrsim 330$ GeV. Moreover, the corresponding Wilson coefficient should be perturbative, $c_l^{(3)} \lesssim \sqrt{4\pi}$. These two facts together lead to $c_l^{(3)}/\Lambda^2 \lesssim 2.5 \times 10^{-5}$ GeV $^{-2}$ for $\Lambda \sim m_\Delta \sim 150$ GeV. Such values of $c_l^{(3)}/\Lambda^2$ are rather small to lead to any significant flux suppression. While this is true for a tree-level generation of this interaction *via* a triplet scalar exchange, such interactions can be generated at the loop-level or by some new dynamics.

The renormalisable case corresponding to the effective interaction in eq. (3.3) is discussed in greater detail in Sec. 3.3.3 and Sec. 3.3.2.

4. There can also be a dimension-seven effective interaction vertex for neutrino-DM scattering:

$$\mathcal{L} \supset \frac{c_l^{(4)}}{\Lambda^3} (\bar{\nu}^c \sigma^{\mu\nu} \nu) (\partial_\mu \Phi^* \partial_\nu \Phi - \partial_\nu \Phi^* \partial_\mu \Phi). \quad (3.5)$$

Bound on this interaction comes from invisible Z decay width and reads $c_l^{(4)}/\Lambda^3 \lesssim 2.0 \times 10^{-3}$ GeV $^{-3}$. There is no counterpart of such an interaction involving the charged leptons. Thus the gauge-invariant form of this vertex does not invite any tighter bounds. Such a bound dictates that this interaction does not lead to any considerable flux

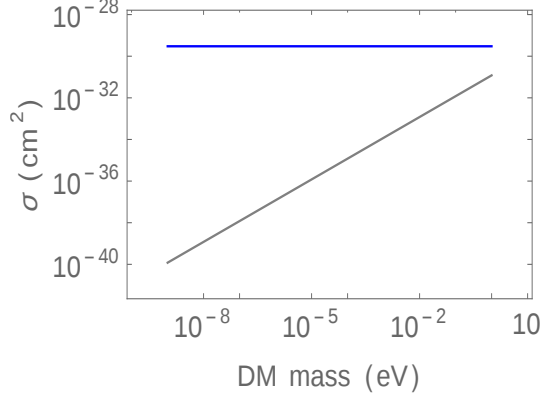


Figure 3.2. Cross-section vs. mass of DM. Blue line represents cross-section for $m_\nu = 0.1$ eV, $c_l^{(3)}/\Lambda = 0.5$ GeV $^{-1}$ for interaction (3) under Topology I. Grey line represents the required cross-section to induce 1% suppression of incoming flux.

suppression.

5. Another seven-dimensional interaction can be given as:

$$\mathcal{L} \supset \frac{c_l^{(5)}}{\Lambda^3} \partial^\mu (\bar{\nu}^c \nu) \partial_\mu (\Phi^* \Phi). \quad (3.6)$$

From invisible Z decay width the constraint on the coupling reads $c_l^{(5)}/\Lambda^3 \lesssim 7.5 \times 10^{-4}$ GeV $^{-3}$. The measurement of $Z \rightarrow l^+ l^-$ or LEP monophoton searches does not invite any further constraint on this interaction due to the same reasons as in case of eq. (3.3) and (3.5). Due to such a constraint, no significant flux suppression can take place in presence of this interaction.

6. Another neutrino-DM interaction of dim-8 can be written as follows:

$$\mathcal{L} \supset \frac{c_l^{(6)}}{\Lambda^4} (\bar{\nu} \partial^\mu \gamma^\nu \nu) (\partial_\mu \Phi^* \partial_\nu \Phi - \partial_\nu \Phi^* \partial_\mu \Phi). \quad (3.7)$$

The coupling $c_l^{(6)}/\Lambda^4$ of interaction given by eq. (3.7) is constrained from invisible Z decay width as $c_l^{(6)}/\Lambda^4 \lesssim 2.5 \times 10^{-5}$ GeV $^{-4}$. The constraint on the gauge-invariant form of this interaction reads $c_l^{(6)}/\Lambda^4 \lesssim 10^{-5}$ GeV $^{-4}$, which is similar for all three charged leptons. The gauge-invariant form of the above effective interaction also gives rise to five-point vertices involving the Z boson. These lead

to bounds from the observations of $Z \rightarrow inv$ and $Z \rightarrow l^+l^-$ which read $c_l^{(6)}/\Lambda^4 \lesssim 4.0 \times 10^{-5} \text{ GeV}^{-4}$ and $c_l^{(6)}/\Lambda^4 \lesssim 2.8 \times 10^{-5} \text{ GeV}^{-4}$ respectively. The bound from the process $e^+e^- \rightarrow \gamma\Phi^*\Phi$ reads $c_e^{(6)}/\Lambda^4 \lesssim 1.2 \times 10^{-6} \text{ GeV}^{-4}$. Even with the least stringent constraint among the different considerations stated above, such an interaction does not lead to any significant flux suppression of the astrophysical neutrinos.

3.2.2 Topology II

1. We consider a vector mediator Z' , with couplings to neutrinos and DM given by:

$$\mathcal{L} \supset \frac{c_l^{(7)}}{\Lambda^2} (\partial^\mu \Phi^* \partial^\nu \Phi - \partial^\nu \Phi^* \partial^\mu \Phi) Z'_{\mu\nu} + f_i \bar{\nu}_i \gamma^\mu P_L \nu_i Z'_\mu. \quad (3.8)$$

This interaction has the same form of interaction as in eq (3.7) of Topology I. Bound on this interaction from invisible Z decay reads $f_l c_l^{(7)}/\Lambda^2 \lesssim 4.2 \times 10^{-2} \text{ GeV}^{-2}$. The constraints on the gauge-invariant form of such interactions are $f_e c_e^{(7)}/\Lambda^2 \lesssim 5.8 \times 10^{-3} \text{ GeV}^{-2}$, $f_\mu c_\mu^{(7)}/\Lambda^2 \sim f_\tau c_\tau^{(7)}/\Lambda^2 \lesssim 8.1 \times 10^{-3} \text{ GeV}^{-2}$. The bound on the process $e^+e^- \rightarrow \gamma\Phi^*\Phi$ reads $f_e c_e^{(7)}/\Lambda^2 \lesssim 1.9 \times 10^{-5} \text{ GeV}^{-2}$.

For this interaction, the $\Phi\Phi^*Z'$ vertex from eq. (3.8) takes the form,

$$i \frac{c_l^{(7)}}{\Lambda^2} (p_2 \cdot p_4 - m_{\text{DM}}^2) (p_2 + p_4)^\mu Z'_\mu \sim i \frac{c_l^{(7)}}{\Lambda^2} m_{\text{DM}} (E_4 - m_{\text{DM}}) (p_2 + p_4)^\mu Z'_\mu,$$

where p_2 and p_4 are the four-momenta of the incoming and outgoing DM respectively. In light of the constraints from Z decay, the factor $\left(c_l^{(7)} m_{\text{DM}} (E_4 - m_{\text{DM}}) / \Lambda^2 \right)$ is much smaller than unity when the dark matter is ultralight, *i.e.*, $m_{\text{DM}} \lesssim 1 \text{ eV}$ and incoming neutrino energy $\sim 1 \text{ PeV}$. The rest of the Lagrangian is identical to the renormalisable vector-mediated process discussed in Sec. 3.3.3 and Sec. 3.3.2. Further the charged counterpart of the second term in eq. (3.8) contributes to $g - 2$ of charged leptons and also leads to new three-

body decay channels of τ . As mentioned in Sec. 4.8, the bounds on these couplings read $f_e \sim 10^{-5}$, $f_\mu \sim 10^{-6}$ and $f_\tau \sim 10^{-2}$ for $m_{Z'} \sim 10$ MeV. So among the constraints from different considerations, even the least stringent one ensures that no significant flux suppression takes place with this interaction in case of ultralight DM.

2. Consider a scalar mediator Δ with a momentum-dependent coupling with DM,

$$\mathcal{L} \supset \frac{c_l^{(8)}}{\Lambda} \partial^\mu |\Phi|^2 \partial_\mu \Delta + f_l \bar{\nu}^c \nu \Delta. \quad (3.9)$$

Here, Δ can be realised as the neutral component of a $SU(2)_L$ -triplet scalar with $Y = 2$. A Majorana neutrino mass term with $m_\nu = f_l v_\Delta$ also exists along with the second term of eq. (3.9), where v_Δ is the vev of the neutral component of the triplet scalar. The measurement of the T -parameter dictates, $v_\Delta \lesssim 4$ GeV [280]. For $v_\Delta \sim 1$ GeV, the smallness of neutrino mass constrains the coupling f_l at $\sim \mathcal{O}(10^{-11})$. The mass of the physical scalar Δ is constrained to be $m_\Delta \gtrsim 150$ GeV [286] for $v_\Delta \sim 1$ GeV. For $f_l \sim \mathcal{O}(10^{-11})$ and $m_\Delta \gtrsim 150$ GeV, such an interaction does not give rise to an appreciable flux suppression for ultralight DM.

3.2.3 Topology III

We consider the vector boson Z' mediating the neutrino-DM interaction, with a renormalisable vectorlike coupling with the DM, but a non-renormalisable dipole-type interaction in the $\nu\nu Z'$ vertex. The interaction terms are given as,

$$\mathcal{L} \supset C_1 (\Phi^* \partial_\mu \Phi - \Phi \partial_\mu \Phi^*) Z'^\mu + \frac{c_l^{(9)}}{\Lambda} (\bar{\nu}^c \sigma_{\mu\nu} P_L \nu) Z'^{\mu\nu}. \quad (3.10)$$

This interaction can be constrained from the measurement of the invisible decay width of Z . The flavour-independent bound on the coefficient $c_l^{(9)}$ reads, $c_l^{(9)}/\Lambda \lesssim 3.8 \times 10^{-3} \text{ GeV}^{-1}$. The interactions in eq. (3.10) can

be realised as the renormalisable description of the effective Lagrangian as mentioned in eq. (3.5). The BBN constraint on this interaction reads, $c_l^{(9)}/\Lambda \lesssim 2.5 \times 10^{-6} \text{ GeV}^{-1}$, which disfavors any significant flux suppression at IceCube.

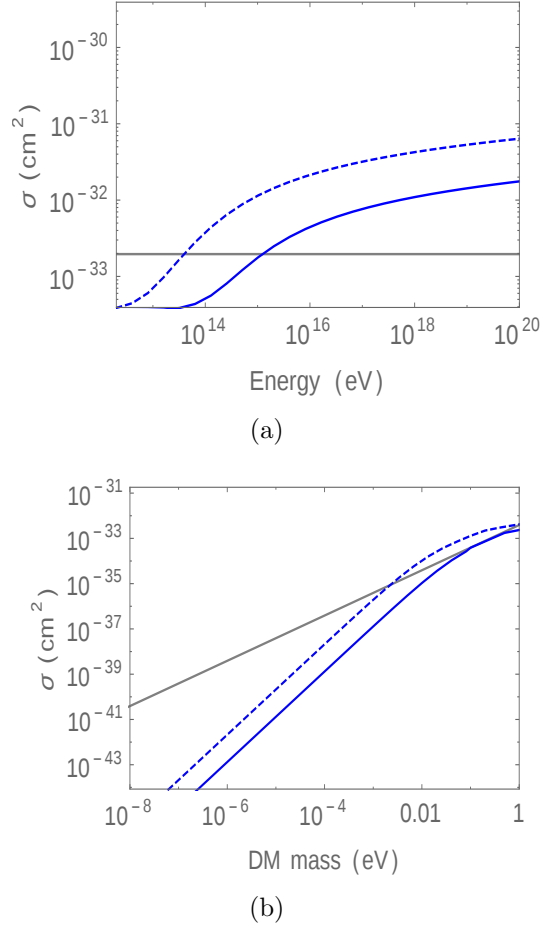


Figure 3.3. (a) Cross-section vs. incoming neutrino energy. (b) Cross-section vs. mass of DM. Grey line represents the required cross-section to induce 1% suppression of incoming flux. The dashed and solid blue lines represent cross-sections for $m_{Z'} = 5, 10$ MeV respectively, (a) with $m_{\text{DM}} = 0.5$ eV and (b) with $E_\nu = 1$ PeV. In both plots, $c_l^{(9)}/\Lambda = 3.8 \times 10^{-3} \text{ GeV}^{-1}$ and $C_1 = 1$.

3.2.4 Topology IV

We consider the fermionic field $F_{L,R}$ mediating the neutrino-DM interaction with

$$\mathcal{L} \supset \frac{c_l^{(10)}}{\Lambda^2} \bar{L} F_R \Phi |H|^2 + C_L \bar{L} F_R \Phi + h.c. \quad (3.11)$$

In eq. (3.11), after the Higgs H acquires vacuum expectation value (vev), the first term reduces to the second term up to a further suppression of (v^2/Λ^2) . Following the discussion in Sec. 3.3.1, such interactions do not lead to a significant flux suppression.

• **Effective interactions with thermal DM**

So far we have mentioned the constraints on several neutrino-DM interactions in case of ultralight DM and whether such interactions can lead to any significant flux suppression. Here we discuss such effective interactions of neutrinos with thermal DM with mass $m_{\text{DM}} \gtrsim 10$ MeV. In case of thermal DM, bounds on the effective interactions considered above can come from the measurement of the relic density of DM, collisional damping and the measurement of the effective number of neutrinos, discussed in detail in Sec. 3.3.2. As mentioned earlier, the case of thermal DM becomes interesting in cases where the cross-section of neutrino-DM scattering increase with DM mass. For example, in topology II with the interaction given by eq. (3.8), the neutrino-DM scattering cross-section is proportional to $\left(c_l^{(7)} m_{\text{DM}} (E_4 - m_{\text{DM}}) / \Lambda^2\right)$ which increases with DM mass. However, considering the bound on $c_l^{(7)} / \Lambda^2$ from Z decay, the relic density and thus the number density of the DM with such an interaction comes out to be quite small, leading to no significant flux suppression. The following argument holds for all effective interactions considered in this chapter for neutrino interactions with thermal DM. The thermally-averaged DM annihilation cross-section is given by $\langle \sigma v \rangle_{th} \propto (1/\Lambda^2) (m_{\text{DM}}^2 / \Lambda^2)^d$, where $d = 0, 1, 2, 3$ for five-, six-, seven- and eight-dimensional effective interactions respectively. In order to have sufficient number density, the DM should account for the entire relic density, *i.e.*, $\langle \sigma v \rangle_{th} \sim 3 \times 10^{-26} \text{cm}^3 \text{s}^{-1}$. To comply with the measured relic density, the required values of Λ come out to be rather large leading to small cross-section.

3.3 The Renormalisable Models

3.3.1 Description of the models

Here we have considered three cases of neutrinos interacting with scalar dark matter at the tree-level *via* a fermion, a vector, and a scalar mediator.

Fermion-mediated process

In this case, the Lagrangian which governs the interaction between neutrinos and DM is given by:

$$\mathcal{L} \supset (C_L \bar{L} F_R + C_R \bar{l}_R F_L) \Phi + h.c. \quad (3.12)$$

Here L and l_R stand for SM lepton doublet and singlet respectively. $F_{L,R}$ are the mediator fermions. As it was discussed earlier, a scalar DM of ultralight nature can only transform as a singlet under the SM gauge group. So, the new fermions F_L and F_R should transform as singlets and doublets under $SU(2)_L$ respectively. In such cases, the LEP search for exotic fermions with electroweak coupling lead to the bound on the masses of these fermions as, $m_F \gtrsim 100$ GeV [287]. A scalar DM candidate can be both self-conjugate and non-self-conjugate. The stability of such DM can be ensured by imposing a discrete symmetry, for example, a Z_2 -symmetry. A non-self-conjugate DM can be stabilised by imposing a continuous symmetry as well. For self-conjugate DM, the neutrino-DM interaction takes place *via* s - and u -channel processes and such contributions tend to cancel each other in the limit $s, u \ll m_F^2$ [270]. In contrary, for non-self-conjugate DM the process is mediated only *via* the u -channel and leads to a larger cross-section compared to the former case. In this chapter, we only concentrate on the non-self-conjugate DM in this scenario.

Such interactions contribute to the anomalous magnetic moment, $\delta a_l \equiv g_l - 2$, of the charged SM leptons, which in turn constrains the value of the coefficients $C_{L,R}$. The contribution of the interaction in eq. (3.12)

to the anomalous dipole moment of SM charged lepton of flavour l is given by [288]:

$$\delta a_l = \frac{m_l^2}{32\pi^2} \int_0^1 dx \frac{(C_L + C_R)^2(x^2 - x^3 + x^2 \frac{m_F}{m_l}) + (C_L - C_R)^2(x^2 - x^3 - x^2 \frac{m_F}{m_l})}{m_l^2 x^2 + (m_F^2 - m_l^2)x + m_{\text{DM}}^2(1-x)},$$

where m_l is the mass of the corresponding charged lepton. In the limit $m_{\text{DM}} \ll m_l \ll m_F$, the anomalous contribution due to new interaction reduces to,

$$\delta a_l \sim \frac{C_L C_R m_l}{16\pi^2 m_F}. \quad (3.13)$$

For electron and muon the bound on the ratio $(C_L C_R / 16\pi^2 m_F)$ reads $1.6 \times 10^{-9} \text{ GeV}^{-1}$ and $2.9 \times 10^{-8} \text{ GeV}^{-1}$ respectively. There is no such bound for the tauon.

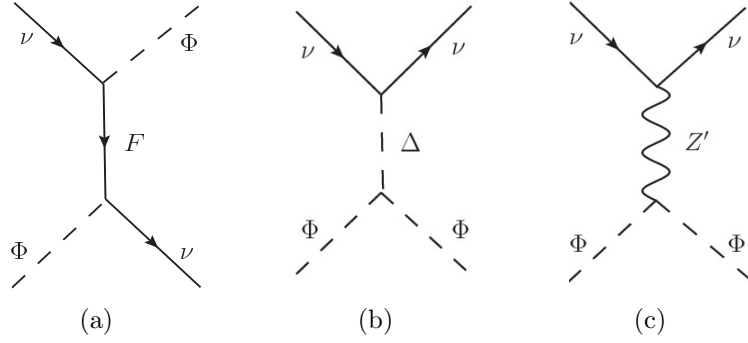


Figure 3.4. Renormalisable cases of neutrino-DM scattering with (a) fermion, (b) scalar and (c) vector mediator.

Scalar-mediated process

The Lagrangian for the scalar-mediated neutrino-DM interaction can be written as:

$$\mathcal{L} \supset f_l \bar{L}^c L \Delta + g_\Delta \Phi^* \Phi |\Delta|^2, \quad (3.14)$$

where L are the SM lepton doublets and Δ is the $SU(2)_L$ -triplet with hypercharge $Y = 2$. When Δ acquires a vev v_Δ , the first term in eq. (3.14)

leads to a non-zero neutrino mass $m_\nu \sim f_l v_\Delta$. For $v_\Delta \sim 1$ GeV and mass of the neutrino $m_\nu \lesssim 0.1$ eV the constraint on the coupling f_l reads $f_l \lesssim 10^{-11}$. The second term in eq. (3.14) contributes to DM mass $m_{\text{DM}}^2 \sim g_\Delta v_\Delta^2$. In case the DM mass is solely generated from such a term, the upper bound on v_Δ dictated by the measurement of ρ -parameter, implies a lower bound on g_Δ . The mass term for DM might also arise from some other mechanisms, for example, by vacuum misalignment in case of ultralight DM. In such a scenario, for a particular value of m_{DM} and v_Δ there exists an upper bound on the value of g_Δ .

The lower bound on the mass of the heavy CP-even neutral scalar arising from the $SU(2)$ -triplet is $m_\Delta \sim 150$ GeV for $v_\Delta \sim 1$ GeV [286], which comes from the theoretical criteria such as perturbativity, stability and unitarity, as well as the measurement of the ρ -parameter and $h \rightarrow \gamma\gamma$.

Light Z' -mediated process

The interaction of a scalar DM with a new gauge boson Z' is given by the Lagrangian,

$$\mathcal{L} \supset f'_l \bar{L} \gamma^\mu P_L L Z'_\mu + i g' (\Phi^* \partial^\mu \Phi - \Phi \partial^\mu \Phi^*) Z'_\mu. \quad (3.15)$$

Here, f'_l are the couplings of the $l = e, \mu, \tau$ kind of neutrinos with the new boson Z' , while g' is the coupling between the dark matter and the mediator. f'_l can be constrained from the $g - 2$ measurements. Due to the same reason as in the fermion-mediated case, the coupling of Z' with τ -flavoured neutrinos is not constrained from $g - 2$ measurements. Constraints for this case from the decay width of Z boson will be discussed in Sec V.

For the mass of the SM charged lepton, m_l and the boson, $m_{Z'}$, the anomalous contribution to the $g - 2$ takes the form [288]:

$$\delta a_l \sim \frac{f_l'^2 m_l^2}{12 \pi^2 m_{Z'}^2}. \quad (3.16)$$

We have considered vector-like coupling between the Z' and charged lep-

tons. For electrons and muons we find the constraints on couplings-to-mediator mass ratio to be rather strong [280],

$$\frac{f'_e}{m_{Z'}} \lesssim \frac{7 \times 10^{-6}}{\text{MeV}}, \quad \frac{f'_\mu}{m_{Z'}} \lesssim \frac{3 \times 10^{-7}}{\text{MeV}}. \quad (3.17)$$

From the measurement of N_{eff} the lower bound on the mass of a light Z' interacting with SM neutrinos at the time of nucleosynthesis reads $m_{Z'} \gtrsim 5 \text{ MeV}$ [93].

3.3.2 Thermal Relic Dark Matter

In this scenario, the DM is initially in thermal equilibrium with other SM particles *via* its interactions with the neutrinos. For models with thermal dark matter interacting with neutrinos, three key constraints come from the measurement of the relic density of DM, collisional damping and the measurement of the effective number of neutrinos. These three constraints are briefly discussed below.

- **Relic density**

If the DM is thermal in nature, its relic density is set by the chemical freeze-out of this particle from the rest of the primordial plasma. The observed value of DM relic density is $\Omega_{\text{DM}} h^2 \sim 0.1188$ [280], which corresponds to the annihilation cross-section of the DM into neutrinos $\langle \sigma v \rangle_{th} \sim 3 \times 10^{-26} \text{ cm}^3 \text{ s}^{-1}$. In order to ensure that the DM does not overclose the Universe, we impose

$$\langle \sigma v \rangle_{th} \gtrsim 3 \times 10^{-26} \text{ cm}^3 \text{ s}^{-1}. \quad (3.18)$$

- **Collisional damping**

Neutrino-DM scattering can change the observed CMB as well as the structure formation. In presence of such interactions, neutrinos scatter off DM, thereby erasing small scale density perturbations, which in turn suppresses the matter power spectrum and disrupts large scale structure formation.

The cross-section of such interactions are constrained by the CMB measurements from Planck and Lyman- α observations as [258, 259],

$$\sigma_{el} \lesssim 10^{-48} \times \left(\frac{m_{\text{DM}}}{\text{MeV}}\right) \left(\frac{T_0}{2.35 \times 10^{-4} \text{eV}}\right)^2 \text{cm}^2. \quad (3.19)$$

• **Effective number of neutrinos**

In standard cosmology, neutrinos are decoupled from the rest of the SM particles at a temperature $T_{dec} \sim 2.3$ MeV and the effective number of neutrinos is evaluated to be $N_{\text{eff}} = 3.045$ [289]. For thermal DM in equilibrium with the neutrinos even below T_{dec} , entropy transfer takes place from dark sector to the neutrinos, which leads to the bound $m_{\text{DM}} \gtrsim 10$ MeV from the measurement of N_{eff} . It can be understood as follows. In presence of n species with thermal equilibrium with neutrinos, the change in N_{eff} is encoded as [91],

$$N_{\text{eff}} = \left(\frac{4}{11}\right)^{-4/3} \left(\frac{T_\nu}{T_\gamma}\right)^4 \left[N_\nu + \sum_{i=1}^n I\left(\frac{m_i}{T_\nu}\right)\right], \quad (3.20)$$

where,

$$\frac{T_\nu}{T_\gamma} = \left[\left(\frac{g_\nu^*}{g_\gamma^*}\right)_{T_{dec}}\right]^{1/3}. \quad (3.21)$$

Here, the effective number of relativistic degrees of freedom in thermal equilibrium with neutrinos is given as

$$g_\nu^* = \frac{14}{8} \left(N_\nu + \sum_{i=1}^n \frac{g_i}{2} F\left(\frac{m_i}{T_\nu}\right)\right). \quad (3.22)$$

In eqs. (4.10) and (4.12), $i = 1, \dots, n$ denotes the number of species in thermal equilibrium with neutrinos, $g_i = 7/8$ (1) for fermions (bosons) and the functions $I(m_i/T_\nu)$ and $F(m_i/T_\nu)$ can be found in ref. [91]. For a DM in thermal equilibrium with neutrinos and $m_{\text{DM}} \lesssim 10$ MeV, the contribution of $F(m_{\text{DM}}/T_\nu)$ to (T_ν/T_γ) is quite large, and such values of

DM mass can be ruled out from $N_{\text{eff}} = 3.15 \pm 0.23$ [47], obtained from the CMB measurements.

We implement the above constraints in cases of the renormalisable models discussed in Sec 3.3. We present the thermally-averaged annihilation cross-section $\langle\sigma v\rangle_{th}$ and the cross-section for elastic neutrino-DM scattering σ_{el} for the respective models in table 3.1. The notations for the couplings and masses follow that of Sec 3.3. In the expressions of $\langle\sigma v\rangle_{th}$, p_{cm} can be further simplified as $\sim m_{\text{DM}}v_r$ where $v_r \sim 10^{-3} c$ is the virial velocity of DM in the galactic halo [92]. In the expressions of σ_{el} , E_ν represents the energy of the incoming relic neutrinos which can be roughly taken as the CMB temperature of the present Universe.

Two of the three renormalisable interactions discussed in this chapter, namely the cases of fermion and vector mediators have been discussed in the literature in light of the cosmological constraints, *i.e.*, relic density, collisional damping and N_{eff} [92]. For a particular DM mass, the annihilation cross-section decreases with increasing mediator mass. Thus, in order for the DM to not overclose the Universe, there exists an upper bound to the mediator mass for a particular value of m_{DM} . With mediator mass less than such an upper bound, the relic density of the DM is smaller compared to the observed relic density, leading to a smaller number density.

	Fermion-mediated	Scalar-mediated	Vector-mediated
$\langle\sigma v\rangle_{th}$	$C_L^4 \frac{p_{cm}^2}{12\pi(m_{\text{DM}}^2 + m_F^2)^2}$	$g_\Delta^2 f_l^2 \frac{2m_{\text{DM}}^2 + p_{cm}^2}{32\pi m_{\text{DM}}^2 (m_\Delta^2 - 4m_{\text{DM}}^2)^2}$	$g'^2 f'^2 \frac{p_{cm}^2}{3\pi(m_{Z'}^2 - 4m_{\text{DM}}^2)^2}$
σ_{el}	$C_L^4 \frac{E_\nu^2}{8\pi(m_{\text{DM}}^2 - m_F^2)^2}$	$\frac{g_\Delta^2 f_l^2 E_\nu^2}{8\pi m_{\text{DM}}^2 m_\Delta^4}$	$\frac{g'^2 f'^2 E_\nu^2}{2\pi m_{Z'}^4}$

Table 3.1. Thermally averaged DM annihilation cross-section and the cross-section for neutrino-DM elastic scattering for thermal DM.

As discussed earlier, the measurement of N_{eff} places a lower bound on DM mass $m_{\text{DM}} \gtrsim 10$ MeV. DM number density is proportional to the relic abundance and inversely proportional to the DM mass. Thus the most ‘optimistic’ scenario in context of flux suppression is when $m_{\text{DM}} = 10$ MeV and the masses of the mediators are chosen in such a way that those correspond to the entire relic density in fig. 3.5. Such a choice leads

to the maximum DM number density while satisfying the constraint of relic density and N_{eff} . As it can be seen from fig. 3.5, such values of mediator and DM mass satisfies the constraint from collisional damping as well. For example, as fig. 3.5(a) suggests, $m_{\text{DM}} \sim 10$ MeV and $m_F \sim 2$ GeV correspond to the upper boundary of the blue region, which represents the point of highest relic abundance. Similarly for the scalar and vector mediated case, the values of mediator masses come out to be ~ 20 MeV and ~ 1 GeV respectively for $m_{\text{DM}} \sim 10$ MeV.

With the above-mentioned values of the DM and mediator masses, the neutrino-DM scattering cross-section for the entire range of energy of astrophysical neutrinos fall short of the cross-section required to produce 1% flux suppression, by many orders of magnitude. The key reason behind this lies in the fact that for the range of allowed DM mass, corresponding number density is quite small and the neutrino-DM scattering cross-section cannot compensate for that. The cross-section in the fermion and scalar mediated cases decrease with energy in the relevant energy range. Such a fall in cross-section is much more faster in the scalar case compared to the fermion one. Though in the vector-mediated case the cross-section remains almost constant in the entire energy range under consideration. The cross-section in the fermion, scalar and vector-mediated cases are respectively $10^6 - 10^8$, $10^{30} - 10^{35}$ and 10^7 orders smaller than the required cross-section in the energy range of 20 TeV - 10 PeV. Thus we conclude that the three renormalisable interactions stated above do not lead to any significant flux suppression of astrophysical neutrinos in case of cold thermal dark matter.

3.3.3 Ultralight Scalar Dark Matter

Here we consider the DM to be an ultralight BEC scalar with mass $10^{-21} - 1$ eV. The centre-of-mass energy for the neutrino-DM interaction in this case always lies between $\mathcal{O}(10^{-3})$ eV to $\mathcal{O}(10)$ MeV for incoming neutrino of energy $\sim \mathcal{O}(10)$ PeV depending on DM mass. We consider below the models described in Sec. 3.3 to calculate the cross-section of neutrino-

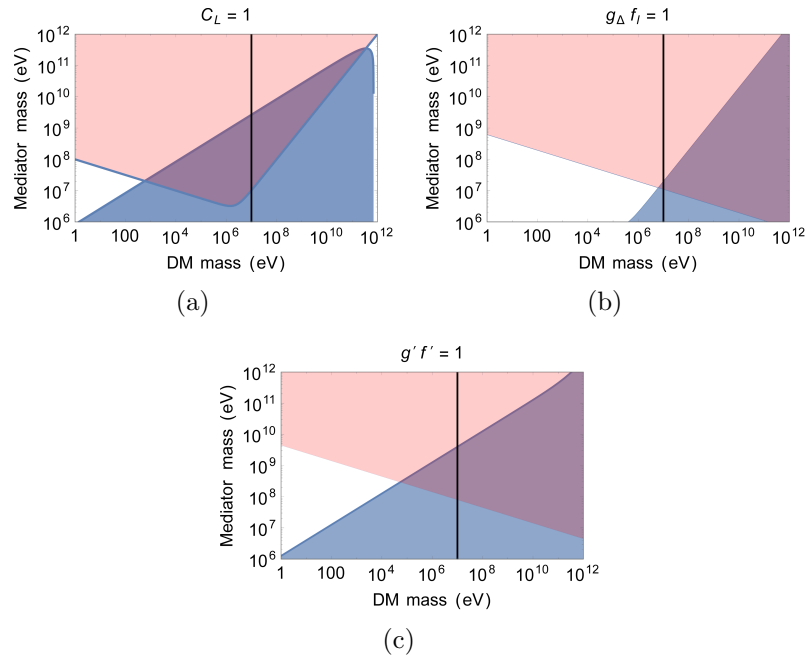


Figure 3.5. Mass of the mediator vs. mass of DM for (a) fermion-mediated, (b) scalar-mediated and (c) vector-mediated neutrino-DM interactions. The blue and pink regions are allowed from relic density of DM and collisional damping respectively. The region at the left side of the vertical black line is ruled out from the constraint coming from N_{eff} .

DM interaction and compare those to the cross-section required for a flux suppression at IceCube.

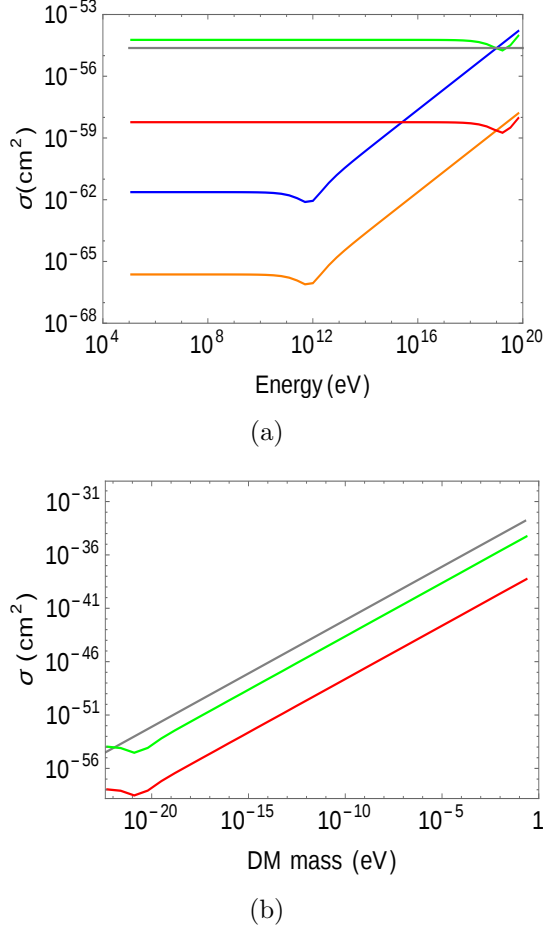


Figure 3.6. Fermion-mediated neutrino-DM scattering. (a) Cross-section vs. incoming neutrino energy. Green and blue lines represent cross-sections for $m_\nu = 10^{-2}, 10^{-5}$ eV respectively with $m_F = 10$ GeV. Red and orange lines represent cross-sections for $m_\nu = 10^{-2}, 10^{-5}$ eV respectively with $m_F = 100$ GeV. Here $C_L = 0.88$, $m_{\text{DM}} = 10^{-22}$ eV. (b) Cross-section vs. mass of DM. Green and red lines represent $m_F = 10, 100$ GeV respectively for $m_\nu = 10^{-2}$ eV. Here $C_L = 0.88$, $E_\nu = 1$ PeV. Grey line represents the required cross-section to induce 1% suppression of incoming neutrino flux.

Fermion-mediated process

The cross-section for neutrino-DM scattering through a fermionic mediator in case of ultralight scalar DM is given as

$$\sigma \sim \frac{C_L^4(m_\nu^2 + 4m_{\text{DM}}E_\nu)}{16\pi m_F^4},$$

where m_ν, E_ν are the mass and energy of the incoming neutrino respectively, m_{DM} is the mass of the ultralight DM, and m_F is the mass of the heavy fermionic mediator. As the mass of the DM is quite small, at lower

neutrino energies $m_\nu^2 > m_{\text{DM}}E_\nu$ and hence, the cross-section remains constant. As the energy increases, the $m_{\text{DM}}E_\nu$ term becomes more dominant and eventually, the cross-section increases with energy.

Such an interaction has been studied in literature in case of ultralight DM [255]. This analysis was improved with the consideration of non-zero neutrino mass in ref. [256]. For example, from fig. 3.6(a) it can be seen that the cross-section for $m_\nu \sim 10^{-2}$ eV is larger compared to that for $m_\nu \sim 10^{-5}$ eV. In fig. 3.6(b), with $m_\nu \sim 10^{-2}$ eV, it is shown that no significant flux suppression takes place for a DM heavier than 10^{-22} eV for $m_F \sim 10$ GeV. However, it has been shown that the quantum pressure of the particles of mass $\lesssim 10^{-21}$ eV suppresses the density fluctuations relevant at small scales ~ 0.1 Mpc, which is disfavoured by the Lyman- α observations of the intergalactic medium [72, 290]. Also, the constraint on the mass of such a mediator fermion, which couples to the Z boson with a coupling of the order of electroweak coupling, reads $m_F \gtrsim 100$ GeV [287]. These facts together suggest that $m_{\text{DM}} \sim 10^{-22}$ eV and $m_F \sim 10$ GeV, as considered in ref. [256], are in tension with Lyman- α observations and LEP searches for exotic fermions respectively. If we consider $m_\nu = 0.1$ eV along with $m_F = 100$ GeV, it leads to a larger cross-section compared to that with $m_\nu = 0.01$ eV, which is still smaller compared to the cross-section required to induce a significant flux suppression. Thus, taking into account such constraints, the interaction in eq. (3.12) does not lead to any appreciable flux suppression in case of ultralight DM.

Scalar-mediated process

As mentioned in Sec. 3.3.1, the bound on the coupling of a scalar mediator Δ with neutrinos is quite stringent, $fv_\Delta \lesssim 0.1$ eV. Moreover, the mass of such a mediator are constrained as $m_\Delta \gtrsim 150$ GeV [286]. In this case, the cross-section of neutrino-DM scattering is independent of the DM as well as the neutrino mass for neutrino energies under consideration. As fig. 3.7 suggests, the neutrino-DM cross-section in this case never reaches

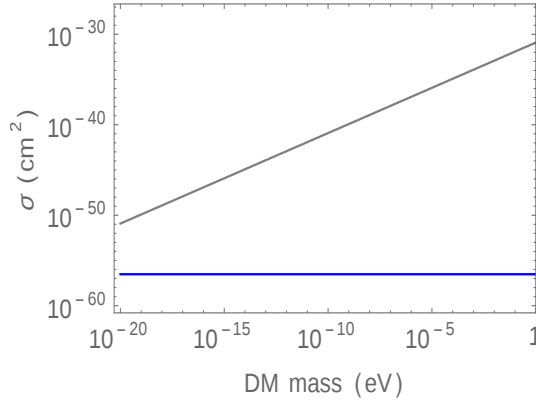


Figure 3.7. Cross-section vs. mass of DM in scalar-mediated neutrino-DM scattering. The blue and grey lines represent the cross-section with scalar mediator and the same required to induce 1% suppression of incoming flux respectively. Here, energy of incoming neutrino $E_\nu = 1$ PeV, mediator mass $m_\Delta = 200$ GeV and $f_l g_\Delta v_\Delta = 0.1$ eV.

the value of cross-section required to induce a significant suppression of the astrophysical neutrino flux for $m_{\text{DM}} \gtrsim 10^{-21}$ eV. As mentioned earlier, DM of mass smaller than $\sim 10^{-21}$ eV are disfavoured from Lyman- α observations.

Vector-mediated process

As it has been discussed in Sec. 4.8, the couplings of electron and muon-flavoured neutrinos to the Z' are highly constrained, $\sim \mathcal{O}(10^{-5} - 10^{-6})$. However, as discussed in appendix 7.4, for the tau-neutrinos such a coupling is less constrained by collider observations, $\sim \mathcal{O}(10^{-2})$. From fig. 3.8(a) it can be seen that, in presence of such an interaction, an appreciable flux suppression can take place for $E_\nu \gtrsim 10$ TeV, with $m_{Z'} = 10$ MeV, $g'f' = 10^{-3}$ and $m_{\text{DM}} = 10^{-6}$ eV. Instead, if we fix $E_\nu = 1$ PeV, it can be seen from fig. 3.8(b) that the entire range of DM mass in the ultralight regime, *i.e.*, 10^{-21} eV to 1 eV, can lead to an appreciable flux suppression. It was also pointed out that a strong neutrino-DM interaction can degrade the energies of neutrinos emitted from core collapse Supernovae and scatter those off by an significant amount to not be seen at the detectors [291–293]. This imposes the following constraint on the neutrino-DM cross-section [91, 293]: $\sigma_{\nu\text{-DM}} \lesssim 3.9 \times 10^{-25} \text{ cm}^{-2} (m_{\text{DM}}/\text{MeV})$ for $E_\nu \sim T_{\text{SN}} \sim 30$ MeV. It can

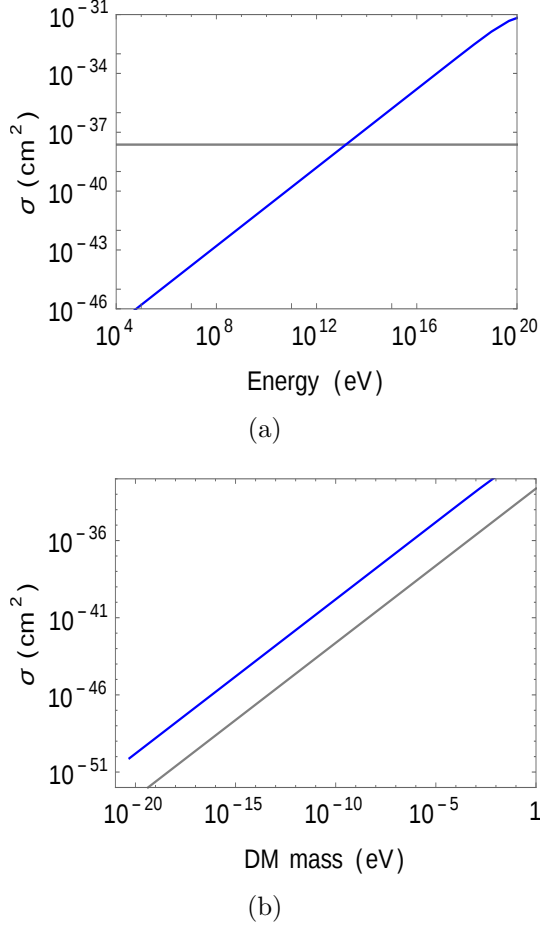


Figure 3.8. Vector-mediated neutrino-DM scattering. (a) Cross-section vs. incoming neutrino energy. (b) Cross-section vs. mass of DM. Blue and grey lines represent the calculated cross-section and required cross-section to induce 1% suppression of incoming flux respectively. Here, the mediator mass $m_{Z'}$ = 10 MeV, and the couplings $g'f' = 10^{-3}$. For (a), $m_{\text{DM}} = 10^{-6}$ eV and for (b), the energy of incoming neutrino $E_\nu = 1$ PeV.

seen from fig. 3.8(a) that such a constraint is comfortably satisfied in our benchmark scenario.

In the standard cosmology, neutrinos thermally decouple from electrons, and thus from photons, near $T_{\text{dec}} \sim 1$ MeV. Ultralight DM with mass m_{DM} forms a Bose-Einstein condensate below a critical temperature $T_c = 4.8 \times 10^{-4} / ((m_{\text{DM}}(\text{eV}))^{1/3} a)$ eV, where a is the scale factor of the particular epoch [63]. When the temperature of the Universe is $T \sim T_{\text{dec}}$, $T_c \sim 480$ MeV for $m_{\text{DM}} \sim 10^{-6}$ eV, *i.e.*, the ultralight DM exists as a BEC. In order to check whether the benchmark scenario presented in fig. 3.8(a) leads to late kinetic decoupling of neutrinos, we verify

if $n_\nu(T_{dec}) \sigma_{\nu\text{-DM}} v_\nu \lesssim H(T_{dec})$. Here, $n_\nu(T)$ and $H(T)$ are the density of relic neutrinos and the Hubble rate at temperature T respectively,

$$\begin{aligned} H(T_{dec}) &\sim \frac{\pi \sqrt{g_{eff}} T_{dec}^2}{\sqrt{90} M_{Pl}} \sim 5 \times 10^{-16} \text{ eV}. \\ n_\nu &\sim 0.091 T_{dec}^3 \sim 1.14 \times 10^{31} \text{ cm}^{-3}. \end{aligned} \quad (3.23)$$

For t -channel process, $m_{\text{DM}} \sim 10^{-6}$ eV, mediator mass $m_{Z'}$ ~ 10 MeV and neutrino-DM coupling $g'f' \sim 10^{-3}$, $\sigma_{\nu\text{-DM}}^t \sim 1.5 \times 10^{-44} \text{ cm}^{-2}$. Thus, at $T \sim T_{dec}$, $n_\nu \sigma_{\nu\text{-DM}}^t v_\nu \sim 4.2 \times 10^{-20} \text{ eV} \ll H(T)$ with $v_\nu \sim c$. However, for s -channel process $\nu\nu \rightarrow \Phi\Phi$, the bound from BBN on the coupling $g'f' \lesssim 6 \times 10^{-8}$, for $m_{Z'} \sim 10$ MeV and $m_{\text{DM}} \lesssim 1$ eV; hence this interaction does not lead to any significant flux suppression at \sim PeV.

3.4 Summary

High energy extragalactic neutrinos travel a long distance before reaching the Earth, through the isotropic dark matter background. The observation of astrophysical neutrino flux at IceCube can bring new insights for a possible interaction between neutrinos and dark matter. While building models of neutrino-DM interactions leading to flux suppressions of astrophysical neutrinos, the key challenge is to obtain the correct number density of dark matter along with the required cross-section. The number density of DM in the WIMP scenario is quite small compared to the ultralight case. However, the neutrino-DM scattering cross-section for some interactions increase with the DM mass. Thus, it is essentially the interplay of DM mass and the nature of neutrino-DM interaction that collectively decide whether a model can lead to a significant flux suppression. So, a study of various types of interactions for the whole range of DM masses is required to comment on which scenarios actually give the right combination of number density and cross-section.

Issues of neutrino flux suppression [255, 256, 260], flavour conversion [257, 261] and cosmological bounds [91, 92, 258, 259] in presence of

neutrino-DM interaction have been addressed in the literature. The existing studies of the flux suppression of astrophysical neutrinos involve only a few types of renormalisable neutrino-DM interactions. The change in the flux of astrophysical neutrinos in presence of only a few renormalisable and effective interactions between neutrinos and DM has been discussed in the literature [255, 256, 260]. As mentioned earlier, such studies suffer from various collider searches and precision tests. We take a rigorous approach to this problem by considering renormalisable as well as effective interactions between neutrinos and DM and mention the constraints on such interactions. Taking into account the bounds from, we investigate whether such interactions can provide the required value of cross-section of neutrino-DM scattering so that they lead to flux suppression of the astrophysical neutrinos.

In this work we have contained our discussion to scalar dark matter. Thermal DM with mass $m_{\text{DM}} \lesssim \mathcal{O}(10)$ MeV can be realised as warm and hot dark matter, whereas for $m_{\text{DM}} \gtrsim \mathcal{O}(10)$ MeV it can be realised as cold DM. However, non-thermal ultralight DM with mass in the range $\mathcal{O}(10^{-21})$ eV – $\mathcal{O}(1)$ eV can exist as a Bose-Einstein condensate, *i.e.*, as a cold DM as well. In contrary to the warm and hot thermal relics, which can only account for $\sim 1\%$ of the total DM density, ultralight BEC DM can account for the total DM abundance. We consider three renormalisable interactions viz. the scalar, fermionic and vector mediation between neutrinos and DM at the tree-level. Moreover, we consider up to dimension-eight contact type interactions in topology I, and dimension-six interactions in one of the vertices in topologies II, III and IV. We find the constraints on such interactions from LEP monophoton searches, measurement of the Z decay width and precision measurements such as anomalous magnetic dipole moment of e and μ . In passing, we also point out that the demand of gauge invariance of the effective interactions can lead to more stringent constraints. For the thermal dark matter, we discuss the cosmological bounds on the models coming from relic density, collisional damping and measurement of effective number of neutrinos.

In case of thermal DM of mass greater than $\mathcal{O}(10)$ MeV, for a particular DM mass, the value of mediator mass for renormalisable cases or the effective interaction scale for non-renormalisable cases, required to comply with the observed relic density, is too large to lead to a significant flux suppression of the astrophysical neutrinos. For ultralight BEC DM, due to stringent constraints from precision tests, collider searches as well as the cosmological observations, only one dim-5 contact-type interaction from topology I can give rise to significant flux suppression. A summary of all the interactions under consideration along with ensuing constraints can be found at appendix 7.3.

The effective neutrino-DM interactions considered in this work can stem from different renormalisable models, at both tree and loop levels. In order to keep the analysis as general as possible, in contrary to the usual effective field theory (EFT) prescription, we do not assume any particular scale of the dynamics which lead to such effective interactions. As a result, it is not possible to *a priori* ensure that the effects of a particular neutrino-DM effective interaction will always be smaller than an effective interaction with a lower mass-dimension. Thus we investigate effective interactions up to mass dimension-8.

The possibility of neutrino-DM interaction in presence of light mediators, for example a Z' with mass $\sim \mathcal{O}(10)$ MeV, points to the fact that effective interaction scale in such processes can be rather low. As it was mentioned earlier, the centre-of-mass energy for the scattering of the astrophysical neutrinos off ultralight DM particles can be quite small, $\sqrt{s} \lesssim 10$ MeV, for neutrino energies up to 1 PeV. Thus, it might be tempting to try to interpret the effective interactions arising out of all the renormalisable scenarios with mediator mass $\gtrsim 10$ MeV, *i.e.*, even the case of a Z' of mass $\sim \mathcal{O}(10)$ MeV, as higher-dimensional operators in an EFT framework. However, it has been shown that the Z -decay and LEP monophoton searches constrain both the renormalisable as well as effective neutrino-DM interactions. Hence such an EFT description of neutrino-DM interaction does not hold below the Z boson mass or $\sqrt{s}_{\text{LEP}} \sim 209$ GeV.

For this reason, it is not meaningful to match the bounds obtained in a renormalisable model with mediator mass less than m_Z or $\sqrt{s_{\text{LEP}}}$, *i.e.*, the model with a light Z' as in Sec. 3.3.3, with the corresponding effective counterpart in eq. (3.2).

It is also worth mentioning that the flavour oscillation length of the neutrinos is much smaller than the mean interaction length with dark matter. Hence, the attenuation in the flux of one flavour of incoming neutrinos eventually gets transferred to all other flavours and leads to an overall flux suppression irrespective of the flavours. The criteria of 1% flux suppression helps to identify the neutrino-DM interactions which should be further taken into account to check potential signatures at IceCube. The flux of astrophysical neutrinos at IceCube also depend upon the specifics of the source flux and cosmic neutrino propagation. In order to find out the precise degree of flux suppression, one needs to solve an integro-differential equation consisting of both attenuation and regeneration effects [294], which is addressed in ref. [295]. But the application of the criteria of 1% flux suppression, as well as the conclusions of the present work are independent of an assumption of a particular type of source flux or details of neutrino propagation.

In brief, we encompass a large canvas of interactions between neutrinos and dark matter, trying to find whether they can lead to flux suppression of the astrophysical neutrinos. The interplay of collider, precision and cosmological considerations affect such an endeavour in many different ways. Highlighting this, we point out the neutrino-DM interaction which may lead to flux suppression at IceCube.

Chapter 4

Astronomy with Energy Dependent Flavour Ratios of Extragalactic Neutrinos

Traditional astronomy based on photons ceases to work for very high energy gamma rays, above a few tens of TeV, as they get absorbed interacting with background photons on their way to the Earth. Hence, it is rather difficult to gather first hand information about the interiors of the astrophysical objects like AGN, GRB, etc. at very high energies. However, these objects are expected not only to emit photons, but also cosmic rays and neutrinos with extreme energies stretching up to EeVs or more. As neutrinos interact only weakly, astronomy with high energy astrophysical neutrinos seem quite promising. IceCube has seen such neutrinos up to a few PeV and future upgrades are designed to improve the statistics. We have already been able to ‘look’ into the interiors of the Sun through neutrinos and now we aspire to do the same for these astrophysical objects. However, the matter density in these astrophysical objects is usually too low to affect neutrino propagation. While this allows the neutrinos to stream out of these objects unhindered, very little information about the interiors are usually carried by these neutrinos. This is the main stumbling block of astronomy with the high energy astrophysical neutrinos, compared to the same with photons, which of course is effective only at lower energies. We propose in this section that if the dark matter is ultralight, then even a feeble interaction of neutrinos with DM inside these objects may help

circumvent such shortcomings of neutrino astronomy.

In the standard scenario, astrophysical neutrinos are produced from charged pion decay, yielding a flavour ratio $\nu_e : \nu_\mu : \nu_\tau = 1 : 2 : 0$. Then these neutrinos undergo vacuum flavour oscillations to reach Earth with a flavour ratio $\nu_e : \nu_\mu : \nu_\tau = 1 : 1 : 1$, independent of the energy of the neutrinos. We show that this picture takes a blow once these neutrinos are allowed to interact with a surrounding ultralight dark matter halo. The results presented in this chapter are based on ref. [296].

Building models for neutrino-dark matter interactions that lead to appreciable flux suppression is rather challenging [254]. Such interactions can lead to a lack of temporal coincidence between the observation of electromagnetic signals and neutrinos from GRBs [297]. On the other hand, the strength of such interactions may be feeble enough to lead to any appreciable flux suppression at the IceCube, but these can severely affect neutrino oscillations in regions where the dark matter number density is significant. We show that this leads to an energy dependent flavour ratio which drastically differs from the standard expectation of flavour-universal flux of such neutrinos. This also predicts different flavour ratios for neutrinos and anti-neutrinos. Although it is the dark matter interactions with the neutrinos that influence the neutrino oscillations, to match the standard literature, we refer to this as ‘matter effects’ in this chapter.

The role of DM-neutrino interactions to preserve the source flux ratio during propagation has been reported [298]. The fact that such interactions might help in finding out DM distribution is not that surprising. But the fact that it does so by imprinting the dark matter halo profile in the energy dependence of neutrino flavour ratios is rather intriguing. Alternatively, such an energy dependence might even originate at the source [299]. Various implications of the measurement of neutrino flavour ratios at IceCube have been studied in the literature, such as constraining certain new physics scenarios [300–302], neutrino decay [303, 304], testing the unitarity of mixing matrix [305], contributions from exotic sources [306, 307], etc.

The chapter is organised as follows: In the next section, we discuss certain general aspects of the neutrino sources relevant for this chapter, such as DM density profile, relation to black hole mass, etc. In Sec. 4.2 we lay down the formalism to evaluate the neutrino flavour ratios in the presence of a DM potential. The energy dependencies of flavour ratios and track to shower ratio at IceCube have been discussed in Sec. 4.3. Subsequently, we summarise our key findings.

4.1 Neutrino Astronomy

From Sec. 1.8.2 we know that ultralight scalar DM, is an attractive candidate to address the problems on smaller galactic scales [308–311]. In the case of BEC ultralight DM the associated quantum pressure compensates for the gravitational pressure, forming a constant density structure at the centre, called ‘solitonic core’ [49, 64, 64–66]. This core has a uniform density at the centre, but the density falls abruptly at some radial distance. This has been confirmed by numerical simulations. Various analytical calculations of ultralight DM profile, both in the presence and the absence of a BH at the centre of the galaxy has been carried out [314–316]. While presenting our results we have considered following DM profile of the solitonic core, in the presence of a SMBH of mass M_{BH} [314]:

$$\rho(r) = \rho_0 \exp(-r/a), \quad (4.1)$$

where

$$a = \frac{1}{GM_{\text{BH}}m_{\text{DM}}^2} \quad (4.2)$$

and ρ_0 is related to the mass of the solitonic core M_{sol} as

$$\rho_0 = \frac{M_{\text{sol}}M_{\odot}}{8\pi a^3} \text{pc}^{-3}, \quad (4.3)$$

with M_{\odot} as the solar mass.

The mass of SMBH and the solitonic core can be related by a scaling

$M_{\text{sol}} \sim M_{\text{halo}}^{1/3}$ for $m_{\text{DM}} \sim 10^{-22}$ eV [316]. On the other hand, an empirical formula has been proposed to relate the SMBH and halo mass using Sersic index and stellar velocity dispersion [317, 318]. There have also been attempts to predict the shape of the core using velocity dispersion [314, 315]. We show that the future neutrino telescopes can complement the traditional telescopes providing valuable inputs related to the shape of the DM profiles of various astrophysical objects. The core models of AGN are examples of the kind of astrophysical objects we are referring to. Although, the acceleration mechanism for the cosmic rays and sites for shocks are not known, for our purpose, it is safe to consider a situation in which neutrinos are produced from the charged pions originating from the interaction of accelerated protons with photons in the corona around a distance $\sim 10\text{--}40R_s$, where $R_s = 2GM_{\text{BH}}$ is the Schwarzschild radius of the black hole [319–321].

To get a feel for the length scales under consideration, let us consider $M_{\text{BH}} \sim 10^5 M_{\odot}$, for which $R_s \sim 5 \times 10^{-8}$ pc. The neutrino emission takes place around a distance 10^{-7} pc from the centre, where the DM density of the solitonic core is uniform, considering $m_{\text{DM}} \sim 3 \times 10^{-17}$ eV. According to eq. (4.2), this combination of M_{BH} and m_{DM} leads to $a = 10^{-6}$ pc, around where the core meets its edge. After this radial distance, the density of DM halo is drastically less. The sharp fall in the DM density at the edge can induce non-adiabaticity in the neutrino oscillation probability, which will in principle make neutrino astronomy possible determining the shape of the core. Here, the oscillation length of a neutrino of energy 1 PeV can only be as large as $\sim 10^{-12}$ pc. This reaffirms the fact that the oscillations do get averaged out while these neutrinos come out of these astrophysical objects. The aforementioned relations between the SMBH, halo, and soliton masses are under substantial investigation in the literature, which we will mention later on. As a consequence, in this chapter, we consider ρ_0 and a as the parameters describing DM profile while demonstrating the energy dependence of the flavour ratios.

As mentioned earlier, due to the low matter density in these environments, the standard matter effect due to electrons is negligible. But

the ultralight mass of the DM results in a sizable number density, leading to a substantial matter effect from ν -DM interactions. As we will show in the next section, the potential induced by such interactions drastically affect neutrino oscillations, so that the DM profile gets imprinted on the energy dependence of the flavour ratios of neutrinos detected at neutrino telescopes.

4.2 Neutrino Oscillations in a dark matter halo

Various aspects of neutrino-DM interactions have been studied in the literature [117, 185, 216, 217, 254, 264, 297, 298, 322–325]. An encyclopedia of interactions of neutrinos with ultralight scalar DM leading to an effective vertex $\nu\bar{\nu}\Phi\Phi^*$ can be found in ref. [254]. Most of these interactions are severely restricted by the ensuing interactions of the corresponding charged leptons implied by the $SU(2)_L$ invariance.

As an example, for the vectorial type of interaction,

$$\mathcal{L} \supset f'_{\alpha\beta} \bar{L}_\alpha \gamma^\mu P_L L_\beta Z'_\mu + ig'(\Phi^* \partial^\mu \Phi - \Phi \partial^\mu \Phi^*) Z'_\mu,$$

the constraints on the effective strength, $\epsilon_{\alpha\beta} = f'_{\alpha\beta} g'/m_{Z'}^2$, are as follows: In order to avoid anomalous energy loss in sun, one must ensure $\epsilon_{ee} \lesssim 10^{-38} \text{ eV}^{-2}$ [326]. LHC bounds from heavy Z' searches can be used to obtain $\epsilon_{\mu\mu} \lesssim 1.5 \times 10^{-26} \text{ eV}^{-2}$ [327]. Bounds on flavour violating charged lepton decays translate to $\epsilon_{\mu\tau} \lesssim 10^{-31} \text{ eV}^{-2}$ [328], $\epsilon_{\mu e} \lesssim 10^{-40} \text{ eV}^{-2}$ [329], and $\epsilon_{\tau e} \lesssim 4 \times 10^{-32} \text{ eV}^{-2}$ [329]. On the other hand, the constraints on $\epsilon_{\tau\tau}$ are comparatively less stringent. The most stringent bound on $\epsilon_{\tau\tau}$ comes from the measurement of partial Z decay width $\Gamma(Z \rightarrow \tau^+ \tau^-)$ which reads $\epsilon_{\tau\tau} \leq 1.3 \times 10^{-20} \text{ eV}^{-2}$ [254]. Hence, we explore the possible impact of matter effect on the flavour ratio of astrophysical neutrinos due to $\epsilon_{\tau\tau}$, at IceCube and future neutrino observatories. For very light dark matter, depending on

the model behind neutrino–DM interactions, given the rather relaxed limit mentioned above, $\epsilon_{\mu\mu}$ can also influence neutrino oscillations. Although for simplicity, here we will consider only $\epsilon_{\tau\tau}$ to be non-zero, the analysis can easily be extended to incorporate effects of $\epsilon_{\mu\mu}$ as well. Note that, as discussed in Sec. 3.3.3, to prevent ultralight DM from being thermalised in the primordial soup, the Big Bang nucleosynthesis (BBN) constraint demands $\epsilon \lesssim 6 \times 10^{-22} \text{ eV}^{-2}$ for all flavours.

In passing, a comment on feasibility to build such a model that allows only the third generation leptons to interact with DM seems quite pertinent. Such a scenario can easily be realised if such an interaction is mediated by a Z' vector boson, that related to a gauged $U(1)_\tau$ symmetry [254]:

$$\mathcal{L} \supset ig'(\Phi^* \partial_\mu \Phi - \Phi \partial_\mu \Phi^*) Z'^\mu + f \bar{\nu}_\tau \gamma_\mu \nu_\tau Z'^\mu. \quad (4.4)$$

On integrating out Z' , for $\sqrt{s} \ll m_{Z'}$, the Lagrangian takes the form

$$\mathcal{L} \supset i \frac{g' f}{m_{Z'}^2} (\Phi^* \partial_\mu \Phi - \Phi \partial_\mu \Phi^*) \bar{\nu}_\tau \gamma_\mu \nu_\tau.$$

This leads to an interaction strength $G'_F = g' f / m_{Z'}^2$. Henceforth, G'_F is synonymous with $\epsilon_{\tau\tau}$ in this chapter. A UV-complete model accommodating the renormalisable neutrino-DM interaction in presence of such a light Z' mediator is discussed in appendix 7.4.

In the non-relativistic limit a complex field can be decomposed as,

$$\phi(\vec{x}, t) = \frac{1}{\sqrt{2} m_{\text{DM}}} e^{-im_{\text{DM}} t} \psi(\vec{x}, t). \quad (4.5)$$

The conserved current for the scalar interaction in eq. (4.4) is $J_\mu = i(\phi^* \partial_\mu \phi - \phi \partial_\mu \phi^*)$. Using eq. (4.5) the conserved charge comes out to be

$$J_0 = i(\phi^* \dot{\phi} - \phi \dot{\phi}^*) = \frac{|\dot{\psi}|^2}{m_{\text{DM}}}. \quad (4.6)$$

Here we have used that in the non-relativistic limit $\dot{\psi} \ll m_{\text{DM}} \psi$. Moreover, the energy-momentum tensor for a complex scalar field is $T^{\mu\nu} = \partial^\mu \phi^* \partial^\nu \phi +$

$\partial^\nu \phi^* \partial^\mu \phi - \delta^{\mu\nu} \mathcal{L}$. Using eq. (4.5) and $\vec{\nabla} \phi, \vec{\nabla} \phi^* = 0$,

$$T^{00} = |\dot{\phi}|^2 + m_{\text{DM}}^2 |\phi|^2 = |\psi|^2.$$

But also, $T^{00} = \rho$. At the non-relativistic limit, the interaction in eq. (4.5) becomes

$$\mathcal{L} \supset i G'_F (\phi^* \dot{\phi} - \phi \dot{\phi}^*) \nu^\dagger \nu. \quad (4.7)$$

Using eqs. (4.6) and (4.7),

$$\mathcal{L} \supset G'_F (\rho/m_{\text{DM}}) \nu^\dagger \nu = G'_F n_{\text{DM}} \nu^\dagger \nu. \quad (4.8)$$

Therefore, while passing through the DM halo, neutrinos will experience a potential

$$V_{\tau\tau} = \frac{G'_F}{m_{\text{DM}}} \rho(r). \quad (4.9)$$

Several other models can also lead to ν -DM interactions of desired strength [254]. For these other interactions with different momentum dependencies, the resultant potentials simply differ by factors of m_{DM} .

In the presence of potential $V_{\tau\tau}$, the Hamiltonian governing the evolution of neutrinos is augmented by a ‘matter’ term as follows:

$$H_{\text{eff}} = \frac{1}{2E(1+z)} U \begin{pmatrix} 0 & 0 & 0 \\ 0 & \Delta m_{21}^2 & 0 \\ 0 & 0 & \Delta m_{32}^2 \end{pmatrix} U^\dagger - \begin{pmatrix} 0 & 0 & 0 \\ 0 & 0 & 0 \\ 0 & 0 & V_{\tau\tau}(r) \end{pmatrix}, \quad (4.10)$$

where U stands for the PMNS matrix in vacuum and the redshift z is indicative of the location of the neutrino source from the Earth. E is the energy of the neutrino at earth. As mentioned in Sec. 1.7, due to CP symmetry for antineutrinos $V_{\tau\tau}$ flips its sign.

H_{eff} has to be diagonalised to compute the modified PMNS matrix in the presence of the DM potential. Owing to the extreme density at the core of these astrophysical objects, the first term in eq. (4.10) is negligible

compared to the second term for extremely energetic neutrinos. As a result, U^S , the PMNS matrix at the source of production, becomes an identity matrix for $E \gtrsim 50$ PeV. At the Earth, however, both the terms in eq. (4.10) should be taken into account for computation of U^D , the PMNS matrix at the detector. In this case, $z = 0$, and U^D depends on energy of the neutrino as recorded on earth and the combination G'_F/m_{DM} , that decide the value of $V_{\tau\tau}$ at the detector.

The mean free path of neutrinos at earth due to neutrino scattering off electrons, in the SM scenario, is around 10^4 km for $E = 1$ PeV [10, 213]. Therefore, around 60% of neutrinos are absorbed for $\cos\theta_Z = -0.3$ [213] (zenith angle $\theta_Z = 107^\circ$). As $n_e\sigma_{\nu e}L \sim 1$, this scattering disrupts the effect of neutrino oscillation, modifying the arrival direction and energy spectrum. Therefore, we do not see any MSW effect for neutrinos passing through the Earth as neutrino absorption is the dominant effect at such energy.

Large DM density at the core leads to a considerable shift of the values of the effective mixing angles from the vacuum mixing angles. Moreover, a sharp change in the density profile may give rise to non-adiabaticity. Following Sec. 1.7, from eq. (1.32), the neutrino flavour oscillation probability is given by,

$$P_{\alpha\beta} = |U_{\alpha i}^S|^2 |U_{\beta i}^D|^2 - P_{ij}^c (|U_{\alpha i}^S|^2 - |U_{\alpha j}^S|^2) (|U_{\beta i}^D|^2 - |U_{\beta j}^D|^2) - P_{ik}^c P_{kj}^c (|U_{\alpha i}^S|^2 - |U_{\alpha k}^S|^2) (|U_{\beta k}^D|^2 - |U_{\beta j}^D|^2). \quad (4.11)$$

Here, we use the convention of summation over repeated indices, which will be followed in the rest of the chapter too. Note that, the first term on the right is the adiabatic contribution after neutrino oscillations get averaged out as the oscillation length is much less than the distance traversed. The rest of the terms contribute only when some non-adiabaticity is present. P_{ij}^c stands for the jumping probability between the two mass eigenstates ν_i

and ν_j and is given by:

$$P_{ij}^c = \frac{\exp(-\frac{\pi}{2}\gamma_{ij}^R F_{ij}) - \exp(-\frac{\pi}{2}\gamma_{ij}^R \frac{F_{ij}}{\sin^2 \theta_{ij}})}{1 - \exp(-\frac{\pi}{2}\gamma_{ij}^R \frac{F_{ij}}{\sin^2 \theta_{ij}})}, \quad (4.12)$$

where γ_{ij} is the non-adiabaticity parameter, which at the resonance is given by

$$\gamma_{ij}^R = \frac{\Delta m_{ij}^2 \sin^2 2\theta_{ij}}{2E \cos 2\theta_{ij} |d \ln \rho / dr|_R}. \quad (4.13)$$

$\gamma_{ij} \sim 0$ corresponds to extreme non-adiabaticity. A significant amount of non-adiabaticity, leading to transitions between different mass eigenstates, can be induced in our case due to the interplay of the extreme energy of the neutrinos and the density gradient of DM at the edge of the solitonic core inside an AGN. For the profile given by eq. (4.1), $|d \ln \rho / dr|_R = 1/a$ and

$$F_{ij} = \frac{4}{\pi} \text{Im} \int_0^i db \frac{(b^2 + 1)^{1/2}}{(b \tan 2\theta_{ij} + 1)} = \begin{cases} 1 - \tan^2 \theta_{ij}, & \text{if } \theta_{ij} \leq \pi/4 \\ 1 - \cot^2 \theta_{ij}, & \text{if } \theta_{ij} > \pi/4. \end{cases} \quad (4.14)$$

Energy dependence in $P_{\alpha\beta}$ creeps in through U^D and P_{ij}^c . Note that in eq. (4.11), $P_{\alpha\beta}$ denotes the probability of oscillation from the flavour α to β and it differs from $P_{\beta\alpha}$ due to the different DM densities at the source and the detector. Within this chapter, due to the only non-zero $V_{\tau\tau}$ component, ν_1 never jumps to ν_2 and vice versa, so that $P_{12}^c = P_{21}^c = 0$. Also, one needs to be cautious in reading off eq. (4.11). Here, for the non-adiabatic contributions only those terms relevant for the scenario has to be taken into account. For example, if the 31 resonance is followed by a 32 resonance, only the term $P_{32}^c P_{31}^c$ has to be included in the term responsible for two resonances. In principle, depending on the density profile of the DM, eq. (4.11) can easily be extended to include terms with more than two resonances.

While presenting numerical estimates we use the following set of parameters obtained from a global fit [37, 330] of solar, atmospheric, reactor

and accelerator neutrino oscillation experiments : $\theta_{12} = 33.8^\circ$, $\theta_{23} = 48.6^\circ$, $\theta_{13} = 8.6^\circ$, $\delta_{\text{CP}} = 1.22\pi$ rad. This set corresponds to the normal hierarchy of the neutrino masses, with $\Delta m_{32}^2 = m_3^2 - m_2^2 = 2.53 \times 10^{-3}$ eV² and $\Delta m_{21}^2 = m_2^2 - m_1^2 = 7.39 \times 10^{-5}$ eV².

Around the Earth, the density of the galactic dark matter halo does not vary rapidly enough to induce any non-adiabaticity to neutrino oscillations. Hence, the results are independent of the choice of DM profiles in our galaxy. However, the DM density at earth is important to estimate the adiabatic contributions to the probability, and we take it to be 0.4 GeV/cm³ [331]. Hence, for the DM profile considered here, there are four quantities that determine the probability of oscillations: the redshift z , the parameters related to the solitonic core ρ_0 and a , and the combination G'_F/m_{DM} .

4.3 Energy dependence of flavour ratios

Neutrino flavour ratios at the detector is related to the same at source as follows

$$f_\beta^D = P_{\alpha\beta} f_\alpha^S. \quad (4.15)$$

Clearly, in the case of vacuum oscillations, for the source flux ratio 1 : 1 : 1, the flavour ratio at earth remains 1 : 1 : 1. If the ratio at source is 1 : 2 : 0, then the flavour ratio at the detector

$$f_\beta^D = P_{e\beta} + 2P_{\mu\beta} = |U_{\beta i}|^2 (|U_{ei}|^2 + 2|U_{\mu i}|^2). \quad (4.16)$$

This leads to $f_e^D : f_\mu^D : f_\tau^D \simeq 1 : 1 : 1$. For $\theta_{13} = 0$, the equality is exact. While these favour ratios at earth are energy independent, as we will further discuss, neutrino-DM interactions may induce an energy dependence.

In the presence of large matter effect, the mixing matrix at the source deviates significantly from that at vacuum. In matter, $\sin 2\theta_{13}^M = \Delta m_{31}^2 \sin 2\theta_{13} / [(2EV_{\tau\tau} - \Delta m_{31}^2 \cos 2\theta_{13})^2 + (\Delta m_{31}^2 \sin 2\theta_{13})^2]^{1/2}$ and as E

is large, $2EV_{\tau\tau} \gg \Delta m_{31}^2 \cos 2\theta_{13}$, leading to a vanishingly small $\sin 2\theta_{13}^M$. Similarly, $\sin 2\theta_{23}^M$ also becomes small at large values of E . As E increases further, the vacuum oscillation term of the Hamiltonian can be neglected and the mixing matrix tends to identity.

In the case of adiabatic oscillation, due to a large matter effect induced by neutrino-DM interaction, the flavour ratios of the (anti)neutrinos at the source are preserved [298]. Here we focus on a more general and interesting possibility of non-adiabatic flavour transition which can change flavour ratio at IceCube. As eq. (4.11) indicates, the probability of flavour transition in such a general scenario depends on U^S , U^D , P_{31}^c , and P_{32}^c . These in turn depends on G'_F/m_{DM} , a , and the DM density at the detector and source. As discussed in Sec. 4.2, with the best-fit values of the PMNS mixing angles considered here, θ_{23} and θ_{13} lie in the second and first quadrants respectively. Thus, the resonance condition, $2E_{ij}^R V_{\tau\tau} = \Delta m_{ij}^2 \cos 2\theta_{ij}$ is satisfied for the negative and positive values of the potential for $ij = 32$ and $ij = 31$ respectively. According to eq. (4.13), for a fixed value of E , the condition for non-adiabatic oscillation, $\gamma_R^{ij} \lesssim 1$ is satisfied for two different values of a for the 32 and 31 transitions. For $E < 1$ PeV, $\gamma_{31} \lesssim 1$ is obtained for $a \lesssim 10^{-3}$ pc for positive $V_{\tau\tau}$, whereas, for negative $V_{\tau\tau}$, $\gamma_{32} \lesssim 1$ for $a \lesssim 10^{-5}$ pc. Henceforth, we consider $V_{\tau\tau}$ to be positive for neutrinos and thus, negative for antineutrinos. In the following, we discuss the energy dependence of the flavour ratios for different values of a with $\rho_0 = 7.4 \times 10^{-3}$ eV⁴ and $G'_F/m_{\text{DM}} = 10^{-13}$ eV⁻³.

- For $E < 1$ PeV, both neutrinos and antineutrinos undergo adiabatic transition for $a \gtrsim 10^{-3}$ pc. Hence, the flavour ratios at the detector can be written as

$$f_\beta^D = P_{\alpha\beta} f_\alpha^S = |U_{\beta i}^D|^2 |U_{\alpha i}^S|^2 f_\alpha^S = |U_{\beta i}^D|^2 |U_{ei}^S|^2 + 2|U_{\beta i}^D|^2 |U_{\mu i}^S|^2.$$

As U^S tends to an identity matrix at high energies, the above relation simplifies to $f_\beta^D = |U_{\beta 1}^D|^2 + 2|U_{\beta 2}^D|^2$. With increasing energy, the off-diagonal terms of U^D decrease as well. Thus the fraction of ν_μ

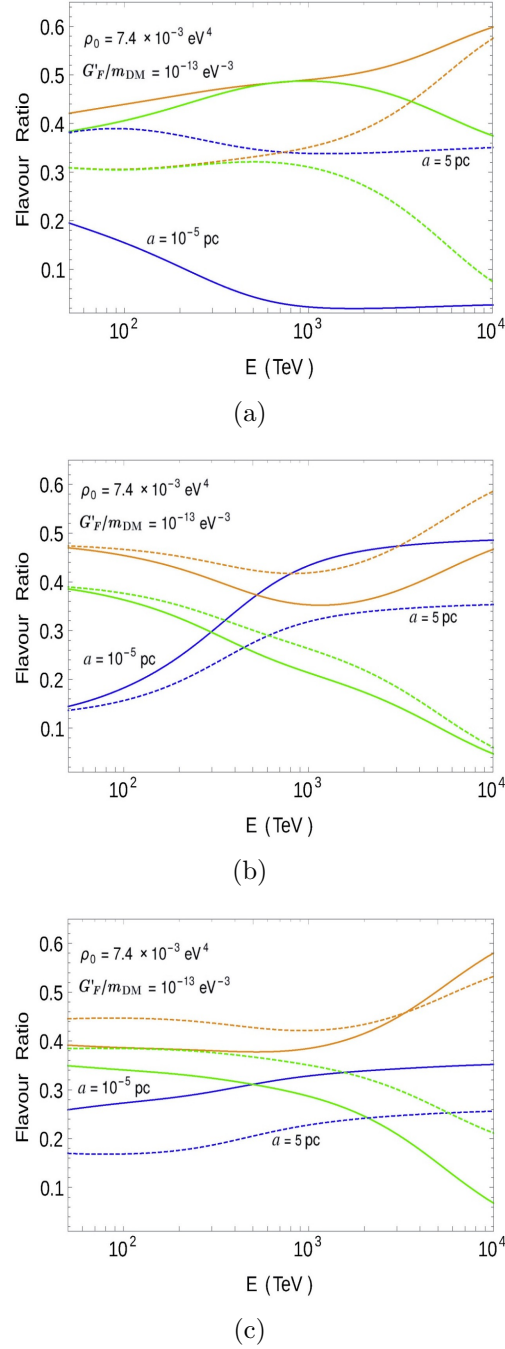


Figure 4.1. Energy dependence of flavour ratios for (a) neutrinos (f_α^D) and (b) antineutrinos ($f_{\bar{\alpha}}^D$), and (c) the average of neutrinos and antineutrinos (F_α^D). The blue, orange and green lines represent flavour ratio for e , μ and τ flavours. Solid and dashed lines stand for $a = 10^{-5} \text{ pc}$ (non-adiabatic case) and $a = 5 \text{ pc}$ (adiabatic case) respectively.

increases and ν_τ nearly diminishes at higher energies. As a result, at energies $E \gtrsim 50 \text{ PeV}$, the flavour ratio at the detector becomes $1 : 2 : 0$, the same as the flavour ratio at source. This can be seen

in fig. 4.1 for $a = 5$ pc, which corresponds to the adiabatic case. As it can be seen from eq. (4.2), such a value of a can be achieved for $M_{\text{BH}} = 10^5 M_{\odot}$ and $m_{\text{DM}} = 1.3 \times 10^{-20}$ eV.

- In the case of neutrinos, for the benchmark $a = 10^{-5}$ pc, there is a significant violation of adiabaticity only for the jumping of ν_1 to ν_3 for $E \gtrsim 1$ PeV. Hence, the ratio of electron neutrinos at the detector is given as

$$f_e^D = |U_{ei}^D|^2 |U_{\alpha i}^S|^2 f_{\alpha}^S - P_{31}^c (|U_{e1}^D|^2 - |U_{e3}^D|^2) (|U_{\alpha 1}^S|^2 - |U_{\alpha 3}^S|^2) f_{\alpha}^S.$$

As mentioned earlier, for fixed value of ρ_0 and G'_F , as the energy increases the effective Hamiltonian is dominated by the matter potential term. Thus the mixing matrices U_S and U_D tend to identity matrix leading to $f_e^D = 1 - P_{31}^c$. For the benchmark shown in fig. 4.1(a) with $a = 10^{-5}$ pc, P_{31}^c increases with energy and finally attains a constant value of $P_{31}^c \sim 0.98$. As a result, f_e^D decreases with energy and eventually saturates. Similarly, the ratio of muon neutrinos at high energies simplifies to,

$$\begin{aligned} f_{\mu}^D &= 2|U_{\mu 2}^D|^2 |U_{\mu 2}^S|^2 - 2P_{31}^c (|U_{\mu 1}^D|^2 - |U_{\mu 3}^D|^2) (|U_{\mu 1}^S|^2 - |U_{\mu 3}^S|^2) \\ &\quad - P_{31}^c (|U_{\mu 1}^D|^2 - |U_{\mu 3}^D|^2) (|U_{e 1}^S|^2 - |U_{e 3}^S|^2) \\ &\simeq 2 - P_{31}^c (|U_{\mu 1}^D|^2 - |U_{\mu 3}^D|^2). \end{aligned}$$

For this benchmark, the combination of the off-diagonal elements $(|U_{\mu 1}^D|^2 - |U_{\mu 3}^D|^2)$ decreases with increasing energy. Thus, f_{μ}^D increases with energy. Also, the fraction of tau neutrinos at high energies simplifies to,

$$\begin{aligned}
 f_\tau^D &= |U_{\tau 1}^D|^2 |U_{e 1}^S|^2 + 2|U_{\tau 2}^D|^2 |U_{\mu 2}^S|^2 - 2P_{31}^c (|U_{\tau 1}^D|^2 - |U_{\tau 3}^D|^2) (|U_{\mu 1}^S|^2 - |U_{\mu 3}^S|^2) \\
 &\quad - P_{31}^c (|U_{\tau 1}^D|^2 - |U_{\tau 3}^D|^2) (|U_{e 1}^S|^2 - |U_{e 3}^S|^2) \\
 &\simeq -P_{31}^c (|U_{\tau 1}^D|^2 - |U_{\tau 3}^D|^2).
 \end{aligned}$$

Subsequently, as it can be seen from fig. 4.1(a), for $a = 10^{-5}$ pc, the flavour ratio for neutrinos tend towards 0 : 2 : 1 at higher energies.

- The flavour ratios for electron and muon antineutrinos after non-adiabatic transition can be simplified to

$$\frac{f_{\bar{e}}^D}{f_{\bar{\mu}}^D} = \frac{|U_{e 1}^D|^2 + 2|U_{e 2}^D|^2 - 2P_{32}^c (|U_{e 2}^D|^2 - |U_{e 3}^D|^2)}{2|U_{\mu 2}^D|^2 (1 - P_{32}^c)}.$$

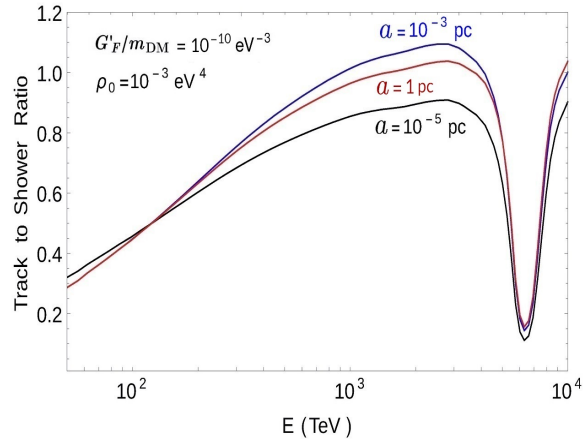
With increasing energy the off-diagonal terms in U^D decrease and P_{32}^c increases before it finally saturates. As an example, for $a = 10^{-5}$ pc, P_{32}^c attains a value of ~ 0.43 for $E \gtrsim 3$ PeV. Thus, $f_{\bar{e}}^D$ increases and $f_{\bar{\mu}}^D$ decreases at higher energies, leading to $f_{\bar{e}}^D / f_{\bar{\mu}}^D = 1 / (2 - 2P_{32}^c) \sim 1$ for $E \gtrsim 10$ PeV. This has been shown in fig. 4.1(b).

At IceCube, the flavour ratios of astrophysical neutrinos are extracted from the track to shower ratio. For bin (E_{min}, E_{max}) the number of tracks (N_T) and shower (N_S) at IceCube are evaluated as

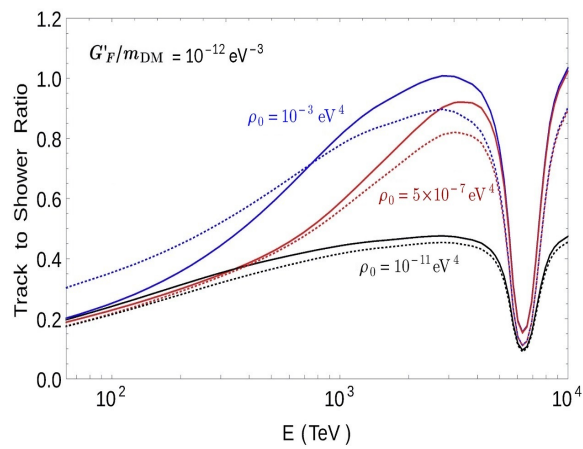
$$\begin{aligned}
 N_S &= 4\pi T \int_{E_{min}}^{E_{max}} dE \{ \phi_e A_e + (1 - p_\tau^T) \phi_\tau A_\tau + (1 - p_\mu^T) \phi_\mu A_\mu \}, \\
 N_T &= 4\pi T \int_{E_{min}}^{E_{max}} dE \{ p_\tau^T \phi_\tau A_\tau + p_\mu^T \phi_\mu A_\mu \}.
 \end{aligned}$$

Here A_l , ϕ_l , and p_l^T are the effective area [332], neutrinos flux at earth and the probability of neutrino of flavour l to produce a track event respectively. Taking small energy bins, ϕ_l and A_l are constants and the ratio of N_T to N_S is approximately

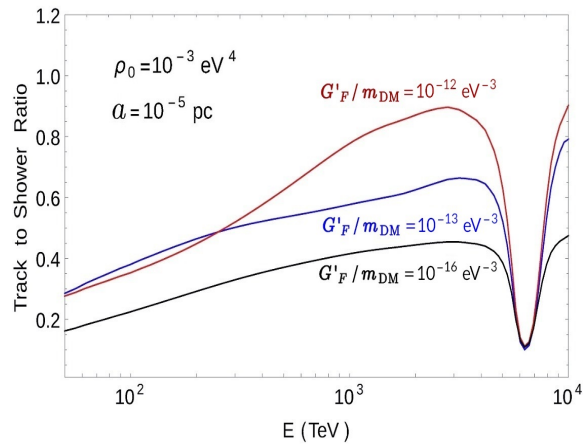
$$\frac{N_T}{N_S} = \frac{p_\tau^T \phi_\tau A_\tau + p_\mu^T \phi_\mu A_\mu}{\phi_e(E) A_e(E) + (1 - p_\tau^T) \phi_\tau A_\tau + (1 - p_\mu^T) \phi_\mu A_\mu}.$$



(a)



(b)



(c)

Figure 4.2. Track to shower ratio vs. neutrino energy for varying values of (a) radius of the solitonic core a , (b) DM density at its centre ρ_0 , and (c) G'_F/m_{DM} . In (b), the solid and dotted lines correspond to $a = 1$ pc (adiabatic case) and 10^{-5} pc (non-adiabatic case) respectively.

The probability of obtaining a track from muon and tauon neutrino is evaluated as

$$p_{\mu}^T = \frac{\sigma_{CC}^{\nu N} M_{\mu}^{CC}}{\sigma_{CC}^{\nu N} M_{\mu}^{CC} + \sigma_{NC}^{\nu N} M_{\mu}^{NC}},$$

$$p_{\tau}^T = \frac{\sigma_{CC}^{\nu N} \times \text{BR}(\tau \rightarrow \nu_{\tau} \mu \bar{\nu}_{\mu}) M_{\tau}^{CC}}{\sigma_{CC}^{\nu N} M_{\tau}^{CC} + \sigma_{NC}^{\nu N} M_{\tau}^{NC}},$$

where $M_l^{CC(NC)}$ is the effective mass of detector for CC (NC) interaction [332]. Using $\text{BR}(\tau \rightarrow \nu_{\tau} \mu \bar{\nu}_{\mu}) \sim 17\%$, the probability of obtaining a track from a ν_{μ} and ν_{τ} are approximated as 0.8 [333] and 0.13 respectively. Thus the track to shower ratio reads:

$$\frac{N_{\text{track}}}{N_{\text{shower}}} = \frac{0.8A_{\mu}f_{\mu}^D + 0.13A_{\tau}f_{\tau}^D}{A_e f_e^D + 0.2A_{\mu}f_{\mu}^D + 0.87A_{\tau}f_{\tau}^D}, \quad (4.17)$$

where $f_l^D = \phi_l / (\phi_e + \phi_{\mu} + \phi_{\tau})$.

At lower energies, both electromagnetic shower produced by ν_e and hadronic shower by ν_{τ} lead to cascade signatures at IceCube. Thus, at lower energies, track to shower ratio is the only probe of the flavour ratios. But for energies higher than \sim PeV, ν_{τ} can leave distinguishable signatures in the form of double bang and lollipop events. Moreover, it has been pointed out that, hadronic showers can be distinguished from electromagnetic showers in the TeV-PeV range by means of a new observable called ‘pion and neutron echos’ [334]. If such a distinction of electron and tau neutrino events are successfully performed, the flavour ratio can be known with an unprecedented accuracy after a substantial livetime of IceCube-Gen2 operation [211].

In the following, we discuss the change in the track to shower ratio for varying values of a , ρ_0 , and G'_F shown in fig. 4.2. Note that, we also take into account the contributions of antineutrinos while computing the track to shower ratio. The effective areas for neutrinos and antineutrinos are the same except for the electron flavour due to the possibility of hadronic shower induced by $\bar{\nu}_e$ at $E \sim 6.3$ PeV.

- **Dependence on a :**

In fig. 4.2(a) we have shown the changes in track to shower ratio for $a = 10^{-5}$ pc, 10^{-3} pc, and 1 pc with fixed values of $\rho_0 = 10^{-3}$ eV⁴ and $G'_F/m_{\text{DM}} = 10^{-10}$ eV⁻³. As mentioned in Sec. 4.2, with the neutrino energies considered in this chapter, both neutrinos and antineutrinos undergo adiabatic transition for $a = 1$ pc. Similarly, for $a = 10^{-5}$ pc, both neutrinos and antineutrinos undergo non-adiabatic transitions. However, for $a = 10^{-3}$ pc, only neutrinos can have non-adiabatic transition.

As can be seen from fig. 4.1(b), for $a = 10^{-5}$ pc, $f_{\bar{\mu}} \sim f_{\bar{e}}$ and $f_{\bar{\tau}} \sim 0$ at higher energies. On the other hand, for $a = 10^{-3}$ pc the antineutrinos propagate adiabatically leading to the flavour ratio $\sim 1 : 2 : 0$ at high energies. Thus, the value of track to shower ratio is larger for $a = 10^{-3}$ pc compared to the case of $a = 10^{-5}$ pc.

Following the previous logic, one may apparently expect the track to shower ratio to be higher for $a = 1$ pc compared to $a = 10^{-3}$ pc. But, as it was shown in fig. 4.1(a), the ratio $f_{\mu}^D / (f_e^D + f_{\tau}^D)$ is higher for the non-adiabatic case compared to the adiabatic case. For $a = 10^{-3}$ pc, neutrinos oscillate non-adiabatically, thereby leading to a higher value of track to shower ratio compared to $a = 1$ pc.

- **Dependence on ρ_0 :**

To understand the dependence of track to shower ratio on DM density at the source, in fig. 4.2(b) we consider three benchmark values $\rho_0 = 10^{-3}$ eV⁴, 5×10^{-7} eV⁴, and 10^{-11} eV⁴, while fixing $a = 1$ pc (10^{-5} pc) and $G'_F/m_{\text{DM}} = 10^{-12}$ eV⁻³. These three benchmark values of ρ_0 lead to $E_{31}^R \sim 10^{11}$ eV, 10^{15} eV and 10^{19} eV respectively.

Let us first discuss the adiabatic case with $a = 1$ pc. For $E \lesssim E_{31}^R$, the vacuum term in the effective Hamiltonian is more significant than the matter term. Thus, in the limit $E \ll E_{ij}^R$, the flavour ratio is close to $1 : 1 : 1$. Though, at much higher energies the matter term becomes more significant, resulting in a flavour ratio of $\sim 1 : 2 : 0$, as it

is expected in a typical adiabatic scenario. This was also shown in fig. 4.1(c) for $a = 5$ pc, where the ratio of averaged muon-flavour contribution (F_μ^D) to the electron and tau (anti)neutrinos increase with energy. Thus, the case with a lower value of E^R will lead to a larger fraction of muon (anti)neutrinos. So, as can be seen from fig. 4.2(b), the benchmark with higher DM density at source has a larger value of track to shower ratio till the resonance energy.

The non-adiabatic case also shows similar features. Note that, the track to shower ratio becomes saturated to its maximum value for $\rho_0 \gtrsim 10^{-3}$ eV⁴ and to its minimum value at $\rho_0 \lesssim 10^{-11}$ eV⁴. In other words, the case with $\rho_0 = 10^{-11}$ eV⁴ almost coincides with the standard scenario with no DM at the source.

- **Dependence on G'_F/m_{DM} :**

In fig. 4.2(c) we consider $G'_F/m_{\text{DM}} = 10^{-16}$ eV⁻³, 10^{-13} eV⁻³, and 10^{-12} eV⁻³, with a fixed DM profile $\rho_0 = 10^{-3}$ eV⁴ and $a = 10^{-5}$ pc. As it can be seen from fig. 4.1(c) at lower energies, though the value of F_μ^D is higher than the individual electron or tau-flavour contributions, the value of $F_\mu^D/(F_e^D + F_\tau^D)$ is slightly lower than one. But for $E \gtrsim 500$ TeV, the muon-flavour contribution F_μ^D increases with energy and the tau-flavour contribution abruptly decreases, leading to $F_\mu^D/(F_e^D + F_\tau^D) > 1$.

The resonance energy is inversely proportional to $V_{\tau\tau}$, and therefore to, G'_F/m_{DM} . Thus, the flavour ratios for $G'_F/m_{\text{DM}} = 10^{-12}$ eV⁻³, $f_i(E)$ can be related to the flavour ratios for $G'_F/m_{\text{DM}} = 10^{-13}$ eV⁻³, $f'_i(E)$, such that $f_i(E) \simeq f'_i(E/10)$. Hence, as can be inferred from fig. 4.1(c), for $E \gtrsim 300$ TeV the case with $G'_F/m_{\text{DM}} = 10^{-12}$ eV⁻³ has a higher muon (anti)neutrino contribution, and in turn, a larger value of track to shower ratio. Also it can be seen from fig. 4.1(c) that, for lower energies, F_e^D slightly increases whereas F_μ^D and F_τ^D do not significantly change. Thus, $G'_F/m_{\text{DM}} = 10^{-12}$ eV⁻³ leads to a larger value of F_e^D , and therefore a smaller value of track to

shower ratio. These effects can be read off fig. 4.2(b). Moreover, for $G'_F/m_{\text{DM}} = 10^{-16} \text{ eV}^{-3}$, the track to shower ratio attains its standard value.

In this chapter, we have considered only positive values of $V_{\tau\tau}$. Although, for negative values of $V_{\tau\tau}$, the ratio $f_\mu^D/(f_e^D + f_\tau^D)$ becomes larger compared to the case of positive $V_{\tau\tau}$. Hence, one can expect a larger value of the track to shower ratio near $E \sim 6.3 \text{ PeV}$.

As it was pointed out in Sec. 4.2, $\epsilon_{\mu\mu}$ is constrained at $\mathcal{O}(10^{-26}) \text{ eV}^{-2}$. Thus, non-zero values of $V_{\mu\mu}$ may also lead to significant changes in the track to shower ratios for rather small values of m_{DM} . Also, scalar-mediated neutrino-DM effective interactions are constrained from invisible Z decay at $\mathcal{O}(10^{-10}) \text{ eV}^{-1}$ [254] and may lead to observable effects in flavour ratios. Though, in a concrete model with a $Y = 2$ triplet scalar, the smallness of neutrino mass renders this effective interaction to be quite small to have any interesting effect on flavour ratios.

As mentioned earlier, the empirical relationship between M_{BH} and M_{halo} is derived from the correlation of M_{BH} and stellar velocity dispersion [317]. Slightly refined versions of such a relationship also exist in the literature [318, 335]. On the other hand, the scaling relation between the masses of solitons and their host halos was found in ref. [316] from structure formation simulations. Utilising $M_{\text{BH}} - M_{\text{halo}}$ relation from ref. [317] and $M_{\text{sol}} - M_{\text{halo}}$ from ref. [316], we had earlier estimated that the combination of $M_{\text{BH}} \sim 10^5 M_\odot$ and $m_{\text{DM}} \sim 3 \times 10^{-17} \text{ eV}$ leads to $a \sim 10^{-6} \text{ pc}$, $M_{\text{sol}} \sim 10^4 M_\odot$, and $\rho_0 \sim 10^{20} \text{ eV}^4$. This is a typical scenario which leads to non-adiabatic flavour transition for both neutrinos and antineutrinos. Though, it has been shown in ref. [315] that the value of M_{sol} in the presence of SMBH can deviate from that predicted by ref. [316]. As example, for $m_{\text{DM}} \sim 10^{-19} \text{ eV}$, the value of soliton mass in the presence of SMBH can be smaller compared to M_{sol} predicted by ref. [316] by an order of magnitude. These issues are under active scrutiny and a better understanding of the interplay between M_{BH} , M_{sol} , and M_{halo} is expected to emerge in

the future, which will further strengthen our prescription by reducing the number of unknown variables in the fit.

Now, building on our previous discussions, we try to point out the region of interest in the parameter space of $\{a, \rho_0, G'_F/m_{\text{DM}}\}$. For the neutrino energy range considered here, non-adiabatic oscillation in neutrino (antineutrino) propagation occurs for $a \lesssim 10^{-3}$ pc ($a \lesssim 10^{-5}$ pc). We have seen that the track to shower ratio is sensitive to the ultralight DM profile for 10^{-11} eV⁴ $\lesssim \rho_0 \lesssim 10^{-3}$ eV⁴. For $\rho_0 \gtrsim 10^{-3}$ eV⁴, the mixing matrix at source U^S becomes an identity matrix, thereby making the flavour ratios independent of ρ_0 . On the other hand, for $\rho_0 < 10^{-11}$ eV⁴, U^S is similar to the mixing matrix in the vacuum. Also, there exists an upper bound on M_{sol} , and thus, ρ_0 from the measurement of total enclosed mass in astrophysical objects. It has been seen that, track to shower ratio is sensitive to G'_F/m_{DM} in the range 10^{-16} eV⁻³ $\lesssim G'_F/m_{\text{DM}} \lesssim 10^{-10}$ eV⁻³. Combining with the BBN constraint $G'_F \lesssim 6 \times 10^{-22}$ eV⁻² mentioned in Sec. 4.2, $G'_F/m_{\text{DM}} \gtrsim 10^{-16}$ eV⁻³ indicates that a non-standard flavour ratio at IceCube can be seen for $m_{\text{DM}} \lesssim 10^{-6}$ eV.

As implied in eq. (4.2), the size of solitonic core depends on M_{BH} and m_{DM} . Along with the lower bound $m_{\text{DM}} \gtrsim 10^{-22}$ eV mentioned in Sec. 4.1, for BH mass as low as $M_{\text{BH}} \sim 10^5 M_{\odot}$, the solitonic core is such that $a \sim 10^4$ pc. Also, for a large BH mass $M_{\text{BH}} \sim 10^{10} M_{\odot}$ and the aforementioned limiting value $m_{\text{DM}} \sim 10^{-6}$ eV, a can attain values as low as $\sim 10^{-33}$ pc. But, in a realistic scenario, such a small DM halo will be fully contained inside the SMBH itself, leading to no effects in neutrino oscillation.

4.4 Summary and outlook

In the astrophysical neutrino sources, such as AGNs, the matter accretion disc and a dark matter halo can surround a super-massive black hole. Sub-eV ultralight scalar dark matter, in a form of Bose-Einstein condensate,

happens to be a suitable candidate for cold dark matter. An interaction of these high energy neutrinos with such ultralight DM is an interesting proposal that helps to address various features of the observed neutrino spectrum, as well as the lack of directional coherence with particular astrophysical objects. In that spirit, in this chapter we have considered if such interactions can be important for neutrino astronomy through the observation of neutrino flavour ratios at earth.

We find that while passing through the DM halo, the details of the halo profile, DM mass, the redshift associated with the AGN, the strength of such interactions, masses of the SMBH and DM halo get encoded into the energy dependence of neutrino flavour ratio at the IceCube. In future, the statistics at IceCube will improve with the Gen2 upgrade. Besides IceCube, KM3NeT/ARCA will also have the potential to detect point-like extragalactic neutrino sources [194]. The accuracy for directionality in ARCA can even be better compared to the IceCube, making it a somewhat better probe of such astrophysical sources [239]. At that point, more such neutrinos can possibly be traced back to the potential astrophysical sources. This will allow the usage of our proposed method to perform neutrino astronomy. The knowledge of some of the parameters like the masses of the SMBH and DM halo, the distance of the AGN from other modes of astronomy may help us improve the fit to the rest of the unknowns.

In spite of the large neutrino energies, the centre of mass energy for neutrino scattering off ultralight DM is much less compared to the mass of the particle mediating such interactions. The latter can be of $\mathcal{O}(\text{MeV})$ for the case of a light Z' . In such cases, the resulting ν -DM cross-section is negligible, to lead to any appreciable neutrino flux suppression [254]. We have shown that, even for ν -DM interactions feeble enough to impart any changes in astrophysical neutrino flux, the track to shower ratios can significantly modify due to the large DM number density. Even if the nature of effective interactions are more complicated with additional momentum dependencies, the DM potentials for neutrinos vary only by factors of m_{DM} . This allows us to define a single effective interaction strength G'_F .

In this chapter, we have used the current best-fit values of neutrino mass and mixing parameters for normal ordering. In the case of inverted ordering, both Δm_{31}^2 and Δm_{32}^2 are negative by definition, whereas the best-fit values of mixing angles remain in the same octants as per the observations [37, 330]. Thus, for $ij = 32$ and $ij = 31$ the resonance condition $2E_{ij}^R V_{\tau\tau} = \Delta m_{ij}^2 \cos 2\theta_{ij}$ is satisfied for a positive and negative value of $V_{\tau\tau}$ respectively. Note that, so far we have restricted our discussion to the best-fit values of Δm_{ij}^2 and θ_{ij} . But, for both the normal and inverted ordering, 3σ allowed ranges on θ_{23} span over the first and second octants, thereby allowing both positive and negative values of $\cos 2\theta_{23}$. So, deviating from the best-fit values opens up the possibility of resonant effects in both 32 and 31 transitions. As mentioned in Sec. 4.2, this effect leads to new terms proportional to $P_{32}^c P_{31}^c$ in the final flavour ratios. However, future reactor experiments, such as JUNO [336], atmospheric neutrino experiments like HyperK [337], PINGU [338], ICAL [342] and accelerator experiments like DUNE [339], T2HK/T2HKK [340] aim to resolve neutrino mass ordering. Out of these HyperK [337], PINGU [338], DUNE [339], T2HK/T2HKK [340] may also resolve octant degeneracy. Certain combinations of these experimental data, for example, JUNO+PINGU [342], Daya Bay II+PINGU [343] can be decisive for this purpose through synergy effects. With a better understanding of the mass ordering and the sign of $\cos 2\theta_{23}$, the determination of G'_F within our framework can be easier.

Another important aspect is the role of local DM density in this proposal. The galactic DM density does not change that rapidly to lead to any non-adiabaticity. For our galaxy, the gradient of DM number density $|d \ln n_\Phi / dr| \sim 1/a$ with Isothermal profile is orders of magnitude smaller than that inside the typical AGN sources. With the NFW profile, DM density very near to the centre of our galaxy can be substantial. But as the density spikes at a very narrow range, the number of neutrinos coming through this region might not be substantial to lead to any major impact to this proposal. So only the local density of DM, $\rho = 0.4 \text{ GeV/cm}^3$, makes an entry in the first term in eq. (4.12), otherwise, it is not sensitive to the

local halo profile.

So far only one IceCube source could be traced back to its origin. With more statistics from the next generation of IceCube and other neutrino telescopes like KM3NeT, it might become possible to point out more such sources of astrophysical neutrinos. With the help of precise observations of mixing matrix parameters from DUNE, JUNO and Hyper-Kamiokande, the future neutrino telescopes like Gen2, will efficiently reduce the error on flavour composition at source to $< 6\%$ in 20 years of running [344]. With such precise measurements Gen2 will put stringent constraints on BSM models like the one we considered in our thesis. Exploiting the theoretical relations between M_{BH} , M_{halo} , and M_{sol} , for a subset of these sources a dedicated fit of the track to shower ratios at various energy bins will provide sensible values of G'_F and m_{DM} . These can in turn be used to probe other astrophysical neutrino sources. With a significant livetime of the future neutrino telescopes we can hope to explore such interesting aspects of neutrino astronomy. This proposed method may then complement other modes of astronomy, in shedding light on the inner dynamics of astrophysical objects.

Chapter 5

Strong constraints on non-standard neutrino interactions: LHC vs. IceCube

The observation of high energy astrophysical neutrinos of extragalactic origin at IceCube [345, 346] can provide several useful insights about production mechanism and interactions of such neutrinos. The potential of IceCube in unravelling neutrino decoherence [347, 348], existence of sterile neutrinos [349–357], neutrino interactions with dark matter [254–257, 260, 261, 265, 295] and cosmic neutrino background [220, 221, 262–264, 266, 267] have been addressed in the literature.

It is also interesting to ask whether the observation of these high energy neutrinos with $E_\nu \gtrsim 20$ TeV provides new information about neutrino interactions with matter (partons and electrons). Non-standard interaction (NSI) of neutrinos is a widely studied issue in the literature for several decades. NSIs lead to confusions in extracting the neutrino oscillation parameters from the solar, atmospheric and reactor neutrino data. The non-standard interactions with only one charged lepton, the so-called charged current NSIs, are somewhat constrained from several considerations [358]: CKM unitarity, electroweak precession tests, reactor experiments, *etc.* The most stringent bound on $\epsilon_{ll}\bar{\nu}_l l \bar{q} q'$ comes from beta decay $\epsilon_{ee} \lesssim 4 \times 10^{-4}$ [116], π^+ semileptonic decay $\epsilon_{\mu\mu} \lesssim 4 \times 10^{-3}$, and tau decay $\epsilon_{\tau\tau} \lesssim 4.5 \times 10^{-3}$ [359]. Thus, in this chapter we do not consider these interactions.

Non-standard interactions with two neutrinos and two partons are rel-

atively less constrained than those of the form $\bar{\nu}_l l \bar{q} q$. Hence, these are the only kind of new interactions we discuss in this chapter and refer to as NSI from now on. If these interactions stem from a gauge-invariant operator, interactions with two charged leptons and two partons should also exist, leading to additional constraints from LEP ($e^+e^- \rightarrow q\bar{q}$) [361], muon/tau decay [358], neutrino-nucleon scattering experiments [115, 362, 363], LHC dilepton searches [364], *etc.* However, it is possible that the new physics (NP) is such that it leads to NSI with neutrinos, but not involving their charged counterparts. Later on, we will mention a renormalisable model involving a new vector boson Z' where this situation can be realised. Also, a dimension eight operator, given by $\mathcal{O}_8 = (\bar{L}H\gamma_\mu H^\dagger L)(\bar{q}\gamma^\mu q)$, leads to an interaction of the form $\bar{\nu}\nu\bar{q}q$, but not to its counterpart involving charged leptons $\bar{l}l\bar{q}q$ [363, 365, 366]. In this case, the constraints on operators with charged leptons do not apply. Hence, here we do not consider the charged lepton counterpart of interactions with two neutrinos and two partons.

While neutrino propagates through the earth, NSI in neutrino oscillation can lead to observable signatures at long baseline and reactor experiments, as well as solar neutrino observations and neutrino-scattering experiments: all of these pertain to low-energy constraints on NSI. Even IceCube has placed significant constraints on certain NSI parameters through the observation of atmospheric ν_μ disappearance at DeepCore [367, 368]. These constraints are vastly studied in the literature. However, the observation of high energy astrophysical neutrinos at IceCube leads to the extraction of neutrino-nucleon deep inelastic scattering cross-sections at unprecedented high energies [213, 360]. The effects of NSI under consideration lead to signatures similar to SM NC neutrino-nucleon scattering at IceCube. Thus, it is possible to constrain the effects of neutrino NSI from the measurement of neutrino-nucleon scattering cross-section at IceCube. The results presented in this chapter are based on ref. [369].

NSI can also show up at the LHC in a final state characterised by missing energy and one or more hard jets. Thus the generic search of new

physics in channels like monojet+ \cancel{E}_T can lead to significant constraints on the NSI parameters. In this chapter, we find out the constraints on NSI from the measurement of neutrino-nucleon cross-section at IceCube, as well as LHC monojet+ \cancel{E}_T searches and perform a comparative study taking into account the bounds from low-energy neutrino scattering experiments. Moreover, we consider not only the NSI with $(V - A)$ structure of neutrino currents, but a complete set of interactions up to dim-7 with even more exotic Lorentz structures.

In Section 5.1 we discuss the general structure of NSI interactions and various existing constraints. Specifics of our implementation of the LHC and IceCube constraints are described in Section 5.2. Whereas, in Section 5.3 we introduce the non-standard interactions under consideration. Here, we divide the effective interactions into two categories: interactions mediated by a new gauge boson Z' that couples to neutrinos up to dim-5, and contact type interactions up to dim-7. Finally, we summarise our findings in Section 5.4.

5.1 NSI and existing constraints

Beyond standard model effects in neutrino interactions with other SM fermions can be encoded in higher dimensional effective interactions, the so-called NSIs. The constraints on such interactions can be obtained from a wide range of considerations, such as EW precession tests, neutrino oscillation experiments, coherent neutrino-nucleon scattering, colliders, *etc.*, and currently at IceCube as well [109]. As mentioned earlier, in this chapter, we do not consider NSI with a single charged lepton. We also do not discuss about NSI with two neutrinos and two charged leptons. Widely studied ‘neutral-current’ NSI involving (axial)-vector-like quark and neutrino currents is given as [370, 371],

$$\mathcal{L}_{\text{NSI}} = 2\sqrt{2}\epsilon_{ij}^{fC} G_F (\bar{\nu}^i \gamma_\mu \nu^j) (\bar{f} \gamma^\mu P_C f), \quad (5.1)$$

where, ν and f are the SM neutrinos and quarks respectively, and G_F is the Fermi coupling constant. Here, ϵ_{ij}^{fC} is the NSI parameter with i, j as generation indices and P_C with $C = L, R$ are the chirality projection matrices. We also use the notation: $\epsilon_{ij}^{fV} = \epsilon_{ij}^{fL} + \epsilon_{ij}^{fR}$. A discussion of key constraints on NSI parameters and a few clarifications related to the present work are appended:

1. **Oscillation experiments:** Interactions in eq. (5.1) can also lead to large effects in neutrino oscillation while propagation through matter via the Mikheev-Smirnov-Wolfenstein (MSW) mechanism [38, 372]. Such matter effects can show up in the oscillation data of solar and atmospheric neutrinos, as well as in the long-baseline and reactor experiments. From these neutrino oscillation experiments, the constraints on the parameter ϵ can vary from $\mathcal{O}(10^{-2}) - \mathcal{O}(10^{-1})$ depending on the flavour indices, for example [373], $\epsilon_{ee}^{uV} - \epsilon_{\mu\mu}^{uV} = [-0.020, 0.456]$, $\epsilon_{\mu\mu}^{uV} - \epsilon_{\tau\tau}^{uV} = [-0.005, 0.130]$, $\epsilon_{ee}^{dV} - \epsilon_{\mu\mu}^{dV} = [-0.027, 0.474]$, $\epsilon_{\mu\mu}^{dV} - \epsilon_{\tau\tau}^{dV} = [-0.005, 0.095]$, etc.

2. **Neutrino scattering off electrons and nucleons:** Coherent neutrino-nucleon scattering at COHERENT [374], coherent neutrino-electron scattering at Borexino [375] and deep-inelastic neutrino-nucleon scattering at CHARM [376] can also constrain the NSI parameters. COHERENT imposes the following constraints on NSI parameters at 90% CL [377]: $\epsilon_{ee}^{qV} = [-0.073, 0.023] \oplus [0.16, 0.25]$, $\epsilon_{\mu\mu}^{qV} = [-0.0070, 0.033] \oplus [0.15, 0.19]$, $|\epsilon_{e\mu}^{qV}| \lesssim 0.055$, $|\epsilon_{e\tau}^{qV}| \lesssim 0.014$ and $|\epsilon_{\mu\tau}^{qV}| \lesssim 0.051$, for $q = u, d$. Also, CHARM can provide significant constraints as well [378], as example, $\epsilon_{ee}^{uV} = [-0.11, 0.27]$, $\epsilon_{\mu\mu}^{uV} = [-0.03, 0.06]$, etc.

3. **Missing energy signatures at LHC:** At the LHC, the non-standard neutrino interactions can be probed in channels with missing energy in the final state along with one or more jets. From the observation of these channels at $\sqrt{s} = 8$ TeV, the constraints on NSI parameters appearing in eq. (5.1) read, $\epsilon_{ij}^{qC} \lesssim 0.17$ [379], whereas the same with $\sqrt{s} = 13$ TeV is given by, $\epsilon_{ij}^{qC} \lesssim 0.02$ [380]. These constraints are independent of chirality or neutrino flavour indices of the NSI parameter, as long as the counterpart

of eq. (5.1) involving the charged leptons are not considered. If DM interactions with partons are also present along with NSI, they can also contribute to the process $pp \rightarrow j + \cancel{E}_T$. In such a scenario, the constraints on NSI can be weaker compared to the case when DM-parton interactions are absent. Thus, the new constraints presented in this chapter are somewhat conservative, as they indicate the maximum allowed strength of NSI.

4. **IceCube:** Observation of atmospheric neutrinos at DeepCore in the energy range 6 – 56 GeV suggests that the disappearance of ν_μ peaks at a neutrino energy, $E_\nu \sim 25$ GeV. This gives rise to the following constraint [368], $-0.0067 \lesssim \epsilon_{\mu\tau}^{dV} \lesssim 0.0081$, which is more stringent than the same from oscillation experiments, $-0.012 \lesssim \epsilon_{\mu\tau}^{dV} \lesssim 0.009$ [373]. As mentioned earlier, in this chapter, we point out that there is another aspect of IceCube observations which can lead to constraints on NSI and has not been addressed in the literature: The measurement of total neutrino-nucleon scattering cross-section ($\sigma_{\nu N}^{tot}$) from the observation of high energy astrophysical neutrinos. Recently, neutrino-nucleon cross-section has been estimated from the shower and track events induced by such high energy neutrinos in refs. [213] and [360] respectively.

In brief, the ‘classical’ searches for NSI, such as the neutrino oscillation experiments, constrain the NSI parameters at the level $\sim \mathcal{O}(10^{-2}) - \mathcal{O}(10^{-1})$. All the experimental constraints discussed above, except LHC and IceCube, deals with much lower neutrino energies. For instance, at IceCube, the centre-of-mass energy of neutrino-nucleon scattering with $E_\nu \sim 400$ TeV comes out to be ~ 280 GeV. Also, at LHC, in the process $pp \rightarrow \nu\bar{\nu}j$, transverse energy of the $\nu\bar{\nu}$ -pair typically attains values up to a few hundreds of GeVs. As mentioned earlier, the constraint on Fermi operator-like dim-6 NSI appearing in eq. (5.1) from LHC is rather significant. Subsequently, measurement of $\sigma_{\nu N}^{tot}$ from observation of high energy neutrinos at IceCube is also expected to place substantial constraints on NSI, due to similar reach in centre-of-mass energy as LHC. Thus, in this chapter, we consider the impact of LHC and IceCube measurements

on the NSI up to dim-7, while we also discuss the implications of other lower energy experiments in passing. The constraints from low energy neutrino scattering experiments on such NSI from have been studied in the literature [378]. Apparently, dim-7 NSI which lead to additional energy enhancement in neutrino-nucleon cross-section compared to the Fermi-type operator in eq. (5.1), are even more promising to be detected at IceCube. We also pay special attention to the case of Z' of mass around a GeV, a well-studied scenario that leads to potentially large NSI effects. As discussed earlier, it is not possible to distinguish the neutrino flavour structure of the NSI parameters at LHC, as the neutrinos of all flavours lead to missing E_T . In the same way, we extract flavour-independent constraints on NSI from the estimation of neutrino-nucleon cross-section at IceCube.

5.2 Implementation of the constraints

In the following, we discuss the specifics about the implementation of LHC and IceCube constraints.

• Implementation of monojet+ \cancel{E}_T constraints from LHC:

Typical search channels of the NSI are characterised by a final state of mono-X ($X = \text{jet}, \gamma$) plus missing energy. The monojet plus missing transverse energy signal considered in this chapter stems from the process:

$$pp \rightarrow \bar{\nu}_\alpha \nu_\beta j, \quad j = q, \bar{q}, g. \quad (5.2)$$

For the evaluation of cross-section of the above process, we employ `Madgraph-2.6.1` [284], which uses the UFO files generated by `FeynRules-2.3.32` [282]. Hadronization of partonic events are performed using `Pythia-8` [381] and hepmc files are created for $\sqrt{s} = 8, 13$ TeV. The hepmc files are passed to `CheckMATE-2` [382] which checks the compatibility of an interaction against various LHC searches, in our case, the LHC monojet+ \cancel{E}_T searches [383, 384]. The allowed values of NSI parameters are

chosen such that the generated monojet+ \cancel{E}_T signal is less than the 95% exclusion limit on the signal.

• **Implementation of constraints from cascade and track searches at IceCube:**

IceCube has observed upgoing as well as downgoing cascade and track events induced by high energy neutrinos [332, 385]. The upgoing neutrinos travel through the earth to reach IceCube whereas the downgoing neutrinos reach the detector almost uninterrupted. The number of upgoing events is dependent on neutrino flux and neutrino-nucleon cross-section at the detector up to a shadowing factor S encoding the effects of propagation through the earth. The shadowing factor can be evaluated as, $S = \exp[-X(\theta)/\Lambda(E_\nu, \theta)]$, where $X(\theta)$ is the distance travelled through the earth by a neutrino that reaches the IceCube detector from a declination angle θ , where mean free path of neutrinos, $\Lambda(E_\nu, \theta) = m_N/[(\sigma_{NC} + \sigma_{CC})\rho(\theta)]$, with m_N as mass of the nucleons and $\rho(\theta)$ as average matter density in earth along angle θ . Thus, for the downgoing neutrinos, the shadowing factor becomes almost unity. Within an energy interval, neutrinos coming from different directions are distinguished by the shadowing factor, which is also sensitive to neutrino-nucleon cross-section. Thus, it is possible to estimate such cross-section from the observation of high energy astrophysical neutrinos at IceCube. Total neutrino-nucleon cross-section has been calculated in this way, taking into account the contained shower events [213]. Non-standard interactions as given in eq. (5.1), cannot be distinguished from the SM neutral current interaction as both lead to cascade events at IceCube. Thus, in the presence of an NSI, the total neutrino-nucleon cross-section receives an additional contribution, which in turn leads to a constraint on the NSI parameter. See Appendix 7.5 for further details.

The neutrino-nucleon interaction at IceCube for neutrino energy greater than 10 TeV corresponds to the centre-of-mass energy, $\sqrt{s} \gtrsim 140$ GeV. Hence, these neutrinos suffer deep inelastic scattering (DIS). The double-differential neutrino-nucleon DIS cross-section of such interaction is

given by [10, 386]:

$$\frac{d^2\sigma_{\nu N}}{dx dy} = \frac{|\mathcal{M}_{\nu q}|^2}{16\pi x s} \left(f_q(x, Q^2) + (1-y)^2 f_{\bar{q}}(x, Q^2) \right). \quad (5.3)$$

Here, x, y are Bjorken scaling parameters, while Q is the momentum transferred to the nucleon. $f_{q,\bar{q}}(x, Q^2)$ are certain combinations of parton distribution function (PDF) of the quarks and antiquarks, discussed in Sec. 1.3.2. In eq. (5.3), $|\mathcal{M}_{\nu q}|^2$ is the square of amplitude for a given neutrino-parton interaction.

As mentioned in Sec. 1.3.2, due to HERA and LHCb observations, PDFs are precisely known for $E_\nu \lesssim \text{PeV}$ [12–16]. Hence, the uncertainties in the neutrino-nucleon cross-sections stemming from QCD effects are rather small. Therefore for high energy astrophysical neutrinos, any significant difference between predicted SM cross-section and the cross-section measured from the observation of IceCube events can be attributed to non-standard interactions. We use the CT10 parton distribution functions [387] in this work.

5.3 Constraints on NSI interactions from LHC and IceCube

The NSI interactions can be generated in various extensions of the SM. A complete set of higher dimensional effective interactions of neutrinos with partons up to dim-7 have been constructed in the literature [378]. In this section, we consider these effective interactions up to dim-7 which can give rise to neutrino-nucleon scattering at IceCube. Here, we investigate and compare the constraints on the NSI parameters from the neutrino-nucleon cross-section measurement facilitated by IceCube and monojet+ \cancel{E}_T search at LHC. The following discussion is separated in two parts: (i) the case of a Z' of mass $\sim \mathcal{O}(\text{GeV})$ with renormalisable and effective couplings to neutrinos and quarks, leading to non-standard effects in neutrino-nucleon

scattering, and (ii), the case of contact type NSI interactions. For the second part, we consider effective operators leading to NSI up to dim-7.

5.3.1 Z' with renormalisable and effective coupling to neutrinos

The NSI generated from a new vector boson coupling to both neutrino and quark currents is particularly important as it can lead to sizable NSI parameters which can be tested at neutrino oscillation and scattering experiments [388–390]. Such a new vector boson Z' can be realised as the gauge boson corresponding to a $U(1)$ symmetry, pertaining to various chiral anomaly-cancelling combinations of baryon and lepton numbers, for example, $B - L$. The coupling of Z' can even violate lepton flavour universality when realised as the gauge boson corresponding to, for example, $U(1)_{L_\mu - L_\tau}$ [391], *etc.* But, as mentioned earlier, all the constraints on NSI derived in this chapter are flavour-independent.

Constraints on a light Z' : Here we briefly discuss the key constraints on a Z' of mass in the range MeV to GeV and tree-level coupling with neutrinos and quarks, from low-energy experiments and cosmological considerations. If a Z' in the aforementioned mass range couples to charged leptons at the tree-level, several other constraints ensue, which do not apply in our context.

1. Z' with tree-level coupling to neutrinos may keep the neutrinos in equilibrium with photons, and thus electrons, even after the thermal decoupling of neutrinos from the rest of the SM particles, which occurs at temperature $T_{\text{dec}} \sim 2$ MeV in standard cosmology. This might contradict the measurement of effective numbers of neutrinos (N_{eff}) and the ratio $Y_{\text{He}}/Y_{\text{H}}$ at the BBN epoch, which makes Z' with masses $m_{Z'} \lesssim 5$ MeV unfavourable [93].

2. Coupling of neutrinos to Z' can lead to non-standard effects in su-

pernova cooling and could leave potential signatures in the observed spectrum of supernova neutrinos, which constrains the Z' coupling to be as small as $g_\nu \sim 10^{-10}$ depending upon $m_{Z'}$. This constraint is not applicable for $m_{Z'} \gtrsim 30$ MeV [326, 392].

3. In the presence of tree-level couplings to quarks, Z' can have kinetic mixing with photons and consequently, several constraints from meson decay apply. For $m_{Z'} = 100 - 200$ MeV, the measurement of the branching ratio for $K_L^0 \rightarrow \pi^0 Z'$ leads to the bound $g_q \lesssim 10^{-8}$ [393]. For even lower masses of Z' up to a MeV, this constraint is even more stringent. In the range, $m_{Z'} = 200 - 600$ MeV, measurements related to decays of η , η' , ϕ put bounds on the Z' coupling, with the measurement of $\eta \rightarrow \pi^0 \gamma \gamma$ providing the most stringent limit of $g_q \lesssim 10^{-5} - 0.01$ depending upon $m_{Z'}$ [394]. Measurements of branching ratios of $\eta' \rightarrow \pi^0 \pi^+ \pi^- \gamma$, $\Psi \rightarrow K^+ K^-$ and $\Upsilon \rightarrow$ hadrons provide comparably weaker constraints, $g_q \lesssim 0.01 - 0.1$ for very narrow ranges of Z' mass at $m_{Z'} = 0.8, 5.5$ and 9.8 GeV respectively, which correspond to masses of the decaying mesons.

4. For $m_{Z'} \lesssim 10$ GeV, BABAR puts a constraint on the electrons- Z' coupling from the measurement of $e^+ e^- \rightarrow \gamma Z'$ [101, 395] which reads $g_e \lesssim 3.3 \times 10^{-2}$. Though in our scenario Z' does not couple to electrons at the tree-level and $e^+ e^- \rightarrow \gamma Z'$ only occurs at one-loop level. Thus, in our case this constraint applies up to a loop factor, significantly downsizing its relevance. This will be addressed in details later.

5. For Z' with tree-level couplings to neutrinos and electrons, Borexino provides significant constraints for $m_{Z'}$ up to a few GeVs. For $m_{Z'} \sim 1$ GeV, this constraint is given by $g_{e,\mu} \lesssim \mathcal{O}(10^{-2})$ [326]. For smaller values of $m_{Z'}$, such a constraint can be even more stringent, as an example, $g_{e,\mu} \lesssim \mathcal{O}(10^{-5})$ for $m_{Z'} \sim 1$ MeV [326]. But similar to the last point, for our case, this constraint is not that relevant as the neutrino-electron scattering suffers a loop suppression.

In light of the above discussions, broadly the constraints on tree-level couplings of Z' to neutrinos and quarks for $m_{Z'} \lesssim 1$ GeV are quite strin-

gent, owing to the decays of various mesons, cosmological/astrophysical observations, etc. On the other hand, as it will be discussed in details later, for $m_{Z'} \gtrsim 100$ GeV, constraints from LHC on such a Z' are significant as well, $\epsilon \equiv g_q g_\nu (v^2/2m_{Z'}^2) \sim 0.01$. Though, for Z' mass of a few GeVs, Z' couplings remain essentially unconstrained from both the low-energy experiments and LHC, keeping aside the constraints from Ψ and Υ decay which affect only small $m_{Z'}$ ranges around the corresponding meson masses. This situation arises because in order to enable detection of generic new physics signatures, the minimum value of missing E_T at LHC is considered to be $\gtrsim 100$ GeV, whereas the highest energy reach of the relevant low-energy experiments is up to a GeV.

In the following, we study the cases of a Z' of mass $\sim \mathcal{O}(\text{GeV})$, with renormalisable and effective coupling to neutrinos up to dim-5.

1. Here we consider the renormalisable Z' interaction terms leading to a tree-level neutrino-quark scattering,

$$\mathcal{L} \supset g_\nu (\bar{\nu} \gamma_\mu P_L \nu) Z'^\mu + g_q (\bar{q} \gamma^\mu q) Z'_\mu. \quad (5.4)$$

As it was mentioned earlier, we do not consider the couplings of Z' with charged leptons at the tree-level. Such a scenario can be realised in renormalisable models [254], where the Z' is realised as the gauge boson corresponding to an additional $U(1)$ symmetry, under which SM quarks, neutrinos, and the new fermions (F) required for cancelling chiral anomalies, transform non-trivially. Thus, as it can be followed from eq. (5.4), the quark couplings with Z' lead to a kinetic mixing of Z' with photon, $\mathcal{L}_{mix} = \epsilon_{loop} F_{\mu\nu} Z'^{\mu\nu}$, with the following mixing factor,

$$\epsilon_{loop} \sim \frac{8}{9} \frac{e g_q}{(4\pi)^2} \ln \left[\frac{(m_u m_c m_t)^2}{(m_d m_s m_b) m_F^3} \right] = 1.3 \times 10^{-2} g_q \ln \left[\left(\frac{100 \text{ GeV}}{m_F} \right)^3 \right] \quad (5.5)$$

Here, m_q is the mass of the quarks, $q = u, c, t, d, s, b$. Masses of the new fermions can be constrained from several LEP searches as,

$m_F \gtrsim 100$ GeV [287]. Due to the loop-induced mixing of Z' and γ , in our scenario, the amplitude of neutrino-electron scattering in Borexino is suppressed by ϵ_{loop} . Thus, in our case, the constraint from Borexino turns out to be, $g_q g_\nu \lesssim 0.25$ for $m_{Z'} = 5$ GeV, and is relaxed compared to the case of a Z' with tree-level coupling to electrons. A similar discussion holds for a gauged $L_\mu - L_\tau$ model [221, 396].

The constraint from LHC monojet+ \cancel{E}_T searches [384] at $\sqrt{s} = 8$ TeV on the interaction in eq. (5.4) comes out to be, $g_q g_\nu \lesssim 9.9 \times 10^{-3}$ for $m_{Z'} = 5$ GeV. Whereas, for the same Z' mass, the constraint from LHC search [383] in the same channel at $\sqrt{s} = 13$ TeV is weaker, $g_q g_\nu \lesssim 1.7 \times 10^{-2}$. This occurs because of a larger background and cuts at larger values of \cancel{E}_T at $\sqrt{s} = 13$ TeV compared to $\sqrt{s} = 8$ TeV for the process under consideration, leading to a smaller signal-to-background ratio when the 13 TeV data is adopted. In the process $pp \rightarrow \nu \bar{\nu} j$ at LHC, the subprocess $qg \rightarrow \nu \bar{\nu} j$ dominates over the $q\bar{q}$ initiated process, due to a large gluon flux. Anyway, this implies, for $m_{Z'} \sim 5$ GeV and interactions as in eq. (5.4), the LHC constraint at $\sqrt{s} = 8$ TeV is more significant compared to the Borexino bound. However, as it can be seen from fig. 5.1, the IceCube observation of the cascade events give a slightly better bound than the LHC monojet+ \cancel{E}_T searches, $g_q g_\nu \lesssim 1.65 \times 10^{-3}$, *i.e.*, $\epsilon \equiv g_q g_\nu (v^2/2m_{Z'}^2) \lesssim 2.0$ for $m_{Z'} = 5$ GeV. The maximum allowed values of ϵ can be read off fig. 5.2 (a) for different values of $m_{Z'}$. As it can be seen from fig. 5.2 (a), for the interaction in eq. (5.4), except the range $m_{Z'} \sim 35 - 500$ GeV, IceCube provides a better constraint than LHC. This happens due to LHC's rather good acceptance in the channel $pp \rightarrow j + \cancel{E}_T$ for the aforementioned Z' mass range with renormalisable interactions [379]. In this case, the dependence of the LHC constraint on $m_{Z'}$ is similar to that previously found in the literature [397].

2. Now, we consider a dim-5 interaction of neutrinos with Z' with a

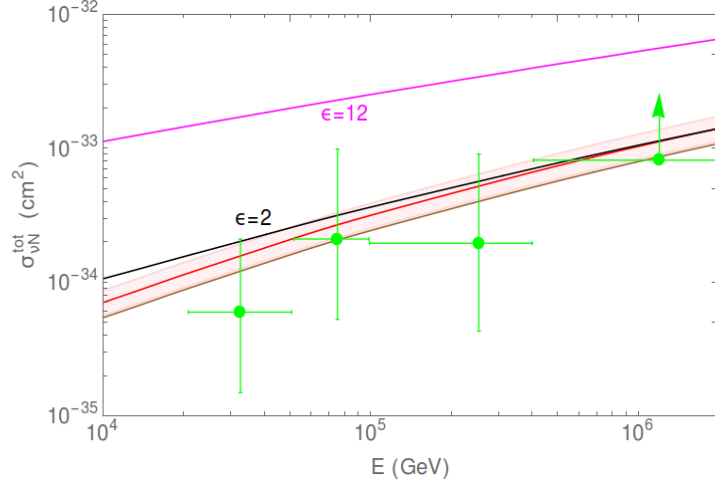
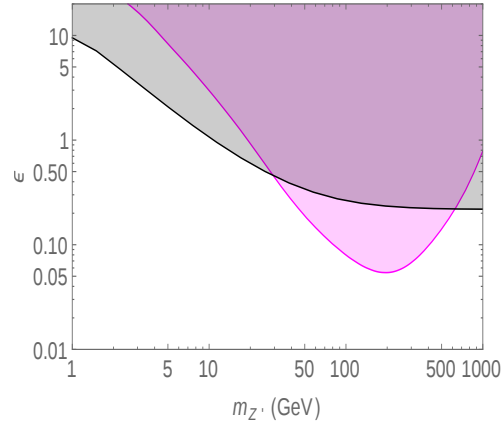


Figure 5.1. Constraints on NSI described by eq. (5.4) for $m_{Z'} = 5$ GeV. The brown line represents the total SM neutrino-nucleon cross-section [10]. The red line and the light red band denote the central value and 1σ allowed range of $\sigma_{\nu N}^{tot}$ from IceCube observation of track events respectively [360]. Similarly, the green points and related error bars in the y -direction stand for the central values and 1σ allowed ranges in $\sigma_{\nu N}^{tot}$ measured from the IceCube observation of shower events at different energy bins respectively [213]. In presence of a Z' with mass $m_{Z'} = 5$ GeV and interactions as in eq. (5.4), (i) the magenta line depicts the value of $\sigma_{\nu N}^{tot}$ with the NSI parameter ϵ set at its maximum allowed value from LHC, $\epsilon = 12$, (ii) the black line represents the value of $\sigma_{\nu N}^{tot}$ with ϵ set at its maximum allowed value from IceCube, $\epsilon = 2$.

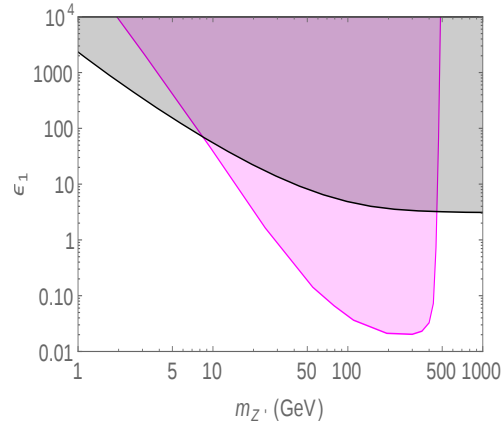
dipole-like vertex structure,

$$\mathcal{L} \supset \frac{c^{(1)}}{\Lambda} (\bar{\nu}_i^c \sigma_{\mu\nu} P_L \nu_j) Z'^{\mu\nu} + g_q (\bar{q} \gamma^\mu q) Z'_\mu, \quad (5.6)$$

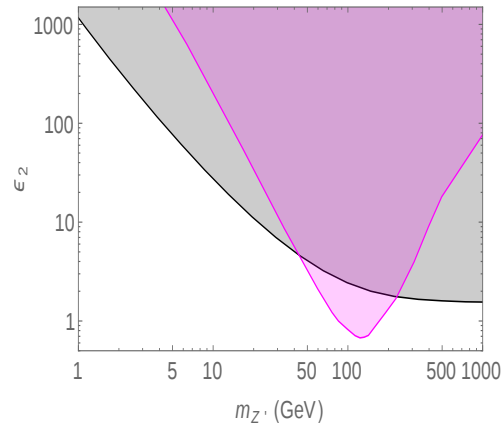
where Λ is the effective interaction scale. By demanding hermiticity of the Lagrangian, it can be noted that the term $(\bar{\nu}_i^c \sigma_{\mu\nu} P_L \nu_j) Z'^{\mu\nu}$ is non-vanishing only if $i \neq j$. Also, as shown for a renormalisable Z' interaction in eq. (5.4), the above interaction also leads to kinetic mixing of Z' with photon via a quark loop. This leads to transitional neutrino dipole moment $\mu_{ij}^M = (c^{(1)}/\Lambda) \epsilon_{loop} (k^2/(k^2 - m_{Z'}^2))$, where k is the momentum of the photon and ϵ_{loop} is a loop factor expressed in eq. (5.5). The most stringent constraint on neutrino dipole moment comes from the study of neutrino-electron scattering at Borexino and is given by, $\mu_{ij}^M \lesssim 10^{-11} \mu_B$ [375]. For $m_{Z'} \sim \text{MeV}$ this leads to a rather stringent bound, $c^{(1)} g_q / \Lambda \lesssim 10^{-5} \text{ GeV}^{-1}$. But for a much heavier Z' the



(a)



(b)



(c)

Figure 5.2. Constraints on Z' induced NSI in presence of interactions expressed in eq. (5.4), (5.6) and (5.7) respectively as functions of Z' mass. The pink and grey regions are excluded from LHC and IceCube respectively.

constraint from Borexino becomes irrelevant: For $m_{Z'} = 5$ GeV, the Borexino bound turns out to be $c^{(1)}g_q/\Lambda \lesssim 4.3 \times 10^3 \text{ GeV}^{-1}$.

For $m_{Z'} = 5$ GeV, LHC constraint from monojet+ \cancel{E}_T search turns out

to be $c^{(1)}g_q/\Lambda \lesssim 1.3 \times 10^{-3} \text{ GeV}^{-1}$, *i.e.*, $\epsilon_1 \equiv (c^{(1)}g_q v/\Lambda)(v^2/2m_{Z'}^2) \lesssim 382$. IceCube constraint on this interaction, as can be followed from fig. 5.3, reads $c^{(1)}g_q/\Lambda \lesssim 4.8 \times 10^{-4} \text{ GeV}^{-1}$, *i.e.*, $\epsilon_1 \lesssim 143$, which is somewhat stronger than the constraints imposed by LHC. For this interaction, the $m_{Z'}$ dependence of LHC and IceCube constraints on ϵ_1 has been shown in fig. 5.2 (b). It can be seen that, the LHC constraint prevails the IceCube bound when $m_{Z'} \gtrsim 15 \text{ GeV}$. However, due to the additional momentum enhancement, the width of Z' becomes quite large in this case. Subsequently, for $m_{Z'} \gtrsim 500 \text{ GeV}$, the cross-section of $pp \rightarrow \nu\bar{\nu}j$ with this interaction does not significantly change with increasing couplings. This implies that there is no relevant constraint on this interaction for $m_{Z'} \gtrsim 500 \text{ GeV}$ from LHC.

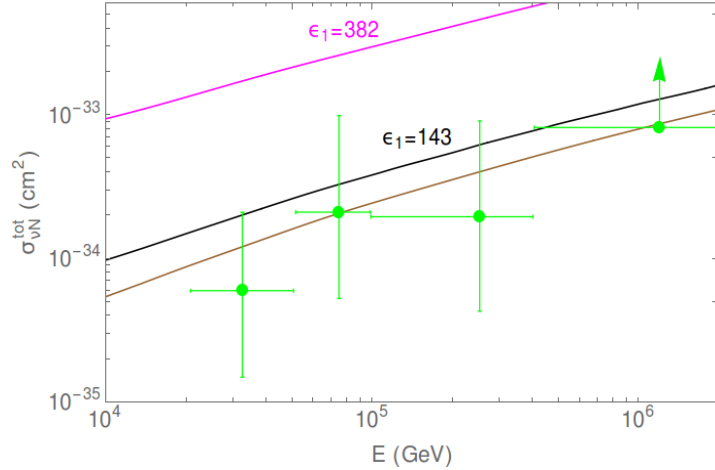


Figure 5.3. Constraints on NSI described by eq. (5.6) in presence of a Z' of mass 5 GeV. Colour coding is the same as in fig. 5.1.

- Another dim-5 vertex for neutrino- Z' interaction leading to neutrino-nucleon scattering can be written as,

$$\mathcal{L} \supset \frac{c^{(2)}}{\Lambda} (\bar{\nu}^c i \partial^\mu \nu) Z'_\mu + g_q (\bar{q} \gamma^\mu q) Z'_\mu, \quad (5.7)$$

where Λ is the effective interaction scale. As shown for the previous cases, the ν - e scattering amplitude is suppressed by a loop factor ϵ_{loop} , which renders the Borexino bound weaker than cases with

tree-level electron- Z' coupling. Thus, for the interaction in eq. (5.7), Borexino bound can be projected as, $c^{(2)}g_q/\Lambda \lesssim 3.4 \times 10^4 \text{ GeV}^{-1}$ for $m_{Z'} = 5 \text{ GeV}$.

Monojet+ \cancel{E}_T search at $\sqrt{s} = 13 \text{ TeV}$ at LHC leads to $c^{(2)}g_q/\Lambda \lesssim 3.3 \times 10^{-3} \text{ GeV}^{-1}$, *i.e.*, $\epsilon_2 \equiv (c^{(2)}g_q v/\Lambda)(v^2/2m_{Z'}^2) \lesssim 982$ for $m_{Z'} = 5 \text{ GeV}$, whereas the measurement of $\sigma_{\nu N}^{tot}$ at IceCube provides a stronger bound, $c^{(2)}g_q/\Lambda \lesssim 2.5 \times 10^{-4} \text{ GeV}^{-1}$, *i.e.*, $\epsilon_2 \lesssim 75.6$. The comparison of $\sigma_{\nu N}^{tot}$ allowed from LHC and IceCube in the presence of the interaction given in eq. (5.7), is shown in fig. 5.4. The LHC and IceCube bounds for different values of $m_{Z'}$ have been depicted in fig. 5.2 (c) which shows that, the LHC bound becomes more significant than IceCube in the range $m_{Z'} \sim 40 - 220 \text{ GeV}$.

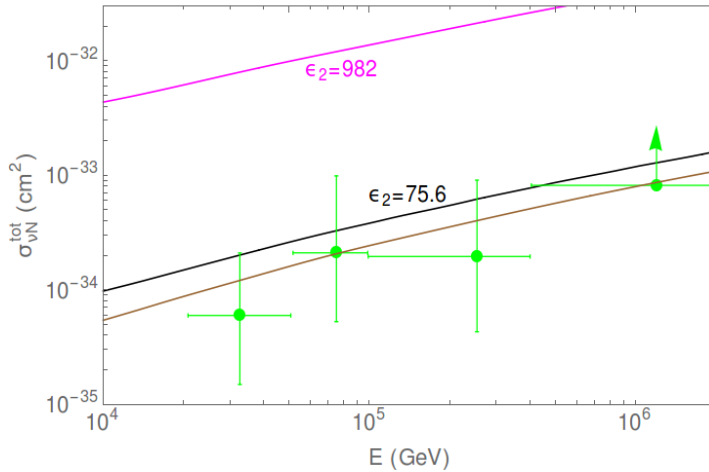


Figure 5.4. Constraints on NSI described by eq. (5.7) in presence of a Z' of mass 5 GeV. Colour coding is the same as in fig. 5.1.

5.3.2 Contact type interactions

Neutrino-nucleon interaction can be realised via effective vertices which lead to neutrino scattering off partons. In addition to the neutrino-quark operators, here we have also considered the case of neutrino-gluon effective interaction. In the following, we study the constraints on these effective interactions up to dim-7 from LHC and IceCube:

4. The dim-6 contact interaction leading to neutrino-quark scattering, which resembles the structure of the four-fermionic operator in eq. (5.1), can be written as,

$$\mathcal{L} \supset \frac{c}{\Lambda^2} (\bar{\nu} \gamma_\mu \nu) (\bar{q} \gamma^\mu q). \quad (5.8)$$

Here we use the notation, $\epsilon \equiv cv^2/\Lambda^2$. As mentioned in Sec. 5.1, a conservative constraint on the maximum allowed value of ϵ from low-energy neutrino DIS experiment CHARM is found to be, $\epsilon \sim 0.06$. Though, for different neutrino flavours, ϵ can take even higher values. We find that the LHC monojet+ \cancel{E}_T search leads to a somewhat stringent constraint, $\epsilon \lesssim 0.02$ which is at par with the findings of refs. [380, 397]. The IceCube constraint from observation of cascade events is given as $-0.004 \lesssim \epsilon \lesssim 0.08$ and is shown in fig. 5.5. It is worth mentioning that, in presence of this interaction, the interference effect of the NSI and SM contributions in the process $pp \rightarrow \nu \bar{\nu} j$ at LHC is rather small. This effect has been discussed in Appendix 7.6 in more detail.

This effective interaction can be interpreted as a dim-6 operator arising from an underlying renormalisable model consisting of a heavy Z' with coupling to neutrinos and quarks at the tree-level as in eq. (5.4). One can also formulate a tree-level matching condition, $\epsilon = (2\sqrt{2}G_F)^{-1}(g_{Z'}/m_{Z'})^2$. But, in order to realise the maximum value of ϵ allowed by LHC in the underlying Z' model, it would require a large coupling, $g_{Z'} \gtrsim 6$ with $m_{Z'} \gtrsim 8$ TeV [380]. For such large values of $g_{Z'}$, the decay width of Z' becomes larger than its mass and the aforementioned matching condition does not hold. Thus it is not sensible to match, or compare the bounds on this dim-6 interaction with the heavy Z' model.

5. A dim-7 effective interaction which leads to neutrino-quark scattering

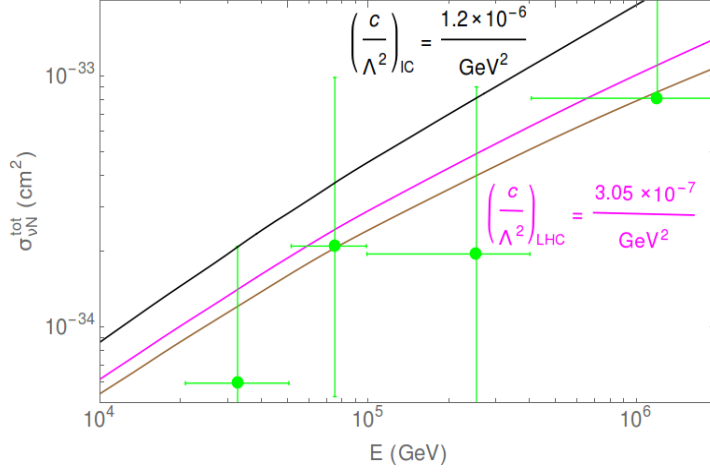


Figure 5.5. The maximum allowed values of NC neutrino-nucleon cross-section in presence of NSI appearing in eq. (5.8). Colour coding is the same as in fig. 5.1.

is given by:

$$\mathcal{L} \supset \frac{c^{(3)}}{\Lambda^3} \partial^\nu (\bar{\nu}_i^c \sigma_{\mu\nu} P_L \nu_j) (\bar{q} \gamma^\mu q). \quad (5.9)$$

Here, in the same rationale as in eq. (5.6), $i \neq j$. Among the low energy experiments, the most stringent constraint on this interaction is imposed by CHARM, $c^{(3)}/\Lambda^3 \lesssim 2.9 \times 10^{-7} \text{ GeV}^{-3}$ [378]. The LHC constraint on this interaction is found to be $c^{(3)}/\Lambda^3 \lesssim 1.8 \times 10^{-10} \text{ GeV}^{-3}$. Measurement of neutrino-nucleon scattering cross-section with IceCube cascade events gives a constraint, $c^{(3)}/\Lambda^3 \lesssim 5.3 \times 10^{-8} \text{ GeV}^{-3}$. Hence, the LHC bound is stronger than the CHARM and IceCube constraints. A comparison of the LHC and IceCube bounds can be followed from fig. 5.6.

6. Another dim-7 effective Lagrangian for the neutrino-quark four-point interaction is given by:

$$\mathcal{L} \supset \frac{c^{(4)}}{\Lambda^3} (\bar{\nu}^c i \partial_\mu \overleftrightarrow{\nu}) (\bar{q} \gamma^\mu q). \quad (5.10)$$

The most relevant constraint among low energy experiments on this interaction comes from neutrino-nucleon scattering cross-section

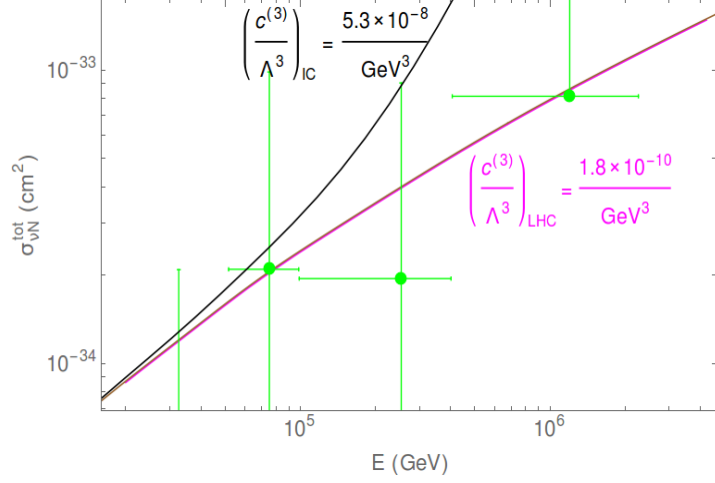


Figure 5.6. Constraints on NSI described by eq. (5.9). Colour coding is the same as in fig. 5.1.

measurement at CHARM, $c^{(4)}/\Lambda^3 \lesssim 1.2 \times 10^{-7} \text{ GeV}^{-3}$ [378]. Monojet+ \cancel{E}_T searches at LHC lead to a stronger constraint, $c^{(4)}/\Lambda^3 \lesssim 8.6 \times 10^{-10} \text{ GeV}^{-3}$, whereas the bound from IceCube reads, $c^{(4)}/\Lambda^3 \lesssim 2.6 \times 10^{-8} \text{ GeV}^{-3}$. As the last two cases, LHC provides a stronger constraint on this interaction compared to low-energy experiments and IceCube. The neutrino-nucleon cross-sections at IceCube due to this interaction, corresponding to the upper limits of the IceCube and LHC constraints, are shown in fig. 5.7.

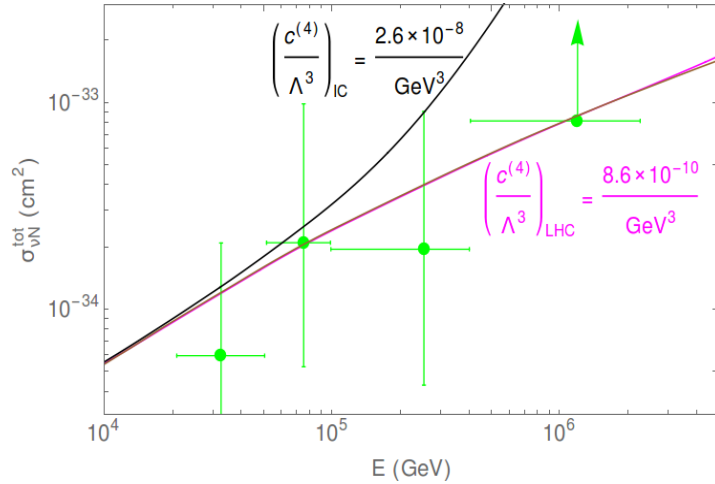


Figure 5.7. Constraints on NSI appearing in eq. (5.10). Colour coding is the same as in fig. 5.1.

7. As mentioned earlier, neutrino-nucleon scattering can take place in

the presence of effective interaction involving neutrinos and gluons as well. A dim-7 term for such neutrino-gluon interaction is given as:

$$\mathcal{L} \supset \frac{c^{(5)}}{\Lambda^3} (\bar{\nu}^c P_L \nu) G_{\mu\nu} G^{\mu\nu}. \quad (5.11)$$

For the above interaction, the most relevant low-energy constraint comes from the measurement of neutrino-nucleon cross-section at CHARM, $c^{(5)}/\Lambda^3 \lesssim 1.6 \times 10^{-6} \text{ GeV}^{-3}$ [378]. LHC monojet+ \cancel{E}_T searches lead to the constraint, $c^{(5)}/\Lambda^3 \lesssim 1.6 \times 10^{-10} \text{ GeV}^{-3}$. The neutrino-nucleon NC cross-section in presence of this interaction, with ϵ fixed at the upper bound obtained from LHC, is shown in fig. 5.8. The IceCube bound from the observation of cascade events is given by, $c^{(5)}/\Lambda^3 \lesssim 5.5 \times 10^{-8} \text{ GeV}^{-3}$. Thus for the interaction given in eq. (5.11), LHC gives a much stronger bound than both IceCube and CHARM.

A possible UV-completion of the operator in eq. (5.11) can be realised in the Type-II seesaw model, where an $SU(2)_L$ triplet (Δ) with hypercharge-2 provides mass to the light neutrinos after it acquires a non-zero vacuum expectation value (vev). The measurement of the T -parameter renders v_Δ to be rather small, $v_\Delta < 4 \text{ GeV}$. The lightest CP-even neutral component of the triplet, namely Δ^0 , mixes with the SM Higgs. The mixing parameter depends on the quartic couplings involving H and Δ , and the vev of the triplet as well. As the SM Higgs, h has an effective coupling to a gluon pair through quark loops, $h - \Delta^0$ mixing leads to an effective coupling of Δ^0 to gluons too. Thus the coefficient $c^{(5)}$ in eq. (5.11) is proportional to $y_\nu \sin \alpha$, where y_ν is the Yukawa coupling of neutrinos to Δ , and α represents the mixing angle of Δ^0 and the SM Higgs. The theoretical constraints, such as unitarity, stability, the measurement of T -parameter and $h \rightarrow \gamma\gamma$ constrain the value of $\sin \alpha$ significantly. The interplay of these bounds ensures that, for $m_H > 200 \text{ GeV}$, $\sin \alpha \lesssim 0.02$ [286]. Also, the Yukawa coupling leads to neutrino mass, $m_\nu \sim y_\nu v_\Delta$. Con-

sidering $m_\nu \lesssim 0.1$ eV, $y_\nu \lesssim 10^{-10}$ for $v_\Delta = 1$ GeV and $y_\nu \lesssim 10^{-6}$ for $v_\Delta = 10^{-4}$ GeV. Thus the coefficient of this effective interaction is rather small if it is generated from such a renormalisable model and does not lead to a significant deviation from the SM value of NC neutrino-nucleon cross-section.

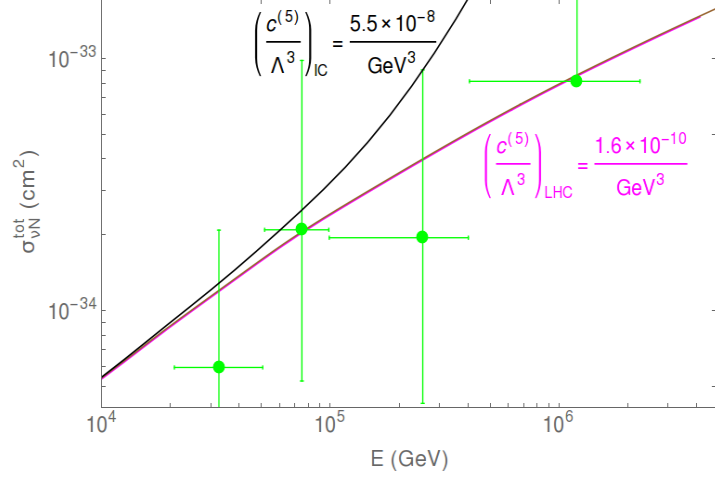


Figure 5.8. Constraints on NSI appearing in eq. (5.11). Colour coding is the same as in fig. 5.1.

We have found that, for the NSIs mediated by Z' of mass $m_{Z'} = 5$ GeV, IceCube provides a superior bound than LHC. Though, for contact-type NSI, the constraints from LHC are more significant than IceCube. However, due to the increasing nature of neutrino-nucleon cross-section in the presence of contact-type NSI, as it can be seen from figs. 5.5, 5.6, 5.7 and 5.8, the measurement of $\sigma_{\nu N}^{tot}$ in the bin 100 – 400 TeV places the most stringent constraints on such interactions. An increase in the number of high energy neutrino events at IceCube-Gen2 will lead to reduced uncertainties in $\sigma_{\nu N}^{tot}$. For instance, the reduction in uncertainties in the bin 100 – 400 TeV can improve the constraint on NSI appearing in eq. (5.10) by nearly a factor of two after 6 years of data from IceCube-Gen2.

No ongoing neutrinos have been observed in the energy range 400 – 2004 TeV. This leads to a lower bound on $\sigma_{\nu N}^{tot}$ which almost coincided with the SM prediction in this bin. Thus, any kind of new physics that leads to a substantial destructive interference with the SM contribution is

disfavoured from the energy bin 400 – 2004 TeV. Note that, all the constraints from IceCube derived in this chapter are independent of the sign of the couplings/Wilson coefficients as the NP contribution does not significantly interfere with SM, except the case described by eq. (5.8). For the case in eq. (5.8), only a small negative value is allowed from the IceCube due to the observation in the energy range 400 – 2004 TeV. It is possible to distinguish the flavour of astrophysical neutrinos based on the CC interactions at the detector [266, 334, 398], which in turn can lead to flavour-dependent constraints on NSI of type $\bar{\nu}\nu\bar{q}q$. Thus, a better understanding of the neutrino flavour ratios at IceCube-Gen2 will also facilitate improved and flavour-dependent constraints on such NSI.

NSIs in eqs. (5.9), (5.10) and (5.11) carry additional momentum dependence compared to the Fermi-type operator. In these cases, the neutrino-nucleon cross-sections increase with energy even faster, leading to more severe constraints from LHC. Moreover, as it can be seen from figs. 5.3-5.8, the value of $\sigma_{\nu N}^{tot}$ increases faster with neutrino energy in presence of the contact-type interactions compared to the non-renormalisable interactions of a light Z' . This can be attributed to the propagator suppression in the Z' -mediated cases which relax the additional momentum enhancement due to the non-renormalisable interactions.

Low-energy experiments, such as MATHUSLA [399], SHiP [400], FASER [401], dedicated to the search for new long-lived particles in the MeV-GeV range can put relevant constraints on the Z' interactions considered in this chapter. Such constraints, although flavour-dependent, can be stronger than that from IceCube, or even IceCube-Gen2. Though, these constraints only affect Z' of mass $\lesssim 4$ GeV.

5.4 Summary

NSIs lead to confusions in extracting the neutrino oscillation parameters by inflicting several degeneracies. Low-energy experiments provide constraints

on the NSI parameters depending on the flavour structure. Among the high energy experiments, LHC leads to sizable constraints on the NSI parameters from generic new physics searches, in channels such as $pp \rightarrow j + \cancel{E}_T$. In IceCube, atmospheric neutrinos detected at DeepCore can also put flavour-specific constraints on NSI parameter at the level $\mathcal{O}(10^{-3})$. The observation of high energy astrophysical neutrinos at IceCube is particularly interesting in this context: It provides an opportunity to measure neutrino-nucleon cross-section at a value of \sqrt{s} comparable to the LHC or even higher. This way it can also point to the existence of new physics at those high energies, if in future, any deviation from the SM neutrino-nucleon cross-section is observed. The similarity in the centre-of-mass energies involved in concerned processes demands a comparative study of constraints on NSI from LHC and IceCube.

The uncertainty in neutrino flux can propagate in the neutrino-nucleon cross-section extracted from the observation of astrophysical neutrinos. High energy neutrinos reaching the IceCube from different directions traverse a different distance within the earth, providing sensitivity to the neutrino-nucleon cross-section which dictates the interaction length. Furthermore, the knowledge of parton distribution functions is also plagued with significant uncertainty for $E_\nu \gtrsim 10$ PeV. But the maximum energy for observed neutrinos goes up to \sim PeV, for which the PDFs are well measured, primarily from HERA, thus making the error due to PDF irrelevant in light of current IceCube data. Thus, IceCube has enormous prospects for testing the non-standard neutrino interactions with high energy astrophysical neutrinos. In light of IceCube observations of shower and track events induced by such neutrinos, estimates of neutrino-nucleon scattering cross-section have been found in the literature [213, 360]. As mentioned earlier, such a direct measurement of $\sigma_{\nu N}^{tot}$ can constrain the NSI parameters.

The non-standard interactions consisting of one charged lepton and one neutrino are constrained quite tightly from several low-energy experiments, EW precision tests, *etc.* We do not consider these kinds of interactions in our chapter. Also, we are not interested in NSI involving two

charged leptons and two partons, which suffer stringent constraints from various LEP measurements, meson decay *etc.* It has been mentioned that, it is possible to generate NSI of form $\bar{\nu}\nu\bar{q}q$ in a renormalisable model with a new vector boson Z' without giving rise to the charged lepton counterpart of these interactions in the presence of new heavy fermions. There also exist other scenarios where this can be attained, for example, in the presence of a specific gauge-invariant dim-8 operator. Though, if the NSIs are assumed to be generated from such operators with $d > 6$, the scale of new physics, Λ can be lower than the case of dim-6 NSI. The implementation of IceCube bounds in this chapter is based on an analysis which assumes equal neutrino flux across flavours. Thus, the constraints on NSI obtained in this chapter are flavour-independent.

We consider two subclasses of new interactions. Firstly, we discuss the case of a Z' of mass $\sim \mathcal{O}(1)$ GeV with renormalisable and effective interactions up to dim-5. As mentioned earlier, in these cases, the IceCube bounds surpass the LHC constraints from monojet+ \cancel{E}_T searches, which we illustrate for a Z' with mass $m_{Z'} = 5$ GeV. In this context, future experiments dedicated to the search for new physics around ~ 1 GeV, such as MATHUSLA, SHiP, FASER, can put quite stringent constraints. The observation of coherent neutrino-nucleon scattering at COHERENT experiment can also lead to quite stringent, though flavour-specific, constraints in the presence of such a Z' [396, 402, 403]. We have also presented a comparison between LHC and IceCube bounds for different masses of Z' . Broadly it has been seen that, for $m_{Z'}$ within a few tens to a few hundreds of GeVs, the LHC bounds are more significant than IceCube. For example, with the renormalisable Z' interactions as in eq. (5.4), within the range $m_{Z'} \sim 35 - 500$ GeV, LHC provides stronger constraints than IceCube. This also means, along with other new physics candidates like extra dimensions [213] and leptoquarks [360], IceCube also has a remarkable discovery potential for Z' of mass \sim TeV. Secondly, we take into account contact-type interactions involving two neutrinos and two partons up to dim-7. For such interactions, the LHC constraints are more significant than that from

both IceCube and lower energy neutrino-scattering experiments.

The extraction of neutrino-nucleon cross-section is also affected by astrophysical neutrino flux and flavour ratios. The constraints from IceCube derived in this chapter can be improved in the upgraded version of this experiment, namely IceCube-Gen2, with a better understanding of neutrino flux and flavour ratios [241]. In case of discovery of even higher energy astrophysical neutrinos, the energy reach of IceCube can supersede that of LHC. With current IceCube data, SM neutrino-nucleon cross-section is still allowed within 95% CL. Any possible deviation from SM neutrino-nucleon cross-section may hint towards the existence of NP. With improved statistics, it might also be possible to distinguish between different kinds of NSIs, by studying the distribution of high energy neutrino events across deposited energy and zenith angle.

Chapter 6

Conclusion

Non-standard neutrino interactions and the nature of DM particles are open issues in particle physics. Beyond Standard Model (BSM) searches at low energy experiments, *e.g.*, BOREXINO, CHARM, COHERENT, *etc.*, and high energy colliders like LHC, LEP, are in the pursuit of new physics to explain the overwhelming astrophysical and cosmological evidences of neutrino mass and the existence of dark matter. Along with the laboratory experiments, cosmological and astrophysical probes are essential tools to explore such BSM interactions. Astrophysical neutrinos interact weakly, and hence, they reach the detector unattenuated and undeflected. However, the same weak interactions and decrease in flux with energy make them difficult to detect. Therefore, we need a massive detector of large volume in order to observe them. At IceCube, the detection of astrophysical neutrinos opens up new opportunities for probing such new interactions.

As these neutrinos pass through large columns of the cosmic dark matter before reaching the Earth, neutrino-DM interactions can get imprinted in the spectrum observed at IceCube. While building models of neutrino-DM interactions leading to flux suppressions of astrophysical neutrinos, the key challenge is to obtain the correct number density of dark matter along with the required cross-section. We consider neutrino-DM interaction of type $\nu\text{-}\bar{\nu}\text{-}\Phi\text{-}\Phi^*$, where Φ represent scalar DM. In order to explore neutrino-DM interaction exhaustively, we take a rigorous approach by considering renormalisable as well as effective interactions between neutrinos and DM and mention the constraints on such interactions. The effective interactions are subdivided into four topologies: Topology I is contact type

interactions up to dimension-eight, and topologies II, III, and IV up to dimension-six contain effective interactions in one of the vertex. For renormalisable interactions, we consider vector, scalar, and fermion mediators. For thermal DM, we find that the cosmological bounds, namely, relic density, collisional damping, and N_{eff} , demand too small DM number density to lead to any significant flux suppression. On the other hand, owing to small mass ultralight BEC DM (m_{DM}), they have a huge number density and are interesting to explore in the context of ν -DM interaction. Taking into account the bounds from precision tests, collider searches as well as the cosmological constraints, we investigate whether such interactions can provide the required value of cross-section of neutrino-DM scattering so that they lead to flux suppression of the astrophysical neutrinos. For ultralight BEC DM only one dim-5 contact-type interaction from topology I, *i.e.*, $(c_i^{(3)}/\Lambda)\bar{\nu}^c\nu\Phi^*\Phi$, can lead to flux suppression at IceCube.

In the astrophysical neutrino sources, such as AGNs, the matter accretion disc and a dark matter halo can surround a supermassive black hole. In spite of the large neutrino energies, the centre of mass energy for neutrino scattering off ultralight DM may be much less compared to the mass of the particle mediating such interactions. The latter can be of $\mathcal{O}(\text{MeV})$ for the case of a light Z' . In such cases, the resulting ν -DM cross-section is too small to lead to any appreciable neutrino flux suppression [254]. We have shown that ν -DM interactions can be feeble enough to impart any changes in astrophysical neutrino flux, but the track to shower ratios can significantly modify due to the large DM number density.

We find that while passing through the DM halo, the details of the halo profile, DM mass, the redshift associated with the AGN, the strength of such interactions, masses of the SMBH (M_{BH}) and DM halo (M_{halo}) get encoded into the energy dependence of neutrino flavour ratio at the IceCube [296]. We show that the track to shower ratio at the detector increases with the increase in DM density at source (ρ_0) and effective interaction strength (G'_F). We found that the track to shower ratio is sensitive to the ultralight DM profile for $10^{-11} \text{ eV}^4 \lesssim \rho_0 \lesssim 10^{-3} \text{ eV}^4$ and

$10^{-16} \text{ eV}^{-3} \lesssim G'_F/m_{\text{DM}} \lesssim 10^{-10} \text{ eV}^{-3}$. Also, sources with a sharp change in DM number density, *i.e.*, $|\text{d} \ln n_\phi/\text{d}r| \gtrsim 100 \text{ pc}^{-1}$, can lead to non-adiabatic propagation of astrophysical neutrinos.

In addition to neutrino-DM interactions, IceCube can probe neutrino interactions with SM quarks. There could be new physics hidden when a neutrino interacts with quarks, the so-called Non-Standard Interactions (NSI). Low-energy experiments provide constraints on the NSI parameters depending on the flavour structure. Among the high energy experiments, LHC leads to sizable flavour independent constraints on the NSI parameters from generic new physics searches, in channels such as $pp \rightarrow j + \cancel{E}_T$. At IceCube, there is an opportunity to measure the neutrino-nucleon cross-section at centre-of-mass energies comparable to or even higher than LHC. In this context, we have studied effective interactions: Both with only SM quarks, gluon, neutrinos, as well as with Z' as their mediator. Owing to the original vectorial structure, the NSI generated from a new vector boson coupling with both neutrino and quark currents is particularly important. Firstly, we discuss the case of a Z' of mass $\sim \mathcal{O}(1) \text{ GeV}$ with renormalisable and effective interactions up to dim-5. Broadly it has been seen that for $m_{Z'}$ within a few tens to a few hundreds of GeVs, the LHC bounds are more significant than IceCube. For example, with the renormalisable Z' interactions, within the range $m_{Z'} \sim 35 - 500 \text{ GeV}$, LHC provides stronger constraints than IceCube, whereas elsewhere IceCube bounds supersede. Secondly, we take into account contact-type interactions involving two neutrinos and two partons up to dim-7. For such interactions, the LHC constraints are more significant than that from both IceCube and lower energy neutrino-scattering experiments.

IceCube has observed 60 neutrino events of astrophysical origin with neutrino energy $E_\nu \gtrsim 60 \text{ TeV}$ in 7.5 years of observations. In the future IceCube-Gen2, with around ten times the volume of present IceCube, the number of events observed will increase by a factor of 10. Thus, with the seven years of running, the statistical error at Gen2 will decrease by a factor of $1/\sqrt{600} \sim 1/25$. This decrease in statistical error will drastically reduce

the uncertainty in the observed flux. Further, with more fiducial volume, the events with $E_\nu \gtrsim \text{PeV}$ can be easily contained within the fiducial volume, which in turn will improve the energy resolution of both tracks and shower events. Hence, various features of the spectrum which have started to show up at present IceCube will be known more precisely. Therefore, Gen-2 is expected to improve the probe of neutrino-DM interactions that can lead to significant flux suppression of astrophysical neutrinos.

So far, as reported, only one IceCube event could be traced back to its origin. In future, the angular resolution of high energy neutrino events is expected to drastically improve at Gen-2, from 15 degrees to 5 degrees for cascade at $E_\nu \gtrsim 100 \text{ TeV}$ [224]. Besides IceCube, KM3NeT/ARCA will also have the potential to detect point-like extragalactic neutrino sources. The accuracy for directionality in ARCA can even be better compared to the IceCube, making it a somewhat better probe of such astrophysical sources. At that point, more such neutrinos can possibly be traced back to the potential astrophysical sources. This will allow the usage of our proposed method for flavour ratio to perform neutrino astronomy. The knowledge of some of the parameters like the masses of the SMBH and DM halo, the distance of the AGN, *etc.*, from other modes of astronomy, may help us improve the fit to the rest of the unknowns. Also, with a better understanding of the mass ordering from the upcoming experiments like JUNO, HyperK, T2HK, PINGU, DUNE, INO, *etc.*, and the sign of $\cos 2\theta_{23}$ from HyperK, T2HK, PINGU, DUNE, *etc.*, the determination of G'_F within our framework can be easier. Exploiting the theoretical relations between M_{BH} , M_{halo} , and M_{sol} for a subset of these sources, a dedicated fit of the track to shower ratios at various energy bins will provide sensible values of G'_F and m_{DM} . These can, in turn, be used to probe other astrophysical neutrino sources. With a significant livetime of the future neutrino telescopes, we can hope to explore such interesting aspects of neutrino astronomy. The proposed method of the energy dependence of neutrino flavour ratio may then complement other modes of astronomy, in shedding light on the inner dynamics of astrophysical objects.

The extraction of neutrino-nucleon cross-section is also affected by astrophysical neutrino flux and flavour ratios. The NSI constraints from IceCube derived in the thesis can be improved in the upgraded version of the experiment, with a better understanding of neutrino flux and flavour ratios. In case of discovery of even higher energy astrophysical neutrinos, the energy reach of IceCube can supersede that of LHC. With current IceCube data, SM neutrino-nucleon cross-section is still allowed within 95% CL. Any possible deviation from SM neutrino-nucleon cross-section may hint towards the existence of BSM physics. With improved statistics, it might also be possible to distinguish between different kinds of NSIs, by studying the distribution of high energy neutrino events across deposited energy and zenith angle.

In brief, we have explored the potential of IceCube in unravelling new interactions of neutrinos with both dark matter and ordinary matter. Considering various collider as well as cosmological constraints, we point out the neutrino-DM interaction that may lead to flux suppression at IceCube. The changes in flavour ratio can be an important probe of the interiors of astrophysical sources. Further, IceCube is a better probe of ν -quark NC NSI than LHC, for both intermediate mass Z' , $m_{Z'} \sim 10$ GeV, and very heavy Z' with $m_{Z'} \gtrsim 500$ GeV. Thus, IceCube has enormous prospects for testing the non-standard neutrino interactions with high energy astrophysical neutrinos. Such a study has vast scopes pertaining to the upcoming experiments, *e.g.*, IceCube-Gen2, PINGU, GRAND, KM3NeT, *etc.*, which will offer improved probes of such new physics interactions.

Chapter 7

Appendices

7.1 Cross-section of neutrino-DM interaction

7.1.1 Kinematics

We consider the process of neutrinos scattering off DM particles. If the incoming neutrino has an energy E_1 , the energy of the recoiled neutrino is [404],

$$E_3 = \frac{E_1 + m_{\text{DM}}}{2} \left(1 + \frac{m_\nu^2 - m_{\text{DM}}^2}{s} \right) + \frac{\sqrt{E_1^2 - m_\nu^2}}{2} \left[\left(1 - \frac{(m_\nu + m_{\text{DM}})^2}{s} \right) \left(1 - \frac{(m_\nu - m_{\text{DM}})^2}{s} \right) \right]^{1/2} \cos \theta,$$

where θ is the scattering angle of the neutrino. The relevant Mandelstam variables are,

$$s = (p_1^\mu + p_2^\mu)^2 = m_\nu^2 + m_{\text{DM}}^2 + 2E_1 m_{\text{DM}},$$
$$t = (p_1^\mu - p_3^\mu)^2 = 2m_\nu^2 + 2(E_1 E_3 - p_1 p_3 \cos \theta) \sim 2m_\nu^2 + 2E_1 E_3 (1 - \cos \theta).$$

The energies of incoming neutrinos are such that, $E_1 \sim p_1$ holds well. The scattering angle θ in the centre-of-momentum frame can take all values between 0 to π , whereas that is the case in the laboratory frame only when $m_\nu < m_{\text{DM}}$. When $m_\nu > m_{\text{DM}}$, there exists an upper bound on the scattering angle in the laboratory frame, $\theta_{\text{max}} \sim m_{\text{DM}}/m_\nu$.

The differential cross-section in the laboratory frame is given by [405]:

$$\frac{d\sigma}{d\Omega} = \frac{1}{64\pi^2 m_{\text{DM}} p_1} \frac{p_3^2}{p_3(E_1 + m_{\text{DM}}) - p_1 E_3 \cos\theta} \sum_{spin} |\mathcal{M}|^2, \quad (7.1)$$

where $d\Omega = \sin\theta d\theta d\phi$.

7.1.2 Amplitudes of various renormalisable neutrino-DM interactions

• Fermion-mediated process

With the renormalisable interaction presented in eq. (3.12), one obtains the amplitude square for the scattering of high energy neutrinos off DM as,

$$\sum_{spin} |\mathcal{M}|^2 = C_L^4 \frac{(m_\nu^2 - m_{\text{DM}}^2)(p_1 \cdot p_3) - 2(m_\nu^2 - p_2 \cdot p_3)(p_1 \cdot p_2)}{(u - m_F^2)^2}. \quad (7.2)$$

Here, p_1, p_2, p_3 and p_4 are the four-momenta of the incoming neutrino, incoming DM, outgoing neutrino and outgoing DM respectively.

• Scalar-mediated process

The amplitude squared for a scalar-mediated process governed by neutrino-DM interaction given by eq. (3.14) reads:

$$\sum_{spin} |\mathcal{M}|^2 = g_\Delta^2 f_t^2 \frac{(p_1 \cdot p_3 - m_\nu^2)}{(t - m_\Delta^2)^2}. \quad (7.3)$$

The neutrinos are Majorana particles in this case and g_Δ has a mass dimension of unity.

• Vector-mediated process

The square of the amplitude for a vector-mediated process described

by eq. (3.15) is given as:

$$\sum_{spin} |\mathcal{M}|^2 = 2g'^2 f'^2 \frac{(p_2 \cdot p_1 + p_4 \cdot p_1)^2 - (p_1 \cdot p_3)(m_{\text{DM}}^2 + p_2 \cdot p_4)}{(t - m_{Z'}^2)^2}. \quad (7.4)$$

7.2 Anomaly cancellation for vector-mediated scalar DM model

The charges of the SM and exotic fermions are arranged in such a way that they cancel the ABJ anomalies pertaining to the triangular diagram with gauge bosons as external lines and fermions running in the loop. Such conditions are read as:

$$\text{Tr}[\gamma^5 t^a \{t^b, t^c\}] = 0, \quad (7.5)$$

where t^a, t^b, t^c correspond to the generators of the corresponding gauge group and the trace is taken over all fermions. In an anomaly-free theory, the sum of such terms for all fermions for a certain set of gauge bosons identically vanishes. Here the gauge symmetry under consideration is $SU(3)_c \times SU(2)_L \times U(1)_Y \times U(1)'$ where $U(1)'$ represents the new gauge symmetry. In our case, third generation leptons, *i.e.*, L_τ and τ_R are charged under $U(1)'$. Thus, a full family of additional chiral fermions, namely Q_4, u_{4R}, d_{4R}, L_4 and l_{4R} are needed in order to cancel anomalies. As the new fermions are an exact replica of one generation of SM fermions, the anomalies involving only SM gauge currents, namely $U(1)_Y^3, U(1)_Y SU(2)_L^2, U(1)_Y SU(3)_c^2$ and $U(1)_Y(\text{Gravity})^2$ are automatically satisfied [406].

Still we need to take care of the chiral anomalies involving $U(1)'$ which lead to the following conditions [407, 408]:

$$\begin{aligned}
U(1)'SU(3)_c^2 : \quad & \text{Tr}[Y'\{\sigma^b, \sigma^c\}] = 0 \implies 3(2Y'_{Q_4} - Y'_{u_{4R}} - Y'_{d_{4R}}) = 0, \\
U(1)'SU(2)_L^2 : \quad & \text{Tr}[Y'\{\sigma^b, \sigma^c\}] = 0 \implies Y'_{L_\tau} + Y'_{L_4} = 0, \\
U(1)'^2U(1)_Y : \quad & \text{Tr}[Y'^2Y] = 0 \implies Y'^2_{L_\tau} + Y'^2_{L_4} - Y'^2_{\tau_R} - Y'^2_{l_{4R}} = 0, \\
U(1)_Y^2U(1)' : \quad & \text{Tr}[Y^2Y'] = 0 \implies Y'_{L_\tau} + Y'_{L_4} - 2Y'_{\tau_R} - 2Y'_{l_{4R}} = 0, \\
U(1)'^3 : \quad & \text{Tr}[Y'^3] = 0 \implies 2Y'^3_{L_\tau} + 2Y'^3_{L_4} - Y'^3_{\tau_R} - Y'^3_{l_{4R}} = 0, \\
\text{Gauge-gravity} : \quad & \text{Tr}[Y'] = 0 \implies 2Y'_{L_\tau} + 2Y'_{L_4} - Y'_{\tau_R} - Y'_{l_{4R}} = 0. \quad (7.6)
\end{aligned}$$

While expanding the trace in above relations, an additional $(-)$ sign for the left-handed fermions is implied. Here, Y'_i stands for the $U(1)'$ hypercharge of the species i , where $i \equiv L_\tau, \tau_R, L_4, l_{4R}$. As the exotic quarks are uncharged under $U(1)'$, the first condition of eqs. (7.6) satisfies. The SM Higgs transforms trivially under $U(1)'$ in order to keep the Yukawa Lagrangian for quarks and the first two generations of leptons $U(1)'$ -invariant. Thus, in order to make the Yukawa term involving τ gauge-invariant, one must put $Y'_{\tau_R} = Y'_{L_\tau}$, which serves as another condition along with eqs. (7.6). Thus the $U(1)'$ hypercharges of the respective fields can be determined from eqs. (7.6) and are mentioned in table 7.3.

7.3 Summary of neutrino-DM interactions for scalar DM

The key constraints on the effective and renormalisable interactions for light DM are summarised in table IV and V.

Topology	Interaction	Constraints	Remarks
I 1	$\frac{c_l^{(1)}}{\Lambda^2} (\bar{\nu} i \not{\partial} \nu) (\Phi^* \Phi)$	$c_l^{(1)}/\Lambda^2 \lesssim 8.8 \times 10^{-3} \text{ GeV}^{-2}$, $c_e^{(1)}/\Lambda^2 \lesssim 1.0 \times 10^{-4} \text{ GeV}^{-2}$, $c_\mu^{(1)}/\Lambda^2 \lesssim 6.0 \times 10^{-3} \text{ GeV}^{-2}$, $c_\tau^{(1)}/\Lambda^2 \lesssim 6.2 \times 10^{-3} \text{ GeV}^{-2}$	disfavoured
I 2	$\frac{c_l^{(2)}}{\Lambda^2} (\bar{\nu} \gamma^\mu \nu) (\Phi^* \partial_\mu \Phi - \Phi \partial_\mu \Phi^*)$	$c_l^{(2)}/\Lambda^2 \lesssim 1.8 \times 10^{-2} \text{ GeV}^{-2}$, $c_e^{(2)}/\Lambda^2 \lesssim 2.6 \times 10^{-5} \text{ GeV}^{-2}$, $c_\mu^{(1)}/\Lambda^2 \lesssim 1.2 \times 10^{-2} \text{ GeV}^{-2}$, $c_\tau^{(1)}/\Lambda^2 \lesssim 1.3 \times 10^{-3} \text{ GeV}^{-2}$	disfavoured
I 3	$\frac{c_l^{(3)}}{\Lambda} \bar{\nu}^c \nu \Phi^* \Phi$	$c_l^{(3)}/\Lambda \leq 0.5 \text{ GeV}^{-1}$	favoured ^a
I 4	$\frac{c_l^{(4)}}{\Lambda^3} (\bar{\nu}^c \sigma^{\mu\nu} \nu) (\partial_\mu \Phi^* \partial_\nu \Phi - \partial_\nu \Phi^* \partial_\mu \Phi)$	$c_l^{(4)}/\Lambda^3 \lesssim 2.0 \times 10^{-3} \text{ GeV}^{-3}$	disfavoured
I 5	$\frac{c_l^{(5)}}{\Lambda^3} \partial^\mu (\bar{\nu}^c \nu) \partial_\mu (\Phi^* \Phi)$	$c_l^{(5)}/\Lambda^3 \lesssim 7.5 \times 10^{-4} \text{ GeV}^{-3}$	disfavoured
I 6	$\frac{c_l^{(6)}}{\Lambda^4} (\bar{\nu} \partial^\mu \gamma^\nu \nu) (\partial_\mu \Phi^* \partial_\nu \Phi - \partial_\nu \Phi^* \partial_\mu \Phi)$	$c_l^{(6)}/\Lambda^4 \lesssim 2.5 \times 10^{-5} \text{ GeV}^{-4}$, $c_e^{(6)}/\Lambda^4 \lesssim 1.2 \times 10^{-6} \text{ GeV}^{-4}$, $c_\mu^{(6)}/\Lambda^4 \sim c_\tau^{(6)}/\Lambda^4 \lesssim 10^{-5} \text{ GeV}^{-4}$	disfavoured
II 1	$\frac{c_l^{(7)}}{\Lambda^2} (\partial^\mu \Phi^* \partial^\nu \Phi - \partial^\nu \Phi^* \partial^\mu \Phi) Z'_{\mu\nu} + f_i \bar{\nu}_i \gamma^\mu P_L \nu_i Z'_\mu$	$f_l c_l^{(7)}/\Lambda^2 \lesssim 4.2 \times 10^{-2} \text{ GeV}^{-2}$, $f_e c_e^{(7)}/\Lambda^2 \lesssim 1.9 \times 10^{-5} \text{ GeV}^{-2}$, $f_\mu c_\mu^{(7)}/\Lambda^2 \sim f_\tau c_\tau^{(7)}/\Lambda^2 \lesssim 8.1 \times 10^{-3} \text{ GeV}^{-2}$, $[f_e, f_\mu, f_\tau] \lesssim [10^{-5}, 10^{-6}, 0.02]$ for $m_{Z'} \sim 10 \text{ MeV}$	disfavoured
II 2	$\frac{c_l^{(8)}}{\Lambda} \partial^\mu \Phi ^2 \partial_\mu \Delta + f_l \bar{\nu}^c \nu \Delta$	$m_\nu \sim f_l v_\Delta \lesssim 0.1 \text{ eV}$, $m_\Delta \gtrsim 150 \text{ GeV}$	disfavoured
III	$C_1 (\Phi^* \partial_\mu \Phi - \Phi \partial_\mu \Phi^*) Z'^\mu + \frac{c_l^{(9)}}{\Lambda} (\bar{\nu}^c \sigma_{\mu\nu} P_L \nu) Z'^{\mu\nu}$	$C_1 c_l^{(9)}/\Lambda \lesssim 3.8 \times 10^{-3} \text{ GeV}^{-1}$ and $C_1 c_l^{(9)}/\Lambda \lesssim 2.5 \times 10^{-6} \text{ GeV}^{-1}$ for $m_{Z'} \sim 10 \text{ MeV}$	disfavoured
IV	$\frac{c_l^{(10)}}{\Lambda^2} \bar{L} F_R \Phi H ^2 + C_L \bar{L} F_R \Phi$	Same as in fermion case in table V	disfavoured

Table 7.1. Summary of neutrino-DM effective interactions. c_l and $c_{e,\mu,\tau}$ represent the coefficients of interactions for the gauge non-invariant and gauge-invariant forms respectively. The colour coding for the constraints is: $Z \rightarrow inv$, LEP monophoton+ \cancel{E}_T , $Z \rightarrow \mu^+ \mu^-$, $Z \rightarrow \tau^+ \tau^-$, BBN and $(g-2)_{e,\mu}$. We also remark whether the interactions are favoured in context of the 1% flux suppression criteria as mentioned earlier.

^a disfavoured if realised with a $SU(2)_L$ triplet scalar.

For DM with higher masses the cosmological constraints, *i.e.*, relic

Mediator	Interaction	Constraints	Remarks
Fermion	$(C_L \bar{L} F_R + C_R \bar{l}_R F_L) \Phi + h.c.$	$m_F \gtrsim 100 \text{ GeV}$, $m_{\text{DM}} \gtrsim 10^{-21} \text{ eV}$, $C_L C_R \lesssim \{2.5, 0.5\} \times 10^{-5}$ for e and μ	disfavoured
Scalar	$f_l \bar{L}^c L \Delta + g_\Delta \Phi^* \Phi \Delta ^2$	$m_\nu \sim f_l v_\Delta \lesssim 0.1 \text{ eV}$, $g_\Delta \sim v_\Delta^2 / m_{\text{DM}}^2$	disfavoured
Vector	$f'_l \bar{L} \gamma^\mu P_L L Z'_\mu + i g' (\Phi^* \partial^\mu \Phi - \Phi \partial^\mu \Phi^*) Z'_\mu$	$[f'_e, f'_\mu, f'_\tau] \lesssim [10^{-5}, 10^{-6}, 0.02]$ and $f' g' \lesssim 6 \times 10^{-8}$ for $m_{Z'} \sim 10 \text{ MeV}$	disfavoured

Table 7.2. Summary of renormalisable neutrino-DM interactions. Colour coding is the same as in table 2.1.

density, collisional damping and N_{eff} ensure that the above-mentioned interactions do not lead to any significant flux suppression. This has been discussed in Sec. 3.2 and 3.3.2.

7.4 A UV-complete model for vector-mediated ultralight scalar DM

Here we present a UV-complete scenario which accommodates an ultralight scalar DM as well as a Z' with mass $\sim \mathcal{O}(10)$ MeV. The Z' mediates the interaction between the DM and neutrinos.

The coupling of such a Z' with the first two generations of neutrinos cannot be significant because of the stringent constraints on the couplings of the Z' with electron and the muon. As it was discussed in Sec. 4.8, those couplings have to be $\sim \mathcal{O}(10^{-5} - 10^{-6})$ for $m_{Z'} \sim 10$ MeV. Thus, only the couplings to the third generation of leptons can be sizable. However, the coupling of the Z' with the b -quark is also constrained from the invisible decay width of Υ . The bound from such invisible decay width dictates $|g_\Phi g_b| \lesssim 5 \times 10^{-3}$, where g_Φ and g_b stand for Z' coupling with DM and the b -quarks respectively [409]. Thus we construct a model such that the Z' couples only to the third generation of leptons among the SM particles.

The Z' boson is realised as the gauge boson corresponding to a $U(1)'$ gauge group, which gets broken at $\sim \mathcal{O}(10)$ MeV due to the vev of the

real component of a complex scalar φ transforming under the $U(1)'$. As the third generation of SM leptons are also charged under $U(1)'$, in order to cancel the chiral anomalies it is necessary to include another generation of heavy chiral fermions to the spectrum [406]. The cancellation of chiral anomalies in presence of the fourth generation of chiral fermions under $SU(3)_c \times SU(2)_L \times U(1)_Y \times U(1)'$ is discussed in appendix 7.2. If the exotic fermions obtain masses from the vev of the scalar φ which is also responsible for the mass of Z' , the mass of the exotic fermion is related to the gauge coupling of $U(1)'$ in the following manner [220, 410],

$$m_{\text{exotic}} \lesssim 100 \text{ GeV} \left(\frac{m_{Z'}}{10 \text{ MeV}} \right) \left(\frac{5.4 \times 10^{-4}}{g_{Z'}} \right) \left(\frac{1}{Y'_\varphi} \right). \quad (7.7)$$

Here, $g_{Z'}$ is gauge coupling of $U(1)'$ and Y'_φ is the $U(1)'$ charge of the scalar φ . It is clear from eq. (7.7) that, in order to satisfy the collider search limit on the masses of exotic leptons $\sim 100 \text{ GeV}$, the gauge coupling of Z' has to be rather small. Such a constraint can be avoided if the exotic fermions obtain masses from a scalar other than φ . This scalar cannot be realised as the SM Higgs, because then the effect of the heavy fourth generation fermions do not decouple in the loop-mediated processes like $gg \rightarrow h$, $h \rightarrow \gamma\gamma$ etc. To evade both these constraints we consider that the exotic fermions get mass from a second Higgs doublet.

In order to avoid Higgs-mediated flavour-changing neutral current at the tree-level, it is necessary to ensure that no single type of fermion obtains mass from both the doublets $\Phi_{1,2}$. Hence, we impose a Z_2 -symmetry to secure the above arrangement under which the fields transform as it is mentioned in table 7.3. After electroweak symmetry breaking, the spectrum of physical states of this model will contain two neutral CP-even scalars h and H , a charged scalar H^\pm , and a pseudoscalar A . The Yukawa sector of this model looks like,

$$\mathcal{L}_{\text{Yukawa}} \supset \frac{m_f}{v} (\zeta_h^f \bar{f} f h + \zeta_H^f \bar{f} f H + \zeta_A^f \bar{f} f A), \quad (7.8)$$

ψ	$SU(3)_c$	$SU(2)_L$	$U(1)_Y$	$U(1)'$	Z_2
Q	3	2	1/6	0	+
u_R	3	1	2/3	0	+
d_R	3	1	-1/3	0	+
L_e, L_μ	1	2	-1/2	0	+
e_R, μ_R	1	1	-1	0	+
L_τ	1	2	-1/2	1	+
τ_R	1	1	-1	1	+
L_4	1	2	-1/2	-1	+
l_{4R}	1	1	-1	-1	-
Q_4	3	2	1/6	0	+
u_{4R}	3	1	2/3	0	-
d_{4R}	3	1	-1/3	0	-
Φ_1	1	2	1/2	0	-
Φ_2	1	2	1/2	0	+
φ	1	1	0	Y_φ	+
ν_R	1	1	0	0	+
Φ	1	1	0	Y_Φ	-

Table 7.3. Quantum numbers of the particles in the model.

with,

$$\begin{aligned} \zeta_h^{SM} &= \cos \alpha / \sin \beta, \quad \zeta_H^{SM} = \sin \alpha / \sin \beta, \quad \zeta_A^{SM} = -\cot \beta, \\ \zeta_h^X &= -\sin \alpha / \cos \beta, \quad \zeta_H^X = \cos \alpha / \cos \beta, \quad \zeta_A^X = \tan \beta. \end{aligned} \quad (7.9)$$

Here, ζ_i^{SM} and ζ_i^X are the coupling multipliers of the SM and exotic fermions to the neutral scalars $i \equiv h, H, A$ respectively. It can be seen that the couplings of the Higgses with SM fermions in this model are the same as in a Type-I 2HDM. α is the mixing angle between the neutral CP-even Higgses and β quantifies the ratio of the vevs of the two doublets, $\tan \beta = v_2/v_1$. The coupling of the SM-like Higgs to the exotic fermions tend to zero as $\alpha \rightarrow 0$. Moreover, the Higgs signal strength measurements dictate $|\cos(\beta - \alpha)| \lesssim 0.45$ at 95% CL [411, 412]. So, the allowed values of $\tan \beta$ for our model are $\tan \beta \gtrsim 1.96$ along with $\alpha \rightarrow 0$. The particle content of our model along with their charges under the SM gauge group as well as $U(1)'$ and Z_2 are given in table 7.3. Chiral fourth generation fermions can also be realised in a Type-II 2HDM in the wrong-sign Yukawa limit [413].

The $Z'\tau\bar{\tau}$ interaction in our model leads to a new four-body decay

channel of τ and three-body decay channels for Z and W^\pm . We consider that the effect of these new interactions must be such that their contribution to the respective decay processes must be within the errors of the measured decay widths at 1σ level. This leads to an upper bound on the allowed value of the coupling g_τ which is enlisted in table 7.4.

Process	Allowed decay width (GeV)	Maximum value of g_τ
$\tau \rightarrow \nu_\tau W^{-(*)} Z'$	3.8×10^{-15}	0.04
$W^- \rightarrow \tau^- \bar{\nu}_\tau Z'$	1.8×10^{-2}	0.05
$Z \rightarrow \tau^+ \tau^- Z'$	2.8×10^{-4}	0.02

Table 7.4. Constraints on coupling of light vector boson Z' of mass 10 MeV.

If we choose the new symmetry to be a $SU(2)$ instead of $U(1)'$, then in addition to Z' we would have W'^\pm in the spectrum. But the existence of a charged vector boson of mass $\sim \mathcal{O}(10)$ MeV opens up a new two-body decay channel for τ . Such decay processes are highly constrained, thus making the coupling of Z' to ν_τ rather small.

7.5 Extracting constraints on NSI from CC neutrino-nucleon cross-section

NC interactions of neutrinos of all flavours and CC interactions of ν_τ (83% times) and ν_e lead to cascade events at the IceCube detector. Moreover, the interaction lengths of high energy neutrinos in earth depend upon the neutrino-nucleon cross-section (NC and CC). These make the extraction of $\sigma_{\nu N}^{tot}$ viable from the observation of cascade events at IceCube induced by high energy neutrinos [213]. The NSIs considered in this thesis provide additional contributions to the NC neutrino-nucleon cross-section, which can be constrained as,

$$\sigma_{\nu N}^{NSI} \lesssim \sigma_{\nu N}^{tot,cas} - \sigma_{\nu N}^{CC,IC} - \sigma_{\nu N}^{NC,SM}. \quad (7.10)$$

Here, $\sigma_{\nu N}^{tot,cas}$ denotes the total neutrino-nucleon cross-section measured from the IceCube observation of cascade events induced by high energy

neutrinos [213]. The second term in RHS of inequality (7.10), *i.e.*, the CC neutrino-nucleon cross-section, $\sigma_{\nu N}^{CC,IC}$, can be measured rather precisely from the track events at IceCube [360], so the related uncertainties are not implemented. This way one can estimate the remaining room for NSI contribution. Extracting the bound on $\sigma_{\nu N}^{NSI}$ in this way comes at the expense of introducing $\sim 2\%$ change in the neutrino flux compared to ref. [213], which is even smaller than the effect of regeneration of high energy neutrinos passing through the earth. Considering the current uncertainties in $\sigma_{\nu N}^{tot}$ found in ref. [213], the effects of regeneration, which cause a change up to $\sim 10\%$ in the neutrino flux, does not have a significant impact on the estimated cross-section. By the same token, relevant bound on $\sigma_{\nu N}^{NSI}$ can be extracted using eq. (7.10).

7.6 Differential cross-sections and interference effects

The differential cross-sections of the process $pp \rightarrow \nu\bar{\nu}j$ for the contact NSI as in eq. (5.8) can be written as the sum of contributions from the SM, NP and interference of these two:

$$\frac{d\sigma}{dp_T d\eta} = \frac{d\sigma_{SM}}{dp_T d\eta} + \frac{d\sigma_{int}}{dp_T d\eta} + \frac{d\sigma_{NP}}{dp_T d\eta}, \quad (7.11)$$

with,

$$\begin{aligned} \frac{d\sigma_{SM}}{dp_T d\eta} &= \frac{G_F^2}{\pi p_T} \left(\frac{M_Z^4}{(Q_{tr}^2 - M_Z^2)^2 + (\Gamma M_Z)^2} \right) Q_{tr}^2 \left(1 + \frac{Q_{tr}^4}{(x_1 x_2 s)^2} \right), \\ \frac{d\sigma_{int}}{dp_T d\eta} &= \frac{2\epsilon G_F^2}{\pi p_T} \left(\frac{M_Z^2 (Q_{tr}^2 - M_Z^2)}{(Q_{tr}^2 - M_Z^2)^2 + (\Gamma M_Z)^2} \right) Q_{tr}^2 \left(1 + \frac{Q_{tr}^4}{(x_1 x_2 s)^2} \right), \\ \frac{d\sigma_{NP}}{dp_T d\eta} &= \frac{\epsilon^2 G_F^2}{\pi p_T} Q_{tr}^2 \left(1 + \frac{Q_{tr}^4}{(x_1 x_2 s)^2} \right). \end{aligned} \quad (7.12)$$

Here, x_1 and x_2 are fractions of proton momentum transferred to the two initial partons involved in $pp \rightarrow \nu\bar{\nu}j$ and Q_{tr} is momentum transferred to the neutrino pair. At LHC with $\sqrt{s} = 8$ TeV the cross-section for

$pp \rightarrow \nu\bar{\nu}j$ gets most of the contribution in the p_T range, 120 – 150 GeV. To compare the relative contributions of the different terms appearing in the RHS of eq. (7.11), we use the fact that, $\langle Q_{tr} \rangle \sim 500$ GeV for $p_T = 150$ GeV, $|\eta| < 2$ and $\sqrt{s} = 8$ TeV [414]. Using the second and third relations of eq. (7.12) one finds the ratio of the NP contribution to that from the interference term to be $\sim 2M_Z^2/(\epsilon\langle Q_{tr}^2 \rangle)$. As $\langle Q_{tr} \rangle \sim 500$ GeV, this ratio turns out to be ~ 0.33 for the maximum allowed value of $\epsilon \sim 0.19$. This implies, the interference term is subleading than the NP term in the cross-section of $pp \rightarrow \nu\bar{\nu}j$ with the dim-6 NSI term, which is somewhat opposite to the common perception. This happens due to an accidental conspiracy between $\langle Q_{tr}^2 \rangle$ and current maximum allowed value of ϵ . If the constraint on ϵ becomes even more stringent, with the value $\langle Q_{tr}^2 \rangle$ not changing significantly, the current picture can be reversed, *i.e.*, the interference term can be dominant over the NP contribution. A similar situation has been discussed in ref. [379].

Bibliography

- [1] Reines F., Cowan C. L., Harrison F. B., McGuire A. D. and Kruse H. W., Detection of the free anti-neutrino, *Phys. Rev.* **117** (1960) 159 (DOI:10.1103/PhysRev.117.159).
- [2] Danby G., Gaillard J. M., Goulianos K. A., Lederman L. M., Mistry N. B., Schwartz M. and Steinberger J., Observation of High-Energy Neutrino Reactions and the Existence of Two Kinds of Neutrinos, *Phys. Rev. Lett.* **9** (1962) 36 (DOI:10.1103/PhysRevLett.9.36).
- [3] Kodama K. *et al.* [DONUT Collaboration], Observation of tau neutrino interactions, *Phys. Lett. B* **504** (2001) 218 (DOI:10.1016/S0370-2693(01)00307-0).
- [4] Hernandez P., Neutrino Physics, CERN Yellow Report CERN 2015-005, pp. 85-142 (DOI:10.5170/CERN-2016-005.85).
- [5] Noether E., Invariant Variation Problems, *Gott. Nachr.* **1918** (1918) 235 [Transp. Theory Statist. Phys. **1** (1971) 186] (DOI:10.1080/00411457108231446).
- [6] Weinberg S., A Model of Leptons, *Phys. Rev. Lett.* **19** (1967) 1264 (DOI:10.1103/PhysRevLett.19.1264).
- [7] Tanabashi M. *et al.* [Particle Data Group], Review of Particle Physics, *Phys. Rev. D* **98** (2018) no.3, 030001 (DOI:10.1103/PhysRevD.98.030001).
- [8] Giunti C. and Kim C. W., *Fundamentals of Neutrino Physics and Astrophysics*, Oxford, UK: Univ. Pr. (2007) 710 p.

- [9] Bjorken J. D., Asymptotic Sum Rules at Infinite Momentum, *Phys. Rev.* **179** (1969) 1547 (DOI:10.1103/PhysRev.179.1547).
- [10] Gandhi R., Quigg C., Reno M. H. and Sarcevic I., Neutrino interactions at ultrahigh-energies, *Phys. Rev. D* **58** (1998) 093009 (DOI:10.1103/PhysRevD.58.093009).
- [11] Connolly A., Thorne R. S. and Waters D., Calculation of High Energy Neutrino-Nucleon Cross Sections and Uncertainties Using the MSTW Parton Distribution Functions and Implications for Future Experiments, *Phys. Rev. D* **83** (2011) 113009 (DOI:10.1103/PhysRevD.83.113009).
- [12] Aaron F. D. *et al.* [H1 and ZEUS Collaborations], Combined Measurement and QCD Analysis of the Inclusive e^+p Scattering Cross Sections at HERA, *JHEP* **1001** (2010) 109 (DOI:10.1007/JHEP01(2010)109).
- [13] Abramowicz H. *et al.* [H1 and ZEUS Collaborations], Combination of measurements of inclusive deep inelastic $e^\pm p$ scattering cross sections and QCD analysis of HERA data, *Eur. Phys. J. C* **75** (2015) no.12, 580 (DOI:10.1140/epjc/s10052-015-3710-4).
- [14] Zenaiev O. *et al.* [PROSA Collaboration], Impact of heavy-flavour production cross sections measured by the LHCb experiment on parton distribution functions at low x , *Eur. Phys. J. C* **75** (2015) no.8, 396 (DOI:10.1140/epjc/s10052-015-3618-z).
- [15] Gauld R., Rojo J., Rottoli L. and Talbert J., Charm production in the forward region: constraints on the small- x gluon and backgrounds for neutrino astronomy, *JHEP* **1511** (2015) 009 (DOI:10.1007/JHEP11(2015)009).
- [16] Cacciari M., Mangano M. L. and Nason P., Gluon PDF constraints from the ratio of forward heavy-quark production at the LHC at $\sqrt{S} = 7$ and 13 TeV, *Eur. Phys. J. C* **75** (2015) no.12, 610 (DOI:10.1140/epjc/s10052-015-3814-x).

- [17] Glashow S. L., Resonant Scattering of Antineutrinos, *Phys. Rev.* **118** (1960) 316 (DOI:10.1103/PhysRev.118.316).
- [18] Berezhinsky V. S. and Gazizov A. Z., Cosmic neutrino and the possibility of Searching for W bosons with masses 30-100 GeV in underwater experiments, *JETP Lett.* **25** (1977) 254 [*Pisma Zh. Eksp. Teor. Fiz.* **25** (1977) 276].
- [19] Berezhinsky V. S. and Gazizov A. Z., Neutrino - electron scattering at energies above the W boson production threshold, *Sov. J. Nucl. Phys.* **33** (1981) 120 [*Yad. Fiz.* **33** (1981) 230].
- [20] Lu L. [IceCube Collaboration], Multi-flavour PeV neutrino search with IceCube, *PoS ICRC 2017* (2018) 1002 (DOI:10.22323/1.301.1002).
- [21] Huang G. y. and Liu Q., Hunting the Glashow Resonance with PeV Neutrino Telescopes, *JCAP* **2003** (2020) no.03, 005 (DOI:10.1088/1475-7516/2020/03/005).
- [22] Higgs P. W., Broken symmetries, massless particles and gauge fields, *Phys. Lett.* **12** (1964) 132 (DOI:10.1016/0031-9163(64)91136-9).
- [23] Higgs P. W., Spontaneous Symmetry Breakdown without Massless Bosons, *Phys. Rev.* **145** (1966) 1156 (DOI:10.1103/PhysRev.145.1156).
- [24] Englert F. and Brout R., Broken Symmetry and the Mass of Gauge Vector Mesons, *Phys. Rev. Lett.* **13** (1964) 321 (DOI:10.1103/PhysRevLett.13.321).
- [25] Higgs P. W., Broken Symmetries and the Masses of Gauge Bosons, *Phys. Rev. Lett.* **13** (1964) 508 (DOI:10.1103/PhysRevLett.13.508).
- [26] Ashie Y. *et al.* [Super-Kamiokande Collaboration], A Measurement of atmospheric neutrino oscillation parameters by SUPER-KAMIOKANDE I, *Phys. Rev. D* **71** (2005) 112005 (DOI:10.1103/PhysRevD.71.112005).

- [27] Kajita T., Atmospheric Neutrinos And Discovery Of Neutrino Oscillations, Proc. Japan Acad. B **86** (2010) 303 (DOI:10.2183/pjab.86.303).
- [28] Back H. *et al.*, Report of the solar and atmospheric neutrino experiments working group of the APS multidivisional neutrino study (arXiv:hep-ex/0412016).
- [29] Ahmad Q. R. *et al.* [SNO Collaboration], Direct evidence for neutrino flavor transformation from neutral current interactions in the Sudbury Neutrino Observatory, Phys. Rev. Lett. **89** (2002) 011301 (DOI:10.1103/PhysRevLett.89.011301).
- [30] Goswami S., Bandyopadhyay A. and Choubey S., Global analysis of neutrino oscillation, Nucl. Phys. Proc. Suppl. **143** (2005) 121 (DOI:10.1016/j.nuclphysbps.2005.01.096).
- [31] Mohapatra R. N. and Pal P. B., Massive neutrinos in physics and astrophysics, Third Edition, World Sci. Lect. Notes Phys. **60** (1998) 1.
- [32] Weinberg S., Baryon and Lepton Nonconserving Processes, Phys. Rev. Lett. **43** (1979) 1566 (DOI:10.1103/PhysRevLett.43.1566).
- [33] Loureiro A. *et al.*, On The Upper Bound of Neutrino Masses from Combined Cosmological Observations and Particle Physics Experiments, Phys. Rev. Lett. **123** (2019) no.8, 081301 (DOI:10.1103/PhysRevLett.123.081301).
- [34] Mohapatra R. N., Physics of neutrino mass, eConf **C040802** (2004) L011 (DOI:10.1088/1367-2630/6/1/082).
- [35] Maki Z., Nakagawa M. and Sakata S., Remarks on the unified model of elementary particles, Prog. Theor. Phys. **28** (1962) 870 (DOI:10.1143/PTP.28.870).
- [36] Pontecorvo B., Inverse beta processes and nonconservation of lepton charge, Sov. Phys. JETP **7** (1958) 172.

- [37] Esteban I., Gonzalez-Garcia M., Hernandez-Cabezudo A., Maltoni M. and Schwetz T., NuFIT 4.1 (2019), <http://www.nu-fit>.
- [38] Wolfenstein L., Neutrino Oscillations in Matter, *Phys. Rev. D* **17** (1978) 2369 (DOI:10.1103/PhysRevD.17.2369).
- [39] Zener C., Nonadiabatic crossing of energy levels, *Proc. Roy. Soc. Lond. A* **137** (1932) 696 (DOI:10.1098/rspa.1932.0165).
- [40] Blennow M. and Smirnov A. Y., Neutrino propagation in matter, *Adv. High Energy Phys.* **2013** (2013) 972485 (DOI:10.1155/2013/972485).
- [41] Parke S. J., Nonadiabatic Level Crossing in Resonant Neutrino Oscillations, *Phys. Rev. Lett.* **57** (1986) 1275-1278 (DOI:10.1103/PhysRevLett.57.1275).
- [42] Kaneko T., Analytic Solution for Resonant Mixing of Solar Neutrinos, *Prog. Theor. Phys.* **78** (1987) 532 (DOI:10.1143/PTP.78.532).
- [43] Toshev S., Exact Analytical Solution of the Two Neutrino Evolution Equation in Matter With Exponentially Varying Density, *Phys. Lett. B* **196** (1987) 170-174 (DOI:10.1016/0370-2693(87)90598-3).
- [44] Zwicky F., Die Rotverschiebung von extragalaktischen Nebeln, *Helv. Phys. Acta* **6** (1933) 110-127 (DOI:10.1007/s10714-008-0707-4).
- [45] Rubin V. C. and Ford, Jr. W. K., Rotation of the Andromeda Nebula from a Spectroscopic Survey of Emission Regions, *Astrophys. J.* **159** (1970) 379-403 (DOI:10.1086/150317).
- [46] Clowe D., Bradac M., Gonzalez A. H., Markevitch M., Randall S. W., Jones C. and Zaritsky D., A direct empirical proof of the existence of dark matter, *Astrophys. J. Lett.* **648** (2006) L109-L113 (DOI:10.1086/508162).
- [47] Ade P. A. R. *et al.* [Planck Collaboration], Planck 2015 results. XIII. Cosmological parameters, *Astron. Astrophys.* **594** (2016) A13 (DOI:10.1051/0004-6361/201525830).

- [48] Blumenthal G. R., Faber S. M., Primack J. R. and Rees M. J., Formation of Galaxies and Large Scale Structure with Cold Dark Matter, *Nature* **311** (1984) 517-525 (DOI:10.1038/311517a0).
- [49] Hu W., Barkana R. and Gruzinov A., Cold and fuzzy dark matter, *Phys. Rev. Lett.* **85** (2000) 1158 (DOI:10.1103/PhysRevLett.85.1158).
- [50] Alcock C. *et al.* [MACHO Collaboration], Possible gravitational microlensing of a star in the Large Magellanic Cloud, CFPA-93-30.
- [51] Randall L., Scholtz J. and Unwin J., Cores in Dwarf Galaxies from Fermi Repulsion, *Mon. Not. Roy. Astron. Soc.* **467** (2017) no.2, 1515-1525 (DOI:10.1093/mnras/stx161).
- [52] Steigman G. and Turner M. S., Cosmological Constraints on the Properties of Weakly Interacting Massive Particles, *Nucl. Phys. B* **253** (1985) 375-386 (DOI:10.1016/0550-3213(85)90537-1).
- [53] A. Tasitsiomi, The Cold dark matter crisis on galactic and subgalactic scales, *Int. J. Mod. Phys. D* **12** (2003) 1157 (astro-ph/0205464).
- [54] Salucci P., Walter F. and Borriello A., The distribution of dark matter in galaxies: The Constant density halo around DDO 47, *Astron. Astrophys.* **409** (2003) 53 (DOI:10.1051/0004-6361:20030646).
- [55] Blok W. J. G. d., Bosma A. and McGaugh S. S. Simulating observations of dark matter dominated galaxies: towards the optimal halo profile, *Mon. Not. Roy. Astron. Soc.* **340** (2003) 657 (DOI:10.1046/j.1365-8711.2003.06330.x).
- [56] Navarro J. F., Frenk C. S. and White S. D. M., The Structure of cold dark matter halos, *Astrophys. J.* **462** (1996) 563 (DOI:10.1086/177173).
- [57] Flores R. A. and Primack J. R., Observational and theoretical constraints on singular dark matter halos, *Astrophys. J. Lett.* **427** (1994) L1-4 (DOI:10.1086/187350).

- [58] Klypin A. A., Kravtsov A. V., Valenzuela O. and Prada F., Where are the missing Galactic satellites?, *Astrophys. J.* **522** (1999) 82 (DOI:10.1086/307643).
- [59] Boylan-Kolchin M., Bullock J. S. and Kaplinghat M., Too big to fail? The puzzling darkness of massive Milky Way subhaloes, *Mon. Not. Roy. Astron. Soc.* **415** (2011) L40 (DOI:10.1111/j.1745-3933.2011.01074.x).
- [60] Spergel D. N. and Steinhardt P. J., Observational evidence for self-interacting cold dark matter, *Phys. Rev. Lett.* **84** (2000) 3760-3763 (DOI:10.1103/PhysRevLett.84.3760).
- [61] Goodenough L. and Hooper D., Possible Evidence For Dark Matter Annihilation In The Inner Milky Way From The Fermi Gamma Ray Space Telescope (arXiv:0910.2998 [hep-ph]).
- [62] Yoshida N., Springel V., White S. D. M. and Tormen G., Weakly self-interacting dark matter and the structure of dark halos, *Astrophys. J. Lett.* **544** (2000) L87-L90 (DOI:10.1086/317306).
- [63] Das S. and Bhaduri R. K., Dark matter and dark energy from a Bose–Einstein condensate, *Class. Quant. Grav.* **32** (2015) no.10, 105003 (DOI:10.1088/0264-9381/32/10/105003).
- [64] Matos T. and Urena-Lopez L. A., Flat rotation curves in scalar field galaxy halos, *Gen. Rel. Grav.* **39** (2007) 1279 (DOI:10.1007/s10714-007-0470-y).
- [65] Su K. Y. and Chen P., Solving the Cusp-Core Problem with a Novel Scalar Field Dark Matter, *JCAP* **1108** (2011) 016 (DOI:10.1088/1475-7516/2011/08/016).
- [66] Peebles P. J. E., Fluid dark matter, *Astrophys. J.* **534** (2000) L127 (DOI:10.1086/312677).

- [67] Arbey A., Lesgourgues J. and Salati P., Galactic halos of fluid dark matter, *Phys. Rev. D* **68** (2003) 023511 (DOI:10.1103/PhysRevD.68.023511).
- [68] Goodman J., Repulsive dark matter, *New Astron.* **5** (2000) 103 (DOI:10.1016/S1384-1076(00)00015-4).
- [69] Fan J., Ultralight Repulsive Dark Matter and BEC, *Phys. Dark Univ.* **14** (2016) 84 (DOI:10.1016/j.dark.2016.10.005).
- [70] Alcubierre M., Guzman F. S., Matos T., Nunez D., Urena-Lopez L. A. and Wiederhold P., Galactic collapse of scalar field dark matter, *Class. Quant. Grav.* **19** (2002) 5017 (DOI:10.1088/0264-9381/19/19/314).
- [71] Harko T., Evolution of cosmological perturbations in Bose-Einstein condensate dark matter, *Mon. Not. Roy. Astron. Soc.* **413** (2011) 3095 (DOI:10.1111/j.1365-2966.2011.18386.x).
- [72] Iršič V., Viel M., Haehnelt M. G., Bolton J. S. and Becker G. D., First constraints on fuzzy dark matter from Lyman- α forest data and hydrodynamical simulations, *Phys. Rev. Lett.* **119** (2017) no.3, 031302 (DOI:10.1103/PhysRevLett.119.031302).
- [73] Fukuyama T., Morikawa M. and Tatekawa T., Cosmic structures via Bose Einstein condensation and its collapse, *JCAP* **0806** (2008) 033 (DOI:10.1088/1475-7516/2008/06/033).
- [74] Avignone F. T., III, Elliott S. R. and Engel J., Double Beta Decay, Majorana Neutrinos, and Neutrino Mass, *Rev. Mod. Phys.* **80** (2008) 481-516 (DOI:10.1103/RevModPhys.80.481).
- [75] Casas J., Chakraborti M. and Quilis J., UV completion of an axial, leptophobic, Z' (arXiv:1907.11207 [hep-ph]).
- [76] Heck J. and Rodejohann W., Neutrinoless Quadruple Beta Decay, *EPL* **103** (2013) no.3, 32001 (DOI:10.1209/0295-5075/103/32001).

- [77] Randall L. and Sundrum R., A Large mass hierarchy from a small extra dimension, *Phys. Rev. Lett.* **83** (1999) 3370-3373 (DOI:10.1103/PhysRevLett.83.3370).
- [78] Gouvêa A. de, Neutrino Mass Models, *Ann. Rev. Nucl. Part. Sci.* **66** (2016) 197-217 (DOI:10.1146/annurev-nucl-102115-044600).
- [79] King S., Neutrino mass models, *Rept. Prog. Phys.* **67** (2004) 107-158 (DOI:10.1088/0034-4885/67/2/R01).
- [80] Schechter J. and Valle J., Neutrino Masses in $SU(2) \times U(1)$ Theories, *Phys. Rev. D* **22** (1980) 2227 (DOI:10.1103/PhysRevD.22.2227).
- [81] Petcov S., The Nature of Massive Neutrinos, *Adv. High Energy Phys.* **2013** (2013) 852987 (DOI:10.1155/2013/852987).
- [82] Borah D., Nanda D., Narendra N. and Sahu N., Right-handed neutrino dark matter with radiative neutrino mass in gauged B - L model, *Nucl. Phys. B* **950** (2020) 114841 (DOI:10.1016/j.nuclphysb.2019.114841).
- [83] Uehara Y., Right-handed neutrinos as superheavy dark matter, *JHEP* **12** (2001) 034 (DOI:10.1088/1126-6708/2001/12/034).
- [84] Chen M., Gouvea A. de and Dobrescu B. A., Gauge Trimming of Neutrino Masses, *Phys. Rev. D* **75** (2007) 055009 (DOI:10.1103/PhysRevD.75.055009).
- [85] Aguilar-Arevalo A. *et al.* [MiniBooNE Collaboration], Improved Search for $\bar{\nu}_\mu \rightarrow \bar{\nu}_e$ Oscillations in the MiniBooNE Experiment, *Phys. Rev. Lett.* **110** (2013) 161801 (DOI:10.1103/PhysRevLett.110.161801).
- [86] Mention G., Fechner M., Lasserre T., Mueller T., Lhuillier D., Cri-bier M. and Letourneau A., The Reactor Antineutrino Anomaly, *Phys. Rev. D* **83** (2011) 073006 (DOI:10.1103/PhysRevD.83.073006).
- [87] Aguilar-Arevalo A. *et al.* [MiniBooNE Collaboration], Significant Excess of ElectronLike Events in the MiniBooNE Short-Baseline

- Neutrino Experiment, *Phys. Rev. Lett.* **121** (2018) no.22, 221801 (DOI:10.1103/PhysRevLett.121.221801).
- [88] de Gouvea A., See-saw energy scale and the LSND anomaly, *Phys. Rev. D* **72** (2005) 033005 (DOI:10.1103/PhysRevD.72.033005).
- [89] Chu X., Dasgupta B., Dentler M., Kopp J. and Saviano N., Sterile neutrinos with secret interactions—cosmological discord?, *JCAP* **11** (2018) 049 (DOI:10.1088/1475-7516/2018/11/049).
- [90] Forastieri F., Lattanzi M. and Natoli P., Cosmological constraints on neutrino self-interactions with a light mediator, *Phys. Rev. D* **100** (2019) no.10, 103526 (DOI:10.1103/PhysRevD.100.103526).
- [91] Boehm C., Dolan M. J. and McCabe C., A Lower Bound on the Mass of Cold Thermal Dark Matter from Planck, *JCAP* **1308** (2013) 041 (DOI:10.1088/1475-7516/2013/08/041).
- [92] Olivares-Del Campo A., Boehm C., Palomares-Ruiz S. and Pascoli S., Dark matter-neutrino interactions through the lens of their cosmological implications, *Phys. Rev. D* **97** (2018) no.7, 075039 (DOI:10.1103/PhysRevD.97.075039).
- [93] Huang G., Ohlsson T. and Zhou S., Observational Constraints on Secret Neutrino Interactions from Big Bang Nucleosynthesis, *Phys. Rev. D* **97** (2018) no.7, 075009 (DOI:10.1103/PhysRevD.97.075009).
- [94] Mangano G., Miele G., Pastor S., Pinto T., Pisanti O. and Serpico P. D., Relic neutrino decoupling including flavor oscillations, *Nucl. Phys. B* **729** (2005) 221-234 (DOI:10.1016/j.nuclphysb.2005.09.041).
- [95] Lesgourgues J. and Pastor S., Massive neutrinos and cosmology, *Phys. Rept.* **429** (2006) 307-379 (DOI:10.1016/j.physrep.2006.04.001).
- [96] Gondolo P. and Gelmini G., Cosmic abundances of stable particles: Improved analysis, *Nucl. Phys. B* **360** (1991) 145-179 (DOI:10.1016/0550-3213(91)90438-4).

- [97] Freitas A. and Westhoff S., Leptophilic Dark Matter in Lepton Interactions at LEP and ILC, *JHEP* **10** (2014) 116 (DOI:10.1007/JHEP10(2014)116).
- [98] Lafferty G. [LHCb Collaboration], Rare decays at LHCb, *Nucl. Part. Phys. Proc.* **263-264** (2015) 32-37 (DOI:10.1016/j.nuclphysbps.2015.04.006).
- [99] Andreassi G., Lepton Flavour Violation searches and scintillating fibre tracker testing in LHCb (DOI:10.5075/epfl-thesis-9251).
- [100] Milanés D. A. and Rodriguez J. A., Review of New Physics Searches at LHCb Experiment, *MOMENTO* **51** (2015) 69-82.
- [101] Essig R., Mardon J., Papucci M., Volansky T. and Zhong Y., Constraining Light Dark Matter with Low-Energy e^+e^- Colliders, *JHEP* **11** (2013) 167 (DOI:10.1007/JHEP11(2013)167).
- [102] Lees J. P. *et al.* [BaBar Collaboration], Search for a muonic dark force at BABAR, *Phys. Rev. D* **94** (2016) no.1, 011102 (DOI:10.1103/PhysRevD.94.011102).
- [103] Altmannshofer W., Gori S., Pospelov M. and Yavin I., Neutrino Trident Production: A Powerful Probe of New Physics with Neutrino Beams, *Phys. Rev. Lett.* **113** (2014) 091801 (DOI:10.1103/PhysRevLett.113.091801).
- [104] Donini A., Hernandez P., Lopez-Pavon J. and Maltoni M., Minimal models with light sterile neutrinos, *JHEP* **07** (2011) 105 (DOI:10.1007/JHEP07(2011)105).
- [105] Trevisani N.[ATLAS and CMS Collaborations], Collider Searches for Dark Matter (ATLAS + CMS), *Universe* **4** (2018) no.11, 131 (DOI:10.3390/universe4110131).
- [106] Keung W. and Senjanovic G., Majorana Neutrinos and the Production of the Right-handed Charged Gauge Boson, *Phys. Rev. Lett.* **50** (1983) 1427 (DOI:10.1103/PhysRevLett.50.1427).

- [107] Aad G. *et al.* [ATLAS Collaboration], Search for heavy neutrinos and right-handed W bosons in events with two leptons and jets in pp collisions at $\sqrt{s} = 7$ TeV with the ATLAS detector, *Eur. Phys. J. C* **72** (2012) 2056 (DOI:10.1140/epjc/s10052-012-2056-4).
- [108] Hayreter A., He X. and Valencia G., LHC constraints on W' , Z' that couple mainly to third generation fermions (arXiv:1912.06344 [hep-ph]).
- [109] Bhupal Dev P. *et al.*, Neutrino Non-Standard Interactions: A Status Report, *SciPost Phys. Proc.* **2** (2019) 001 (DOI:10.21468/SciPostPhysProc.2.001).
- [110] Sirunyan A. M. *et al.* [CMS Collaboration], Search for contact interactions and large extra dimensions in the dilepton mass spectra from proton-proton collisions at $\sqrt{s} = 13$ TeV, *JHEP* **04** (2019) 114 (DOI:10.1007/JHEP04(2019)114).
- [111] Terol-Calvo J., Tórtola M. and Vicente A., High-energy constraints from low-energy neutrino non-standard interactions (arXiv:1912.09131 [hep-ph]).
- [112] Calibbi L. and Signorelli G., Charged Lepton Flavour Violation: An Experimental and Theoretical Introduction, *Riv. Nuovo Cim.* **41** (2018) no.2, 71-174 (DOI:10.1393/ncr/i2018-10144-0).
- [113] Barranco J., Miranda O., Moura C. and Valle J., Constraining non-standard neutrino-electron interactions, *Phys. Rev. D* **77** (2008) 093014 (DOI:10.1103/PhysRevD.77.093014).
- [114] Hayasaka K. *et al.*, Search for Lepton Flavor Violating Tau Decays into Three Leptons with 719 Million Produced Tau+Tau- Pairs, *Phys. Lett. B* **687** (2010) 139-143 (DOI:10.1016/j.physletb.2010.03.037).
- [115] Farzan Y. and Tortola M., Neutrino oscillations and Non-Standard Interactions, *Front. in Phys.* **6** (2018) 10 (DOI:10.3389/fphy.2018.00010).

- [116] Bischer I. and Rodejohann W., General neutrino interactions from an effective field theory perspective, *Nucl. Phys. B* **947** (2019) 114746 (DOI:10.1016/j.nuclphysb.2019.114746).
- [117] Blennow M., Fernandez-Martinez E., Olivares-Del Campo A., Pascoli S., Rosauero-Alcaraz S. and Titov A., Neutrino Portals to Dark Matter, *Eur. Phys. J. C* **79** (2019) no.7, 555 (DOI:10.1140/epjc/s10052-019-7060-5).
- [118] Kelner S. R., Aharonian F. A. and Bugayov V. V., Energy spectra of gamma-rays, electrons and neutrinos produced at proton-proton interactions in the very high energy regime, *Phys. Rev. D* **74** (2006) 034018, Erratum: *Phys. Rev. D* **79** (2009) 039901 (DOI:10.1103/PhysRevD.74.034018, 10.1103/PhysRevD.79.039901).
- [119] Berezhinsky V. S. and Gazizov A. Z., Production of high-energy cosmic neutrinos in p gamma and n gamma scattering. 2. Arbitrary spectra of nucleons and photons, *Phys. Rev. D* **47** (1993) 4217 (DOI:10.1103/PhysRevD.47.4217).
- [120] Bahcall J. N., How the sun shines, *SLAC Beam Line* **31N1** (2001) 2 (arXiv:astro-ph/0009259).
- [121] Arteaga-Velázquez J. C., Neutrino production from photo-hadronic interactions of the gamma flux from Active Galactic Nuclei with their gas content, *Astropart. Phys.* **37**, 40 (2012) (DOI:10.1016/j.astropartphys.2012.07.002).
- [122] Bhattacharjee P. and Sigl G., Origin and propagation of extremely high-energy cosmic rays, *Phys. Rept.* **327** (2000) 109 (DOI:10.1016/S0370-1573(99)00101-5).
- [123] Cherry M. L., Approaching the knee - balloon-borne observations of cosmic ray composition, *J. Phys. Conf. Ser.* **47** (2006) 31 (DOI:10.1088/1742-6596/47/1/004).

- [124] Bellido J. [Pierre Auger Collaboration], Depth of maximum of air-shower profiles at the Pierre Auger Observatory: Measurements above $10^{17.2}$ eV and Composition Implications, PoS ICRC **2017** (2018) 506 (DOI:10.22323/1.301.0506).
- [125] Hanlon W. *et al.* [Telescope Array Collaboration], Energy Spectrum and Mass Composition of Ultra-High Energy Cosmic Rays Measured by the hybrid technique in Telescope Array, PoS ICRC **2015** (2016) 362 (DOI:10.22323/1.236.0362).
- [126] Hillas A. M., The Origin of Ultrahigh-Energy Cosmic Rays, Ann. Rev. Astron. Astrophys. **22** (1984) 425 (DOI:10.1146/annurev.aa.22.090184.002233).
- [127] Kachelriess M., Lecture notes on high energy cosmic rays (arXiv:0801.4376 [astro-ph]).
- [128] Fermi E., On the Origin of the Cosmic Radiation, Phys. Rev. **75** (1949) 1169-1174 (DOI:10.1103/PhysRev.75.1169).
- [129] Alves Batista R. *et al.*, Open Questions in Cosmic-Ray Research at Ultrahigh Energies, Front. Astron. Space Sci. **6** (2019) 23 (DOI:10.3389/fspas.2019.00023).
- [130] Longair M., High Energy Astrophysics, Second Edition, (1994) Cambridge: Cambridge University Press (DOI:10.1017/CBO9781139170505).
- [131] Allard D., Talk presented at NPAC 2016.
- [132] Ahlers M. and Halzen F., IceCube: Neutrinos and multimessenger astronomy, PTEP **2017** (2017) no.12, 12A105 (DOI:10.1093/ptep/ptx021).
- [133] Pisanti O., Astrophysical neutrinos: theory, J. Phys. Conf. Ser. **1263** (2019) no.1, 012004 (DOI:10.1088/1742-6596/1263/1/012004).

- [134] Ackermann M. *et al.* [Fermi-LAT Collaboration], The spectrum of isotropic diffuse gamma-ray emission between 100 MeV and 820 GeV, *Astrophys. J.* **799** (2015) 86 (DOI:10.1088/0004-637X/799/1/86).
- [135] Murase K., Guetta D. and Ahlers M., Hidden Cosmic-Ray Accelerators as an Origin of TeV-PeV Cosmic Neutrinos, *Phys. Rev. Lett.* **116** (2016) no.7, 071101 (DOI:10.1103/PhysRevLett.116.071101).
- [136] Zacharias M., Chen X. and Wagner S. J., Attenuation of TeV γ -rays by the starlight photon field of the host galaxy, *Mon. Not. Roy. Astron. Soc.* **465** (2017) no.3, 3767-3774 (DOI:10.1093/mnras/stw3032).
- [137] Murase K., Ahlers M. and Lacki B. C., Testing the Hadronuclear Origin of PeV Neutrinos Observed with IceCube, *Phys. Rev. D* **88** (2013) no.12, 121301 (DOI:10.1103/PhysRevD.88.121301).
- [138] Bechtol K., Ahlers M., Di Mauro M., Ajello M. and Vandenbroucke J., Evidence against star-forming galaxies as the dominant source of IceCube neutrinos, *Astrophys. J.* **836** (2017) no.1, 47 (DOI:10.3847/1538-4357/836/1/47).
- [139] Ahlers M. and Halzen F., Opening a New Window onto the Universe with IceCube, *Prog. Part. Nucl. Phys.* **102** (2018) 73-88 (DOI:10.1016/j.pnpnp.2018.05.001).
- [140] Ahlers M. and Halzen F., Pinpointing Extragalactic Neutrino Sources in Light of Recent IceCube Observations, *Phys. Rev. D* **90** (2014) no.4, 043005 (DOI:10.1103/PhysRevD.90.043005).
- [141] Waxman E. and Bahcall J. N., High-energy neutrinos from astrophysical sources: An Upper bound, *Phys. Rev. D* **59** (1999) 023002 (DOI:10.1103/PhysRevD.59.023002).
- [142] Bahcall J. N. and Waxman E., High-energy astrophysical neutrinos: The Upper bound is robust, *Phys. Rev. D* **64** (2001) 023002 (DOI:10.1103/PhysRevD.64.023002).

- [143] Murase K. and Beacom J. F., Neutrino Background Flux from Sources of Ultrahigh-Energy Cosmic-Ray Nuclei, *Phys. Rev. D* **81** (2010) 123001 (DOI:10.1103/PhysRevD.81.123001).
- [144] Ho L. C., Nuclear Activity in Nearby Galaxies, *Ann. Rev. Astron. Astrophys.* **46** (2008) 475-539 (DOI:10.1146/annurev.astro.45.051806.110546).
- [145] Kimura S. S., Murase K. and Toma K., Neutrino and Cosmic-Ray Emission and Cumulative Background from Radiatively Inefficient Accretion Flows in Low-Luminosity Active Galactic Nuclei, *Astrophys. J.* **806** (2015) 159 (DOI:10.1088/0004-637X/806/2/159).
- [146] Stecker F. W. and Salamon M. H., High-energy neutrinos from quasars, *Space Sci. Rev.* **75** (1996) 341 (DOI:10.1007/BF00195044).
- [147] Alvarez-Muniz J. and Meszaros P., High energy neutrinos from radio-quiet AGNs, *Phys. Rev. D* **70** (2004) 123001 (DOI:10.1103/PhysRevD.70.123001).
- [148] Pe'er A., Murase K. and Meszaros P., Radio Quiet AGNs as Possible Sources of Ultra-high Energy Cosmic Rays, *Phys. Rev. D* **80** (2009) 123018 (DOI:10.1103/PhysRevD.80.123018).
- [149] Murase K., Active Galactic Nuclei as High-Energy Neutrino Sources (DOI:10.1142/9789814759410-0002).
- [150] Meszaros P., Astrophysical Sources of High Energy Neutrinos in the IceCube Era, *Ann. Rev. Nucl. Part. Sci.* **67** (2017) 45 (DOI:10.1146/annurev-nucl-101916-123304).
- [151] Boettcher M., Modeling the Emission Processes in Blazars, *Astrophys. Space Sci.* **309** (2007) 95-104 (DOI:10.1007/s10509-007-9404-0).
- [152] Sahu S., Osorio Oliveros A. F. and Sanabria J. C., Hadronic-origin orphan TeV flare from 1ES 1959+650, *Phys. Rev. D* **87** (2013) no.10, 103015 (DOI:10.1103/PhysRevD.87.103015).

- [153] Reimer A., Bottcher M. and Postnikov S., Neutrino emission in the hadronic synchrotron mirror model: The Orphan TeV flare from 1ES 1959+650, *Astrophys. J.* **630** (2005) 186-190 (DOI:10.1086/431948).
- [154] Muecke A., Protheroe R. J., Engel R., Rachen J. P. and Stanev T., BL Lac Objects in the synchrotron proton blazar model, *Astropart. Phys.* **18** (2003) 593-613 (DOI:10.1016/S0927-6505(02)00185-8).
- [155] Aartsen M. G. *et al.* [IceCube and Fermi-LAT and MAGIC and AGILE and ASAS-SN and HAWC and H.E.S.S. and INTEGRAL and Kanata and Kiso and Kapteyn and Liverpool Telescope and Subaru and Swift NuSTAR and VERITAS and VLA/17B-403 Collaborations], Multimessenger observations of a flaring blazar coincident with high-energy neutrino IceCube-170922A, *Science* **361** (2018) no.6398, eaat1378 (DOI:10.1126/science.aat1378).
- [156] Böttcher M., Spectral and Polarization Signatures of Relativistic Shocks in Blazars, *Galaxies* **4** (2016) no.3, 22 (DOI:10.3390/galaxies4030022).
- [157] Dermer C. D., Murase K. and Inoue Y., Photopion Production in Black-Hole Jets and Flat-Spectrum Radio Quasars as PeV Neutrino Sources, *JHEAp* **3-4** (2014) 29 (DOI:10.1016/j.jheap.2014.09.001).
- [158] Aartsen M. G. *et al.* [IceCube Collaboration], The contribution of Fermi-2LAC blazars to the diffuse TeV-PeV neutrino flux, *Astrophys. J.* **835** (2017) no.1, 45 (DOI:10.3847/1538-4357/835/1/45).
- [159] Volk H. J., Aharonian F. A. and Breitschwerdt D., The nonthermal energy content and gamma-ray emission of starburst galaxies and clusters of galaxies, *Space Sci. Rev.* **75** (1996) 279.
- [160] Berezhinsky V. S., Blasi P. and Ptuskin V. S., Clusters of Galaxies as a Storage Room for Cosmic Rays, *Astrophys. J.* **487** (1997) 529 (DOI:10.1086/304622).

- [161] Zandanel F., Pfrommer C. and Prada F., On the physics of radio haloes in galaxy clusters: scaling relations and luminosity functions, *Mon. Not. Roy. Astron. Soc.* **438** (2014) no.1, 124 (DOI:10.1093/mnras/stt2250).
- [162] Loeb A. and Waxman E., Gamma-ray background from structure formation in the intergalactic medium, *Nature* **405** (2000) 156 (DOI:10.1038/35012018).
- [163] Ackermann M. *et al.* [Fermi-LAT Collaboration], Resolving the Extragalactic γ -Ray Background above 50 GeV with the Fermi Large Area Telescope, *Phys. Rev. Lett.* **116** (2016) no.15, 151105 (DOI:10.1103/PhysRevLett.116.151105).
- [164] Madau P. and Dickinson M., Cosmic Star Formation History, *Ann. Rev. Astron. Astrophys.* **52** (2014) 415 (DOI:10.1146/annurev-astro-081811-125615).
- [165] Senno N., Mészáros P., Murase K., Baerwald P. and Rees M. J., Extragalactic star-forming galaxies with hypernovae and supernovae as high-energy neutrino and gamma-ray sources: the case of the 10 TeV neutrino data, *Astrophys. J.* **806** (2015) no.1, 24 (DOI:10.1088/0004-637X/806/1/24).
- [166] Hasinger G., Miyaji T. and Schmidt M., Luminosity-dependent evolution of soft x-ray selected AGN: New Chandra and XMM-Newton surveys, *Astron. Astrophys.* **441** (2005) 417 (DOI:10.1051/0004-6361:20042134).
- [167] Meszaros P., Gamma Ray Bursts, *Astropart. Phys.* **43** (2013) 134 (DOI:10.1016/j.astropartphys.2012.03.009).
- [168] Aartsen M. G. *et al.* [IceCube Collaboration], Search for Prompt Neutrino Emission from Gamma-Ray Bursts with IceCube, *Astrophys. J.* **805** (2015) no.1, L5 (DOI:10.1088/2041-8205/805/1/L5).

- [169] Hussain R. *et al.* [IceCube Collaboration], A Search for IceCube Neutrinos from the First 33 Detected Gravitational Wave Events, PoS **ICRC2019** (2020) 918 (DOI:10.22323/1.358.0918).
- [170] Murase K., Ioka K., Nagataki S. and Nakamura T., High Energy Neutrinos and Cosmic-Rays from Low-Luminosity Gamma-Ray Bursts?, *Astrophys. J.* **651** (2006) L5 (DOI:10.1086/509323).
- [171] Gupta N. and Zhang B., Neutrino Spectra from Low and High Luminosity Populations of Gamma Ray Bursts, *Astropart. Phys.* **27** (2007) 386 (DOI:10.1016/j.astropartphys.2007.01.004).
- [172] Murase K. and Ioka K., TeV–PeV Neutrinos from Low-Power Gamma-Ray Burst Jets inside Stars, *Phys. Rev. Lett.* **111** (2013) no.12, 121102 (DOI:10.1103/PhysRevLett.111.121102).
- [173] Razzaque S., Meszaros P. and Waxman E., Neutrino tomography of gamma-ray bursts and massive stellar collapses, *Phys. Rev. D* **68** (2003) 083001 (DOI:10.1103/PhysRevD.68.083001).
- [174] Senno N., Murase K. and Meszaros P., Choked Jets and Low-Luminosity Gamma-Ray Bursts as Hidden Neutrino Sources, *Phys. Rev. D* **93** (2016) no.8, 083003 (DOI:10.1103/PhysRevD.93.083003).
- [175] Mucke A., Engel R., Rachen J. P., Protheroe R. J. and Stanev T., SOPHIA: Monte Carlo simulations of photohadronic processes in astrophysics, *Comput. Phys. Commun.* **124** (2000) 290 (DOI:10.1016/S0010-4655(99)00446-4).
- [176] Ahlers M., High-energy Cosmogenic Neutrinos, *Phys. Procedia* **61** (2015) 392 (DOI:10.1016/j.phpro.2014.12.080).
- [177] Aartsen M. G. *et al.* [IceCube Collaboration], Constraints on Ultrahigh-Energy Cosmic-Ray Sources from a Search for Neutrinos above 10 PeV with IceCube, *Phys. Rev. Lett.* **117** (2016) no.24, 241101, Erratum: *Phys. Rev. Lett.* **119** (2017)

- no.25, 259902 (DOI:10.1103/PhysRevLett.117.241101, 10.1103/PhysRevLett.119.259902).
- [178] Berezhinsky V. S. and Smirnov A. Y., Cosmic neutrinos of ultra-high energies and detection possibility, *Astrophys. Space Sci.* **32** (1975) 461 (DOI:10.1007/BF00643157).
- [179] Ahlers M., Anchordoqui L. A., Gonzalez-Garcia M. C., Halzen F. and Sarkar S., GZK Neutrinos after the Fermi-LAT Diffuse Photon Flux Measurement, *Astropart. Phys.* **34** (2010) 106-115 (DOI:10.1016/j.astropartphys.2010.06.003).
- [180] Murase K., Inoue Y. and Dermer C. D., Diffuse Neutrino Intensity from the Inner Jets of Active Galactic Nuclei: Impacts of External Photon Fields and the Blazar Sequence, *Phys. Rev. D* **90** (2014) no.2, 023007 (DOI:10.1103/PhysRevD.90.023007).
- [181] Aartsen M. G. *et al.* [IceCube Collaboration], Differential limit on the extremely-high-energy cosmic neutrino flux in the presence of astrophysical background from nine years of IceCube data, *Phys. Rev. D* **98** (2018) no.6, 062003 (DOI:10.1103/PhysRevD.98.062003).
- [182] Ahlers M. and Halzen F., Minimal Cosmogenic Neutrinos, *Phys. Rev. D* **86** (2012) 083010 (DOI:10.1103/PhysRevD.86.083010).
- [183] Aartsen M. G. *et al.* [IceCube Collaboration], Search for neutrinos from decaying dark matter with IceCube, *Eur. Phys. J. C* **78** (2018) no.10, 831 (DOI:10.1140/epjc/s10052-018-6273-3).
- [184] Chianese M., Miele G. and Morisi S., Interpreting IceCube 6-year HESE data as an evidence for hundred TeV decaying Dark Matter, *Phys. Lett. B* **773** (2017) 591-595 (DOI:10.1016/j.physletb.2017.09.016).
- [185] Argüelles C. A., Diaz A., Kheirandish A., Olivares-Del-Campo A., Safa I. and Vincent A. C., Dark Matter Annihilation to Neutrinos:

- An Updated, Consistent & Compelling Compendium of Constraints (arXiv:1912.09486 [hep-ph]).
- [186] Boucenna S. M., Chianese M., Mangano G., Miele G., Morisi S., Pisanti O. and Vitagliano E., Decaying Leptophilic Dark Matter at IceCube, *JCAP* **12** (2015) 055 (DOI:10.1088/1475-7516/2015/12/055).
- [187] Feldstein B., Kusenko A., Matsumoto S. and Yanagida T. T., Neutrinos at IceCube from Heavy Decaying Dark Matter, *Phys. Rev. D* **88** (2013) no.1, 015004 (DOI:10.1103/PhysRevD.88.015004).
- [188] Pandey M., Majumdar D., Halder A. and Banerjee S., Mass and Life Time of Heavy Dark Matter Decaying into IceCube PeV Neutrinos, *Phys. Lett. B* **797** (2019) 134910 (DOI:10.1016/j.physletb.2019.134910).
- [189] Cohen T., Murase K., Rodd N. L., Safdi B. R. and Soreq Y., γ -ray Constraints on Decaying Dark Matter and Implications for IceCube, *Phys. Rev. Lett.* **119** (2017) no.2, 021102 (DOI:10.1103/PhysRevLett.119.021102).
- [190] Hiroshima N., Kitano R., Kohri K. and Murase K., High-energy neutrinos from multibody decaying dark matter, *Phys. Rev. D* **97** (2018) no.2, 023006 (DOI:10.1103/PhysRevD.97.023006).
- [191] Roberts A., The Birth of high-energy neutrino astronomy: A Personal history of the DUMAND project, *Rev. Mod. Phys.* **64** (1992) 259 (DOI:10.1103/RevModPhys.64.259).
- [192] Balkanov V. A. *et al.* [BAIKAL Collaboration], The BAIKAL neutrino project: Status report, *Nucl. Phys. Proc. Suppl.* **118** (2003) 363 (DOI:10.1016/S0920-5632(03)01334-3).
- [193] Aguilar J. A. *et al.* [ANTARES Collaboration], First results of the Instrumentation Line for the deep-sea ANTARES neutrino telescope, *Astropart. Phys.* **26** (2006) 314 (DOI:10.1016/j.astropartphys.2006.07.004).

- [194] Adrian-Martinez S. *et al.* [KM3Net Collaboration], Letter of intent for KM3NeT 2.0, *J. Phys. G* **43** (2016) no.8, 084001 (DOI:10.1088/0954-3899/43/8/084001).
- [195] Andres E. *et al.*, The AMANDA neutrino telescope: Principle of operation and first results, *Astropart. Phys.* **13** (2000) 1 (DOI:10.1016/S0927-6505(99)00092-4).
- [196] Abbasi R. *et al.* [IceCube Collaboration], Search for Point Sources of High Energy Neutrinos with Final Data from AMANDA-II, *Phys. Rev. D* **79** (2009) 062001 (DOI:10.1103/PhysRevD.79.062001).
- [197] Aartsen M. G. *et al.* [IceCube Collaboration], Observation of High-Energy Astrophysical Neutrinos in Three Years of IceCube Data, *Phys. Rev. Lett.* **113** (2014) 101101 (DOI:10.1103/PhysRevLett.113.101101).
- [198] Aartsen M. G. *et al.* [IceCube Collaboration], Measurement of Atmospheric Neutrino Oscillations at 6–56 GeV with IceCube DeepCore, *Phys. Rev. Lett.* **120** (2018) no.7, 071801 (DOI:10.1103/PhysRevLett.120.071801).
- [199] Aartsen M. G. *et al.* [IceCube Collaboration], Measurement of the Atmospheric ν_e flux in IceCube, *Phys. Rev. Lett.* **110** (2013) no.15, 151105 (DOI:10.1103/PhysRevLett.110.151105).
- [200] Aartsen M. G. *et al.* [IceCube Collaboration], Measurement of Atmospheric Tau Neutrino Appearance with IceCube DeepCore, *Phys. Rev. D* **99** (2019) no.3, 032007 (DOI:10.1103/PhysRevD.99.032007).
- [201] Andeen K. *et al.* [IceCube Collaboration], Latest Cosmic Ray Results from IceTop and IceCube, *EPJ Web Conf.* **210** (2019) 03005 (DOI:10.1051/epjconf/201921003005).
- [202] Soldin D. [IceCube Collaboration], Recent Results of Cosmic Ray Measurements from IceCube and IceTop (arXiv:1909.04423 [astro-ph.HE]).

- [203] Madsen J. [IceCube Collaboration], Ultra-High Energy Neutrinos (arXiv:1901.02528 [astro-ph.HE]).
- [204] Stettner J. [IceCube Collaboration], Measurement of the Diffuse Astrophysical Muon-Neutrino Spectrum with Ten Years of IceCube Data (arXiv:1908.09551 [astro-ph.HE]).
- [205] Kopper C. [IceCube Collaboration], Observation of Astrophysical Neutrinos in Six Years of IceCube Data, PoS ICRC **2017** (2018) 981 (DOI:10.22323/1.301.0981).
- [206] Abbasi R. *et al.* [IceCube Collaboration], The IceCube high-energy starting event sample: Description and flux characterization with 7.5 years of data (arXiv:2011.03545 [astro-ph.HE]).
- [207] Schneider A., Characterization of the Astrophysical Diffuse Neutrino Flux with IceCube High-Energy Starting Events (arXiv:1907.11266 [astro-ph.HE]).
- [208] Resconi E., Neutrino Astronomy at Very High Energy Scale, Conference Talk at Hillas Symposium (2018).
- [209] Stachurska J. [IceCube Collaboration], First Double Cascade Tau Neutrino Candidates in IceCube and a New Measurement of the Flavor Composition (arXiv:1908.05506 [astro-ph.HE]).
- [210] Abbasi R. *et al.* [IceCube Collaboration], Measurement of Astrophysical Tau Neutrinos in IceCube's High-Energy Starting Events (arXiv:2011.03561 [hep-ex]).
- [211] Bustamante M., Talk presented at PAHEN 2019.
- [212] Robertson S. [IceCube Collaboration], Measurement of the multi-TeV neutrino cross section with IceCube using Earth absorption (arXiv:1908.06123 [astro-ph.HE]).
- [213] Bustamante M. and Connolly A., Extracting the Energy-Dependent Neutrino-Nucleon Cross Section above 10 TeV Us-

- ing IceCube Showers, *Phys. Rev. Lett.* **122** (2019) no.4, 041101 (DOI:10.1103/PhysRevLett.122.041101).
- [214] Yuan T. [IceCube Collaboration], Measurement of the high-energy all-flavor neutrino-nucleon cross section with IceCube, (arXiv:1908.07027 [astro-ph.HE]).
- [215] Abbasi R. *et al.* [IceCube Collaboration], Measurement of the high-energy all-flavor neutrino-nucleon cross section with IceCube, (arXiv:2011.03560 [hep-ex]).
- [216] Alvey J. and Fairbairn M., Linking Scalar Dark Matter and Neutrino Masses with IceCube 170922A, *JCAP* **07** (2019) 041 (DOI:10.1088/1475-7516/2019/07/041).
- [217] Choi K., Kim J. and Rott C., Constraining dark matter-neutrino interactions with IceCube-170922A, *Phys. Rev. D* **99** (2019) no.8, 083018 (DOI:10.1103/PhysRevD.99.083018).
- [218] Aartsen M. G. *et al.* [IceCube Collaboration], Neutrino emission from the direction of the blazar TXS 0506+056 prior to the IceCube-170922A alert, *Science* **361** (2018) no.6398, 147 (DOI:10.1126/science.aat2890).
- [219] Wiebusch C., Talk presented at 7th Symposium on Symmetries in Subatomic Physics 2018 on behalf of IceCube Collaboration.
- [220] DiFranzo A. and Hooper D., Searching for MeV-Scale Gauge Bosons with IceCube, *Phys. Rev. D* **92** (2015) no.9, 095007 (DOI:10.1103/PhysRevD.92.095007).
- [221] Araki T., Kaneko F., Ota T., Sato J. and Shimomura T., MeV scale leptonic force for cosmic neutrino spectrum and muon anomalous magnetic moment, *Phys. Rev. D* **93** (2016) no.1, 013014 (DOI:10.1103/PhysRevD.93.013014).

- [222] Bustamante M., Rosenstroem C. A., Shalgar S. and Tamborra I., Bounds on secret neutrino interactions from high-energy astrophysical neutrinos (arXiv:2001.04994 [astro-ph.HE]).
- [223] Yacobi L., Guetta D. and Behar E., Implication of the Non-detection of gzk Neutrinos, *Astrophys. J.* **823** (2016) no.2, 89 (DOI:10.3847/0004-637X/823/2/89).
- [224] Van Eijk D., Tau Neutrinos in IceCube, KM3NeT and the Pierre Auger Observatory, *SciPost Phys. Proc.* **1** (2019) 030 (DOI:10.21468/SciPostPhysProc.1.030).
- [225] Spurio M. [ANTARES Collaboration], Results from the ANTARES neutrino telescope, *EPJ Web Conf.* **116** (2016) 11006 (DOI:10.1051/epjconf/201611611006).
- [226] Illuminati G. [ANTARES and IceCube Collaborations], ANTARES and IceCube combined search for neutrino point-like and extended sources in the Southern Sky (arXiv:1908.07439 [astro-ph.HE]).
- [227] Silvestri A. *et al.* [ANITA Collaboration], Results from the ANITA experiment, *Mod. Phys. Lett. A* **22** (2007) 2237 (DOI:10.1142/S0217732307024279).
- [228] Gorham P. W. *et al.* [ANITA Collaboration], Observation of an Unusual Upward-going Cosmic-ray-like Event in the Third Flight of ANITA, *Phys. Rev. Lett.* **121** (2018) no.16, 161102 (DOI:10.1103/PhysRevLett.121.161102).
- [229] Gorham P. W. *et al.* [ANITA Collaboration], Characteristics of Four Upward-pointing Cosmic-ray-like Events Observed with ANITA, *Phys. Rev. Lett.* **117** (2016) no.7, 071101 (DOI:10.1103/PhysRevLett.117.071101).
- [230] Fox D. B., Sigurdsson S., Shandera S., Mészáros P., Murase K., Mostafá M. and Coutu S., The ANITA Anomalous Events as Sig-

- natures of a Beyond Standard Model Particle, and Supporting Observations from IceCube (arXiv:1809.09615 [astro-ph.HE]).
- [231] Ishihara A. [IceCube Collaboration], The IceCube Upgrade – Design and Science Goals (arXiv:1908.09441 [astro-ph.HE]).
- [232] Nagai R. *et al.* [IceCube Collaboration], Electronics Development for the New Photo-Detectors (PDOM and D-Egg) for IceCube-Upgrade (arXiv:1908.11564 [astro-ph.IM]).
- [233] van Eijk D. *et al.* [IceCube Collaboration], Characterization of Two PMT Models for the IceCube Upgrade mDOM (arXiv:1908.08446 [astro-ph.IM]).
- [234] Aartsen M. G. *et al.* [IceCube Collaboration], IceCube-Gen2: A Vision for the Future of Neutrino Astronomy in Antarctica (arXiv:1412.5106 [astro-ph.HE]).
- [235] Sanguineti M. [ANTARES and KM3NeT Collaborations], ANTARES and KM3NeT: The Latest Results of the Neutrino Telescopes in the Mediterranean, *Universe* **5** (2019) no.2, 65 (DOI:10.3390/universe5020065).
- [236] Avrorin A. D. *et al.* [Baikal-GVD Collaboration], Baikal-GVD: status and prospects, *EPJ Web Conf.* **191** (2018) 01006 (DOI:10.1051/epjconf/201819101006).
- [237] Álvarez-Muñiz J. *et al.* [GRAND Collaboration], The Giant Radio Array for Neutrino Detection (GRAND): Science and Design, *Sci. China Phys. Mech. Astron.* **63** (2020) no.1, 219501 (DOI:10.1007/s11433-018-9385-7).
- [238] Fermani P. [KM3NeT and Antares Collaborations], Status and results from the ANTARES and KM3NeT-ARCA neutrino telescopes, *PoS NuFact2019* (2020) 032 (DOI:10.22323/1.369.0032).
- [239] Aiello S. *et al.* [KM3NeT Collaboration], Sensitivity of the KM3NeT/ARCA neutrino telescope to point-like

- neutrino sources, *Astropart. Phys.* **111** (2019) 100-110 (DOI:10.1016/j.astropartphys.2019.04.002).
- [240] Kowalski M., IceCube-Gen2 and IceCube-Upgrade, Conference Talk at the VLVnT 2018 Conference (2018).
- [241] van Santen J. [IceCube Gen2 Collaboration], IceCube-Gen2: the next-generation neutrino observatory for the South Pole, *PoS ICRC 2017* (2018) 991 (DOI:10.22323/1.301.0991).
- [242] Katz U., Future neutrino telescopes in water and ice, Conference Talk at the Neutrino 2018 Conference (2018) (DOI:10.5281/zenodo.1287686).
- [243] Denton P. B., Marfatia D. and Weiler T. J., The Galactic Contribution to IceCube's Astrophysical Neutrino Flux, *JCAP* **1708** (2017) no.08, 033 (DOI:10.1088/1475-7516/2017/08/033).
- [244] Aartsen M. G. *et al.* [IceCube Collaboration], The IceCube Neutrino Observatory - Contributions to ICRC 2017 Part II: Properties of the Atmospheric and Astrophysical Neutrino Flux (arXiv:1710.01191 [astro-ph.HE]).
- [245] Dhuria M. and Rentala V., PeV scale Supersymmetry breaking and the IceCube neutrino flux, *JHEP* **1809** (2018) 004 (DOI:10.1007/JHEP09(2018)004).
- [246] Borah D., Dasgupta A., Dey U. K., Patra S. and Tomar G., Multi-component Fermionic Dark Matter and IceCube PeV scale Neutrinos in Left-Right Model with Gauge Unification, *JHEP* **1709** (2017) 005 (DOI:10.1007/JHEP09(2017)005).
- [247] Zavala J., Galactic PeV neutrinos from dark matter annihilation, *Phys. Rev. D* **89** (2014) no.12, 123516 (DOI:10.1103/PhysRevD.89.123516).

- [248] Dev P. S. B., Mohapatra R. N. and Zhang Y., Heavy right-handed neutrino dark matter in left-right models, *Mod. Phys. Lett. A* **32** (2017) 1740007 (DOI:10.1142/S0217732317400077).
- [249] Lambiase G., Mohanty S. and Stabile A., PeV IceCube signals and Dark Matter relic abundance in modified cosmologies, *Eur. Phys. J. C* **78** (2018) no.4, 350 (DOI:10.1140/epjc/s10052-018-5821-1).
- [250] Murase K., Laha R., Ando S. and Ahlers M., Testing the Dark Matter Scenario for PeV Neutrinos Observed in IceCube, *Phys. Rev. Lett.* **115** (2015) no.7, 071301 (DOI:10.1103/PhysRevLett.115.071301).
- [251] Chen C. Y., Bhupal Dev P. S. and Soni A., Standard model explanation of the ultrahigh energy neutrino events at IceCube, *Phys. Rev. D* **89** (2014) no.3, 033012 (DOI:10.1103/PhysRevD.89.033012).
- [252] Murase K. and Waxman E., Constraining High-Energy Cosmic Neutrino Sources: Implications and Prospects, *Phys. Rev. D* **94** (2016) no.10, 103006 (DOI:10.1103/PhysRevD.94.103006).
- [253] Aab A. *et al.* [Pierre Auger Collaboration], Observation of a Large-scale Anisotropy in the Arrival Directions of Cosmic Rays above 8×10^{18} eV, *Science* **357** (2017) no.6537, 1266 (DOI:10.1126/science.aan4338).
- [254] Pandey S., Karmakar S. and Rakshit S., Interactions of Astrophysical Neutrinos with Dark Matter: A model building perspective, *JHEP* **1901**, 095 (2019) (DOI:10.1007/JHEP01(2019)095).
- [255] Barranco J., Miranda O. G., Moura C. A., Rashba T. I. and Rossi-Torres F., Confusing the extragalactic neutrino flux limit with a neutrino propagation limit, *JCAP* **1110** (2011) 007 (DOI:10.1088/1475-7516/2011/10/007).
- [256] Reynoso M. M. and Sampayo O. A., Propagation of high-energy neutrinos in a background of ultralight scalar dark matter, *Astropart. Phys.* **82** (2016) 10 (DOI:10.1016/j.astropartphys.2016.05.004).

- [257] Huang G. Y. and Nath N., Neutrinophilic Axion-Like Dark Matter, *Eur. Phys. J. C* **78** (2018) no.11, 922 (DOI:10.1140/epjc/s10052-018-6391-y).
- [258] Wilkinson R. J., Boehm C. and Lesgourgues J., Constraining Dark Matter-Neutrino Interactions using the CMB and Large-Scale Structure, *JCAP* **1405** (2014) 011 (DOI:10.1088/1475-7516/2014/05/011).
- [259] Escudero M., Mena O., Vincent A. C., Wilkinson R. J. and Boehm C., Exploring dark matter microphysics with galaxy surveys, *JCAP* **1509** (2015) no.09, 034 (DOI:10.1088/1475-7516/2015/9/034).
- [260] Argüelles C. A., Kheirandish A. and Vincent A. C., Imaging Galactic Dark Matter with High-Energy Cosmic Neutrinos, *Phys. Rev. Lett.* **119** (2017) no.20, 201801 (DOI:10.1103/PhysRevLett.119.201801).
- [261] de Salas P. F., Lineros R. A. and Tórtola M., Neutrino propagation in the galactic dark matter halo, *Phys. Rev. D* **94** (2016) no.12, 123001 (DOI:10.1103/PhysRevD.94.123001).
- [262] Ng K. C. Y. and Beacom J. F., Cosmic neutrino cascades from secret neutrino interactions, *Phys. Rev. D* **90** (2014) no.6, 065035, Erratum: *Phys. Rev. D* **90** (2014) no.8, 089904 (DOI:10.1103/PhysRevD.90.065035, 10.1103/PhysRevD.90.089904).
- [263] Mohanty S., Narang A. and Sadhukhan S., Cutoff of IceCube Neutrino Spectrum due to t-channel Resonant Absorption by $C\nu B$ (arXiv:1808.01272 [hep-ph]).
- [264] Chauhan B. and Mohanty S., Signature of light sterile neutrinos at IceCube, *Phys. Rev. D* **98** (2018) no.8, 083021 (DOI:10.1103/PhysRevD.98.083021).
- [265] Kelly K. J. and Machado P. A. N., Multimessenger Astronomy and New Neutrino Physics, *JCAP* **1810** (2018) no.10, 048 (DOI:10.1088/1475-7516/2018/10/048).

- [266] Shoemaker I. M. and Murase K., Probing BSM Neutrino Physics with Flavor and Spectral Distortions: Prospects for Future High-Energy Neutrino Telescopes, *Phys. Rev. D* **93** (2016) no.8, 085004 (DOI:10.1103/PhysRevD.93.085004).
- [267] Cherry J. F., Friedland A. and Shoemaker I. M., Short-baseline neutrino oscillations, Planck, and IceCube (arXiv:1605.06506 [hep-ph]).
- [268] Ibe M. and Kaneta K., Cosmic neutrino background absorption line in the neutrino spectrum at IceCube, *Phys. Rev. D* **90** (2014) no.5, 053011 (DOI:10.1103/PhysRevD.90.053011).
- [269] Bode P., Ostriker J. P. and Turok N., Halo formation in warm dark matter models, *Astrophys. J.* **556** (2001) 93 (DOI:10.1086/321541).
- [270] Boehm C. and Fayet P., Scalar dark matter candidates, *Nucl. Phys. B* **683** (2004) 219 (DOI:10.1016/j.nuclphysb.2004.01.015).
- [271] Sikivie P. and Yang Q., Bose-Einstein Condensation of Dark Matter Axions, *Phys. Rev. Lett.* **103** (2009) 111301 (DOI:10.1103/PhysRevLett.103.111301).
- [272] Duffy L. D. *et al.* [ADMX Collaboration], A high resolution search for dark-matter axions, *Phys. Rev. D* **74** (2006) 012006 (DOI:10.1103/PhysRevD.74.012006).
- [273] Tada M., Kishimoto Y., Kominato K., Shibata M., Funahashi H., Yamamoto K., Masaike A. and Matsuki S., CARRACK II: A new large scale experiment to search for axions with Rydberg-atom cavity detector, *Nucl. Phys. Proc. Suppl.* **72** (1999) 164 (DOI:10.1016/S0920-5632(98)00519-2).
- [274] Dev P. S. B., Lindner M. and Ohmer S., Gravitational waves as a new probe of Bose–Einstein condensate Dark Matter, *Phys. Lett. B* **773** (2017) 219 (DOI:10.1016/j.physletb.2017.08.043).

- [275] Graham P. W., Mardon J. and Rajendran S., Vector Dark Matter from Inflationary Fluctuations, *Phys. Rev. D* **93** (2016) no.10, 103520 (DOI:10.1103/PhysRevD.93.103520).
- [276] Aprile E. *et al.* [XENON Collaboration], Physics reach of the XENON1T dark matter experiment, *JCAP* **1604** (2016) no.04, 027 (DOI:10.1088/1475-7516/2016/04/027).
- [277] Akerib D. S. *et al.* [LUX Collaboration], Results from a search for dark matter in the complete LUX exposure, *Phys. Rev. Lett.* **118** (2017) no.2, 021303 (DOI:10.1103/PhysRevLett.118.021303).
- [278] Athron P. *et al.* [GAMBIT Collaboration], Status of the scalar singlet dark matter model, *Eur. Phys. J. C* **77** (2017) no.8, 568 (DOI:10.1140/epjc/s10052-017-5113-1).
- [279] Schawinski K. *et al.*, The Sudden Death of the Nearest Quasar, *Astrophys. J.* **724** (2010) L30 (DOI:10.1088/2041-8205/724/1/L30).
- [280] Olive K. A. *et al.* [Particle Data Group], Review of Particle Physics, *Chin. Phys. C* **38** (2014) 090001 (DOI:10.1088/1674-1137/38/9/090001).
- [281] Abdallah J. *et al.* [DELPHI Collaboration], Photon events with missing energy in e^+e^- collisions at $s^{1/2} = 130\text{-GeV}$ to 209-GeV , *Eur. Phys. J. C* **38** (2005) 395 (DOI:10.1140/epjc/s2004-02051-8).
- [282] Christensen N. D. and Duhr C., FeynRules - Feynman rules made easy, *Comput. Phys. Commun.* **180** (2009) 1614 (DOI:10.1016/j.cpc.2009.02.018).
- [283] Belyaev A., Christensen N. D. and Pukhov A., CalcHEP 3.4 for collider physics within and beyond the Standard Model, *Comput. Phys. Commun.* **184** (2013) 1729 (DOI:10.1016/j.cpc.2013.01.014).
- [284] Alwall J. *et al.*, The automated computation of tree-level and next-to-leading order differential cross sections, and their

- matching to parton shower simulations, *JHEP* **1407** (2014) 079 (DOI:10.1007/JHEP07(2014)079).
- [285] Schael S. *et al.* [ALEPH and DELPHI and L3 and OPAL Collaborations and LEP Working Group for Higgs Boson Searches], Search for neutral MSSM Higgs bosons at LEP, *Eur. Phys. J. C* **47** (2006) 547 (DOI:10.1140/epjc/s2006-02569-7).
- [286] Das D. and Santamaria A., Updated scalar sector constraints in the Higgs triplet model, *Phys. Rev. D* **94**, no. 1, 015015 (2016) (DOI:10.1103/PhysRevD.94.015015).
- [287] Achard P. *et al.* [L3 Collaboration], Search for heavy neutral and charged leptons in e^+e^- annihilation at LEP, *Phys. Lett. B* **517** (2001) 75 (DOI:10.1016/S0370-2693(01)01005-X).
- [288] Leveille J. P., The Second Order Weak Correction to $(G-2)$ of the Muon in Arbitrary Gauge Models, *Nucl. Phys. B* **137** (1978) 63 (DOI:10.1016/0550-3213(78)90051-2).
- [289] de Salas P. F. and Pastor S., Relic neutrino decoupling with flavour oscillations revisited, *JCAP* **1607** (2016) no.07, 051 (DOI:10.1088/1475-7516/2016/07/051).
- [290] Armengaud E., Palanque-Delabrouille N., Yèche C., Marsh D. J. E. and Baur J., Constraining the mass of light bosonic dark matter using SDSS Lyman- α forest, *Mon. Not. Roy. Astron. Soc.* **471** (2017) no.4, 4606 (DOI:10.1093/mnras/stx1870).
- [291] Bertoni B., Ipek S., McKeen D. and Nelson A. E., Constraints and consequences of reducing small scale structure via large dark matter-neutrino interactions, *JHEP* **1504** (2015) 170 (DOI:10.1007/JHEP04(2015)170).
- [292] Fayet P., Hooper D. and Sigl G., Constraints on light dark matter from core-collapse supernovae, *Phys. Rev. Lett.* **96** (2006) 211302 (DOI:10.1103/PhysRevLett.96.211302).

- [293] Mangano G., Melchiorri A., Serra P., Cooray A. and Kamionkowski M., Cosmological bounds on dark matter-neutrino interactions, *Phys. Rev. D* **74** (2006) 043517 (DOI:10.1103/PhysRevD.74.043517).
- [294] Naumov V. A., and Perrone L., Neutrino propagation through matter, *Astropart. Phys.* **10**, 239 (1999) (DOI:10.1016/S0927-6505(98)00046-2).
- [295] Karmakar S., Pandey S. and Rakshit S., Are We Looking at Neutrino Absorption Spectra at IceCube? (arXiv:1810.04192 [hep-ph]).
- [296] Karmakar S., Pandey S. and Rakshit S., Astronomy with energy dependent flavour ratios of extragalactic neutrinos *JHEP* **10** (2021) 004 (DOI:10.1007/JHEP10(2021)004).
- [297] Koren S., Neutrino – Dark Matter Scattering and Coincident Detections of UHE Neutrinos with EM Sources, *JCAP* **1909** (2019) 013 (DOI:10.1088/1475-7516/2019/09/013).
- [298] Farzan Y. and Palomares-Ruiz S., Flavor of cosmic neutrinos preserved by ultralight dark matter, *Phys. Rev. D* **99** (2019) no.5, 051702 (DOI:10.1103/PhysRevD.99.051702).
- [299] Mehta P. and Winter W., Interplay of energy dependent astrophysical neutrino flavor ratios and new physics effects, *JCAP* **1103** (2011) 041 (DOI:10.1088/1475-7516/2011/03/041).
- [300] Bustamante M., Beacom J. F. and Winter W., Theoretically palatable flavor combinations of astrophysical neutrinos, *Phys. Rev. Lett.* **115** (2015) no.16, 161302 (DOI:10.1103/PhysRevLett.115.161302).
- [301] Argüelles C. A., Katori T. and Salvado J., New Physics in Astrophysical Neutrino Flavor, *Phys. Rev. Lett.* **115** (2015) 161303 (DOI:10.1103/PhysRevLett.115.161303).

- [302] Brdar V. and Hansen R. S. L., IceCube Flavor Ratios with Identified Astrophysical Sources: Towards Improving New Physics Testability, *JCAP* **02** (2019) 023 (DOI:10.1088/1475-7516/2019/02/023).
- [303] Pagliaroli G., Palladino A., Villante F. L. and Vissani F., Testing nonradiative neutrino decay scenarios with IceCube data, *Phys. Rev. D* **92** (2015) no.11, 113008 (DOI:10.1103/PhysRevD.92.113008).
- [304] Bustamante M., Beacom J. F. and Murase K., Testing decay of astrophysical neutrinos with incomplete information, *Phys. Rev. D* **95** (2017) no.6, 063013 (DOI:10.1103/PhysRevD.95.063013).
- [305] Ahlers M., Bustamante M. and Mu S., Unitarity Bounds of Astrophysical Neutrinos, *Phys. Rev. D* **98** (2018) no.12, 123023 (DOI:10.1103/PhysRevD.98.123023).
- [306] Mena O., Mocioiu I. and Razzaque S., Oscillation effects on high-energy neutrino fluxes from astrophysical hidden sources, *Phys. Rev. D* **75** (2007) 063003 (DOI:10.1103/PhysRevD.75.063003).
- [307] Carpio J. and Murase K., Oscillation of high-energy neutrinos from choked jets in stellar and merger ejecta, *Phys. Rev. D* **101** (2020) no.12, 123002 (DOI:10.1103/PhysRevD.101.123002).
- [308] Harko T., Bose-Einstein condensation of dark matter solves the core/cusp problem, *JCAP* **1105** (2011) 022 (DOI:10.1088/1475-7516/2011/05/022).
- [309] Böhmer C. G. and Harko T., Can dark matter be a Bose-Einstein condensate?, *JCAP* **0706** (2007) 025 (DOI:10.1088/1475-7516/2007/06/025).
- [310] Matos T. and Ureña-Lopez L. A., A Further analysis of a cosmological model of quintessence and scalar dark matter, *Phys. Rev. D* **63** (2001) 063506 (DOI:10.1103/PhysRevD.63.063506).

- [311] Guzman F. S., Lora-Clavijo F. D., Gonzalez-Aviles J. J. and Rivera-Paleo F. J., Stability of BEC galactic dark matter halos, *JCAP* **1309** (2013) 034 (DOI:10.1088/1475-7516/2013/09/034).
- [312] Li B., Rindler-Daller T. and Shapiro P. R., Cosmological Constraints on Bose-Einstein-Condensed Scalar Field Dark Matter, *Phys. Rev. D* **89** (2014) no.8, 083536 (DOI:10.1103/PhysRevD.89.083536).
- [313] Davoudiasl H. and Denton P. B., Ultralight Boson Dark Matter and Event Horizon Telescope Observations of M87*, *Phys. Rev. Lett.* **123** (2019) no.2, 021102 (DOI:10.1103/PhysRevLett.123.021102).
- [314] Davies E. Y. and Mocz P., Fuzzy Dark Matter Soliton Cores around Supermassive Black Holes (arXiv:1908.04790 [astro-ph.GA]).
- [315] Bar N., Blum K., Lacroix T. and Panci P., Looking for ultralight dark matter near supermassive black holes, *JCAP* **07** (2019) 045 (DOI:10.1088/1475-7516/2019/07/045).
- [316] Schive H. Y., Liao M. H., Woo, T. P. Wong S. K., Chiueh T., Broadhurst T. and Hwang W. Y. P., Understanding the Core-Halo Relation of Quantum Wave Dark Matter from 3D Simulations, *Phys. Rev. Lett.* **113** (2014) no.26, 261302 (DOI:10.1103/PhysRevLett.113.261302).
- [317] Bandara K., Crampton D. and Simard L., A Relationship between Supermassive Black Hole Mass and the Total Gravitational Mass of the Host Galaxy, *Astrophys. J.* **704** (2009) 1135 (DOI:10.1088/0004-637X/704/2/1135).
- [318] Sun A. L., Greene J. E., Impellizzeri C. M. V., Kuo C. Y., Braatz J. A. and Tuttle S., Refining the $M_{BH} - V_c$ Scaling Relation with H I Rotation Curves of Water Megamaser Galaxies, *Astrophys. J.* **778** (2013) 47 (DOI:10.1088/0004-637X/778/1/47).
- [319] Inoue Y., Khangulyan D., Inoue S. and Doi A., On high-energy particles in accretion disk coronae of supermassive black holes: implica-

- tions for MeV gamma rays and high-energy neutrinos from AGN cores (DOI:10.3847/1538-4357/ab2715).
- [320] Kimura S. S., Murase K. and Mészáros P., Multimes-
senger tests of cosmic-ray acceleration in radiatively ineffi-
cient accretion flows, *Phys. Rev. D* **100** (2019) no.8, 083014
(DOI:10.1103/PhysRevD.100.083014).
- [321] Kimura S. S., Murase K. and Mészáros P., Soft MeV Gamma-Ray
Background from Low-Luminosity Active Galactic Nuclei and Con-
nection to the Origin of IceCube PeV Neutrinos (arXiv:2005.01934
[astro-ph.HE]).
- [322] Berlin A., Neutrino Oscillations as a Probe of Light Scalar
Dark Matter, *Phys. Rev. Lett.* **117** (2016) no.23, 231801
(DOI:10.1103/PhysRevLett.117.231801).
- [323] Murase K. and Shoemaker I. M., Neutrino Echoes from Multimes-
senger Transient Sources, *Phys. Rev. Lett.* **123** (2019) no.24, 241102
(DOI:10.1103/PhysRevLett.123.241102).
- [324] Nieves J. F. and Sahu S., Neutrino decoherence in a fermion
and scalar background, *Phys. Rev. D* **100** (2019) no.11, 115049
(DOI:10.1103/PhysRevD.100.115049).
- [325] Cherry J. F., Friedland A. and Shoemaker I. M., Neutrino Portal
Dark Matter: From Dwarf Galaxies to IceCube (arXiv:1411.1071 [hep-
ph]).
- [326] Harnik R., Kopp J. and Machado P. A. N., Exploring ν Signals in
Dark Matter Detectors, *JCAP* **1207** (2012) 026 (DOI:10.1088/1475-
7516/2012/07/026).
- [327] Sirunyan A. M. *et al.* [CMS], Search for an $L_\mu - L_\tau$ gauge boson using
 $Z \rightarrow 4\mu$ events in proton-proton collisions at $\sqrt{s} = 13$ TeV, *Phys. Lett.*
B 792 (2019) 345-368 (DOI:10.1016/j.physletb.2019.01.072).

- [328] Heeck J., Lepton flavor violation with light vector bosons, *Phys. Lett. B* **758** (2016) 101 (DOI:10.1016/j.physletb.2016.05.007).
- [329] Farzan Y. and Shoemaker I. M., Lepton Flavor Violating Non-Standard Interactions via Light Mediators, *JHEP* **1607** (2016) 033 (DOI:10.1007/JHEP07(2016)033).
- [330] Esteban I., Gonzalez-Garcia M., Hernandez-Cabezudo A., Maltoni M. and Schwetz T., Global analysis of three-flavour neutrino oscillations: synergies and tensions in the determination of θ_{23} , δ_{CP} , and the mass ordering, *JHEP* **01** (2019) 106 (DOI:10.1007/JHEP01(2019)106).
- [331] Read J., The Local Dark Matter Density, *J. Phys. G* **41** (2014) 063101 (DOI:10.1088/0954-3899/41/6/063101).
- [332] Aartsen M. G. *et al.* [IceCube Collaboration], Evidence for High-Energy Extraterrestrial Neutrinos at the IceCube Detector, *Science* **342** (2013) 1242856 (DOI:10.1126/science.1242856).
- [333] Palladino A., Pagliaroli G., Villante F. L. and Vissani F., What is the Flavor of the Cosmic Neutrinos Seen by IceCube?, *Phys. Rev. Lett.* **114** (2015) no.17, 171101 (DOI:10.1103/PhysRevLett.114.171101).
- [334] Li S. W., Bustamante M. and Beacom J. F., Echo Technique to Distinguish Flavors of Astrophysical Neutrinos, *Phys. Rev. Lett.* **122** (2019) no.15, 151101 (DOI:10.1103/PhysRevLett.122.151101).
- [335] Kormendy J. and Ho L. C., Coevolution (Or Not) of Supermassive Black Holes and Host Galaxies, *Ann. Rev. Astron. Astrophys.* **51** (2013) 511-653 (DOI:10.1146/annurev-astro-082708-101811).
- [336] An F. *et al.* [JUNO Collaboration], Neutrino Physics with JUNO, *J. Phys. G* **43** (2016) no.3, 030401 (DOI:10.1088/0954-3899/43/3/030401).
- [337] Abe K. *et al.* [Hyper-Kamiokande Collaboration], Hyper-Kamiokande Design Report (arXiv:1805.04163 [physics.ins-det]).

- [338] Aartsen M. G. *et al.* [IceCube PINGU Collaboration], Letter of Intent: The Precision IceCube Next Generation Upgrade (PINGU) (arXiv:1401.2046 [physics.ins-det]).
- [339] Acciarri R. *et al.* [DUNE Collaboration], Long-Baseline Neutrino Facility (LBNF) and Deep Underground Neutrino Experiment (DUNE): Conceptual Design Report, Volume 2: The Physics Program for DUNE at LBNF (arXiv:1512.06148 [physics.ins-det]).
- [340] Abe K. *et al.* [Hyper-Kamiokande Collaboration], Physics potentials with the second Hyper-Kamiokande detector in Korea, PTEP **2018** (2018) no.6, 063C01 (DOI:10.1093/ptep/pty044).
- [341] S. Ahmed *et al.* [ICAL], Pramana **88** (2017) no.5, 79 doi:10.1007/s12043-017-1373-4 [arXiv:1505.07380 [physics.ins-det]].
- [342] Aartsen M. G. *et al.* [IceCube Gen2 and JUNO members], Combined sensitivity to the neutrino mass ordering with JUNO, the IceCube Upgrade, and PINGU, Phys. Rev. D **101** (2020) no.3, 032006 (DOI:10.1103/PhysRevD.101.032006).
- [343] Blennow M. and Schwetz T., Determination of the neutrino mass ordering by combining PINGU and Daya Bay II, JHEP **09** (2013) 089 (DOI:10.1007/JHEP09(2013)089).
- [344] Song N., Li S. W., Argüelles C. A., Bustamante M. and Vincent A. C., The Future of High-Energy Astrophysical Neutrino Flavor Measurements, JCAP **04** (2021) 054 (DOI:10.1088/1475-7516/2021/04/054).
- [345] Aartsen M. G. *et al.* [IceCube Collaboration], A combined maximum-likelihood analysis of the high-energy astrophysical neutrino flux measured with IceCube, Astrophys. J. **809** (2015) no.1, 98 (DOI:10.1088/0004-637X/809/1/98).
- [346] Aartsen M. G. *et al.* [IceCube Collaboration], Searches for Sterile Neutrinos with the IceCube Detector, Phys. Rev. Lett. **117** (2016) no.7, 071801 (DOI:10.1103/PhysRevLett.117.071801).

- [347] Coloma P., Lopez-Pavon J., Martinez-Soler I. and Nunokawa H., Decoherence in Neutrino Propagation Through Matter, and Bounds from IceCube/DeepCore, *Eur. Phys. J. C* **78** (2018) no.8, 614 (DOI:10.1140/epjc/s10052-018-6092-6).
- [348] Hooper D., Morgan D. and Winstanley E., Probing quantum decoherence with high-energy neutrinos, *Phys. Lett. B* **609** (2005) 206 (DOI:10.1016/j.physletb.2005.01.034).
- [349] Esmaili A. and Nunokawa H., On the robustness of IceCube's bound on sterile neutrinos in the presence of non-standard interactions, *Eur. Phys. J. C* **79** (2019) no.1, 70 (DOI:10.1140/epjc/s10052-019-6595-9).
- [350] Liao J. and Marfatia D., Impact of nonstandard interactions on sterile neutrino searches at IceCube, *Phys. Rev. Lett.* **117** (2016) no.7, 071802 (DOI:10.1103/PhysRevLett.117.071802).
- [351] Liao J., Marfatia D. and Whisnant K., MiniBooNE, MINOS+ and IceCube data imply a baroque neutrino sector, *Phys. Rev. D* **99** (2019) no.1, 015016 (DOI:10.1103/PhysRevD.99.015016).
- [352] Moss Z., Moulai M. H., Argüelles C. A. and Conrad J. M., Exploring a nonminimal sterile neutrino model involving decay at IceCube, *Phys. Rev. D* **97** (2018) no.5, 055017 (DOI:10.1103/PhysRevD.97.055017).
- [353] Denton P. B., Farzan Y. and Shoemaker I. M., Activating the fourth neutrino of the 3+1 scheme, *Phys. Rev. D* **99** (2019) no.3, 035003 (DOI:10.1103/PhysRevD.99.035003).
- [354] Dey U. K., Nath N. and Sadhukhan S., Non-Standard Neutrino Interactions in a Modified ν 2HDM, *Phys. Rev. D* **98** (2018) no.5, 055004 (DOI:10.1103/PhysRevD.98.055004).
- [355] Salvado J., Mena O., Palomares-Ruiz S. and Rius N., Non-standard interactions with high-energy atmospheric neutrinos at IceCube, *JHEP* **1701** (2017) 141 (DOI:10.1007/JHEP01(2017)141).

- [356] Day M. [IceCube Collaboration], Non-standard neutrino interactions in IceCube, *J. Phys. Conf. Ser.* **718** (2016) no.6, 062011 (DOI:10.1088/1742-6596/718/6/062011).
- [357] Esmaili A. and Smirnov A. Y., Probing Non-Standard Interaction of Neutrinos with IceCube and DeepCore, *JHEP* **1306** (2013) 026 (DOI:10.1007/JHEP06(2013)026).
- [358] Biggio C., Blennow M. and Fernandez-Martinez E., General bounds on non-standard neutrino interactions, *JHEP* **0908** (2009) 090 (DOI:10.1088/1126-6708/2009/08/090).
- [359] Carpentier M. and Davidson S., Constraints on two-lepton, two quark operators, *Eur. Phys. J. C* **70** (2010) 1071 (DOI:10.1140/epjc/s10052-010-1482-4).
- [360] Aartsen M. G. *et al.* [IceCube Collaboration], Measurement of the multi-TeV neutrino cross section with IceCube using Earth absorption, *Nature* **551** (2017) 596 (DOI:10.1038/nature24459).
- [361] Falkowski A., González-Alonso M. and Mimouni K., Compilation of low-energy constraints on 4-fermion operators in the SMEFT, *JHEP* **1708** (2017) 123 (DOI:10.1007/JHEP08(2017)123).
- [362] Bergmann S., Guzzo M. M., de Holanda P. C., Krastev P. I. and Nunokawa H., Status of the solution to the solar neutrino problem based on nonstandard neutrino interactions, *Phys. Rev. D* **62** (2000) 073001 (DOI:10.1103/PhysRevD.62.073001).
- [363] Davidson S., Pena-Garay C., Rius N. and Santamaria A., Present and future bounds on nonstandard neutrino interactions, *JHEP* **0303** (2003) 011 (DOI:10.1088/1126-6708/2003/03/011).
- [364] Aaboud M. *et al.* [ATLAS Collaboration], Search for new high-mass phenomena in the dilepton final state using 36 fb^{-1} of proton-proton collision data at $\sqrt{s} = 13 \text{ TeV}$ with the ATLAS detector, *JHEP* **1710** (2017) 182 (DOI:10.1007/JHEP10(2017)182).

- [365] Gavela M. B., Hernandez D., Ota T. and Winter W., Large gauge invariant non-standard neutrino interactions, *Phys. Rev. D* **79** (2009) 013007 (DOI:10.1103/PhysRevD.79.013007).
- [366] Davidson S. and Sanz V., Non-Standard Neutrino Interactions at Colliders, *Phys. Rev. D* **84** (2011) 113011 (DOI:10.1103/PhysRevD.84.113011).
- [367] Aartsen M. G. *et al.* [IceCube Collaboration], Determining neutrino oscillation parameters from atmospheric muon neutrino disappearance with three years of IceCube DeepCore data, *Phys. Rev. D* **91** (2015) no.7, 072004 (DOI:10.1103/PhysRevD.91.072004).
- [368] Aartsen M. G. *et al.* [IceCube Collaboration], Search for Nonstandard Neutrino Interactions with IceCube DeepCore, *Phys. Rev. D* **97** (2018) no.7, 072009 (DOI:10.1103/PhysRevD.97.072009).
- [369] Pandey S., Karmakar S. and Rakshit S., Strong constraints on non-standard neutrino interactions: LHC vs. IceCube, *JHEP* **11** (2019) 046 (DOI:10.1007/JHEP11(2019)046).
- [370] Antusch S., Baumann J. P. and Fernandez-Martinez E., Non-Standard Neutrino Interactions with Matter from Physics Beyond the Standard Model, *Nucl. Phys. B* **810** (2009) 369 (DOI:10.1016/j.nuclphysb.2008.11.018).
- [371] Berezhiani Z. and Rossi A., Limits on the nonstandard interactions of neutrinos from e^+e^- colliders, *Phys. Lett. B* **535** (2002) 207 (DOI:10.1016/S0370-2693(02)01767-7).
- [372] Mikheyev S. P. and Smirnov A. Y., Resonance Amplification of Oscillations in Matter and Spectroscopy of Solar Neutrinos, *Sov. J. Nucl. Phys.* **42** (1985) 913 [*Yad. Fiz.* **42** (1985) 1441].
- [373] Esteban I., Gonzalez-Garcia M. C., Maltoni M., Martinez-Soler I. and Salvado J., Updated Constraints on Non-Standard Interactions

- from Global Analysis of Oscillation Data, JHEP **1808** (2018) 180 (DOI:10.1007/JHEP08(2018)180).
- [374] Akimov D. *et al.* [COHERENT Collaboration], Observation of Coherent Elastic Neutrino-Nucleus Scattering, Science **357** (2017) no.6356, 1123 (DOI:10.1126/science.aao0990).
- [375] Agostini M. *et al.* [Borexino Collaboration], Limiting neutrino magnetic moments with Borexino Phase-II solar neutrino data, Phys. Rev. D **96** (2017) no.9, 091103 (DOI:10.1103/PhysRevD.96.091103).
- [376] Dorenbosch J. *et al.* [CHARM Collaboration], Experimental Verification of the Universality of ν_e and ν_μ Coupling to the Neutral Weak Current, Phys. Lett. B **180** (1986) 303 (DOI:10.1016/0370-2693(86)90315-1).
- [377] Denton P. B., Farzan Y. and Shoemaker I. M., Testing large non-standard neutrino interactions with arbitrary mediator mass after COHERENT data, JHEP **1807** (2018) 037 (DOI:10.1007/JHEP07(2018)037).
- [378] Altmannshofer W., Tammaro M. and Zupan J., Non-standard neutrino interactions and low energy experiments (arXiv:1812.02778 [hep-ph]).
- [379] Friedland A., Graesser M. L., Shoemaker I. M. and Vecchi L., Probing Nonstandard Standard Model Backgrounds with LHC Monojets, Phys. Lett. B **714** (2012) 267 (DOI:10.1016/j.physletb.2012.06.078).
- [380] Choudhury D., Ghosh K. and Niyogi S., Probing nonstandard neutrino interactions at the LHC Run II, Phys. Lett. B **784** (2018) 248 (DOI:10.1016/j.physletb.2018.07.053).
- [381] Sjöstrand T. *et al.*, An Introduction to PYTHIA 8.2, Comput. Phys. Commun. **191** (2015) 159 (DOI:10.1016/j.cpc.2015.01.024).

- [382] Dercks D., Desai N., Kim J. S., Rolbiecki K., Tattersall J. and Weber T., CheckMATE 2: From the model to the limit, *Comput. Phys. Commun.* **221** (2017) 383 (DOI:10.1016/j.cpc.2017.08.021).
- [383] ATLAS Collaboration, Search for dark matter and other new phenomena in events with an energetic jet and large missing transverse momentum using the ATLAS detector (ATLAS-CONF-2017-060).
- [384] Aad G. *et al.* [ATLAS Collaboration], Search for new phenomena in final states with an energetic jet and large missing transverse momentum in pp collisions at $\sqrt{s} = 8$ TeV with the ATLAS detector, *Eur. Phys. J. C* **75** (2015) no.7, 299, Erratum: *Eur. Phys. J. C* **75** (2015) no.9, 408 (DOI:10.1140/epjc/s10052-015-3517-3, 10.1140/epjc/s10052-015-3639-7).
- [385] Aartsen M. G. *et al.* [IceCube Collaboration], Search for a diffuse flux of astrophysical muon neutrinos with the IceCube 59-string configuration, *Phys. Rev. D* **89** (2014) no.6, 062007 (DOI:10.1103/PhysRevD.89.062007).
- [386] Ahlers M., Helbing K. and de los Heros C. Pérez, Probing Particle Physics with IceCube, *Eur. Phys. J. C* **78**, no.11, 924 (2018) (DOI:10.1140/epjc/s10052-018-6369-9).
- [387] Lai H. L., Guzzi M., Huston J., Li Z., Nadolsky P. M., Pumplin J. and Yuan C.-P., New parton distributions for collider physics, *Phys. Rev. D* **82** (2010) 074024 (DOI:10.1103/PhysRevD.82.074024).
- [388] Ohlsson T., Status of non-standard neutrino interactions, *Rept. Prog. Phys.* **76** (2013) 044201 (DOI:10.1088/0034-4885/76/4/044201).
- [389] Farzan Y., A model for large non-standard interactions of neutrinos leading to the LMA-Dark solution, *Phys. Lett. B* **748** (2015) 311 (DOI:10.1016/j.physletb.2015.07.015).

- [390] Miranda O. G. and Nunokawa H., Non standard neutrino interactions: current status and future prospects, *New J. Phys.* **17** (2015) no.9, 095002 (DOI:10.1088/1367-2630/17/9/095002).
- [391] Altmannshofer W., Gori S., Martín-Albo J., Sousa A. and Wallbank M., Neutrino Tridents at DUNE (arXiv:1902.06765 [hep-ph]).
- [392] Dent J. B., Ferrer F. and Krauss L. M., Constraints on Light Hidden Sector Gauge Bosons from Supernova Cooling (arXiv:1201.2683 [astro-ph.CO]).
- [393] Nelson A. E. and Tetradis N., Constraints On A New Vector Boson Coupled To Baryons, *Phys. Lett. B* **221** (1989) 80 (DOI:10.1016/0370-2693(89)90196-2).
- [394] Tulin S., New weakly-coupled forces hidden in low-energy QCD, *Phys. Rev. D* **89** (2014) no.11, 114008 (DOI:10.1103/PhysRevD.89.114008).
- [395] Aubert B. *et al.* [BaBar Collaboration], Search for Invisible Decays of a Light Scalar in Radiative Transitions $v_{3S} \rightarrow \gamma A_0$ (arXiv:0808.0017 [hep-ex]).
- [396] Abdullah M., Dent J. B., Dutta B., Kane G. L., Liao S. and Strigari L. E., Coherent elastic neutrino nucleus scattering as a probe of a Z- through kinetic and mass mixing effects, *Phys. Rev. D* **98** (2018) no.1, 015005 (DOI:10.1103/PhysRevD.98.015005).
- [397] Buarque Franzosi D., Frandsen M. T. and Shoemaker I. M., New or ν missing energy: Discriminating dark matter from neutrino interactions at the LHC, *Phys. Rev. D* **93** (2016) no.9, 095001 (DOI:10.1103/PhysRevD.93.095001).
- [398] Bustamante M. and Ahlers M., Inferring the flavor of high-energy astrophysical neutrinos at their sources, *Phys. Rev. Lett.* **122** (2019) 241101 (DOI:10.1103/PhysRevLett.122.241101).

- [399] Evans J. A., Detecting Hidden Particles with MATHUSLA, *Phys. Rev. D* **97** (2018) no.5, 055046 (DOI:10.1103/PhysRevD.97.055046).
- [400] Mermoud P. [SHiP Collaboration], Prospects of the SHiP and NA62 experiments at CERN for hidden sector searches, *PoS NuFact* **2017** (2017) 139 (DOI:10.22323/1.295.0139).
- [401] Ariga A. *et al.* [FASER Collaboration], FASER: ForwArd Search Experiment at the LHC (arXiv:1901.04468 [hep-ex]).
- [402] Liao J. and Marfatia D., COHERENT constraints on non-standard neutrino interactions, *Phys. Lett. B* **775** (2017) 54 (DOI:10.1016/j.physletb.2017.10.046).
- [403] Papoulias D. K. and Kosmas T. S., COHERENT constraints to conventional and exotic neutrino physics, *Phys. Rev. D* **97** (2018) no.3, 033003 (DOI:10.1103/PhysRevD.97.033003).
- [404] Jackson John D., *Classical Electrodynamics*, Third Edition, (1998) John Wiley & Sons Inc.
- [405] Pal Palash B., *An Introductory Course of Particle Physics*, First Edition, (2014) CRC Press, Taylor and Francis Group.
- [406] Frampton P. H., Hung P. Q. and Sher M., Quarks and leptons beyond the third generation, *Phys. Rept.* **330** (2000) 263 (DOI:10.1016/S0370-1573(99)00095-2).
- [407] Ellis J., Fairbairn M. and Tunney P., Anomaly-Free Dark Matter Models are not so Simple, *JHEP* **1708** (2017) 053 (DOI:10.1007/JHEP08(2017)053).
- [408] Carena M., Daleo A., Dobrescu B. A. and Tait T. M. P., Z' gauge bosons at the Tevatron, *Phys. Rev. D* **70** (2004) 093009 (DOI:10.1103/PhysRevD.70.093009).
- [409] Fayet P., Invisible Upsilon decays into Light Dark Matter, *Phys. Rev. D* **81** (2010) 054025 (DOI:10.1103/PhysRevD.81.054025).

- [410] Dobrescu B. A. and Frugiuele C., Hidden GeV-scale interactions of quarks, *Phys. Rev. Lett.* **113** (2014) 061801 (DOI:10.1103/PhysRevLett.113.061801).
- [411] Haber H. E. and Stål O., New LHC benchmarks for the \mathcal{CP} -conserving two-Higgs-doublet model, *Eur. Phys. J. C* **75** (2015) no.10, 491, Erratum: *Eur. Phys. J. C* **76** (2016) no.6, 312 (DOI:10.1140/epjc/s10052-015-3697-x, 10.1140/epjc/s10052-016-4151-4).
- [412] Dorsch G. C., Huber S. J., Mimasu K. and No J. M., Hierarchical versus degenerate 2HDM: The LHC run 1 legacy at the onset of run 2, *Phys. Rev. D* **93** (2016) no.11, 115033 (DOI:10.1103/PhysRevD.93.115033).
- [413] Das D., Kundu A. and Saha I., Higgs data does not rule out a sequential fourth generation with an extended scalar sector, *Phys. Rev. D* **97** (2018) no.1, 011701 (DOI:10.1103/PhysRevD.97.011701).
- [414] Busoni G., De Simone A., Morgante E. and Riotto A., On the Validity of the Effective Field Theory for Dark Matter Searches at the LHC, *Phys. Lett. B* **728** (2014) 412 (DOI:10.1016/j.physletb.2013.11.069).